



Haggarty, Jennifer (2017) *Biofilm metabolomics: the development of mass spectrometry and chromatographic methodology for the analysis of dual-species pathogenic biofilms*. PhD thesis.

<http://theses.gla.ac.uk/8616/>

Copyright and moral rights for this work are retained by the author

A copy can be downloaded for personal non-commercial research or study, without prior permission or charge

This work cannot be reproduced or quoted extensively from without first obtaining permission in writing from the author

The content must not be changed in any way or sold commercially in any format or medium without the formal permission of the author

When referring to this work, full bibliographic details including the author, title, awarding institution and date of the thesis must be given

Enlighten:Theses  
<http://theses.gla.ac.uk/>  
theses@gla.ac.uk

**Biofilm Metabolomics: the  
development of mass  
spectrometry and  
chromatographic methodology  
for the analysis of dual-species  
pathogenic biofilms**

**Jennifer Haggarty  
BSc(Hons) MRes**

**Submitted in fulfilment of the requirements for the Degree of  
Doctor of Philosophy**

**School of Life Sciences  
College of Medical, Veterinary and Life Sciences  
Institute of Infection, Immunity and Inflammation  
University of Glasgow**

## Abstract

Polymicrobial diseases arise when multiple microorganisms colonize a host and form multi-species biofilms. Within polymicrobial communities bacteria, fungi, viruses and/or parasites directly and indirectly interact with one another in a multitude of ways. The composition and the interactions between organisms within polymicrobial biofilms govern disease severity and patient outcomes. Polymicrobial infections are of significant interest because of the escalating development of antimicrobial resistance and the increasing involvement polymicrobial biofilms in chronic and systemic infections.

The Gram-positive bacteria *Staphylococcus aureus* and dimorphic fungi *Candida albicans* have been shown to coexist within the human host in polymicrobial biofilm communities which often result in increased disease severity and mortality. Both of these commensals are opportunistic human pathogens that cause a plethora of infections ranging from relatively non-lethal local infections to life-threatening systemic infections in immunocompromised individuals. *S. aureus* and *C. albicans* have been co-associated with a number of polymicrobial diseases including cystic fibrosis and polymicrobial sepsis. Furthermore, *S. aureus* and *C. albicans* dual-infections have been associated with increased virulence and antimicrobial resistance. Although an effort has been made to unravel the relationship between *S. aureus* and *C. albicans*, metabolomics offers a powerful analytical tool to gain a better understanding of the interactions between this bacteria and fungus. To gain a better understanding of these interactions novel methods must be developed to modulate biofilm growth.

Metabolomics is intended to analyse the complete small molecule component of a biological system. Analytically, the diversity present in these compounds presents huge opportunities for improvement. The overall aim of this research

was to develop novel metabolomics methods and to apply these methods to the analysis of a *S. aureus*/*C. albicans* dual species biofilm to aid in the understanding of the relationship between this bacteria and fungi.

Characterisation of the *S. aureus*/*C. albicans* biofilm in comparison in to the mono-species was carried out using a number of techniques, including fluorescence microscopy, SEM imaging, qPCR and transcriptional analysis, which indicated that these two organisms interact with each other on a physical and molecular lever. Although the presence of *C. albicans* facilitates *S. aureus* biofilm formation in sera, the presence of the bacteria reduced the number of *C. albicans* within the dual-species biofilm compared to the fungal mono-species and caused ‘crinkled’ hyphae which suggested possible antagonistic behaviour towards the fungi.

An untargeted liquid chromatography-mass spectrometry separation method was developed that effectively retained both polar and nonpolar compounds by serially coupling a reversed-phase liquid chromatography (RPLC) column to a hydrophilic interaction liquid chromatography (HILIC) column via a T-piece. Two independent pumps were incorporated into the system to allow independent gradient control of the two columns. The high dilution between the columns, achieved by the difference in flow rates, enabled the retention and separation of both polar and nonpolar standards and numerous polar and non-polar metabolites extracted from beer. Good peak shapes and retention time reproducibility was achieved across all compound classes analysed.

Next, a targeted ion-chromatography mass-spectrometry method was developed for the analysis of central carbon metabolism intermediates, specifically those involved in glycolysis, the tricarboxylic acid (TCA) cycle and the Electron Transport Chain (ETC). A total mix of all of the energy metabolites standards analysed were able to be separated and detected using IC-MS, with the exception of DHAP, G3P, oxaloacetate, acetyl-CoA,

succinyl-CoA, NAD and NADP. The method displayed good reproducibility and limits of detection.

The complexity of the extracted biofilms proved challenging to the IC-MS. Sample variation and low intensities in some sample groups (particularly the *S. aureus* samples) resulted in lower detection than expected. The RPLC/HILIC method provided hundreds of metabolite detections, but suffered in comparison to the conventional HILIC method, likely due to far greater optimisation of the original technique, leading to the utilisation of the routine pHILIC method in place of the serially combined method.

Untargeted metabolomics analysis highlighted significant changes in a number of metabolic pathways including purine, pyrimidine, methionine and cysteine metabolism between the *S. aureus* and *C. albicans* mono-species and the dual-species biofilms. The differences detected within individual pathways suggest a difference in behaviour when the microorganisms are cultured with one another. The dramatic downregulation of a large portion of essential metabolites within purine, pyrimidine, cysteine and methionine pathways is indicative of the bacteria struggling to proliferate and form strong biofilms in sera. Down-regulation of many of the pathways in the dual-species biofilm compared to the *C. albicans* mono-species biofilm suggests that the presence of *S. aureus* within the biofilm could be having an adverse effect on the *C. albicans*.

The results and conclusions herein provide greater understanding of the clinically important interaction between *S. aureus* and *C. albicans*. Microscopic and molecular characterisation enabled visualisation of the dual-species biofilm. The development and application of metabolomics techniques highlighted changes in metabolism between the mono- and dual-species biofilms, indicating that the relationship between *S. aureus* & *C. albicans* may not be completely synergistic, as previously suggested.

Although the metabolomics methods developed during this study performed well, with regards to the separation of simple standard mixes and the complex beer sample, were not suitable for biofilm analysis. Through continued sample preparation and chromatographic optimisation these novel methods could offer relatively simple alternatives to more time consuming and complex chromatographic procedures.

# Table of Contents

Abstract .....	2
List of Tables.....	9
List of Figures .....	11
List of Accompanying Material.....	17
Acknowledgement .....	19
Author's Declaration .....	20
Definitions/Abbreviations .....	21
Chapter 1. Introduction .....	28
1.1 Polymicrobial infections: bacteria, fungi and biofilms .....	29
1.1.1 Polymicrobial interactions.....	29
1.1.2 <i>Staphylococcus aureus</i> .....	31
1.1.3 <i>Candida albicans</i> .....	36
1.1.4 The role of Candida-Staph polymicrobial biofilms in disease .....	40
1.1.5 <i>S. aureus</i> and <i>C. albicans</i> dual-species biofilms.....	41
1.2 Metabolomics .....	46
1.3 Analytical methods .....	49
1.3.1 Mass spectrometry .....	49
1.3.2 Chromatography.....	60
1.3.3 Identification .....	86
1.4 Aims and Hypothesis .....	88
Chapter 2. Materials and methods.....	90
2.1 Bacterial and fungal biofilm characterisation .....	91
2.1.1 Bacterial and fungal strains and growth.....	91
2.1.2 Biofilm formation .....	91
2.1.3 Biofilm characterisation .....	91
2.1.4 Growth curves .....	92
2.1.5 Biomass assays.....	92
2.1.6 Fluorescence microscopy .....	93
2.1.7 Scanning electron microscopy (SEM) .....	93
2.1.8 Cell numbers.....	93
2.1.9 Gene expression analysis of biofilm associated genes.....	94
2.2 Serially combined method .....	96
2.2.1 Chemicals and reagents.....	96
2.2.2 Standards.....	96

2.2.3 Beer samples.....	97
2.2.4 Instrumentation .....	97
2.2.5 Chromatographic conditions.....	100
2.2.6 Evaluation of reproducibility .....	100
2.2.7 Extracellular-metabolite extraction .....	102
2.2.8 Intracellular-metabolite extraction .....	102
2.2.9 Identification .....	102
2.3 Ion chromatography - mass spectrometry .....	104
2.3.1 Chemicals and reagents.....	104
2.3.2 Standards.....	104
2.3.3 Instrumentation .....	106
2.3.4 Chromatographic conditions.....	107
2.3.5 Evaluation of reproducibility and limits of detection .....	109
2.3.6 Extracellular-metabolite extraction .....	110
2.3.7 Intracellular-metabolite extraction .....	111
2.3.8 Identification .....	111
Chapter 3. <i>S. aureus</i> and <i>C. albicans</i> dual-species biofilm characterisation..	112
3.1 Introduction.....	113
3.2 Material and methods .....	116
3.3 Results .....	116
3.3.1 Growth curves .....	116
3.3.2 Biomass assay.....	118
3.3.3 Biofilm visualisation .....	123
3.3.4 Transcriptional analysis .....	131
3.4 Discussion .....	133
Chapter 4. Serially combined Reverse phase (RP)/Hydrophilic Interaction Liquid Chromatography (HILIC) method development .....	140
4.1 Introduction.....	141
4.1.1 Metabolomics techniques .....	141
4.2 Materials and methods .....	147
4.3 Results .....	147
4.3.1 Standards - Organic acids.....	147
4.1.2 Standards - Bile acids.....	151
4.1.3 Beer sample.....	156
4.4 Discussion .....	159

Chapter 5. Ion chromatography - mass spectrometry (IC-MS) method development for central carbon metabolism (CCM) analysis .....	167
5.1 Introduction.....	168
5.1.1 Central carbon metabolism.....	168
5.1.2 Methods to analyse central carbon metabolism (CCM) .....	171
5.2 Materials and methods .....	179
5.3 Results .....	179
5.3.1 Make-up flow composition.....	179
5.2.2 Standards.....	185
5.3 Discussion .....	218
Chapter 6. Metabolomics analysis of <i>S. aureus</i> and <i>C. albicans</i> mono- and dual-species biofilms.....	226
6.1 Introduction.....	227
6.2 Materials and methods .....	227
6.3 Results .....	228
6.3.1 Targeted analysis - IC-MS method .....	228
6.3.2 Untargeted analysis - RPLC/HILIC method .....	239
6.4 Discussion .....	254
6.4.1 IC-MS .....	255
6.4.2 LC-MS .....	257
6.4.3 Conclusions .....	280
Chapter 7. General discussion.....	281
7.1 <i>S. aureus</i> and <i>C. albicans</i> biofilm characterisation .....	283
7.2 Serially combined Reverse phase (RP)/Hydrophilic Interaction Liquid Chromatography (HILIC) method development.....	284
7.3 Ion chromatography - mass spectrometry (IC-MS) method development for central carbon metabolism (CCM) analysis .....	285
7.4 Metabolomics analysis of <i>S. aureus</i> and <i>C. albicans</i> mono- and dual-species biofilms .....	287
7.5 Future work .....	290
Appendices .....	293
References .....	294

## List of Tables

Table 1-1 List of the minimum metadata relative to metabolite identification required for each MSI level (Sumner et al., 2007).....	87
Table 2-1 A list of the Forward (F) and Reverse (R) Primers used to quantify <i>Candida albicans</i> ( <i>C. albicans</i> ) and <i>Staphylococcus aureus</i> ( <i>S. aureus</i> ) cell numbers.....	95
Table 2-2 Summary of the chromatographic conditions for the combined RPLC/pHILIC method.....	101
Table 2-3 A list of the glycolysis standards.....	105
Table 2-4 A list of the TCA standards .....	106
Table 2-5 A list of the coenzymes and nucleoside phosphates standards.....	106
Table 2-6 Summary of the chromatographic conditions used for the targeted ion chromatography - mass spectrometry (ICMS) analysis .....	108
Table 2-7 Summary of the energy metabolite concentrations used to determine the limits of detection.....	110
Table 4-1 Average retention times (RTs) and relative standard deviations (%RSDs) of the organic and bile acid standards .....	155
Table 4-2 Average retention times (RT) and RSDs of selected beer metabolites .....	158
Table 4-3 Comparison of dual- and single-column methods.....	163
Table 5-1 Ion intensities of pyruvate ( $m/z$ 87.0084), glucose ( $m/z$ 179.0562) and 2-oxoglutarate ( $m/z$ 145.0143).....	185
Table 5-2 A list of the glycolysis standards elemental formulae (EF), molecular weights (MW) and $m/z$ values ([M-H]).....	187
Table 5-3 A list of the TCA cycle intermediates elemental formulae (EF), molecular weights (MW) and $m/z$ values ([M-H]) .....	197
Table 5-4 A list of the coenzymes and nucleoside phosphates intermediates elemental formulae (EF), molecular weights (MW) and $m/z$ values ([M-H]).....	209
Table 5-5 The average retention times (RTs), standard deviations (SD) and relative standard deviations (%RSDs) of each detectable energy metabolism standard. (n=3). .....	212
Table 5-6 A list of the elemental formulae (EF), peak areas and linear regression coefficients ( $R^2$ ) for the energy metabolites at 2 pmol - 1nmol.....	216
Table 5-7 A list of the elemental formulae (EF), peak areas and linear regression coefficients ( $R^2$ ) for the energy metabolites at 200 fmol - 100 pmol.....	217

Table 6-1 A list of detected (+) and undetected (-) energy intermediates in <i>C. albicans</i> (CA), <i>S. aureus</i> (SA), dual-species (CASA) biofilms and fresh media (FM) .....	230
Table 6-2 The elemental formulae (EF), $m/z$ values ([M-H]), expected retention times (RTs), average RTs, standard deviations (SDs) and relative standard deviations (RSDs) of the energy metabolism intermediates detected in the biofilm samples. ....	231
Table 6-3 Heat map comparison of the energy metabolites detected in the spent media of the <i>C. albicans</i> (CAM), <i>S. aureus</i> (SAM) and the dual species (SCM) biofilms .....	239
Table 6-4 Comparison of the RPLC/pHILIC combined and the routine pHILIC methods.....	240
Table 6-5 Heat map comparison of the intracellular purine metabolite abundances detected in the <i>C. albicans</i> (CAC), <i>S. aureus</i> (SAC) and the dual species (SCC) biofilms. ....	244
Table 6-6 Heat map comparison of the intracellular rimidine metabolite abundances detected in the <i>C. albicans</i> (CAC), <i>S. aureus</i> (SAC) and the dual species (SCC) biofilms. ....	247
Table 6-7 Heat map comparison of the intracellular cysteine and methionine metabolite abundances detected in the <i>C. albicans</i> (CAC), <i>S. aureus</i> (SAC) and the dual species (SCC) biofilms.....	251

## List of Figures

Figure 1-1 Diagram of structure of <i>S. aureus</i> cell. ....	33
Figure 1-2 The ‘omics’ cascade and their related molecules. ....	47
Figure 1-3 Schematic diagram of MS. ....	49
Figure 1-4 An example of a mass spectrum. ....	50
Figure 1-5 Schematic of electrospray ionisation (ESI). ....	51
Figure 1-6 The production of gas-phase charged species. ....	53
Figure 1-7 Quadrupole parallel cylindrical rods with opposing charges. ....	54
Figure 1-8 Stability diagram produced from the Mathieu equation ....	56
Figure 1-9 Stability areas for three ions with different masses ....	57
Figure 1-10 Position of the quadrupole mass analyser ....	57
Figure 1-11 Schematics illustration the diversity of the Orbitrap range. ....	58
Figure 1-12 Simple diagram of chromatogram. ....	61
Figure 1-13 Diagram of Gaussian peak. ....	62
Figure 1-14 A simple diagram of two peaks which are not baseline resolved. ...	63
Figure 1-15 Diagram illustration the factors that affect resolution. ....	64
Figure 1-16 Diagram illustration the relationship between selectivity and efficiency. ....	65
Figure 1-17 An example of a Van Deemter plot. ....	68
Figure 1-18 Schematic representation of RPLC stationary phase. ....	71
Figure 1-19 A comparison of common elution solvents used in RPLC. ....	72
Figure 1-20 Schematic illustrating the acid and base equilibrium. ....	74
Figure 1-21 Neutral ion pairs. ....	76
Figure 1-22 Structures of (A) unmodified silica hydride (SH); (B) modified SH (C <sub>8</sub> ); (C) amino; (D) diol and (E) cyano stationary phases that can be bonded to silica gel. ....	78
Figure 1-23 Structure of the sulfoalkylbetaine stationary phase. ....	78
Figure 1-24 Simple diagram depicting partitioning in HILIC. ....	79
Figure 1-25 A comparison of common elution solvents used in HILIC. ....	80
Figure 1-26 Schematic representation of a membrane-based suppressor. ....	85
Figure 2-1 Chemical structures of the test compounds. ....	97
Figure 2-2 Schematic diagram of the RPLC/pHILIC/ESI-FTMS. ....	99
Figure 2-3 Summary of the chromatographic conditions used for the targeted ion chromatography - mass spectrometry (ICMS) ....	108

Figure 3-1 A comparison of the growth curves of <i>C. albicans</i> , <i>S. aureus</i> and their co-culture in various media.....	118
Figure 3-2 Biomass comparison of <i>C. albicans</i> , <i>S. aureus</i> and their co-culture .	119
Figure 3-3 Bar charts comparing the average colony-forming equivalents (CFE) for <i>C. albicans</i> (CA) and <i>S. aureus</i> (SA) in their mono- and co-cultures.....	120
Figure 3-4 Bar charts comparing the average colony-forming equivalents (CFE) for <i>C. albicans</i> (CA) and <i>S. aureus</i> (SA) in their mono- and co-cultures.....	122
Figure 3-5 Fluorescent image of <i>S. aureus</i> .....	123
Figure 3-6 Fluorescent image of <i>C. albicans</i> .....	124
Figure 3-7 Fluorescent image of <i>S. aureus</i> and <i>C. albicans</i> co-culture .....	125
Figure 3-8 Secondary electron images of <i>S. aureus</i> (SA).....	127
Figure 3-9 Secondary electron images of <i>C. albicans</i> (CA) .....	128
Figure 3-10 Secondary electron images of the co-cultured biofilm .....	129
Figure 3-11 Secondary electron images of the <i>S. aureus</i> and <i>C. albicans</i> dual-species biofilm .....	130
Figure 3-12 Bar charts comparing the percentage expression of (A) <i>HWP1</i> (a filamentation protein) and (B) <i>ALS3</i> (an adhesion protein) in mono-cultured <i>C. albicans</i> compared to its co-culture with <i>S. aureus</i> .....	132
Figure 4-1 Schematic of the novel column switching method developed by Li <i>et al.</i> (2015) .....	144
Figure 4-2 Typical configuration for 2D-LC separations.....	145
Figure 4-3 Extracted ion chromatograms (EICs) of selected organic acids.....	149
Figure 4-4 EICs of (A): citrate and (B) isocitrate using the combined RPLC/HILIC method.....	150
Figure 4-5 Extracted ion chromatograms (EICs) of (A): <i>m/z</i> 115.00368 from the organic acid mix and (B): malate ( <i>m/z</i> 133.01425). .....	151
Figure 4-6 Equation showing water loss from malic acid .....	151
Figure 4-7 Extracted ion chromatograms (EICs) of selected bile acids .....	153
Figure 4-8 Extracted ion chromatograms (EICs) of selected beer metabolites with annotations. ....	157
Figure 5-1 Schematic of the glycolysis pathway. ....	169
Figure 5-2 Schematic of the tricarboxylic acid (TCA) cycle. ....	170
Figure 5-3 Mass spectra of pyruvate ( <i>m/z</i> 87.0084) with different make-up flow compositions .....	182

Figure 5-4 Mass spectra of glucose ( $m/z$ 179.0562) with with different make-up flow compositions .....	183
Figure 5-5 Mass spectra of 2-oxoglutarate ( $m/z$ 145.0140) with different make-up flow compositions .....	184
Figure 5-6 The conductivity chromatograms of (A) dihydroxyacetone (DHAP) and (B) glyceraldehyde 3-phosphate (G3P) .....	188
Figure 5-7 Extracted ion chromatograms (EICs) of $m/z$ 168.9908 from the (A) dihydroxyacetone (DHAP) and (B) glyceraldehyde 3-phosphate (G3P) standards. ....	189
Figure 5-8 Mass spectrums (MS) of (A) dihydroxyacetone (DHAP) and (B) glyceraldehyde 3-phosphate (G3P) with possible elemental compositions.. ....	190
Figure 5-9 The (A) IC conductivity chromatogram and (B) EIC from MS of 2- and 3-phosphoglycerate.....	191
Figure 5-10 The extracted ion chromatogram (EIC) of phosphoenolpyruvate ...	192
Figure 5-11 The extracted ion chromatogram (EIC) of the pyruvate standard ..	192
Figure 5-12 The extracted ion chromatograms (EICs) of the glycolysis metabolites.....	193
Figure 5-13 The (A) ion conductivity (IC) chromatogram (B) mass spectrum and (C) an extracted ion chromatogram (EIC) of glucose.....	194
Figure 5-14 The extracted ion chromatograms (EICs) of (A) citrate and (B) isocitrate obtained using the combined RPLC/pHILIC LCMS method .....	198
Figure 5-15 The extracted ion chromatogram (EIC) of a citrate and isocitrate mix using the IC-MS method.....	198
Figure 5-16 The (A) extracted ion chromatogram (EIC) ( $m/z$ 173.0092) and (B) mass spectrum (MS) of the <i>cis</i> -aconitate standard. ....	199
Figure 5-17 Comparison of the (A) IC chromatogram of (1) malate & succinate and (2) fumarate and (B) the extracted ion chromatograms (EICs) of (a) the full MS of a malate, succinate and fumarate mix (b) malate ( $m/z$ 133.0143), (c) fumarate ( $m/z$ 115.0038) and (d) succinate ( $m/z$ 117.0194) .....	200
Figure 5-18 The (A) conductivity chromatogram and (B) extracted ion chromatogram (EIC) of the oxaloacetate .....	201
Figure 5-19 The extracted ion chromatograms (EICs) of the individual intermediates in the TCA mix .....	201
Figure 5-20 EICs of the base peak of (A) acetyl-CoA, (B) succinyl-CoA and (C) CoA. ....	204

Figure 5-21 Mass spectrum of (A) the direct injection of acetyl-CoA into the mass spectrometer and (B) acetyl-CoA injected on to the column with a 100 mM isocratic gradient.....	205
Figure 5-22 Mass spectrum of (A) the direct injection of succinyl-CoA into the mass spectrometer and (B) succinyl-CoA injected on to the column with a 100 mM isocratic gradient.....	206
Figure 5-23 Mass spectrum of (A) the direct injection of CoA into the mass spectrometer and (B) CoA injected on to the column with a 100 mM isocratic gradient.....	207
Figure 5-24 The extracted ion chromatograms (EICs) of $m/z$ 426.0222 from the (A) adenosine triphosphate (ATP) and (B) adenosine diphosphate (ADP) standards .....	208
Figure 5-25 The (A) extracted ion chromatogram (EIC) of the molecular ion of flavin adenine dinucleotide (FAD) $m/z$ 784.1499 and (B) the mass spectrum (MS) at the RT of the FAD standard (53.36 min) .....	210
Figure 5-26 IC conductivity chromatogram of the total mix of the energy metabolism standards using IC-MS. ....	211
Figure 5-27 Graph illustrating the peak areas detected for a selection of energy metabolites.....	214
Figure 5-28 Graph illustrating the peak areas detected for fructose 1,6-bisphosphate, ADP and ATP ranging from 200 fmol - 100 pmol.....	215
Figure 6-1 Extracted ion chromatograms (EICs) of (A) glucose ( $m/z$ 179.0562) and (B) G6P and F6P.....	233
Figure 6-2 Schematic diagrams of the stereoisomers of (A) glucose and (B) sorbose in D- and L- configurations. ....	234
Figure 6-3 Schematic diagram of the ring configuration of $\alpha$ - and $\beta$ -D-glucose. ....	234
Figure 6-4 EICs of (A) citrate and isocitrate ( $m/z$ 191.0198) and (B) succinate ( $m/z$ 117.0194) .....	236
Figure 6-5 Bar chart comparing the average peak areas calculated for each of the intracellular energy metabolites detected in <i>C. albicans</i> (CA), <i>S. aureus</i> (SA) and the dual-species biofilm (SC) .....	238
Figure 6-6 An example of the peak shapes obtained using (A) the RPLC/pHILIC combined method and (B) the standard pHILIC method.....	240
Figure 6-7 An example of peak splitting observed using the RPLC/pHILIC combined method. ....	241

Figure 6-8 Bar charts comparing the relative abundance of intracellular (A) L-glutamine and (B) adenosine monophosphate (AMP) detected in the mono-species <i>C. albicans</i> (CAC), <i>S. aureus</i> (SAC) and their co-culture (SCC).....	244
Figure 6-9 Bar charts comparing the relative abundance of intracellular (A) uridine diphosphate (UDP)-glucose; (B) deoxyuridine; (C) ureidopropionic acid; (D) uridine; (E) thymidine and (F) pseudouridine detected in the mono-species <i>C. albicans</i> (CAC), <i>S. aureus</i> (SAC) and their co-culture (SCC) .....	248
Figure 6-10 Bar charts comparing the relative abundance of intracellular (A) L-glutamine and (B) orotate detected in the mono-species <i>C. albicans</i> (CAC), <i>S. aureus</i> (SAC) and their co-culture (SCC) .....	249
Figure 6-11 Bar charts comparing the relative abundance of intracellular (A) 5'methylthioadenosine; (B) glutathione; (C) S-adenosyl-L-homocysteine; (D) L-methionine and (E) S-adenosyl-L-methionine detected in the mono-species <i>C. albicans</i> (CAC), <i>S. aureus</i> (SAC) and their co-culture (SCC).....	252
Figure 6-12 Bar charts comparing the relative abundance of intracellular (A) L-aspartate; (B) L-homoserine and (C) O-succinyl-L-homoserine detected in the mono-species <i>C. albicans</i> (CAC), <i>S. aureus</i> (SAC) and their co-culture (SCC) ...	253
Figure 6-13 Bar charts comparing the relative abundance of O-succinyl-L-homoserine detected in (A) the mono-species <i>C. albicans</i> (CAC), <i>S. aureus</i> (SAC) and their co-culture (SCC) and (B) the individual <i>C. albicans</i> samples.....	253
Figure 6-14 Bar charts comparing the relative abundance of intracellular (A) L-cystathionine; (B) O-acetyl-L-homoserine and (C) 3-sulfino-L-alanine detected in the mono-species <i>C. albicans</i> (CAC), <i>S. aureus</i> (SAC) and their co-culture (SCC). .....	254
Figure 6-15 Schematic diagram depicting identified and annotated metabolites within the purine metabolism pathway in relation to known <i>S. aureus</i> enzymes .....	260
Figure 6-16 Adenosine triphosphate (ATP) and deoxyadenosine triphosphate (dATP) synthesis from inosine monophosphate (IMP). .....	261
Figure 6-17 Salvage pathways for purines .....	264
Figure 6-18 Schematic diagram of the purine metabolism pathway in relation to known <i>C. albicans</i> enzymes .....	265
Figure 6-19 Schematic diagram depicting identified and annotated metabolites within the pyrimidine metabolism pathway in relation to known <i>S. aureus</i> enzymes.....	267

- Figure 6-20 Schematic diagram of pyrimidine biosynthetic *de novo* pathway in *S. aureus*. .....269
- Figure 6-21 Schematic diagram depicting identified and annotated metabolites within the (A) methionine and S-adenosyl-L-methionine (SAM) biosynthetic pathway and (B) the alternative reactions for the *O*-acylation of homoserine in relation to known *S. aureus* enzymes .....271
- Figure 6-22 A simple diagram highlighting the relationship between the (A) methionine, (B) tetrahydrofolate and (C) pyrimidine synthesis pathways .....274
- Figure 6-23 Schematic diagram depicting identified and annotated metabolites within the (A) methionine and S-adenosyl-L-methionine (SAM) biosynthetic pathway .....276
- Figure 6-24 Schematic diagram of the reverse transsulfuration pathway for the conversion of methionine to cysteine .....279

# List of Accompanying Material

## Appendices

- I. Standard curves of *Staphylococcus aureus* and *Candida albicans*.
- II. Supplementary data: The average retention times, standard deviations and relative standard deviations of the organic acids, bile acids and putative metabolites detected in a beer sample.
- III. Supplementary data: IC-MS retention time reproducibility of the energy metabolism standards.
- IV. Supplementary data: IC-MS metabolic data set of the intracellular metabolome of *S. aureus*, *C. albicans* and their dual-species biofilm.
- V. Supplementary data: IC-MS metabolic data set of the extracellular metabolome of *S. aureus*, *C. albicans* and their dual-species biofilm.
- VI. Supplementary data: *S. aureus* versus *C. albicans* versus dual-species biofilm metabolomics dataset - Polyomic's in-house Metabolic Pipeline spreadsheet.

## Published papers

- Kean, R., Rajendran, R., Haggarty, J., Townsend, E.M., Short, B., Burgess, K. E. V., Lang, S., Millington, O., Mackay, W.G., Williams, C., and Ramage, G. (2017) *Candida albicans* mycofilms support *Staphylococcus aureus* colonisation and enhances miconazole resistance in dual-species interactions. *Frontiers in Microbiology*, 8: 258.
- Haggarty, J. and Burgess, K. E. V. (2017) Review: Recent advances in liquid and gas chromatography methodology for extending the coverage of the metabolome. *Current Opinion in Biotechnology*. 43:77-85. (Invited author).
- Weidt, S., Haggarty, J., Cococarieu, C., Silcock, P., and Burgess, K. E. V. (2016) A novel targeted/untargeted GC-Orbitrap metabolomics methodology applied to *Candida albicans* and *Staphylococcus aureus* biofilms. *Metabolomics*, 12: 189.
- Haggarty, J., Oppermann, M., Dalby, M. J., Burchmore, R. J., Cook, K., Weidt, S., and Burgess, K. E.V. (2015). Serially coupling hydrophilic interaction and reversed-phase chromatography with simultaneous gradients provides greater coverage of the metabolome. *Metabolomics*, 11: 1465-1470.

## Presentations

Parts of the following thesis have been presented at the following conferences and meetings.

- Thermo Scientific IC User Meeting, Stirling, UK, 2015.
- Metabolomics, San Francisco, 2015.
- Glasgow Dental School & the University of the West of Scotland Away Day, Glasgow, UK, 2015.
- DTC Symposium, Glasgow, 2014 and 2015.
- Metabolite Profiling Forum, London, UK, 2014. (Travel award).
- Joint centres for Doctoral Training Conference, Warwick, UK, 2014.

# Acknowledgements

First and foremost I would like to thank all of my academic and industrial supervisors, Karl E. V. Burgess, Ken Cook, Matthew J. Dalby, Richard J. Burchmore, and Magdalena Oppermann. Karl, I would like to thank you for your astute guidance and encouragement during my PhD (and for repeatedly reassuring me that my data was okay!).

I would also like to thank Stefan Weidt. Thank you for taking time to teach me about the many aspects of LC and MS instrumentation, saving the day when things went wrong and for offering friendship and support throughout my PhD. Without your help this research would not have been completed and, for that, I am unbelievably grateful.

I am incredibly thankful for Gordon Ramage who as good as adopted me as a student during my PhD: - thank you for your collaboration and expert guidance. I would also like to take this opportunity to show my appreciation to the Ramage group for all of their help (and for putting up with me in the lab!) throughout my time at the Dental School, in particular Ryan Kean, Eleanor Townsend, Lindsay O'Donnell, Ranjith Rajendran and Leighann Sherry.

Many thanks to my industrial partners, Thermo Scientific and to Glasgow Polyomics: - where I have been based during my studies. I would also like to thank the following people for their support and advice: Laurence Stipetic, James Newton, Wai Chi Man, Peter Dewsbury, Suzanne McGill, Aruna Prakash, Erin Manson, Ana Monteiro, Yoann Gloaguen, Justin van der Hooft, Gavin Blackburn, Amy Cattanach, Allison Jackson and Rachael Murray.

Thank you to my family. Words cannot express how much I appreciate the love, support, kindness and understanding that you show me each and everyday. Mum and Dad, there is no doubt in my mind that I would not have started this journey if it wasn't for your encouragement and belief in me. I owe you both so much and hope that I can make you proud. Thank you to my brother David for your love and unwavering enthusiasm. To my sister Louise, thank you for your motivational speeches, sympathetic ear and expert stir-frying skills- I would not have survived this without you!

## Author's Declaration

I declare that, except where explicit reference is made to the contribution of others, that this dissertation is the result of my own work and has not been submitted for any other degree at the University of Glasgow or any other institution.

Signature:

Printed name: Jennifer Haggarty

## Definitions/Abbreviations

°C	Degrees Celsius
µL	Microlitre
µM	micrometre
µM	Micromolar
µm	Micrometre
1,3-BPG	1,3-bisphosphoglycerate
2D	Two-dimensional
2-PG	2-Phosphoglycerate
3-PG	3-Phosphoglycerate
AC	Alternating current
ace.a	Acetic acid
ACN	Acetonitrile
ADP	Adenosine diphosphate
AEX	Anion exchange chromatography
AFM	Atomic force microscopy
AMP	Adenosine monophosphate
Amp B	Amphotericin B
ATP	Adenosine triphosphate
BHI	Brain heart infusion
C	Carbon
<i>C. albicans</i>	<i>Candida albicans</i>
CA	<i>Candida albicans</i>
CAC	<i>C. albicans</i> intracellular
CAM	<i>C. albicans</i> spent media
CASA	Dual-species biofilm
CCM	Central carbon metabolism
cDNA	Complementary deoxyribonucleic acid
CDP	Cytidine diphosphate
CE	Capillary electrophoresis
CEX	Cation exchange chromatography
CFE	Colony-forming equivalents
CFU	Colony forming unit

ChCl <sub>3</sub>	Chloroform
CID	Collision induced dissociation
ClfA	Clumping factor A
ClfB	Clumping factor B
CLSM	Confocal scanning laser microscopy
CMP	Cytidine monophosphate
CO <sub>2</sub>	Carbon dioxide
CoA	Co-enzyme A
CoNS	Coagulase negative staphylococci
CRM	Charged residue model
CTP	Cytidine triphosphate
CV	Crystal violet
Da	Daltons
dADP	Deoxyadenosine diphosphate
dATP	Deoxyadenosine triphosphate
DC	Direct current
DESI	Desorption electrospray ionisation
dGMP	Deoxyguanosine monophosphate
dH <sub>2</sub> O	Dionised water
DHAP	Dihydroxyacetone phosphate
DHF	Dihydrofolate
DNA	Deoxyribonucleic acid
DNAse	Deoxyribonuclease
dTMP	Deoxythymidine monophosphate
dUMP	Deoxyuridine monophosphate
<i>E. coli</i>	<i>Escherichia coli</i>
E4P	Erythrose 4-phosphate
ECG	Eluent Generator Cartridge
ECM	Extracellular matrix
eDNA	Extracellular deoxyribonucleic acid
EF	Elemental formula
EIC	Extracted ion chromatogram
ELISA	Enzyme-linked immunosorbent assay
ESI	Electrospray ionisation
ETC	Electron transport chain

eV	Electron Volt
F	Flow rate
F1,6-BP	Fructose 1,6-bisphosphate
F6P	Fructose 6-phosphate
FAD	Flavin adenine dinucleotide
FADH <sub>2</sub>	Flavin adenine dinucleotide reduced
FBS	Foetal bovine serum
FISH	Fluorescent <i>in situ</i> hybridisation
FM	Fresh media
Fnbp A	Fibronectin-binding protein A
Fnbp B	Fibronectin-binding protein B
FTMS	Fourier Transform mass spectrometry
FWHM	Full-Width-at-Half-Maximum
g	Gram
G3P	Glyceraldehyde 3-phosphate
G6P	Glucose 6-phosphate
GC	Gas chromatography
GDP	Guanosine diphosphate
GI	Gastrointestinal
GMP	Guanosine monophosphate
GMP	Guanosine monophosphate
GTP	Guanosine triphosphate
h	Hour(s)
H <sup>+</sup>	Hydrogen ion
H <sub>2</sub> O	Water
HBF	High biofilm formers
HESI	Heated electrospray ionisation
HETP	Height equivalent to the theoretical plate
HILIC	Hydrophilic interaction chromatography
Hla	α-Haemolysin
HMDB	Human metabolite database
HPLC	High performance liquid chromatography
HRMS	High-resolution mass spectrometry
HRMS <sup>1</sup> <sub>a</sub>	High-resolution full scan mass spectrum matched to an authentic standard

HRMS <sup>1</sup> MS <sup>2</sup> <sub>PL</sub>	High-resolution MS <sup>2</sup> mass spectrum matched to a public library/database
IC	Ion chromatography
IC-MS	Ion chromatography- mass spectrometry
IEM	Ion evaporation model
IEX	Ion exchange chromatography
IMP	Inosine monophosphate
IPA	Isopropanol
<i>k</i>	Retention factor
K <sub>a</sub>	Ionisation constant
KEGG	Kyoto Encyclopedia of Genes and Genomes
KOH	Potassium hydroxide
kV	Kilovolts
LB	Luria Bertani
LBF	Low biofilm formers
LC	Liquid chromatography
LC-MS	Liquid chromatography- mass spectrometry
LD	Longitudinal diffusion
LOD	Limit of Detection
LogFC	Log fold change
LogP	Partition coefficient
M	Molar
<i>m/z</i>	mass-to-charge
M+H	Protonated mass
MALDI	Matrix assisted laser desorption ionisation
MeOH	Methanol
Me-THF	Methyl-tetrahydrofolate
MFA	Metabolic flux analysis
M-H	Deprotonated mass
min(s)	Minute(s)
mL	Millilitre
mM	Millimolar
mm	Millimetre
MMC	Mixed-mode column
MP	Mobile phase

MS	Mass spectrometry
MS/MS	Tandem Mass Spectrometry
MSCRAMM	Microbial surface component recognising adhesive matrix molecules
MSI	Metabolics Standards Initiative
MTA	5'Methylthioadenosine
MW	Molecular weight
N	Plate number
NAD	Nicotinamide adenine dinucleotide
NADP	Nicotinamide adenine dinucleotide phosphate
NaOH	Sodium hydroxide
nm	Nanometres
NMR	Nuclear magnetic resonance
NP	Normal phase
NPLC	Normal phase liquid chromatography
O	Oxygen
O-BHA	O-benzylhydroxylamine
OD	Optical density
OH <sup>-</sup>	Hydroxide ion
OPC	Oropharyngeal candidiasis
P	Phosphorus
<i>P. aeruginosa</i>	<i>Pseudomonas aeruginosa</i>
PBS	Phosphate buffered saline
PC	Principal component
PCA	Principal component analysis
PEP	Phosphoenolpyruvate
pH	Potential of hydrogen
PIA	Polysaccharide intracellular adhesion
pKa	Partial dissociation coefficient
PMA	Poly(methacrylate)
pmol	Picomole
ppm	Parts-per-million
(p)ppGpp	guanosine tetra- or penta-phosphate
PPP	Pentose phosphate pathway
PRPP	Phosphoribosyl pyrophosphate

PS-DVB	Poly(styrene-divinylbenzene)
PS-EVB	Poly(styrene-ethylvinylbenzene)
PTR	Phosphoribosyl transferase
PVA	Poly(vinyl alcohol)
PVL	Panton-Valentine leukocidin
qPCR	Quantitative polymerase chain reaction
$R^2$	Linear regression coefficient
R5P	Ribose 5-phosphate
RF	Radio frequency
RNA	Ribonucleic acid
RPLC	Reversed phase liquid chromatography
RPM	Revolutions per minute
RPMI	Roswell Park Memorial Institute medium
$R_s$	Resolution
RSD	Relative standard deviation
RT	Retention time
$R_{ta}$	Retention time matched to an authentic standard
s	Second(s)
S	Sulphur
<i>S. aureus</i>	<i>Staphylococcus aureus</i>
SA	<i>Staphylococcus aureus</i>
SAB	Sabouraud's dextrose
SAC	<i>S. aureus</i> intracellular
SAH	S-Adenosyl-L-homocysteine
SAM	<i>S. aureus</i> spent media
SAM	S-Adenosyl-L-methionine
SasA	Staphylococcal protein A
SCC	Staph/Candida co-culture
SCC	Dual-species intracellular
SCM	Dual-species spent media
sec	Second(s)
SEM	Scanning electron microscopy
SERAMs	Secreted expanded-repertoire adhesive molecules
SNM3	Synthetic nasal media
SP	Stationary phase

spp	Species
STDev	Standard deviation
$t'_R$	Adjusted retention time of analyte
$t_0$	Dead time
TBA	Tributylamine
TCA	Tricarboxylic acid
THF	Tetrahydrofolate
TOF	Time-of-flight
$t_r$	Retention time of analyte
TSB	Trypic soy broth
TSS	Toxic shock syndrome
UDP-glucose	Uridine diphosphate glucose
UHPLC	Ultra high pressure liquid chromatography
UMP	Uridine monophosphate
V	Volt
$V_R$	Retention volume
X5P	Xylulose 5-phosphate
XMP	xanthine monophosphate
YPD	Yeast peptone dextrose
z	Number of charges
ZDV	Zero dead volume
ZIC-HILIC	Zwitterionic-HILIC

# **Chapter 1. Introduction**

## **1.1 Polymicrobial infections: bacteria, fungi and biofilms**

Polymicrobial diseases are acute and chronic diseases that are caused by various combinations of bacteria, fungi, viruses and parasites (Brogden, Guthmiller, & Taylor, 2005). A host can become infected with multiple microorganisms in a number of ways. In synergistic polymicrobial infections a microorganism can generate a niche that is favourable for infection and colonization by pathogens, which is often seen between some periodontal pathogens (Palmer et al., 2001). Other polymicrobial infections occur when the presence of one microorganism predisposes the host to colonisation or infection by a second microorganism. For example, respiratory tract viruses can destroy respiratory epithelium. This can create adhesions which can enable bacteria to adhere to the surface causing superinfections (Peltola & Mccullers, 2004). In additive polymicrobial infections two or more non-pathogenic microorganisms can cause infections such as bacteraemia, abdominal abscesses, lung abscesses, odontogenic infections, brain abscesses and liver infections (Myres et al., 2002). Through culture independent community analysis methodologies, several diseases that were previously characterised as being mono-microbial are now recognised as polymicrobial infections, including diseases of the oral cavity, otitis media, diabetic foot wound infections and chronic infections in the cystic fibrosis lung. The composition of microbial populations predicts disease severity and outcomes.

### **1.1.1 Polymicrobial interactions**

There are a number of bacterial-fungal interactions that can occur when these micro-organisms come into contact with one another, both direct and indirect. These interactions can influence behaviour, growth, virulence and survival (De Sordi & Mühlischlegel, 2009; Anton Y Peleg, Hogan, & Mylonakis, 2010). Interactions include the secretion of molecules into the environment

for the purpose of signalling (Short, Murdoch, & Ryan, 2014). Bacteria can use these diffusible molecules to monitor aspects of their environment, such as population density, termed quorum sensing, and they modulate their behaviour accordingly (De Sordi & Mühlischlegel, 2009; Short et al., 2014). For a compound to be classified as an intercellular signal, it has to adhere to guidelines set out by Monds & O'Toole (2008): the compound has to be secreted and identified by the receiving organism; the organism has to possess a receptor to sense the signal and a mechanism to respond specifically to it; the concentration of the signal to elicit a response cannot be toxic to the cell; the response is separate from the metabolism of the signal; the purified signal can reproduce the response; and the signal network is adaptive at the level of the community (Monds & O'Toole, 2008). Some types of signal molecules produced for intracellular signalling can be recognized and influence other non-producing species through 'eavesdropping' (Fugère et al., 2014; Riedel et al., 2001). There are various types of inter-kingdom cross talk (De Sordi & Mühlischlegel, 2009). In one-way sensing, an organism senses and responds to a signal produced by another organism. One organism can use the signal produced by another organism to regulate its own gene, known as co-opting for a signal. An organism can also alter the production or stability of a signal from another organism, known as modulation of a signal. In two-way communication, multiple signals are exchanged between organisms (Cugini, Kolter, & Hogan, 2008).

Another indirect interaction is the modification of the environment, whereby one organism causes a change in the surrounding environment, e.g. pH. Changes in pH can modulate hyphae formation in *C. albicans* (Buffo, Herman, & Soll, 1984).

As well as diffused molecules bacteria and fungi can have physical interactions. Bacteria can attach to hyphae and yeast cells (Harriott & Noverr,

2009; A. Y. Peleg et al., 2008; Tampakakis, Peleg, & Mylonakis, 2009). Bacterial biofilms can also be found on the surface of the fungal hyphae (D. A. Hogan & Kolter, 2002). Physical interactions have been associated with reduced fungal viability. This could be due to the bacteria secreting antifungals into the environment, through direct transfer of bacterial toxins into fungal cells or through the depletion of nutrients (Anton Y Peleg et al., 2010).

The nature of polymicrobial interactions are species and environment dependent. Interspecies interactions can be symbiotic. Cross feeding of metabolites from the enzymatic breakdown of a carbon source or the presence of different species within a niche can provide protection against the host's immune response or anti-microbial agents (Harriott & Noverr, 2010). Interspecies interactions can also be antagonistic, e.g. one organism can secrete lethal quantities of antibiotics, antifungals or bacteriocins that cause harm to another organism. Cross kingdom interactions can also benefit one organism, without damage to another organism through the secretion of molecules termed 'cues'. 'Coercion' can also occur, through which one organism manipulates another organisms to benefit itself, without serious damage to the other (Short et al., 2014).

*S. aureus* and *C. albicans* have been shown to coexist within the human host in polymicrobial biofilm communities which often result in increased disease severity and mortality (Adam, Baillie, & Douglas, 2002; Baena-Monroy et al., 2005; Tawara, Honma, & Naito, 1996).

### **1.1.2 *Staphylococcus aureus***

*Staphylococcus aureus* (*S. aureus*) are non-motile, Gram-positive cocci with a diameter of 0.5 – 1.5  $\mu\text{M}$  (Harris, Foster, & Richards, 2002). These facultative anaerobes are a human commensal that asymptotically colonize

20% of the normal population, transiently colonize 60% of the population, while 20% of the population are rarely or never colonized (Williams, 1963). *S. aureus* primarily colonize anterior nares and are also found on the skin, rectum, pharynx, vagina, axillae and gastrointestinal (GI) tract (Wertheim et al., 2005).

*S. aureus* can grow by aerobic respiration or fermentation and cell division occurs in more than one plane to produce grape-like clusters (Tzagoloff & Novick, 1977). Staphylococci are tolerant to high salt concentrations and also show resistance to elevated temperatures (W. E. Kloos & Lambe, 1991). *S. aureus* are coagulase positive, i.e. can produce a blood clotting enzyme (W. E. Kloos & Musselwhite, 1975). *S. aureus* form golden colonies when grown on a solid media, which can be used to differentiate the bacteria from coagulase negative staphylococci (CoNS), which produce white or translucent colonies (Howard & Kloos, 1987).

The cell membrane, comprised of a phospholipid bi-layer, is surrounded by a cell wall (Fig. 1-1). The cell wall encasing *S. aureus* is a 20 – 40 nM thick protective coat, mainly composed of peptidoglycan and teichoic acid (a phosphate-containing polymer), which account for 50% and 40% of cell wall mass, respectively (Knox & Wicken, 1973; Shockman & Barrett, 1983). The remaining 10% of the cell wall is made up of surface proteins, exoproteins and peptidoglycan hydrolases (Harris et al., 2002). Peptidoglycan enables the construction of a tight multi-layered network that is capable of withstanding the high osmotic pressure of staphylococcus (B. Wilkinson, 1997), while the teichoic acid aids in the acquisition and localisation of metal ions and the activities of autolytic enzymes (B. Wilkinson, 1997). The remaining components are involved in surface attachment and *S. aureus* virulence (Harris et al., 2002). As well as the cell membrane and the cell wall, over 90%

of clinical strains of *S. aureus* have capsular polysaccharides (Arbeit, Karakawa, Vann, & Robbins, 1984; Thakker, Park, Carey, & Lee, 1998).

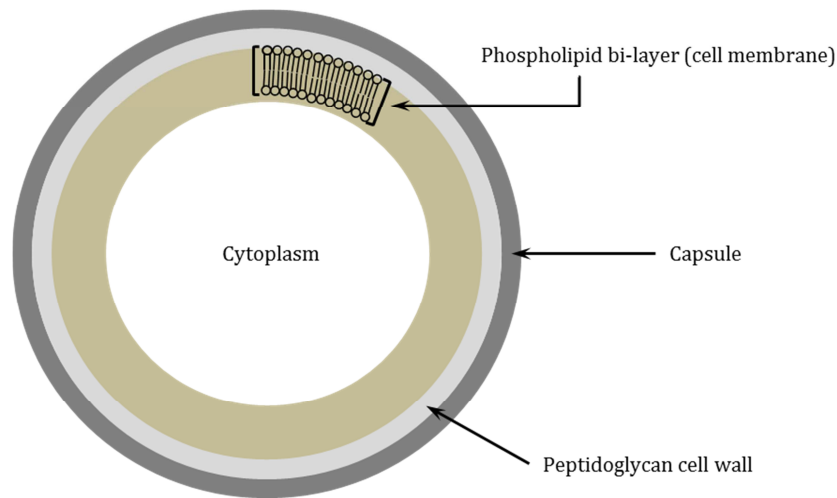


**Figure 1-1** Diagram of structure of *S. aureus* cell.

### 1.1.2.1 *S. aureus* virulence factors and biofilm formation

*S. aureus* possess a plethora of virulence factors which enable the bacteria to infect hosts successfully and increase disease severity through suppression and evasion of host immune response and increase its pathogenicity (Bien, Sokolova, & Bozko, 2011). These virulence factors include the production of adhesions, the secretion of toxins and the formation of biofilms (Bien et al., 2011).

*S. aureus* secrete cytotoxins, superantigens, proteases, lipase and coagulase. The cytolytic toxins produced by *S. aureus* cause cell leakage and lysis through the formation of  $\beta$ -barrel pores in cell membranes (Foster, 2005; Kaneko & Kamio, 2004). Each toxin targets specific mammalian cell types. For example, leukocytes are targeted by leukocidin and Panton-Valentine leukocidin (PVL) while  $\alpha$ -haemolysin (Hla) exhibits specificity towards platelets and monocytes (Kaneko & Kamio, 2004; Menestrina, Dalla Serra, &

Prévost, 2001). Superantigens, which cause nonspecific T-cell activation and massive cytokines release, include enterotoxins which cause food poisoning, toxic shock toxin-1 which causes toxic shock syndrome (TSS) and exfoliative toxin which causes degradation and exfoliation of the epidermis.

Adhesins enable *S. aureus* to adhere to surfaces within the host and initiate the formation of a biofilm. The bacteria can adhere to host plasma or extracellular matrix (ECM) components, such as collagen, fibrinogen and fibronectin using a group of covalently anchored peptidoglycan proteins collectively known as microbial surface component recognising adhesive matrix molecules (MSCRAMMs) (Foster & Höök, 1998; Maresso & Schneewind, 2008; Marraffini, DeDent, & Schneewind, 2006; Speziale et al., 2009). These proteins, which include staphylococcal protein A (SasA), collagen-binding protein, clumping factor A and B (ClfA and ClfB), and fibronectin-binding proteins A and B (FnbpA and FnbpB), mediate the initial attachment stage of biofilm formation, a key virulence factor which is essential for host colonization (Archer et al., 2011; Bien et al., 2011; Foster & Höök, 1998; Lowy, 1998; Yarwood, Bartels, Volper, & Greenberg, 2004). A second group of adhesins, collectively known as secreted expanded-repertoire adhesive molecules (SERAMs), are partially bound to the cell wall (Clarke & Foster, 2006). This group of proteins modulate the host immune system (Chavakis, Wiechmann, Preissner, & Herrmann, 2005; Hammel, Nemecek, Keightley, Thomas, & Geisbrecht, 2007). The expression of the capsule exopolysaccharides and polysaccharide intracellular adhesin (PIA) are other important *S. aureus* virulence factors. Capsule polysaccharides encase many pathogenic strains of *S. aureus* and provide protection from the host immune response by decreasing the susceptibility of the bacteria to phagocytosis (Thakker et al., 1998; B. J. Wilkinson & Holmes, 1979). PIA, composed of poly-*N*-acetyl-glucosamine, is important for staphylococcal aggregation during biofilm formation (Götz, 2002).

The ability to form biofilms is a characteristic shared by most bacteria species and is an important mechanism required for host colonization and infection (McDougald, Rice, Barraud, Steinberg, & Kjelleberg, 2011; Stewart & William Costerton, 2001) Through a highly regulated multi-step process planktonic bacteria adhere to a biotic or abiotic surface and secrete adhesions to cement themselves to the surface as well as bind themselves to other bacterial cells (Götz, 2002).

Biofilm formation undergoes several stages of development (McDougald et al., 2011; Moormeier, Bose, Horswill, & Bayles, 2014; O'Toole, Kaplan, & Kolter, 2000). The first stage of biofilm formation is attachment of the bacteria to a surface (McDougald et al., 2011). Contact with a surface causes a change in gene expression that initiates MSCRAMMs biosynthesis along with other cell surface proteins (Foster & Höök, 1998; Gabriela Bowden et al., 2002; McCrea et al., 2000; J. M. Patti, Allen, McGavin, & Hook, 1994; Peschel, Vuong, Otto, & Gotz, 2000). After initial attachment, the next stage in biofilm formation is maturation. During maturation PIA is synthesised and secreted by *S. aureus*. Bacterial cells are stuck together through the electrostatic interaction of positively charged PIA and the negatively charged teichoic acids on the cell surface (Gross, Cramton, Götz, & Peschel, 2001; Otto, 2008).

The mature biofilm is surrounded by ECM consisting of exopolysaccharides, teichoic acids, extracellular genomic DNA (eDNA), proteins and nucleic acids (Flemming & Wingender, 2010; Gross et al., 2001; Rice et al., 2007). The ECM creates a scaffold to support biofilm structure, acts as a protective barrier against external stressors, e.g. antimicrobials, as well as exhibiting digestive properties to enable large nutrients to be metabolized and distributed amongst the bacteria within the biofilm (Costerton, Lewandowski, Caldwell,

Korber, & LappinScott, 1995; Flemming & Wingender, 2010; Hall-Stoodley, Costerton, & Stoodley, 2004; Monds & O'Toole, 2009; Otto, 2008)

Once a biofilm has matured, dispersion of planktonic cells from the biofilm allows the bacteria to migrate and colonize other areas within the host (McDougald et al., 2011). Dispersal cues can be cell density dependent, or environmental, including nutrient availability (McDougald et al., 2011).

### **1.1.3 *Candida albicans***

*Candida albicans* is a dimorphic fungus which is able to morphologically transform from unicellular yeast cells into a filamentous invasive hyphae form (Sudbery, Gow, & Berman, 2004). The ability to morphologically switch is crucial for *C. albicans* ability to adhere to surfaces and for host tissue colonization during infection (Saville, Lazzell, Monteagudo, & Lopez-ribot, 2003). *C. albicans* is the most abundant fungal species of healthy human microbiota and is found in the GI tract, reproductive tract, oral cavity and skin (Achkar & Fries, 2010; Ganguly & Mitchell, 2011; Kennedy & Volz, 1985; Kumamoto, 2002, 2011). However, *C. albicans* is also one of the few fungal species that can cause disease (Nobile & Johnson, 2015). *C. albicans* is an opportunistic pathogen that can cause fungal infections when there are alterations in host microbiota (use of antibiotics), host immune response (during stress or infection by another microbe) or favourable variations in the environment (changes in nutrient content) (Nobile & Johnson, 2015).

#### **1.1.3.1 *C. albicans* biofilm formation and infection**

Infections arise when *C. albicans* adheres to a surface and forms a biofilm. The developmental stages of biofilm formation in *C. albicans* are similar to most other microorganisms, consisting of four temporal stages; attachment,

early stage growth (initiation), maturation and dispersal (Chandra et al., 2001; Douglas, 2003; Hawser & Douglas, 1994; Nobile & Mitchell, 2006; Uppuluri et al., 2010). During the attachment stage, spherical yeast cells adhere to a surface. These yeast cells then proliferate to form a basal layer of anchoring cells. The biofilm then enters a stage of maturation in which pseudohyphae (ellipsoid cells joined end to end) and hyphae (chains of cylindrical cells) are formed, alongside the production of ECM. After maturation, yeast-form cells are dispersed from the biofilm to seed new sites within the host (Chandra et al., 2001; Douglas, 2003; Hawser & Douglas, 1994; Nobile & Mitchell, 2006; Uppuluri et al., 2010).

The ability to form biofilms is an important virulence factor in *C. albicans*. Sherry et al. (2014) categorized *C. albicans* isolates as either high biofilm formers (HBF) or low biofilm formers (LBF) based on biomass quantification (Sherry et al., 2014). HBF were more resistant to antifungal treatment with amphotericin B (Amp B) and resulted in higher mortality rates in an infection model (Sherry et al., 2014). Anti-microbial resistance in *C. albicans* biofilms are due to the up-regulation of efflux pumps, the presence of recalcitrant persister cells and the presence of ECM.

The two major classes of efflux pumps; the ATP-binding cassette transporter superfamily and the major facilitator class, modulate drug exportation from cells (Anderson, 2005; Cowen, 2008; Ramage, Bachmann, Patterson, Wickes, & López-Ribot, 2002). In planktonic cells efflux pumps are upregulated in response to antifungal drugs. However in *C. albicans* efflux pumps are upregulated within the first few hours of surface contact and remain upregulated throughout biofilm development (Mateus, Crow, & Ahearn, 2004; Mukherjee, Chandra, Kuhn, & Ghannoum, 2003; J. E. Nett, Lepak, Marchillo, & Andes, 2009; Nobile et al., 2012; Ramage et al., 2002; Yeater et al., 2007). This automatic upregulation contributes to the increased antifungal

resistance of *C. albicans* biofilms. Persister cells also contribute to drug-resistance in biofilms.

Persister cells are a sub-set of metabolically dormant yeast cells that exhibit phenotypic variation within the biofilm and are extremely resistant to antimicrobial drugs (LaFleur, Kumamoto, & Lewis, 2006). Drug resistance exhibited by persister cells is the result of the metabolically dormant state of the cells, rather than being dictated by cell membrane composition and efflux pump expression (Knot, Suci, Miller, Nelson, & Tyler, 2006; LaFleur et al., 2006). Although persister cells are an important component of drug resistance in *C. albicans*, little is known about their formation and roles in *C. albicans* biofilms. ECM is another major contributor to *C. albicans* antifungal resistance.

The ECM secreted by *C. albicans* is predominantly composed of proteins and glycoproteins (55%), carbohydrates (25%), lipids (15%) and nucleic acids (5%) (Zarnowski et al., 2014). As well as acting as a physical barrier to antimicrobial drugs, ECM also contains constituents that contribute to drug resistance (Al-Fattani & Douglas, 2006; J. Nett et al., 2007; J. E. Nett, Sanchez, Cain, & Andes, 2010). For example, the addition of polysaccharides  $\beta$ -1,3-glucans to *C. albicans* planktonic cells increased tolerance of the cells to fluconazole and the addition of  $\beta$ -1,3-glucanase to *C. albicans* biofilms increased biofilm susceptibility to fluconazole treatment (Mitchell et al., 2013; J. Nett et al., 2007). Extracellular DNA may also indirectly contribute to anti-microbial resistance (Martins et al., 2010). One study reported that treating biofilms with DNase enhanced the disruption of *C. albicans* biofilms when treated with caspofungin and Amp B (Martins, Henriques, Lopez-Ribot, & Oliveira, 2012). *C. albicans* ECM contains over 500 proteins, mainly predicted to be enzymes, including hydrolysing enzymes, which can

breakdown molecules as a protective response or to access a nutrient resource (Zarnowski et al., 2014).

*C. albicans* infections can range in severity from superficial mucosal and dermal infections, such as thrush and nappy rash, to severe systemic fungal infections of tissues and organs with mortality rates of up to 40% (Calderone & Fonzi, 2001; Rex et al., 2004; Wisplinghoff et al., 2004). *C. albicans* can have serious implications for immunocompromised individuals (AIDS patients and those undergoing anticancer or immunosuppression therapies) and healthy individuals with implanted medical devices (Weig, Gross, & Muhlschlegel, 1998). Urinary and central venous catheters, pacemakers, mechanical heart valves, joint prostheses, contact lenses and dentures are all susceptible to *C. albicans* infections (Cauda, 2009; Donlan, 2002; Kojic & Darouiche, 2004; Seddiki et al., 2013). *C. albicans* infections account for 15% of all sepsis cases, are the 4<sup>th</sup> most common cause of clinically acquired bloodstream infections and are the most common fungal species isolated from medical device infections (Pfaller & Diekema, 2007; Saldanha Dominic, Shenoy, & Baliga, 2007; Wenzel, 1995; Wisplinghoff et al., 2004).

Fungal biofilms are more resistant to antifungals, therefore higher doses are required for treatment, along with removal of any infected medical device (Andes et al., 2012; Cornely et al., 2012; Lortholary et al., 2012; Mermel et al., 2009). Unfortunately, the cost and danger of device removal, along with the complications associated with high doses of antifungal drugs (e.g. kidney and liver damage), often means that treatments are not possible for critically ill patients. Multiple antifungal-resistant forms of *C. albicans* are being increasingly encountered in clinical settings (Ramage et al., 2002).

Although infections by *C. albicans* and *S. aureus* single-species biofilms are well documented, microbes are often found in complex polymicrobial communities.

#### 1.1.4 The role of *Candida-Staph* polymicrobial biofilms in disease

It is estimated that 27-56% of hospital acquired bloodstream infections are polymicrobial with *S. aureus* as the third most common microorganism isolated in conjunction with *C. albicans* (Klotz, Chasin, Powell, Gaur, & Lipke, 2007). The clinical outcomes of polymicrobial sepsis compared with monomicrobial sepsis are grave, with significantly higher mortality rates (Pulimood, Ganesan, Alangaden, & Chandrasekar, 2002). These pathogens have been co-associated with a number of polymicrobial diseases including ventilator-associated pneumonia, cystic fibrosis, superinfection of burn wounds, urinary tract infections and denture stomatitis (Dahlén, Blomquist, & Carlén, 2009; Ekwempu, Lawande, & Egler, 1981; Siegman-Igra, Schwartz, & Konforti, 1988; A. J. Smith et al., 2003; Valenza et al., 2008).

Using an *in vivo* model of systemic intraperitoneal infection, co-inoculation of *C. albicans* and *S. aureus* had a synergistic effect on mortality in mice (E. Carlson, 1982). Infection with sub-lethal doses of either species in isolation resulted in no mortality in mice. However, co-infection with both these pathogens at the same doses resulted in a mortality rate of 100%. Heat-inactivation of either *C. albicans* or *S. aureus* before co-infection reversed this effect (E. Carlson, 1982). Each species could influence gene expression *in vivo*, resulting in increased virulence and resistance to host defences as was reported *in vitro* (Peters et al., 2010a).

*C. albicans* in conjunction with other bacterial species have been isolated from several types of oral infections, including oropharyngeal candidiasis (OPC) (or thrush) and denture stomatitis. OPC affect the soft and hard palate,

buccal mucosa, the floor of the mouth and the tongue and appears as red patches or white curd-like lesions. Fluorescent *in situ* hybridisation (FISH) and 16S RNA analysis revealed the presence of bacterial species, including *Lactobacillus/Enterococcus* species and *Staphylococcus* species (Dongari-Bagtzoglou, Kashleva, Dwivedi, Diaz, & Vasilakos, 2009). Denture stomatitis is an inflammatory process of the oral mucous that leads to the formation of lesions. *S. aureus* was the most common bacteria isolated with *C. albicans* from the oral mucosa and dental prosthesis in patients with denture stomatitis (Baena-Monroy et al., 2005).

Polymicrobial biofilms are prevalent in chronic wounds, such as diabetic foot, pressure and venous leg ulcers (Bertesteanu et al., 2014). Aerobic or facultative anaerobes including *S. aureus*, coagulase-negative staphylococci, *P. aeruginosa*, *E. coli*, *Enterobacter* spp. and *Candida* spp. can cause delayed wound healing and infection in both acute and chronic wounds, especially surgical wounds (Duerden, 1994; Mangram, Horan, Pearson, Silver, & Jarvis, 1999). The presence of bacteria within wounds can induce excessive inflammatory response and tissue damage, which can lead to abscesses, cellulitis, osteomyelitis or limb loss (Bertesteanu et al., 2014).

Due to the severity of dual-infections, various studies have been carried out to investigate the relationship between *S. aureus* and *C. albicans* in dual-species biofilms.

### **1.1.5 *S. aureus* and *C. albicans* dual-species biofilms**

Dual-infections involving *C. albicans* and *S. aureus* result in increased mortality in mice (Eunice Carlson, 1983; Eunice Carlson & Johnson, 1985a, 1985b). Carlson (1983) found that the presence of *C. albicans* stimulated toxin production in different strains of *S. aureus* and increased mouse mortality and morbidity when combined with sublethal doses of *C. albicans*

(Eunice Carlson, 1983). Carlson and Johnson (1985) went on to study this disease synergism in further detail (Eunice Carlson & Johnson, 1985a). Carlson and Johnson found that *S. aureus* was always associated with *C. albicans* growth even when the two microorganisms were injected at different sites on a mouse model (Eunice Carlson & Johnson, 1985a). Furthermore, they discovered that the bacteria was always found within the fungal biofilm rather than at the peripherals and that mixed infections were only found at the fungal injection sites, which suggested fungal growth was essential for bacterial growth and that the fungus may have played a protective role in the dual-infection (Eunice Carlson & Johnson, 1985a).

*S. aureus* does not form strong biofilms in serum (Harriott & Noverr, 2009). Harriott and Noverr (2009) found that sera did not affect the initial attachment of the bacteria but was unable to support subsequent biofilm formation (Harriott & Noverr, 2009). CFU assays, along with fluorescence microscopy and antimicrobial testing revealed that *C. albicans* and *S. aureus* form a polymicrobial biofilm in serum and increase *S. aureus* resistance to antimicrobials compared to *S. aureus* monocultures (Harriott & Noverr, 2009). Although the presence of *C. albicans* increased *S. aureus* vancomycin resistance, the presence or absence of *S. aureus* had no effect on the susceptibility of *C. albicans* to Amp B (Harriott & Noverr, 2009). When *C. albicans* was killed off in the polymicrobial biofilms using very high concentrations of Amp B, *S. aureus* became susceptible to vancomycin. This trend was observed when *C. albicans* and *S. aureus* were cultured using a using a 0.4µm polyester (PET) Transwell membrane, which physically separated the microorganisms but allowed free movement of small molecules between the membrane (Harriott & Noverr, 2009). However, when *S. aureus* was cultured with *C. albicans* matrix, *S. aureus* antimicrobial resistance increased and were comparable to the results obtained when the bacteria and fungi were cultured together (Harriott & Noverr, 2009). Harriott and Noverr

concluded that *C. albicans* facilitated *S. aureus* biofilm formation in serum and that *C. albicans* ECM played a role in the increased resistance of *S. aureus* in polymicrobial biofilms, either by limiting the penetration of the drug, allowing *S. aureus* to up-regulate drug resistance genes or that the matrix material itself altered the growth and gene expression of *S. aureus* resulting in the up-regulation of anti-microbial genes (Harriott & Noverr, 2009). As well as antimicrobial resistance and biofilm formation, the use of fluorescence microscopy revealed that *S. aureus* adhered to *C. albicans* hyphae (Harriott & Noverr, 2009).

In a further study, Harriott and Noverr (2010) investigated the mechanism of *C. albicans*-induced vancomycin resistance during biofilm formation by analysing *C. albicans* mutant strains deficient in regulators of morphogenesis (Harriott & Noverr, 2010). As *S. aureus* preferentially adhered to *C. albicans* hyphae, they investigated mutants with various ECM and hyphae formation deficiencies (Harriott & Noverr, 2010). A mutant that was indistinguishable from the wild-type strain supported polymicrobial biofilm formation and vancomycin resistance (Harriott & Noverr, 2010). Other mutants with short or no hyphae and no ECM did not support *S. aureus* polymicrobial biofilm formation or vancomycin resistance. Adjusting the initial concentrations *C. albicans* mutants which formed very poor biofilms to concentrations similar to the wild-type *C. albicans* did not make a difference with regards to polymicrobial biofilm formation, so it was concluded that the lack of hyphae, and not the lack of cell number dictated phenotype (Harriott & Noverr, 2010). Interestingly, *S. aureus* cell numbers increased when it was cultured with a *C. albicans* mutant defective in adherence, but could still produce hyphae (Harriott & Noverr, 2010). Harriott and Noverr then went on to investigate the role of different adhesins, in particular the members of the ALS family of adhesions that mediate aggregation with bacteria and other yeasts (S. A. Klotz et al., 2007). However, they concluded that it may be a unique combination of

these adhesions, rather than a single adhesion that is required for adherence (Harriott & Noverr, 2010). Overall, it was concluded that surface-associated adhesions and the ECM facilitate *S. aureus* polymicrobial biofilm formation and subsequent vancomycin resistance, although nonspecific interactions could also play a role in polymicrobial biofilm formation (Harriott & Noverr, 2010).

Peters et al. (2010) elucidated the nature and spatial relationship of the interactions between *C. albicans* and *S. aureus* using confocal scanning laser microscopy (CLSM), characterised proteomic changes and identified differentially regulated metabolic, stress and virulence proteins during polymicrobial biofilm growth (Peters et al., 2010a). Similar to Harriott and Noverr (2009), the imaging analysis revealed that *S. aureus* adhered to *C. albicans* hyphae and not the round yeast cells (Harriott & Noverr, 2009; Peters et al., 2010a). Preference for binding to the hyphae of *C. albicans* has been reported in a number of other species including *Streptococcus pyogenes*, *Acinetobacter baumannii* and *P. aeruginosa* (Bamford et al., 2009; Cunningham, 2000; D. A. Hogan & Kolter, 2002; A. Y. Peleg et al., 2008). However, many of these interactions result in fungal and/or bacterial killing during co-culture. Unlike Harriott and Noverr, Peters found that the bacteria were dispersed throughout the entire biofilm, whereas Harriott found that the bacteria adhered to *C. albicans* hyphae in the uppermost region of the biofilm. Peters cultured the biofilms on glass coverslips using RPMI-FBS media, whereas Harriott cultured biofilms on permanox chamber slides using 50% FBS in water, which could be responsible for the differences observed by Peters et al. (Harriott & Noverr, 2009; Peters et al., 2010a). The *C. albicans* – *S. aureus* interaction was found to be non-lethal through a LIVE/DEAD cell viability assay. Through proteomic analysis it was observed that candidal germination may induce *S. aureus* virulence and biofilm formation through the downregulation of CodY expression which is a transcriptional repressor of

a variety of *S. aureus* virulence factors (Levdikov, Blagova, Joseph, Sonenshein, & Wilkinson, 2006). Interestingly, several stress-related proteins were upregulated in *S. aureus* when it was cultured with *C. albicans*. Similarly, stress response proteins were upregulated in *C. albicans* when it was cultured with *S. aureus*, suggesting the presence of one of the microorganisms elicits a stress response in the other microorganism (Peters et al., 2010a).

In another study, Peters et al. (2012) investigated the role that Als3 played in mediating the adherence of *S. aureus* to *C. albicans* hyphae (Peters, Ovchinnikova, et al., 2012). Peters compared various adherence mutants as well as a strain lacking the hyphal cell wall protein Hwp1 and determined the level of staphylococcal binding to *C. albicans* hyphae using scanning electron microscopy, confocal microscopy, adherence ELISA and atomic force microscopy (AFM). The findings suggested that strains lacking Als3 displayed reduced ability to adhere to *S. aureus*. However, some adhesin mutants showed increased *S. aureus* binding when compared to the parental strain (Peters, Ovchinnikova, et al., 2012). The authors suggest that this could be the result of increased expression of other known adhesins or through the exposure of other adhesive moieties on the surface of *C. albicans* resulting in increased *S. aureus* adherence. Other molecules or biofilm matrix components could also play a role or could be due to non-specific attachment (Peters, Ovchinnikova, et al., 2012). Strains expressing Als3 exhibited stronger binding forces to *S. aureus*. Significantly, Peters observed *S. aureus* cells beneath epithelial barriers of co-infected mouse tongues. These findings suggest a mechanism of infection by which *C. albicans* hyphae penetrate host tissue enabling *S. aureus* to breach the biological barriers and initiate infection (Peters, Ovchinnikova, et al., 2012).

Dual-species infections are notoriously difficult to treat due to increased antimicrobial resistance and disease severity. Although an effort has been made to unravel the relationship between *S. aureus* and *C. albicans*, metabolomics offers a powerful analytical tool to gain a better understanding of the interactions between this bacteria and fungus.

## 1.2 Metabolomics

Metabolites are small organic molecules that are chemically changed during metabolic reactions. They are necessary for the correct growth, maintenance and function of cells (Dettmer, Aronov, & Hammock, 2007; Haggarty & Burgess, 2017). Although metabolic analysis had been carried out previously, Oliver et al. were the first to describe the full complement of small molecules synthesised by an organism as the metabolome (Oliver, Winson, Kell, & Baganz, 1998). The metabolome can be defined on all levels of complexity such as organisms, tissues, cells or cell complements (Fiehn, 2002). Conceptually, metabolomics is the study of metabolic reactions through the identification and quantitation of all the metabolites, the metabolome, within a biological system (Blow, 2008; Fiehn, 2002). Metabolomics is at the end of the ‘omics’ cascade (Fig. 1-2) and, unlike genes and proteins, the functions of which are subject to epigenetic regulation and post-translational modifications, respectively, metabolites are changed as a direct result of biochemical activity (Dettmer et al., 2007; G. J. Patti, Yanes, & Siuzdak, 2012a). As metabolites are the direct products of biochemical reactions their concentrations can provide a quantitative, rather than qualitative, description of cellular regulation and control. The direct correlation of metabolite concentrations to metabolic activity provides an insight into the phenotype and changes in phenotype as a result of cellular response to genetic or environmental stimuli (Dettmer et al., 2007; Fiehn, 2002; Haggarty & Burgess, 2017; G. J. Patti et al., 2012a). The ability to utilize metabolomics

to quantitatively describe the cellular state of a biological system has led to its recognition as an important tool in cell and systems biology (Johnson & Gonzalez, 2012; G. J. Patti, Yanes, & Siuzdak, 2012b).



**Figure 1-2** The ‘omics’ cascade and their related molecules.

In order to gain an insight into the biology and physiology of a biological system using metabolomics, it is essential to detect and quantify as many of the metabolites as possible within that system (García-Cañaveras, López, Castell, Donato, & Lahoz, 2016). The number of metabolites varies dramatically between different biological systems, e.g. an estimated 2000 are present in mammals compared to 200 000 in the plant kingdom (Saito & Matsuda, 2010; Weckwerth, 2003). The mass of metabolites can range from 50 – 2500 Daltons (Da) with low picomolar concentrations to molar concentrations (Forcisi et al., 2013; Wang, Liu, Hu, Li, & Wan, 2015). As well as number, mass and abundance, stereochemistry leads to different biological functions. Metabolites can also vary in polarity, pKa, solubility and charge (J. Chen et al., 2008; Forcisi et al., 2013; Saito & Matsuda, 2010; Wang et al., 2015; Weckwerth, 2003). García-Cañaveras et al. described the metabolomics concept as ‘the unbiased determination of all the metabolites present in a sample independently of their chemical structure’ (García-Cañaveras et al., 2016). Global (or untargeted) metabolomics aims to provide an unbiased insight into the metabolome through the detection and quantitation of as many metabolites as possible within a given biological sample.

Unlike global (untargeted) metabolomics, the ambitious goal of which is to detect and quantify all of the small molecules within a biological sample, targeted metabolomics has the comparatively more modest goal of detecting and quantifying a pre-defined group of chemically characterised compounds from known biochemical pathways (Lu, Bennett, & Rabinowitz, 2008; Nielsen & Oliver, 2005; Roberts, Souza, Gerszten, & Clish, 2012). A typical targeted metabolomics experiment generally aims to analyse dozens to hundreds of metabolites in a quantitative or semi-quantitative manner with the use of internal standards (Lu et al., 2008; Roberts et al., 2012).

Targeting a particular pathway, specific part of metabolism or a group of metabolites can provide a powerful tool for systems biology and biotechnology (Cakir et al., 2006; Fiehn, 2002; Kümmel, Panke, & Heinemann, 2006; Nielsen & Oliver, 2005; Stitt & Fernie, 2003). Measurement of specific classes of metabolites or selected key metabolites can aid in the elucidation of metabolic networks, which opens the door for many types of data analysis such as identification of reporter reactions, network-embedded thermodynamic analysis, kinetic modelling and novel associations between analytes to be identified (Cakir et al., 2006; Kümmel et al., 2006; Roberts et al., 2012).

Through targeting a specific metabolite or a specific group of metabolites, all other supplementary compounds can be ignored (Fiehn, 2002). As the compounds to be analysed are known, and have been chemically defined, sample preparation methods for their extraction and purification can be optimized and the analytical platform used can be tuned for their separation and detection (Fiehn, 2002; Roberts et al., 2012).

Due to the number and complexity of metabolites in existence sophisticated instrumentation is required for their detection, quantitation and identification.

## 1.3 Analytical methods

### 1.3.1 Mass spectrometry

Metabolites exhibit wide ranging chemical diversity and concentrations. This diversity leads to a need for sensitive instrumentation for their detection and identification. The two most popular platforms that researchers rely on for metabolomics analyses are nuclear magnetic resonance (NMR) and mass spectrometry (MS).

Mass spectrometry is a technology in which analyte ions are separated and detected based on their mass-to-charge ( $m/z$ ) ratios. The  $m/z$  ratio is then used to calculate the compounds molar mass, which in turn is used for identification. Although there are a large number of different mass spectrometers available, the basic components of a MS are the same (Fig. 1-3).

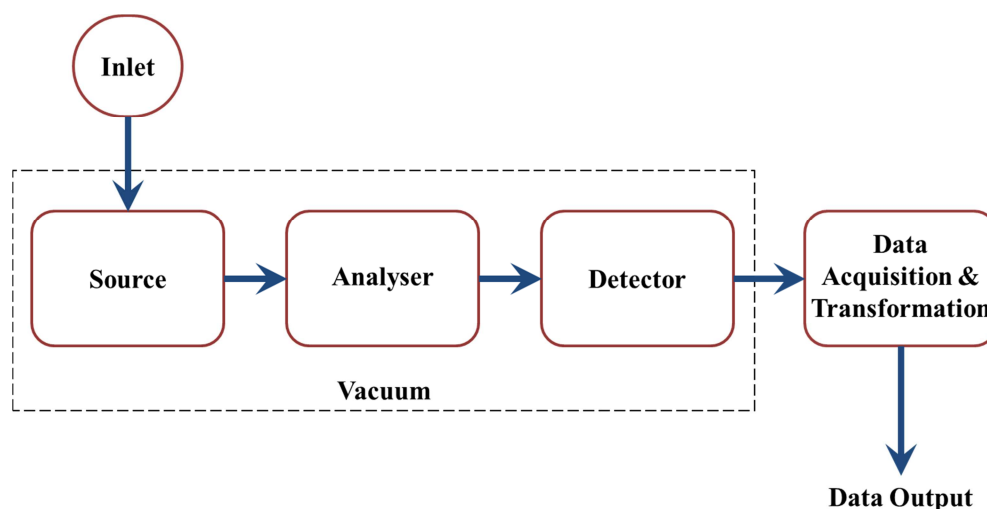


**Figure 1-3** Schematic diagram of the major components of a mass spectrometer.

A sample is introduced to the MS source at the inlet. The compounds within the sample are ionised to produce charged molecules in the gaseous phase.

Ion optics, operated under a vacuum, focus and accelerate ions through the MS to the mass analyser. As the ions move through the MS they can be excluded or included in the final analysis based on their  $m/z$  values using quadrupoles. A variety of detection systems are used to detect resolved ions. A computer is used for instrument control and data acquisition. Instrument software automatically generates the  $m/z$  ratios for all of the detected ions which are displayed as mass spectra, an example of which can be seen in Fig. 1-4.

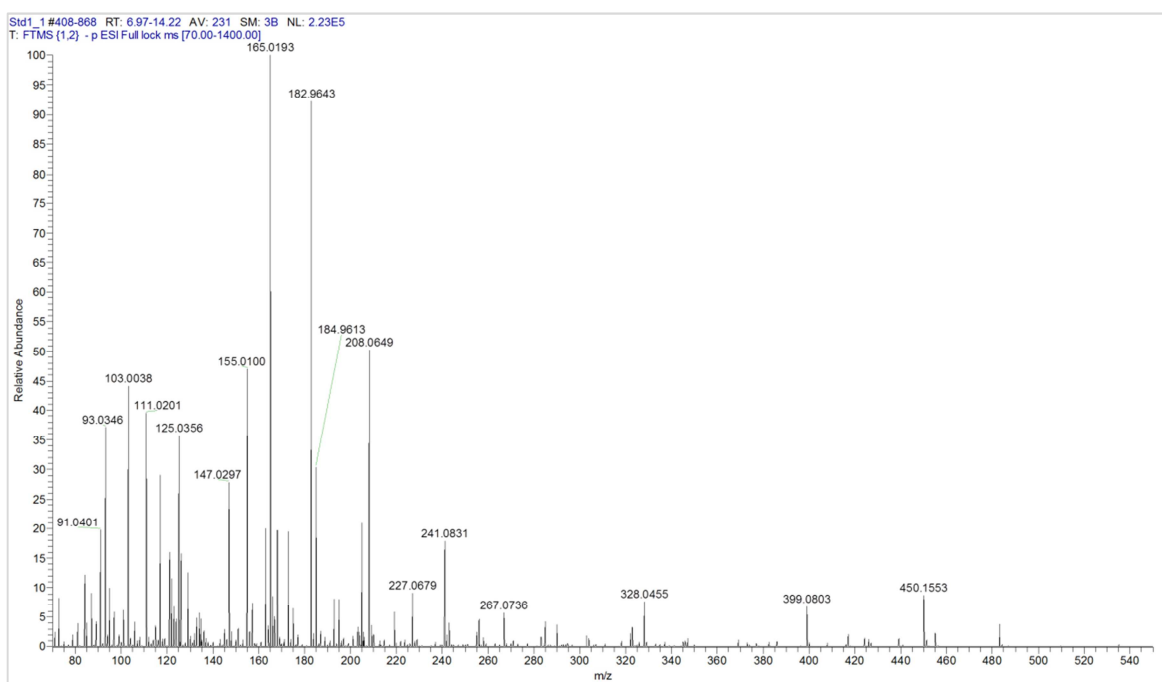


**Figure 1-4** An example of a mass spectrum. Detection: ESI-FTMS, negative mode.

As the MS detects ions in the gas phase, ionisation of the compounds within a sample is the first stage of MS analysis.

### 1.3.1.1 Electrospray Ionisation (ESI)

There are numerous techniques available for the production of analyte ions, and the method adopted is dependent on the type of analysis a researcher

wishes to carry out. For example, to determine the spatial distribution of metabolites within a sample, matrix assisted laser desorption ionisation (MALDI) (Karas, Bachmann, & Hillenkamp, 1985; Tanaka et al., 1988) or desorption electrospray ionisation (DESI) (Takats, 2004) could be used.

Unlike MALDI and DESI, in which metabolites are ionised from the surface of a sample, electrospray ionisation (ESI) is predominantly used to ionize analytes that are in the liquid phase. Developed by Dole et. al (1968), ESI is a soft ionisation technique carried out at atmospheric pressure that produces mainly intact molecular ions (Dole, Mack, & Hines, 1968; L. . Mack, Kralik, Rheude, & Dole, 1970). It is compatible with continual flow systems and therefore is often utilized at the LC-MS interface to enable the transport of analytes in solution into the MS, through desolvation of charged analyte species. Fig. 1-5 depicts a simplified diagram of the ESI process, which can be divided into three stages; droplet formation, droplet shrinkage and gaseous ion formation (Gaskell, 1997; Kebarle & Tang, 1993).

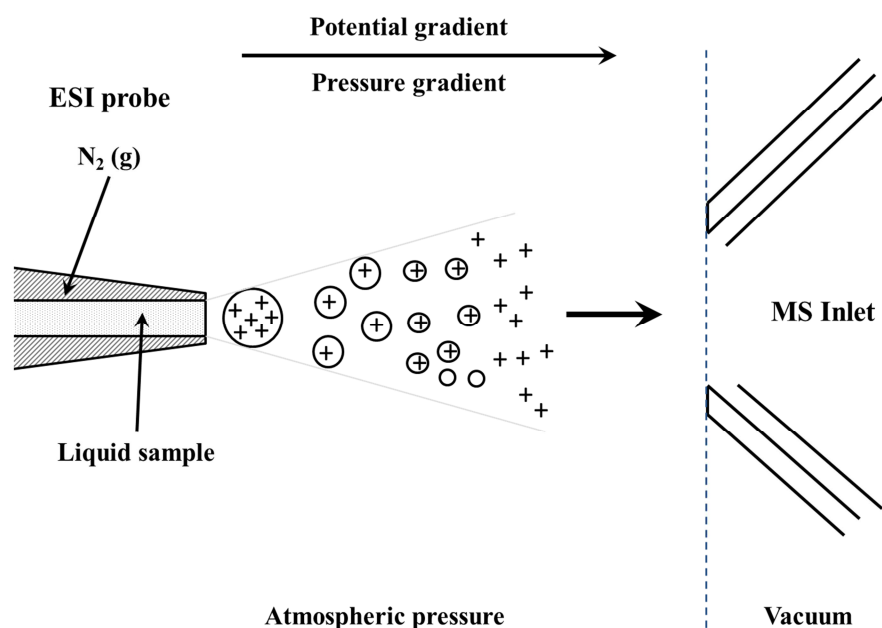


**Figure 1-5** Schematic of electrospray ionisation (ESI), operating in positive mode.

ESI can operate in both positive and negative modes, producing protonated and deprotonated ions, respectively. The simplest ES ion source configuration is a two electrode system. A solution is flowed through a metal capillary, which is held at a potential. The counter electrode is the inlet capillary and the lens elements and detector of the MS. A high potential difference ( $\sim\pm 3\text{-}6\text{kV}$ ) is maintained between the ESI probe and the MS (Van Berkel & Kertesz, 2007). Positively charged analyte ions are primarily produced when the analyte molecules interact with charged species present in the solution, which include  $\text{H}^+$ ,  $\text{Na}^+$  and  $\text{K}^+$ , to produce  $[\text{M}+n\text{H}]^{n+}$ ,  $[\text{M}+n\text{Na}]^{n+}$  or  $[\text{M}+n\text{K}]^{n+}$ , respectively. In negative mode, the deprotonated molecular ion is commonly observed at  $[\text{M}-n\text{H}]^{n-}$ , although adducts may also still be observed such as  $[\text{M}+\text{Cl}]^-$  or  $[\text{M}+\text{HCOO}]^-$  (Van Berkel & Kertesz, 2007; Yamashita & Fenn, 1984). As ions accumulate at the surface of the liquid, the liquid is drawn down a filament and forms a ‘Taylor cone’ (Taylor, 1964). When the electrostatic force applied to the capillary exceeds the surface tension of the liquid, droplets break away from the main body of the liquid and travel along the pressure and potential gradient towards the MS inlet with the spray emission aided by coaxial nitrogen gas. A number of parameters influence the diameter of the droplets produced including the applied potential, the solvent properties and the flow rate (Wilm & Mann, 1994).

As a droplet travels along the pressure gradient towards the MS inlet solvent evaporation occurs, causing a reduction in droplet size. When the magnitude of the charge is great enough to overcome the surface tension holding the droplet together, the ‘Rayleigh limit’, the droplet will break apart, ‘Coulomb explosion’. The droplet continues to deplete in size through evaporation and fission, respectively, to form droplets that contain a single ion. The non-solvated ions result from further evaporation of solvent. This mechanism for the production of ions is known as the charged residue model (CRM) (Fig. 1-6A). A second mechanism for the production of gas-phase ions is the ion

evaporation model (IEM) (Fig. 1-6B), in which a charged ion is expelled from a small highly charged droplet. The solvated ion experiences two opposing forces as it tries to leave the droplet. The solvent within the droplet creates a charge that pulls the ion back into the droplet, while at the same time the repulsive forces by excess droplet charge pushes the ion away from the droplet (Konermann, Ahadi, Rodriguez, & Vahidi, 2013). The ion is initially attached to the droplet via a solvent bridge, which eventually ruptures when the ion is released (Ahadi & Konermann, 2011) (Fig. 1-6B).

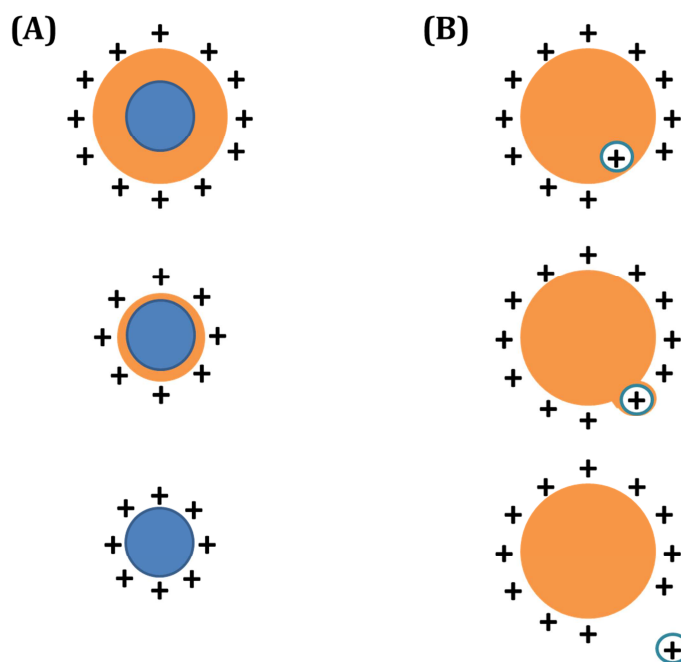


**Figure 1-6** The production of gas-phase charged species through the (A) charged residue (CRM) and (B) ion evaporation (IEM) models (Van Berkel & Kertesz, 2007).

The newly produced desolvated ions then travel to the inlet of the MS where they can be detected. There are a large number of mass analysers commercially available today; therefore the instrumentation discussed in this chapter will focus on the mass spectrometers that have been utilized in this

research; a quadrupole mass analyser (along with hexapoles and octapoles which are used for the transfer of ions through the MS) and an Orbitrap mass analyser, which was used for analyte detection and quantitation.

### 1.3.1.2 Mass analysers

#### 1.3.1.2.1 Quadrupole mass analysers

Quadrupole mass analysers are composed of a square array of four circular rods, which are perfectly parallel (Holzscheiter, 1995; Paul & Raether, 1955). The rods are grouped into two pairs of opposing rods with the same polarity applied to each of the rods within that pair (Fig. 1-7). Direct current (DC) and radio frequency (RF) voltages are applied to the rods to produce a quadrupolar field (Mallet & Down, 2009). The total electric field is made up of the generated quadrupolar field superimposed on a constant field resulting from the potentials applied to the rods (de Hoffmann & Stroobant, 2002). The positively or negatively charged ions entering the quadrupole travel along the z-axis and are attracted to the negatively or positively charged rods, respectively.

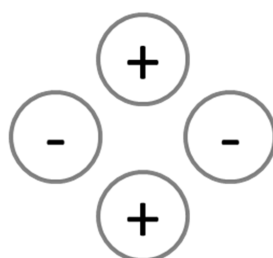


**Figure 1-7** Quadrupole parallel cylindrical rods with opposing charges.

Ions travelling along the z-axis in the space between the rods will maintain their velocity, but are subjected to accelerations along the x- and y-axes as a result of the forces induced by the electric field. As long as the ion does not

hit one of the rods its trajectory will remain stable and the ion will be detected (de Hoffmann & Stroobant, 2002). The x-direction is a high-pass mass filter; only ions with high masses will be transmitted to the end of the quadrupole as ions with low  $m/z$  gain energy from the RF field and oscillate with increasing amplitude until they encounter one of the x-electrodes. Conversely, the y-direction acts as low-pass mass filter. In the y-direction, as a result of the defocusing effect of the DC component, heavy ions become unstable. However, the trajectories of some lower mass ions can be corrected (when their amplitude increases) by the RF component which stops these ions from colliding with the y-electrodes.

Within the quadrupole there are regions along the x- and y-axes that are stable and the ions travelling within these regions will have a stable trajectory. Mathieu equations are used to determine where ions will be stable in the x- and y-axes (Equation 1 & 2):

$$a_u = \frac{8zeU}{m\omega^2r_0^2} \quad (1)$$

$$q_u = \frac{4zeV}{m\omega^2r_0^2} \quad (2)$$

Where:  $a_u/q_u$  = related to the x- & y-coordinate of the ion travelling through the quadrupole,  $z$  = no. of charges on the ion,  $e$  = charge of electron,  $U$  = DC voltage applied to the rods,  $V$  = amplitude of the RF voltage,  $M$  = the mass of the ion,  $\omega$  = the angular frequency constant,  $r_0$  = radius of the quadrupole.

To determine where ions will be stable in both the x- and y-axes simultaneously, individual stability diagrams of each axis are overlaid to determine the stability areas within the quadrupole. A specific area is commonly used in MS, area A (Fig. 1-8).

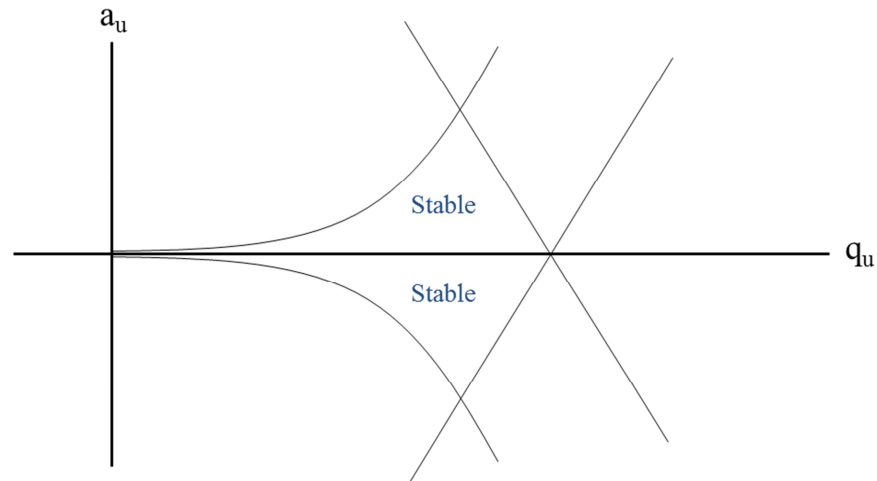


**Figure 1-8** Stability diagram produced from the Mathieu equation.  $u$  can be either  $x$  or  $y$ . The direct potential part is shown for positive  $U$  and negative  $U$ .

Ions with different  $m/z$  ratios require different voltages to keep them in the stable region. The direct potential ( $U$ ) applied to the rods and the RF voltage ( $V$ ) are two variables that are altered to manipulate the position of ions within the quadrupole. An ion in an unstable region will be ejected from the analyser; hence by altering the  $U/V$  (RF/DC) ratio individual  $m/z$  can be transmitted to the end of the quadrupole to the exclusion of all others.

Scanning along a  $U/V$  ratio constant allows successive detection of different masses (as long as the line goes through the stability area of that ions mass (Fig. 1-9)). The higher the  $U/V$  ratio is within the stable area of a specific ion the greater the resolution. This allows the quadrupole to focus, store or eject ions based on their  $m/z$  ratios.

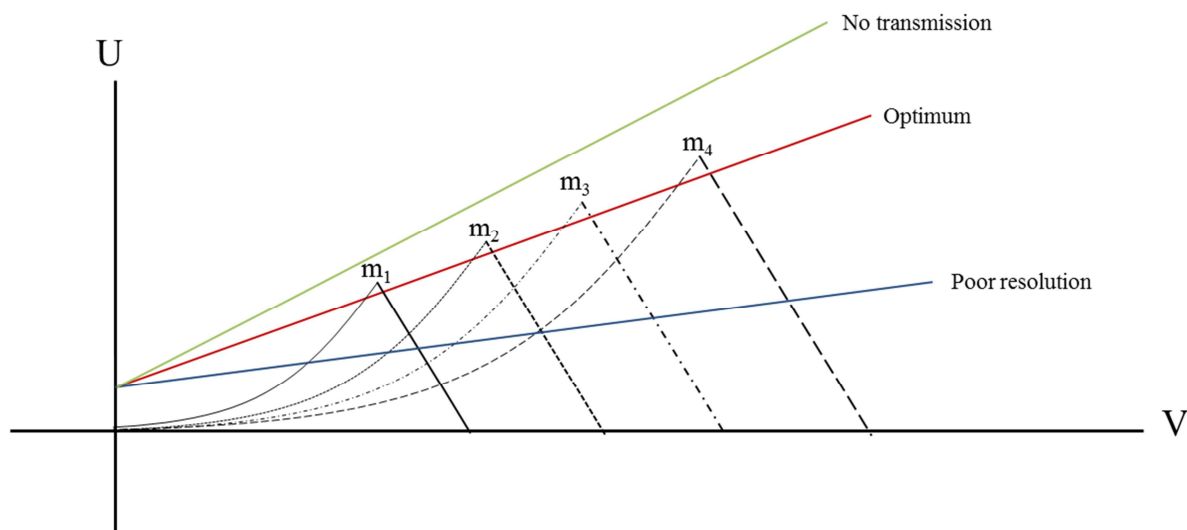


**Figure 1-9** Stability areas for three ions with different masses ( $m_1 < m_2 < m_3 < m_4$ ). The red line represents the U/V ratio.

Quadrupole mass analysers include Q-time of flight (TOF), triple quads and bench-top single quads. However, due to their relatively low resolution capabilities, quadrupoles are not often used as the sole mass analyser within an MS, instead they are often utilized for ion focusing and selection before fragmentation and/or detection. Figure 1-10 illustrates the position of a quadrupole mass analyser within an Orbitrap Fusion<sup>TM</sup>.

*Figure has been removed due to Copyright restrictions.*

**Figure 1-10** Position of the quadrupole mass analyser within an Orbitrap Fusion<sup>TM</sup> (Image taken from <https://www.planetorbitrap.com>. Accessed on 12<sup>th</sup> June 2017).

### 1.3.1.2.2 The Orbitrap

Invented in 1999, the Orbitrap is a Fourier transform mass analyser that has been commercially available since 2005 (Hu et al., 2005; a Makarov, 2000). This orbital trapping mass analyser utilizes a spindle-shaped central electrode surrounded by two symmetrical outer electrodes that precisely complement the shape of the inner electrode ( a Makarov, 2000).

The outer electrodes are electrically separated from one another and are used to establish an ion trapping field and also act as receiver plates for image current detection (Hu et al., 2005; a Makarov, 2000). Ions that successfully enter the orbital trap oscillate around the centre electrode and the image current from these oscillating ions are detected by the receiver plates as a time-domain signal. The signal detected from coherent ions is then used to generate a mass spectrum through fast Fourier transforms.

Although there is a wide range of MS instruments that implement the Orbitrap mass analyser, with various layouts and levels of complexities (Fig. 1-11), there remains a common feature amongst all of them. The mass analyser is always preceded by a gas-filled curved quadrupole, known as a C-trap, that traps ions before injection into the mass analyser (Hu et al., 2005; A. Makarov & Scigelova, 2010; a Makarov, 2000).

*Figure has been removed due to Copyright restrictions.*

**Figure 1-11** Schematics illustration the diversity of the Orbitrap range. The (A) Fusion; (B) QExative Plus and (C) LTQ Orbitrap XL differ in layout and complexities, but all the instruments comprise of a C-trap and Orbitrap mass analyser (Image taken from <https://www.planetorbitrap.com>. Accessed on 12th June 2017).

In the C-trap, ions enter RF-only bent quadrupole and get stored there during which time they lose energy ( a Makarov, 2000). The RF voltage is then ramped down and a high-voltage pulse is applied across the trap, ejecting ions orthogonally to its curved axis. As the original thread of ions disperses into short packets of different  $m/z$ , dedicated bent ion optics focuses these packets onto the aperture of the analyser.

Ion packets enter the Orbitrap analyser at an offset from its equator and experience strong radial and axial fields. The axial components of the field forces axial acceleration, and hence, so-called excitation by injection, while the radial component sets ions on a circular orbit around the central electrode. As the voltage on this electrode increases during the injection process, the radius of the ion packet rotation gets squeezed down.

Because of the strong dependence of the rotational frequencies on the ion energies, angles and initial positions, each ion packet soon spreads over the angular coordinate and forms a thin rotating ring. After voltages are stabilized the differential amplifier detects a current induced by these rings on the split outer electrodes of the trap.

Due to the complexity of the metabolome and sheer number of metabolites in existence many have the same mass, but have different chemical compositions or different chemical structures. To allow these metabolites to be detected and identified, a separation step based on the metabolites differing chemical properties is required before detection. Liquid (LC) or gas (GC) chromatography are often the analytical platforms of choice for analyte separation before MS detection.

### 1.3.2 Chromatography

In chromatography, analytes within a mixture are pushed through a column using a mobile phase (MP) and separated based on their affinity (or attraction) for the packing material, i.e. the stationary phase (SP) within the column. In gas chromatography (GC) metabolites and a carrier gas are transported through a column which is gradually heated using a temperature controlled oven. The metabolites interact with the stationary phase within the column and are separated due to their volatilities (Mozzi, Ortiz, Bleckwedel, De Vuyst, & Pescuma, 2013). Within LC systems analyte molecules are eluted through a column in a liquid MP using a pump (Pal & Sharma, 2010). The column is filled with a chemically specific SP (Pal & Sharma, 2010). The SP can be composed of various types of material depending on the LC technique used. As analytes elute through the column they interact with the SP. It is the interactions between the analyte molecules, the SP and the MP that determines how long each analyte is retained on the column (Xiang, Liu, & Lee, 2006). The detected analytes are plotted onto a chromatogram (Fig. 1-12).

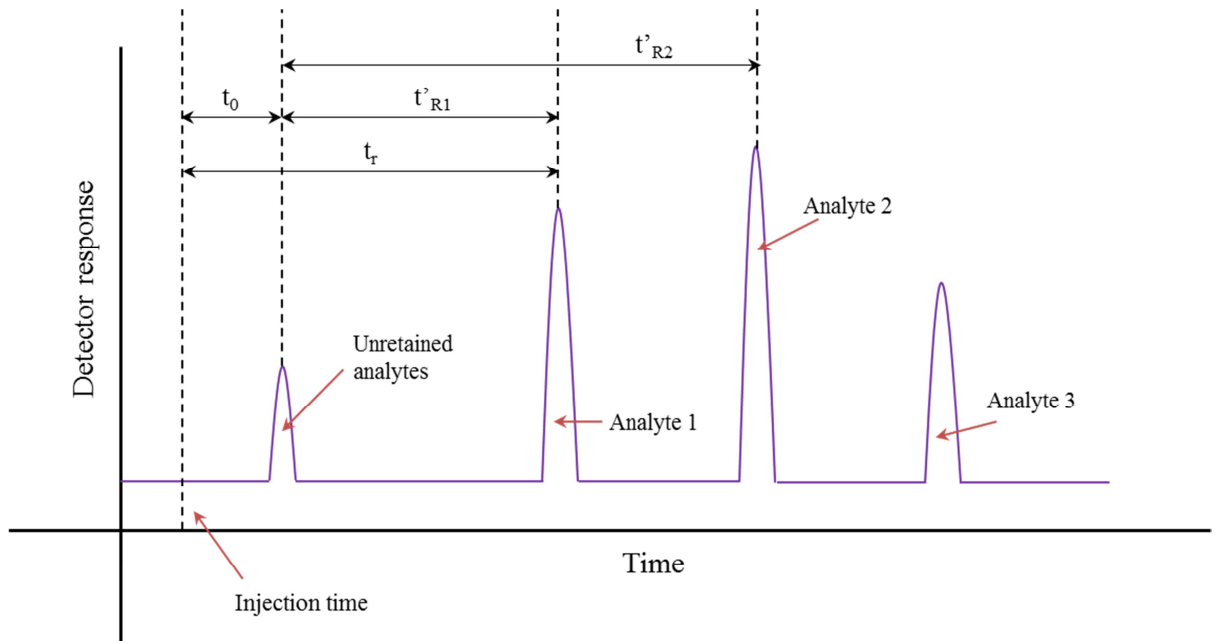


**Figure 1-12** Simple diagram of chromatogram.

From the example chromatogram (Fig. 1-11), the retention time (RT) for each analyte,  $t_r$ , is the time it takes for the analyte to reach the detector after it has been injected onto the column. The dead time,  $t_0$ , is the time it takes for unretained analytes and MP to reach the detector. The RT of each analyte can be taken as the time from injection of the sample,  $t_{R1}$ , or as an adjusted RT from the elution of the dead volume,  $t'_{R1}$ , which can be calculated using Equation 3.

$$t'_{R1} = t_{R1} - t_0 \quad (3)$$

The retention volume,  $V_R$ , is the volume of MP required to elute a specific analyte from a column and can be calculated using Equation 4.

$$V_R = t_R \times F \quad (4)$$

Where  $F$  = to the MP flow rate.

Analytes moving through a column spread into a Gaussian peak, with a standard deviation of  $\sigma$  (Fig. 1-13). The breadth of peaks can be measured at half the height of the peak ( $w_{1/2}$ ) or at the baseline, between two tangents drawn from the inflection points at either side of the peak, i.e. the steepest part of the peak.

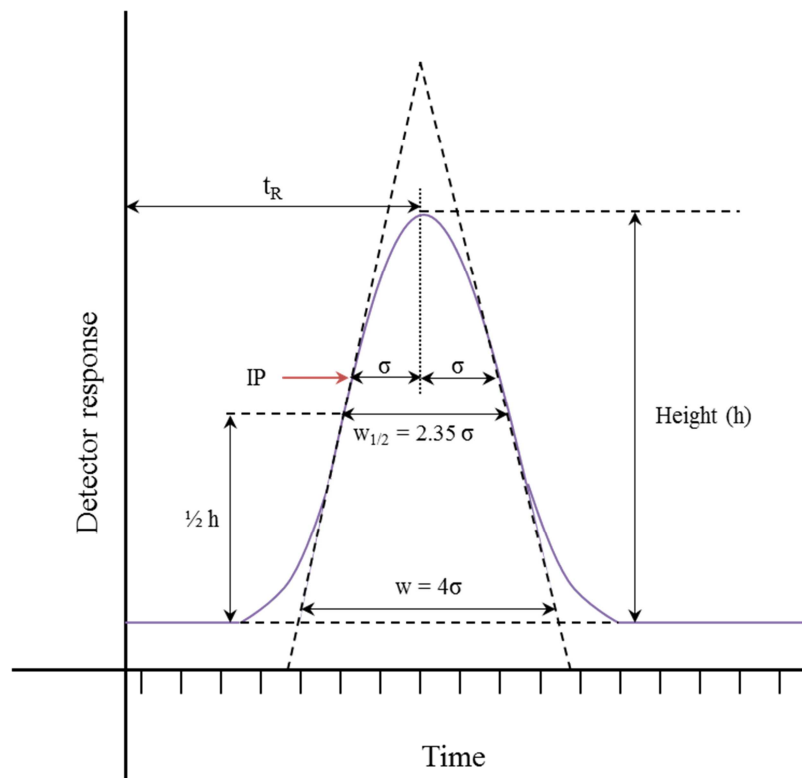


**Figure 1-13** Diagram of Gaussian peak.

Resolution ( $R_s$ ), i.e. the ability of a chromatographic method to separate analyte peaks, is the most important function of an HPLC system. Resolution can be calculated from the ratio of the difference in retention of the two analyte peaks over the average width of the two peaks (Fig. 1-14 & Equation 5).

$$R_s = \frac{(t_{R2} - t_{R1})}{(w_{b1} + w_{b2})/2} \quad \text{or} \quad R_s = \frac{2(t_{R2} - t_{R1})}{w_{b1} + w_{b2}} \quad \text{or} \quad R_s = \frac{\Delta t_R}{w_{av}} \quad (5)$$

Where  $t_{R1}$  &  $t_{R2}$  = the RT of the apices of the peaks,  $w_{b1}$  and  $w_{b2}$  = the full width at base of the peaks,  $\Delta t_R$  = the difference in RT of  $t_{R2}$  &  $t_{R1}$  and  $w_{av}$  = the average of the widths at the base of the analyte peaks.

Most publications utilise full width at half maximum (FWHM) to calculate resolution. In a peak with a Gaussian distribution the peak width ( $W$ ) =  $4\sigma$  and FWHM ( $W_{1/2}$ ) =  $2.354\sigma$  (Fig. 1.13). When these are substituted into Equation 5, resolution can be calculated using Equation 6.

$$R_s = 1.18 \frac{(t_{R2} - t_{R1})}{(w_{1/2b1} + w_{1/2b2})} \quad (6)$$

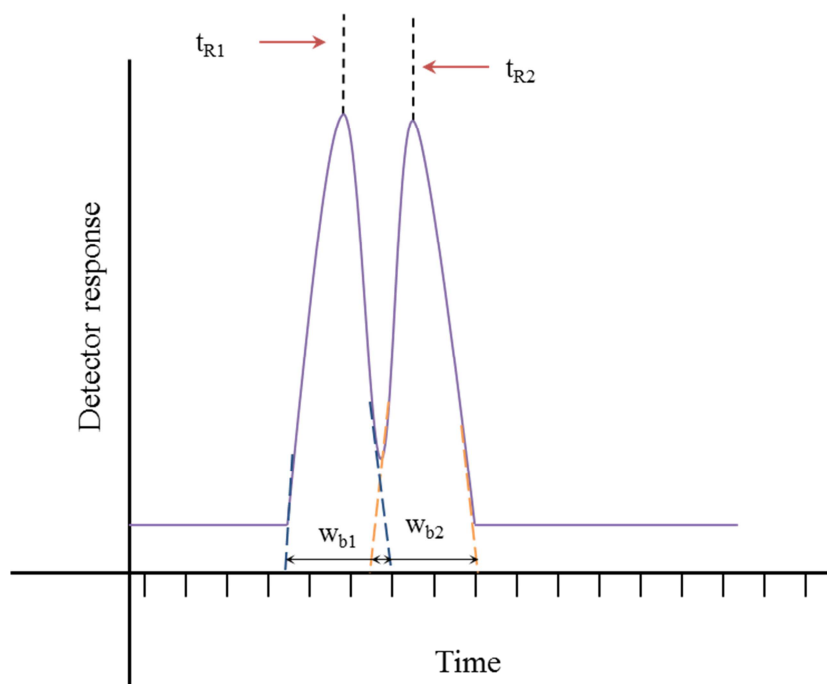


**Figure 1-14** A simple diagram of two peaks which are not baseline resolved.  $t_{R1}$  &  $t_{R2}$  = the RT of the apices of the peaks and  $w_{b1}$  and  $w_{b2}$  = the full width at base of the peaks.

Resolution can be effected by the retention factor (or capacity), the selectivity (or separation factor) and the efficiency of a chromatographic system (Fig. 1-

15). Figure 1-16 describes the relationship between selectivity and efficiency in a chromatographic system. The relationship of efficiency, selectivity, capacity to resolution can be expressed as the Fundamental Resolution Equation (Equation 7).

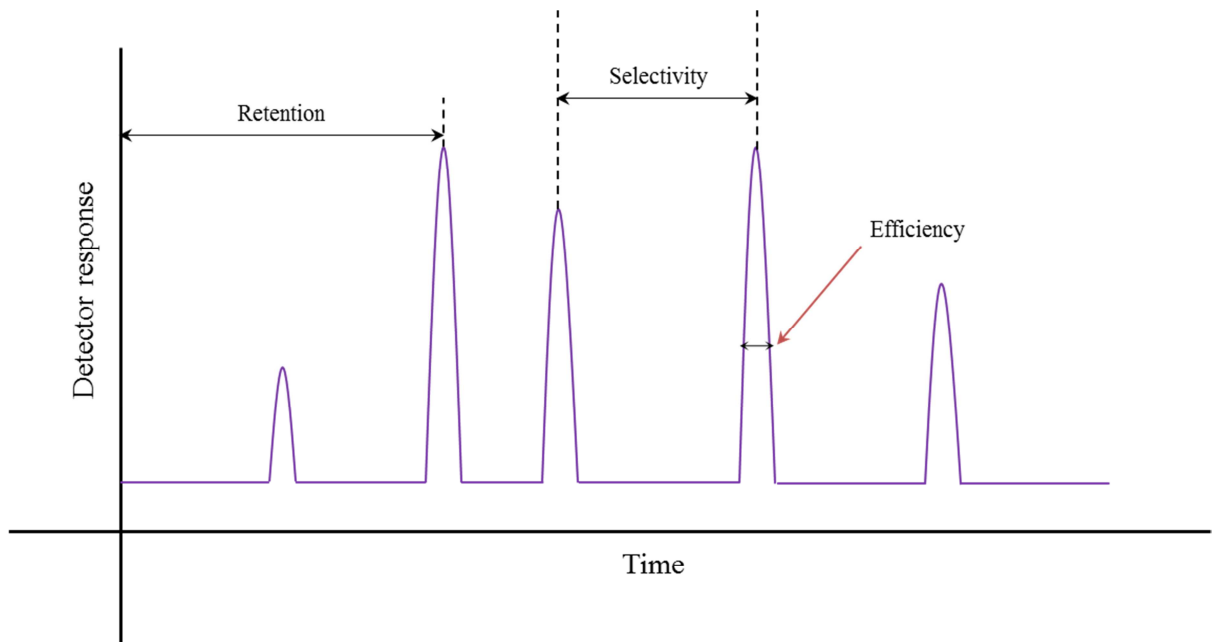


**Figure 1-15** Diagram illustration the factors that affect resolution in chromatography; retention, selectivity and efficiency. Retention is a measure of how well the SP attracts an analyte. The stronger the interaction between the SP and the analyte, the longer the analyte is retained. Selectivity describes how well the system distinguishes between analytes. Efficiency is a measurement of how well the system can elute analytes off the SP. An efficient chromatographic system will produce narrow peaks.

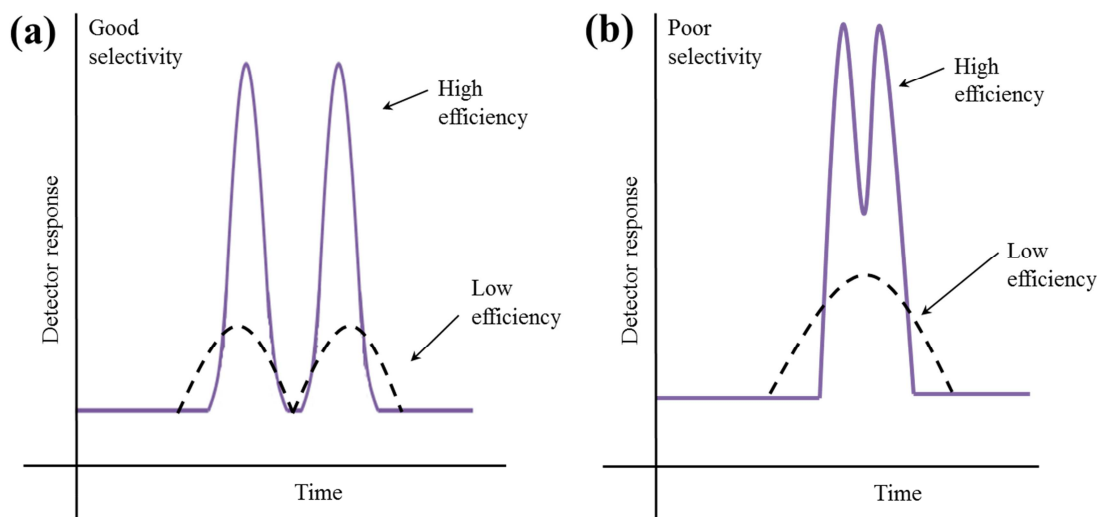


**Figure 1-16** Diagram illustration the relationship between selectivity and efficiency. (A) A chromatographic system that displays good selectivity and high efficiency will produce narrow well separated peaks. A system that displays good selectivity, but low efficiency, will produce broad peaks that are separated. (B) A chromatographic system that has bad selectivity, but good efficiency will produce narrow peaks that are not resolved. A system that displays bad selectivity and low efficiency will often produce one broad peak over the RT where two peaks should be detected.

$$R_s = \underbrace{\frac{1}{4} \sqrt{N}}_{\text{Efficiency}} \times \underbrace{\frac{\alpha-1}{\alpha}}_{\text{Selectivity}} \times \underbrace{\frac{k}{1+k}}_{\text{Capacity}} \quad (7)$$

The retention factor (or capacity),  $k$ , is a measurement of an analytes retention on the column (Fig. 1-14). Equation 8 summarises how the retention factor is calculated.  $k$  is equal to the RT of the analyte on the column to the RT of the unretained compounds.

$$k = \frac{(t_R - t_0)}{t_0} = \frac{t'_R}{t_0} \quad (8)$$

$k$  can be altered by altering the solvent strength of the MP. This is a relatively simple way to increase or decrease the level of interaction between the analytes and the SP, which in turn can increase or decrease  $k$ .  $k$  ignores

variables such as flow rate variations and column dimensions, so is useful for comparing the RT of specific analytes between HPLC systems.

The selectivity (or separation factor),  $\alpha$ , is a measurement of the chromatographic systems ability to ‘chemically’ distinguish between sample components.  $\alpha$  is measured as a ratio of the retention factors ( $k$ ) of the analytes in question and can be visualised as the distance between the apices of two peaks (Fig. 1-14 & Equation 9).

$$\alpha = \frac{k_2}{k_1} = \frac{t'_{R2}}{t'_{R1}} \quad (9)$$

High values of  $\alpha$  indicate a good separation of the apex of each peak. By definition the selectivity is always greater than one, as if  $\alpha = 1$ , the peaks would be co-eluting. The greater the selectivity value the further apart the peaks are on the chromatogram. As  $\alpha$  is dependent on the chemical properties of the analytes, the chemistry of the MP and/or the SP and/or the analytes in solution can be altered to optimise the selectivity of the system.

Some of the parameters that can be altered include the organic solvent used in the MP, e.g. acetonitrile (ACN) over methanol (MeOH) or isopropanol (IPA); the MP pH, which will alter the degree of ionization of some metabolites (altering hydrophobicity); different solvent strengths and additives, e.g. ion pairing agents, can alter selectivity as well as retention; column temperature (and hence MP temperature) can also have a small effect on certain analytes especially on ionisable and chiral compounds. Altering the selectivity can have a dramatic effect on resolution, i.e. small changes in selectivity can result in large improvements on resolution.

Column efficiency is the ability of the chromatogram to produce thin peaks (limited band broadening) and can be determined using the Plate Theory which was developed by Martin and Synge (1941) or by the Rate Theory

(Martin & Synge, 1941; Mayer & Tompkins, 1947; Muzenda, 2012). Martin and Synge (1941) introduced the theory of applying the ‘theoretical plate’ concept of distillation to a liquid-liquid chromatographic column (Martin & Synge, 1941). Within each theoretical plate complete equilibration of the analytes between the SP and the MP occurs. It was concluded that greater separation occurs with the greater the number of theoretical plate and as plate height (H or HETP) becomes smaller. Columns often act as if they have different numbers of plates for different analytes present in the sample. The number of plates on a column can be calculated using Equation 10.

$$N = 16 \left[ \frac{t_R}{w_b} \right]^2 \quad (10)$$

Where  $t_R$  = the retention time and  $w_b$  = base width of the peak.

For asymmetric peaks the equation is altered slightly (Equation 11).

$$N = 41.7 \frac{(t_R/w_{0.1})^2}{A/B + 1.25} \quad (11)$$

The Rate Theory takes into consideration the mechanism of band broadening, the effect of rate elution on band broadening, the availability of different paths an analyte can follow through a column and the diffusion of a solute along the length of the column.

When determining theoretical plate height using Rate Theory, longitudinal diffusion (LD), equilibration time and the resistance to mass transfer have to be considered. The Van Deemter Equation takes these variables into consideration (Equation 12). The Van Deemter Equation can be used to determine the optimum flow rate to achieve the smallest theoretical plate height using a Van Deemter plot (Fig. 1-17).

$$H = A + \frac{B}{u_x} + Cu_x \quad (12)$$

Where  $A$  = multiple paths,  $\frac{B}{u_x}$  = longitudinal diffusion,  $Cu_x$  = equilibration time.

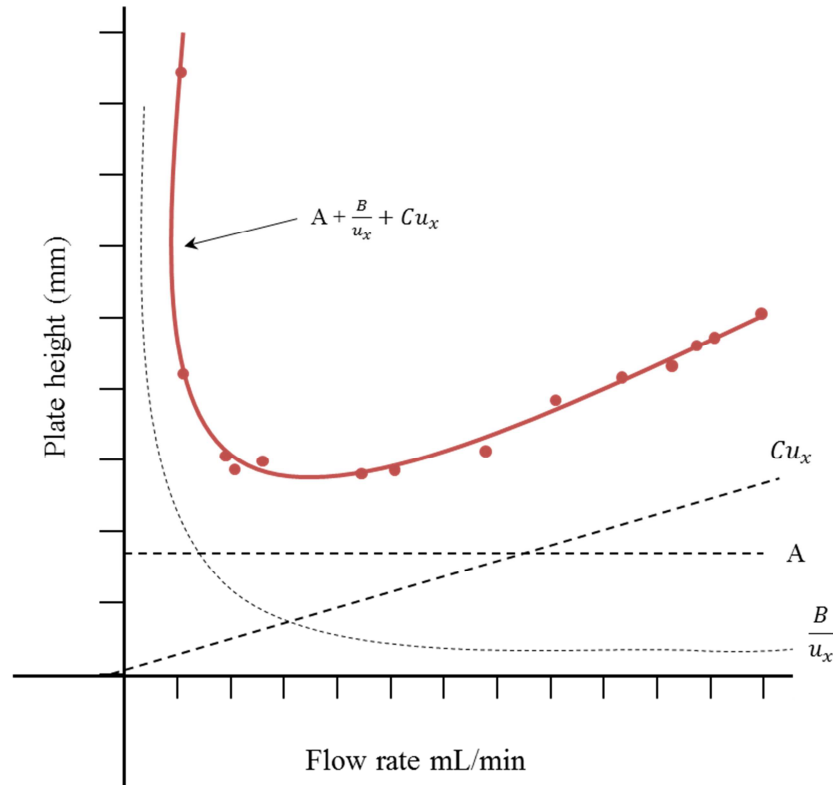


**Figure 1-17** An example of a Van Deemter plot. Where  $Cu_x$  = the equilibration time,  $A$  = Eddy diffusion and  $\frac{B}{u_x}$  = longitudinal diffusion.

LD occurs as a solute moves through the column; solute continuously diffuses away from its centre. The higher the flow rate the less time the solute has to diffuse. The plate height due to LD can be calculated using Equation 13.

$$H_{LD} = \frac{\sigma^2}{L} = \frac{2\gamma D_m}{u_x} = \frac{B}{u_x} \quad (13)$$

Where  $\sigma^2$  = variance resulting from LD,  $L$  = length of column,  $\gamma$  = irregular diffusion pattern,  $D_m$  = the diffusion coefficient of solute in MP.

Resistance to mass transfer (or nonequilibrium) is the time required for the solute to equilibrate between the MP and the SP. As the analyte travels through the column, some of the analyte is stuck to the SP while the remainder in the MP moves further down the column, resulting in band broadening. The slower the flow rate the more complete the equilibration is and the less band broadening occurs. The plate height due to finite equilibration time can be calculated according to Equation 14.

$$H_{\text{mass transfer}} = Cu_x = (C_s + C_m)u_x \quad (14)$$

Where,  $C_s$  and  $C_m$  are the rates of mass transfer through the SP and MP, respectively. There are specific equations for  $C_s$  and  $C_m$  depending on the type of chromatography used.

Efficiency can be improved by decreasing the SP thickness, reducing the column radius and increasing the MP temperature.

A solute can take a multitude of flow paths through a column (Eddy Diffusion). Determining  $A$  through Equation 15, takes this phenomenon into account with regards to chromatographic efficiency.

$$A = 2\lambda d_p \quad (15)$$

Where  $\lambda$  = the dimensionless constant characteristic of the SP packing material and  $d_p$  = particle diameter.

Eddy diffusion can be minimised by eliminating the column packing, reducing the particle size or packing the column with particles of similar size.

The Van Deemter Equation can be used to calculate the height (H) or height equivalent to a theoretical plate (HETP), and because  $H = \frac{L}{N}$ , the number of theoretical plates within the chromatographic system.

To improve the efficiency of a chromatographic system the particle diameter can be reduced, the column diameter can be reduced, changing the column temperature, reducing the thickness of the liquid film, optimizing the flow rate of the MP or lengthening the column.

There are various types of HPLC systems which can be used to separate various types of analytes. (1) Adsorption chromatography separates analytes based on their polarity (Mozzi et al., 2013). There are two classes of adsorption chromatography – (i) normal phase (NPLC) in which the SP is polar (e.g. silica) and the MP is non-polar (e.g. chloroform). The least polar analytes elute first and the most polar are retained for longer; and (ii) reversed phase (RPLC) in which the SP is non-polar (e.g. C<sub>18</sub>) and the MP is polar (e.g. acetonitrile (ACN)). The most polar analytes elute first and the least polar are retained for longer (Mozzi et al., 2013). (2) Ion exchange chromatography separates analyte ions based on the strength of their charge (Mozzi et al., 2013). The SP has an ionically charged surface, opposite to the charge of the target ions, with which the target ions are attracted. The stronger the charge on the target ion the longer it will be retained. Ion exchange chromatography can only be used for ionic or ionisable samples (Mozzi et al., 2013). (3) Size exclusion chromatography separates analytes by their solvated molecular size (Mozzi et al., 2013). Controlled pore sizes in the packing material allow for the penetration and retention of analytes under a specified size with the exclusion and elution of larger analytes (Mozzi et al., 2013).

Although reverse phase (RPLC) is better suited for the analysis of nonpolar compounds, due to its ease of use and wide ranging applicability, it is the most commonly used method in LC for metabolic analysis.

### 1.3.2.1 Reverse phase liquid chromatography (RPLC)

In RPLC the MP is more polar than the SP. The SP is typically hydrophobic and chemically bonded to the surface of a silica support (Fig. 1-18).

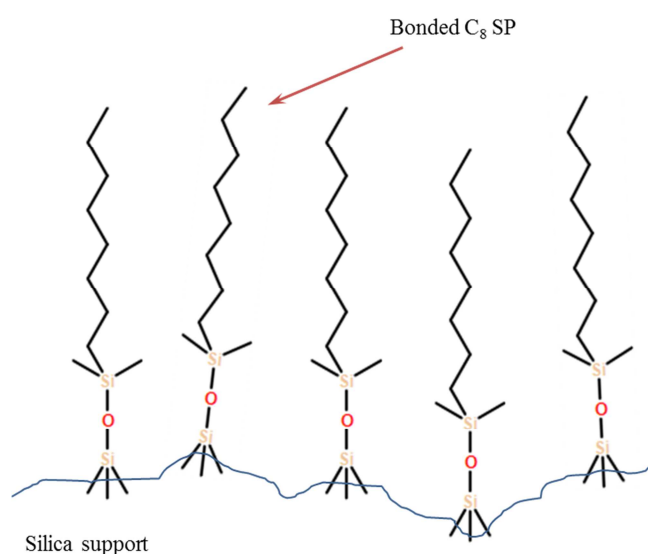


**Figure 1-18** Schematic representation of RPLC stationary phase.

The MP in RPLC is composed of water (polar) and an organic solvent which acts as a modifier to vary the retention of analytes by lowering the polarity of the MP. Hydrophobic analytes are repelled by the polar MP into the non-polar SP where they reside for a time until 'partitioning' out into the MP. The hydrophobicity of an analyte is the primary indicator of how long the analyte will be retained in RPLC. Hydrophobicity is often expressed as LogP which is a measure of the way an analyte in its neutral form partitions between two immiscible solvents (usually water and octanol) under standard conditions. The LogP of a compound can be determined using Equation 15. The higher

the value of LogP (-1 to 1), the more hydrophobic the molecule is. The more hydrophobic an analyte is the greater its retention on column.

$$\log P_{\text{oct/water}} = \log \left( \frac{[\text{solute}]_{\text{octanol}}}{[\text{solute}]_{\text{unionised water}}} \right) \quad (15)$$

A compound's structure can also indicate how well it will be retained in RPLC. Generally retention increases with: - (1) decreasing water solubility; (2) increasing carbon numbers; (3) branched chain compounds; (4) increasing compound saturation. Neutral polar and charged species are the least well retained using RPLC, followed by weak acids and bases which all elute early, and ionic compounds tend to elute with the void volume of the column.

The MP in RPLC consists of a water/aqueous solution and an organic modifier. As water is the most polar solvent, it is chromatographically the weakest as it repels hydrophobic analytes into the SP more than any other solvent which results in long RT. As the organic modifier added lowers the polarity of the MP, the hydrophobic analyte will no longer be as strongly repelled and will spend less time in the SP. As organic modifiers reduce RT, they are classed as chromatographically 'strong'. The more organic modifier that is added the more analyte RT will decrease. Examples of some common organic modifiers are listed in Fig. 1-19.

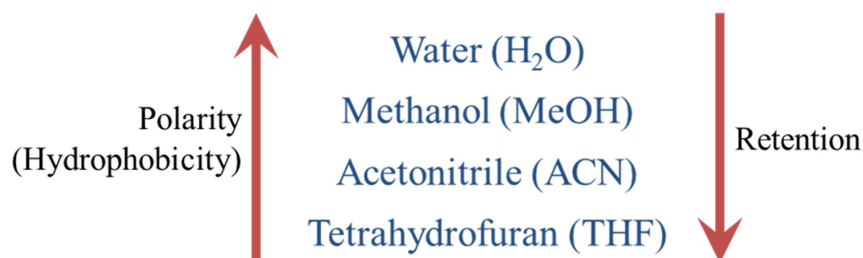
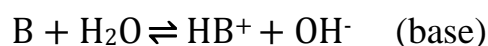
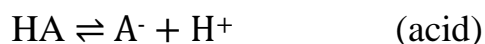


**Figure 1-19** A comparison of common elution solvents used in RPLC.

Although not the optimum method, RPLC can be used to analyse ionisable compounds, however the pH of the MP has to be considered. All acids and bases have a unique ionisation constant ( $K_a$ ) which specifies their degree of ionisation in an aqueous solution. The greater the degree of ionisation, the greater the influence the species has on the hydrogen ion ( $H^+$ ) concentration of a solution, and hence, the 'stronger' the acid or base. For example a strong acid that completely ionises in a solution increases the  $H^+$  concentration and therefore lowers the pH of that solution. A strong base will completely ionise removing  $H^+$  ions which in turn raises the pH of that solution. When an acid or a base is dissolved in water an equilibrium is established:



The dissociation constants of acids and bases can be determined using the following equation (Equation 17 & 18).

$$K_a = \frac{[A^-][H^+]}{[HA]} \quad (\text{acid}) \quad (17)$$

$$K_b = \frac{[HB^+][OH^-]}{[B]} \quad (\text{base}) \quad (18)$$

Weaker acids and bases will only partially dissociate in solution. The partial acid or base dissociation constant is defined as the negative logarithm of the

dissociation coefficient of the neutral and charged forms of the compound (Equation 19 & 20).

$$pK_a = -\log_{10}K_a \quad (\text{acid}) \quad (19)$$

$$pK_b = -\log_{10}K_b \quad (\text{base}) \quad (20)$$

The addition of acid to aqueous solution of a basic analyte will increase the concentration of the charged analyte in solution as the concentration of  $H^+$  increases and the addition of a base will increase the concentration of the neutral form of the base. Conversely, the addition of a basic solution to an acidic analyte will increase the concentration of the charged analyte and the addition of an acid will increase the neutral form of the acid. If the MP is at the exact  $pK_a$  of an analyte, that analyte will exist 50% in its ionised form and 50% in its non-ionised form. The pH of the MP dictates if the average extend of ionisation is hydrophobic or hydrophilic (Fig. 1-20). As pH is related to the degree of ionisation of analytes, and the degree of ionization dictates analytes hydrophobicity, the MP pH can be used to control retention.

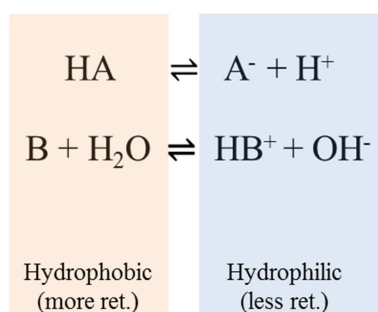


**Figure 1-20** Schematic illustrating the acid and base equilibrium.

Buffers can be added to the MP to control pH to resist small changes that may occur in the HPLC system. The definition of a buffer is a weak acid or base in co-solution with its salt, e.g. acetic acid and sodium acetate. The compounds that are used to make buffering agents can also be used on their own to alter the pH of the MP and as ion pairing agents.

To improve the retention of strongly acidic or basic analytes salt modifiers or ionic liquids, ion-pairing agents, can be added to the mobile phase. Ion pairing agents contain an ionic functional group and a hydrophobic portion. Neutral ion pairs are formed by the electrostatic interaction of the ion pairing agent with any counter ions in solution (Equation 21), forming pseudo-neutral complexes (Fig. 1-21A).



Where  $A^{+}$  = the cationic analyte of interest,  $B^{-}$  = the anionic pairing agent and  $A \cdot B$  = the neutral ion pair formed. (Note: if the analyte is anionic, then similar analysis can be performed using a cationic pairing agent).

Another possible interaction is the hydrophobic portion of the ion-pairing agents partitioning into the alkyl bonded stationary phase of the column forming transitory ion-exchange sites (Fig. 1-21B). The use of ion-pairing agents has increased the coverage of RPLC by facilitating the retention of some polar analytes but these agents can yield inconsistent and irreproducible results, have lengthy equilibrium times, can limit gradient runs, irreversibly modify and reduce column life-times and have significant ion suppression effects on mass spectrometry instrumentation, leading to a far more restricted range of available ion pairs than for chromatography as a whole (García, Hogenboom, Zappey, & Irth, 2002).

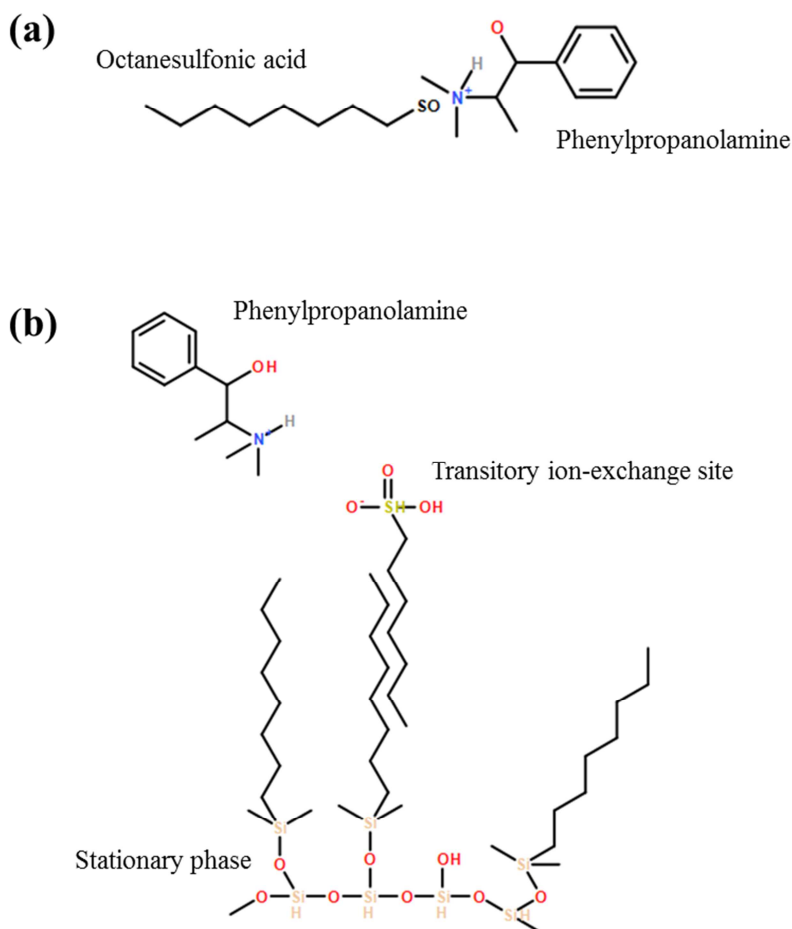


**Figure 1-21** Neutral ion pairs formed in (a) solution between the ion pairing agent (octanesulfonic acid) and a counter ion (phenylpropanolamine) and (b) the formation of transitory ion-exchange sites by the partitioning of the ion pairing agent into the stationary phase. The charged region of the ion-pairing agent attracts counter analyte ions in solution.

Traditionally, polar and ionic analytes do not retain well on RPLC columns without the addition of non-volatile ion-pairing agents to the MP (Bennett, Kimball, & Gao, 2009; Buescher, Moco, Sauer, & Zamboni, 2010; Kimball & Rabinowitz, 2006; Lu et al., 2010, 2014, 2008; Luo, Groenke, Takors, Wandrey, & Oldiges, 2007; Rabinowitz & Kimball, 2007). The addition of some ion pairing agents, such as tributylamine (TBA) enables the retention of polar and charged analytes. However, these reagents can cause irreversible contamination of MS instrumentation, therefore may not be suitable for use in some laboratories (Buescher et al., 2010). Some of the most important

compound classes in metabolomics are polar and ionic: carbohydrates, organic acids, amino acids and nucleotides chromatograph poorly on RP HPLC without the aid of ion-pairing agents, but retain and separate well with some Hydrophilic interaction liquid chromatography (HILIC) columns.

### **1.3.2.2 Hydrophilic interaction liquid chromatography (HILIC)**

First applied to HPLC by Yu & Hartwick (1989), hydrophilic interaction liquid chromatography (HILIC) is an alternative to NPLC, and similar to NPLC, the elution order of HILIC is inverted to RPLC (Alpert, 1990; Yu & Hartwick, 1989). Analytes that have little to no retention on RPLC tend to exhibit good retention on HILIC. HILIC utilizes a NP polar stationary phase with a RP mobile phase containing at least 50% organic solvent (usually ACN) in water (Alpert, 1990). The polar SP retains the strongly polar compounds which are then eluted using the organic solvent/water MP (Kahsay, Song, Van Schepdael, Cabooter, & Adams, 2014). Typical eluents for HILIC consists of 40 – 97% ACN in water or a volatile organic buffer. Due to the high organic concentration in the MP, HILIC is favourable for use with MS detection and shows a 10 – 1000 fold increase in sensitivity for hydrophilic analytes.

The HILIC SP is hydrophilic and often charged at least in some region of the pH scale. Various columns can be used in HILIC, including bare silica gel, silica-based cyano-, diol-, amino-, amido, carbamate-, polyol-, or zwitterionic sulfobetaine and other polar SP chemically bonded on a silica gel support (Guo & Gaiki, 2005; Jandera, 2011). Figure 1-22 shows some examples of the HILIC SPs available. Compounds interact with the SP and retention is generally stronger for more hydrophilic compounds.

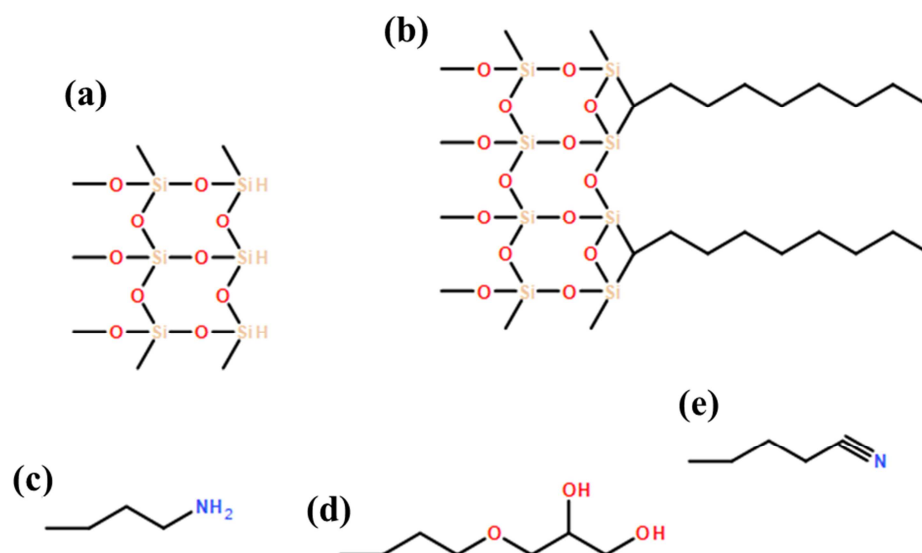


**Figure 1-22** Structures of (A) unmodified silica hydride (SH); (B) modified SH (C<sub>8</sub>); (C) amino; (D) diol and (E) cyano stationary phases that can be bonded to silica gel.

The sulfoalkylbetaine zwitterionic SP (Fig. 1-23) was introduced by Irgum's group for HILIC separations of inorganic salts, small organic ionic compounds and peptides (Jiang, Fischer, Girmay, & Irgum, 2006; Jiang & Irgum, 1999; Viklund & Irgum, 2000). The active layer is bonded onto a wide-pore silica gel or polymer support. The active SP contains both strongly acidic sulfonic acid groups and strongly basic ammonium groups separated by a short alkyl chain, which acts as a spacer. The two oppositely charged groups enable the simultaneous separation of anionic and cationic analytes.

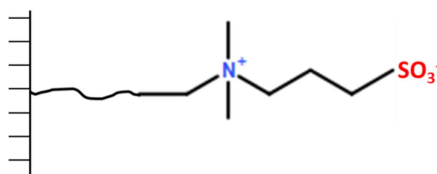


**Figure 1-23** Structure of the sulfoalkylbetaine stationary phase.

The sulfoalkylbetaine SP strongly absorbs water. A water enriched liquid layer will be absorbed on the surface of polar adsorbents or bonded phases. This creates a water-rich adsorbed diffuse liquid-multilayer (Alpert, 1990) (Fig. 1-24). Separation in HILIC is achieved by the partitioning of analytes from the eluent into the hydrophilic environment, in a process that is typically exothermic (Guo & Gaiki, 2005). Polar interactions, such as hydrogen-bonding and dipole-dipole interactions, which are governed by the acidity/basicity of the analytes and dipole moments and the polarizability of the analytes, respectively, are the primary factors that determine retention in HILIC. Electrostatic interactions can also affect the retention of analytes carrying a charge, which may require the addition of salts or buffers to the MP for analyte elution.

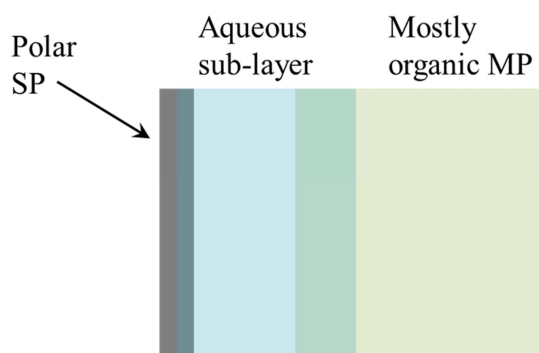


**Figure 1-24** Simple diagram depicting partitioning in HILIC.

In HILIC chromatography analytes elute in an order of decreasing hydrophobicity. Ikegami et al. (2008) carried out a comparison of the separation efficiencies of 9 different HILIC columns, including a bare silica, amino-silica, polymer-coated silica, cyano-silica and ZIC-HILIC (Ikegami, Tomomatsu, Takubo, Horie, & Tanaka, 2008). ZIC-HILIC can be applied to a wide range of analytes but the optimal flow-rate was lower than the other columns, so is not suitable for fast elution. The level of organic solvent in the

MP has the biggest influence on retention (Guo & Gaiki, 2005). Generally the elution time decreases as the water content in the MP increases (Fig. 1-25). Typically increasing the column temperature decreases retention. Unlike RPLC, the type of salt used in the buffer and its concentration has an effect on retention in HILIC (Guo & Gaiki, 2005). Guo & Gaiki (2005) found that increasing the salt concentration increased the retention of some analytes. The increase in retention of analytes occurred regardless of functional group. This suggests that increase of retention as a function of increasing the salt concentration in the MP may be a result of the partitioning process rather than any specific interactions between the SP and analyte functional groups (Guo & Gaiki, 2005). A high level of organic content in the MP leads to a higher salt concentration in the aqueous layer. This results in an increase in volume or hydrophilicity of the liquid layer, leading to longer retention of analytes (Alpert, 1990; Guo & Gaiki, 2005).

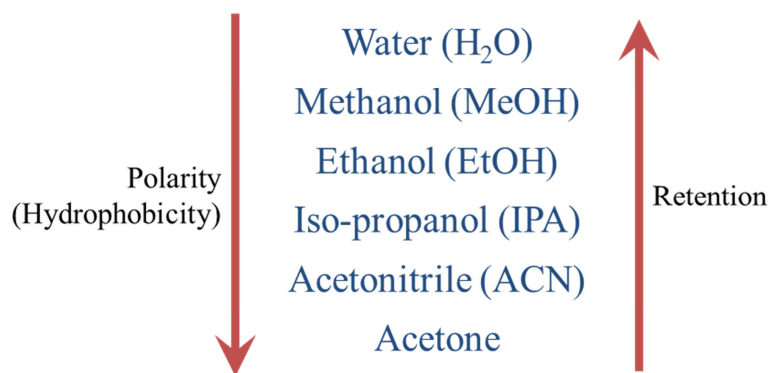


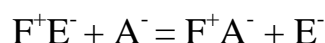
**Figure 1-25** A comparison of common elution solvents used in HILIC.

HILIC has many advantages including: that good peak shapes can be obtained for bases, it can be easily coupled to MS especially in ESI mode, it can enhance MS sensitivity and the order of the solutes is different and generally opposite (complementary) to that of RPLC (McCalley, 2007). One drawback

encountered when using HILIC is that the separation mode is not as well understood and so a change in condition could have an unexpected outcome on separation (McCalley, 2010). Another drawback when using HILIC is the lack of retention seen for analytes that are neutral and non-polar (McCalley, 2010). Negatively charged ions are often not retained either due to the repulsion of the ion from the negatively charged groups on the column (e.g. silanol groups) (McCalley, 2010). Originally applied to carbohydrates, amino acids and peptides, HILIC now has various applications including the analysis of small molecules, metabolites, toxins and drugs of abuse (Dell'Aversano, Hess, & Quilliam, 2005; Gheorghe et al., 2008; Hsieh, 2008; Hsieh & Chen, 2005; Jandera, 2011).

### 1.3.2.3 Ion exchange chromatography (IEX)

Ion exchange chromatography (IEX) (a branch of LC) is utilized for the separation and detection of charged or ionisable analytes (Boyd, Adamson, & Myers, 1947; Ketelle & Boyd, 1947; Mayer & Tompkins, 1947; Moore, Spackman, & Stein, 1958). Analytes are separated in IEX based on differences in their net surface charge. The SP or medium used in IEX is charged and the separation mechanism is based on the reversible adsorption of charged analytes to ion exchange groups of opposite charge. The analyte ions interact with charged functional groups on the SP until they are displaced by competing eluent ions. The basic exchange process can be described by:



Where  $F^+$  = the functional group,  $E^-$  = the eluent ion and  $A^-$  = the analyte ion.

In addition to ion exchange interaction other types of bonding may occur such as van der Waals forces and non-polar interactions. However, the effects of this non-specific binding are usually very small. If there are no other interactions present the RT of an ion is proportional to its charge, polarizability and ionic radius (Nesterenko & Paull, 2017).

A typical IEX run begins with equilibration of the IEX SP with the eluent buffer. After equilibration, a sample is injected onto the column. Oppositely charged analytes interact with the charged SP at varying degrees depending on differences in their overall charge, charge density and surface charge distribution. Neutral and analytes with the same charge as the SP will not be retained. Retained analytes are eluted off of the column using a gradient which increases the ion concentration in the MP. These ions displace the bound analytes from the column as they compete for sites. As the eluent concentration increases higher charged analytes are eluted off the column. Once the analytes have been eluted, a final high ionic strength wash is used to remove any ionically bound analytes before re-equilibration.

Although efficient separations of anions and cations had been carried out previously, the term ion chromatography appeared in 1975 when Small et al. separated small organic ions on an ion exchange column improving on previous methods through the development of conductimetric detection after post-column suppression of the eluent conductivity (Small, Stevens, & Bauman, 1975).

SPs utilised in IEX are made from porous or non-porous matrices. Porous matrices are beneficial as high porosity provides the maximum surface area for exchange sites, whereas non-porous matrices are good for high resolution separations where diffusion effects are not wanted. The matrices are physically stable to withstand high salt or pH concentrations and are

composed of an inert material to ensure low levels of non-specific interactions. Organic polymer-based ion-exchangers are commonly used in anion exchange chromatography (AEX) and include highly crosslinked poly(styrene-divinylbenzene) (PS-DVB), poly(methacrylate) (PMA), poly(vinyl alcohol) (PVA) and poly(styrene-ethylvinylbenzene) (PS-EVB) (Nesterenko & Paull, 2017). PMA, PVA, PS-DVB and PS-EVB-based anion exchangers are reasonably stable in alkaline eluents. These anion exchangers are functionalised with quaternary ammonium groups (account for over 95% of all AEX in IC) (Nesterenko & Paull, 2017). There are two main types of ammonium quaternary columns available; 'Type I' in which a trialkyl-ammonium head is connected to the surface using an alkyl spacer ('carbonate-type selectivity') and 'Type II' which contain two alkyl substituents and one hydroxyalkyl substituent at the nitrogen ('hydroxyl-type selectivity'). For cation exchange chromatography (CEX) silica-based ion-exchangers are commonly used with three main types of functionalities; sulfonic acid for strong acid CEX; weak acid CEX, including carboxylic and phosphoric groups; and complexation-type ion-exchangers (Haddad, Nesterenko, & Buchberger, 2008; Nesterenko & Paull, 2017; Terborg et al., 2012).

IEX mediums are considered strong or weak depending on the extent to which the ionisation state of the functional group varies with pH. For example, a strong ion exchanger has no variation in ion exchange capacity with a change in pH, i.e. this exchanger does not take up or lose protons with changing pH therefore remains fully charged over a broad pH range. This enables easy optimisation and development of methods as the charge characteristics of the SP do not change with pH, there are no intermediate forms of interaction so the mechanism is simple and the column capacity remains constant. Weak ion exchangers offer different selectivity compared to strong exchangers. However, as they can gain or lose protons with changing pH, the ion capacity changes with pH.

As has been mentioned previously, binding analytes are eluted from the column using either a salt or pH gradient. The type of compounds that are being analysed and the instrument used will dictate how the analytes is eluted.

Many eluents utilised in IEX are water based and can range from dilute electrolyte solutions to complex multicomponent buffer solutions (Nesterenko & Paull, 2017). Some common eluents utilised in AEX include hydroxide (Na or K), carbonate/bicarbonate (Na or K), aliphatic carboxylic acids (e.g. citric or formic acid) and aromatic sulfonic acids (Nesterenko & Paull, 2017). The two main types of eluents used in CEX are dilute inorganic or organic acids.

Conductivity or suppressed conductivity is the common detection mode for IEX. Conductivity detection measures the resistance (or impedance) between two electrodes within a flow cell. The response of a conductivity cell for AEX can be described using Equation 22.

$$\Delta G = \frac{(\lambda_{s-} - \lambda_{g-})C_s}{10^{-3}K} \quad (22)$$

Where  $\Delta G$  = conductance signal,  $\lambda_{s-}$  &  $\lambda_{g-}$  = limiting ionic conductances of the analyte and the eluent ions, respectively,  $C_s$  = the concentration of the analyte anion and  $K$  = the cell constant, which takes the physical dimensions of the cell into account.

Conductivity detection without suppression can result in very high background noise and very weak analyte signals. Suppressed conductivity reduces the background conductivity of the eluent by exchanging eluent ions with counter ions across an ion exchange membrane or through a high capacity IEX resin (Nesterenko & Paull, 2017; Small et al., 1975). Developed by Dionex Inc. (now part of Thermo Scientific) eluent suppressors convert highly conductive hydroxide and carbonate eluents into pure water and



Once metabolites have been separated and detected using an LC-MS system, the detected metabolites have to be identified.

### 1.3.3 Identification

Before any biological relevance can be drawn from a metabolomics study, the MS raw data files have to be processed using computer software, so that analytes can be identified and their abundances compared.

Instrument specific data output files are converted to universally recognised data files (e.g. XML & MZmine). The converted files are then run through software where peaks are detected based on a predetermined set of rules, which may include ion abundance, peak shape, signal-to-noise thresholds and RT. The peak picking software carries out this processing across all replicate samples and using a defined set of rules detects, combines and filters features based on relative standard deviation (RSD) of related peaks. The features from each chromatographic run are then combined into one dataset, which then allows further analysis.

After data processing, metabolite identification and annotation is carried out using compound databases such as the Kyoto Encyclopaedia of Genes and Genomes (KEGG), PubChem, ChemSpider and MassBank which aid in the annotation and identification of analytes (Horai et al., 2010; Kanehisa & Goto, 2000; S. Kim et al., 2016; Pence & Williams, 2010).

A standard method for reporting metabolomics analysis was suggested by the Chemical Analysis Working Group (CAWG) as part of the Metabolomics Standards Initiative (MSI) (Sumner et al., 2007). To ensure good practices in the field of metabolomics the CAWG set out a number of minimum reporting standards which included sample preparation, experimental analysis, quality control, metabolite identification and data processing. Sumner et al. proposed

four levels of metabolite identification (Table 1-1). Although this created a simple standardised method for reporting metabolite identification, it did not address the identification of metabolites in the absence of an authentic chemical standard (Sumner et al., 2014).

**Table 1-1** List of the minimum metadata relative to metabolite identification required for each MSI level (Sumner et al., 2007).

MSI Level	Description
1	Identification of compound using at least two independent orthogonal data relative to an authentic standard compound analysed under identical conditions.
2	Putatively annotated compounds (without authentic chemical standard) based on physiochemical properties&/or spectral similarities with public or commercial libraries.
3	Putatively characterised compound classes- either through physiochemical characterisation or by similarity to spectra of compounds of a known chemical class.
4	Unknown compound- although unidentified or unclassified compound can still be differentiated and quantified based on spectral data.

More recently, Sumner et al. (2014) proposed a quantitative and alphanumeric metabolite identification reporting method (Sumner et al., 2014).

The proposed quantitative system would give a numerical score to each of the techniques used in the analysis and then the score is multiplied by 2 or 1.5 depending on whether the compound was matched to an authentic chemical standard or to literature values/spectral libraries, respectively (Sumner et al., 2014). Using a quantitative approach, a minimum score value for a confident identification can be set and takes into account the identification of a metabolite through a variety of methods (Sumner et al., 2014).

The alphanumeric system uses a string of letters and numbers to summarise the data that composed the bases of the identification. Basic codes are employed to detail how the metabolite was matched (e.g.  $R_t$  = retention time match,  $MS^1$  = full scan MS match,  $MS^2$  = tandem MS match, subscript 'a' = matched to authentic chemical standard, subscript 'PL' = matched to public library, etc.).

The alphanumeric metabolite identification, although more complex than the MSI level system for identification, is more descriptive and is more intuitive than the quantitative method. As such, the Sumner alphanumeric method for describing metabolite identification has been utilised throughout this thesis and subsequent publications arising from this research.

## 1.4 Aims and Hypothesis

The number and complexity of metabolites in existence leads to a need for novel chromatographic methods to extend the coverage of the metabolome. We hypothesise that the development of these novel metabolomics methodologies will extend the coverage of the metabolome in a simple and efficient manner. We further hypothesise that *S. aureus* and *C. albicans* interact with one another on a molecular level and that the application of the developed metabolomics methods to the analysis of *S. aureus* and *C. albicans* biofilms will highlight significant metabolic differences between the mono- and dual-cultured biofilms which will provide further insight into the relationship between this prokaryote and eukaryote within their dual-species biofilm.

The overall aim of this research is to develop novel metabolomics methods and to apply these methods to the analysis of a *S. aureus/C. albicans* dual species biofilm to aid in the understanding of the relationship between this bacteria and fungi.

1. We aim to carry out microscopic and molecular characterisation of a dual-species *S. aureus*/*C. albicans* biofilm.
2. Develop an untargeted 2D LC-MS method for the identification of polar and nonpolar compounds within one analytical run.
3. Develop a targeted IC-MS metabolomics method for the analysis of central carbon metabolism intermediates in a single chromatographic run.
4. Apply the developed metabolomics methods to the analysis of single and dual species *S. aureus* and *C. albicans* biofilms.

## **Chapter 2. Materials and methods**

## 2.1 Bacterial and fungal biofilm characterisation

### 2.1.1 Bacterial and fungal strains and growth

*Candida albicans* laboratory strain SC5314 (ATCC MYA-2876) was used in this study. *C. albicans* was sub-cultured on Sabouraud's dextrose (SAB) agar (Fluka Analytical, India) and grown at 37°C for 48 h and maintained at 4°C. Broths were prepared by inoculating yeast peptone dextrose (YPD) medium (Sigma Life Sciences, USA), followed by incubation at 37°C, at 188 rpm, for 16-18 h.

*Staphylococcus aureus* Newman strain (NCTC 8178/ATCC) was cultured on Luria Bertani (LB) agar (Sigma Life Sciences, USA) and incubated for 48 h at 37°C before being maintained at 4°C. Overnight cultures were incubated aerobically in LB broth (Sigma Life Sciences, USA) in a shaking incubator set to 37°C, at a speed of 188 rpm, for 16-18 h.

### 2.1.2 Biofilm formation

Overnight cultures of *C. albicans* and *S. aureus* were centrifuged at 3000 rpm for 5 minutes (Heraeus Megafuge 16R, Thermo Fisher Scientific, Germany) and washed twice using sterile phosphate buffered saline (PBS) (Fisher Chemicals, Leicestershire, UK). *C. albicans* and *S. aureus* were standardised to  $10^6$  cells/mL in an appropriate culture medium. Culture media with no inoculum were used as negative controls.

### 2.1.3 Biofilm characterisation

For biofilm characterisation, pure and co-cultures of the *S. aureus* and *C. albicans* strains were first grown in four different media. Tryptic soy broth (TSB), brain-heart infusion (BHI), RPMI and 50% foetal bovine serum (FBS)

(all Sigma-Aldrich) were selected. Growth curves and crystal violet (CV) staining were used to determine the most appropriate culture medium.

#### **2.1.4 Growth curves**

Pure and co-cultures of the *S. aureus* and *C. albicans* strains were grown in flat-bottomed 96 well microtitre plates at 37 °C for 24 hours in each of the four media. Their growth rates were analysed spectrophotometrically by reading the absorbance every hour at 590 nm in a microtitre plate reader (FluoStar Omega, BMG Labtech). The well plate was agitated before each reading to re-suspend the cells in the media. All absorbance values were blank corrected based upon the negative control where no growth had occurred.

#### **2.1.5 Biomass assays**

Biofilms were carefully washed with PBS and allowed to air dry. 100 µL of 0.05% crystal violet (CV) solution was added to each biofilm and incubated at room temperature for 20 mins to allow uptake of the dye. Following incubation, The CV solution was discarded and the biofilms were washed with running tap water to remove any unbound dye, and 200 µL of 100% ethanol applied to de-stain each biofilm. The contents of the wells were mixed thoroughly by pipetting and 100 µL from each well were transferred to a new flat-bottomed 96 well-plate for OD measurement. The biomass was quantified spectrophotometrically by reading the absorbance at 570 nm in a microtitre plate reader (FluoStar Omega, BMG Labtech). All absorbance values were blank corrected based upon the negative control where no biofilms were formed.

For biofilm visualisation the pure and co-cultures were grown within 12 well flat-bottomed tissue culture plates for 24 h. The biofilms were carefully washed with PBS and allowed to air dry. 1 mL of 0.05% crystal violet (CV)

solution was added to each biofilm and incubated at room temperature for 20 mins to allow uptake of the dye. Following incubation, the CV solution was discarded and the biofilms were washed with running tap water to remove any unbound dye. The stained biofilms were allowed to air dry and were then digitally imaged (Canon IXUS 22 HS).

### **2.1.6 Fluorescence microscopy**

Biofilms were grown in 12 well flat-bottomed tissue culture plates for 24 h on Thermanox Cell Culture coverslips. The cover slips were carefully washed in sterile water and placed in clean wells of a new well-plate containing 100% methanol. The fixed biofilms were stored at 4 °C overnight, washed carefully in sterile water and placed in a clean well-plate. 1 mL of 1.5 µL/mL of calcufluor white and 2.5 µL/mL of SYTO 9 were added to each well and left in the dark for 20 min.

### **2.1.7 Scanning electron microscopy (SEM)**

Biofilms were grown in 12 well flat-bottomed tissue culture plates for 24 h on Thermanox Cell Culture coverslips. The cover slips were carefully washed in PBS and placed in clean wells of a new well plate. The coverslips were rinsed in a 2% gluteraldehyde/2% paraformaldehyde/0.15M sodium cacodylate for 5 mins (x3) and then stored in the fixative at 4 °C until SEM could be carried out. The fixed and dried samples were sputter-coated with gold and viewed under a JEOL JSM-6400 scanning electron microscope.

### **2.1.8 Cell numbers**

The effect of the presence of *S. aureus* and *C. albicans* on cell numbers in the co-cultured biofilms were analysed using real-time quantitative PCR. Biofilms were grown in 12 well flat-bottomed tissue culture plates for 24 h on

Thermanox Cell Culture coverslips. The cover slips were carefully washed in PBS and each coverslip placed in a bijoux containing 1 mL of PBS. For qPCR the biofilm sonicate was used for DNA extraction using the MasterPure Gram Positive DNA Purification Kit (Epicentre®, Cambridge, UK), following manufacturer's instructions. The extracted DNA underwent quality checks using the NanoDrop spectrophotometer (Fischer Scientific, Loughborough). Briefly, 1 µL of extracted DNA was added to a mastermix containing 12.5 µL SYBR® GreenER™, 9.5 µL UV-treated RNase-free water and 1 µL of 10 µM forward/reverse primers for the bacterial or fungal species. Three independent replicates from each parameter were analysed in triplicate using MxProP Quantitative PCR machine and MxProP 3000 software (Stratagene, Amsterdam, Netherlands). Samples were quantified to calculate the colony forming equivalent (CFE) based upon a previously established standard curve of bacterial and fungal colony forming units ranging from  $1 \times 10^3$  to  $10^8$  cfu/mL (Appendix I). The R<sup>2</sup> values for these standard curves ranged from 0.980 to 0.999.

### **2.1.9 Gene expression analysis of biofilm associated genes**

The effect of the presence of *S. aureus* on *C. albicans* SC5314 adhesion (ALS3) and filamentation (HWP1) was analysed by quantitative transcriptional analysis. Standardised cells ( $1 \times 10^6$  cells/mL) were grown in 12 well flat-bottomed tissue culture plates for 24 h. The supernatant was removed and RNA was extracted using the TRIzol® method (Invitrogen, Paisley, UK) . After DNase treatment (QIAGEN, Crawley, UK) and purification (RNeasy MinElute Cleanup Kit; QIAGEN), cDNA was synthesised using a High-Capacity RNA-to-cDNA™ Kit (Life Technologies, Paisley, UK), and quantitative PCR (qPCR) was performed using a SYBR® GreenER™ assay (Life Technologies). The primers (Table 2-1) and conditions used for real-time qPCR throughout this study are described

elsewhere (Sherry et al., 2014). Each parameter was analysed in triplicate using an MxProP Quantitative PCR machine and MxProP 3000 software (Stratagene, Amsterdam, The Netherlands). Gene expression was normalised to the housekeeping gene *act-1* according to the  $2^{-\Delta\Delta CT}$  method, and the percentage of gene expression was expressed as the log<sub>10</sub> mean  $\pm$  standard deviation (Livak & Schmittgen, 2001).

**Table 2-1** A list of the Forward (F) and Reverse (R) Primers used to quantify *Candida albicans* (*C. albicans*) and *Staphylococcus aureus* (*S. aureus*) cell numbers in the mono- and dual-species biofilms, and the Forward (F) and Reverse (R) Primers used to determine expression of the surface protein Als3 (ALS3) and hyphal wall protein (HWP1) in *C. albicans*.

Species-specific Primers	Sequence (5'-3')
<i>C. albicans</i>	F - ACTTCTGTAAGAGTGCTGGTTC R - TGTCGTAATCAAACCTCGGTAGC
<i>S. aureus</i>	F - ATTTGGTCCCAGTGGTGTGGGTAT R - GCTGTGACAATTGCCGTTTGTTCGT
<b><i>C. albicans</i> Biofilm genes</b>	
<i>ALS3</i>	F - CAACTTGGGTTATTGAAACAAAAACA R - AGAAACAGAAACCCAAGAACAACCT
<i>HWP1</i>	F - GCTCAACTTATTGCTATCGCTTATTACA R - GACCGTCTACCTGTGGGACAGT
<b><i>C. albicans</i> Housekeeping gene</b>	
<i>ACT1</i>	F - AAGAATTGATTGGCTGGTAGAGA R - TGGCAGAAGATTGAGAAGAAGTTT

### 2.1.10 Statistical analysis

Graph production, data distribution, and statistical analysis were performed using GraphPad Prism (version 5; La Jolla, CA, USA). Student *t*-tests were used to analyse experiments comparing independent sample data. Statistical significance was achieved if  $P < 0.05$ . All statistical analysis was carried out

using data obtained from three independent biological replicates for each sample group ( $n = 3$ ). Error bars depict the standard deviation of the sample group.

## 2.2 Serially combined method

### 2.2.1 Chemicals and reagents

HPLC gradient grade water was purchased from VWR (Chicago, USA). Absolute ethanol and acetonitrile were purchased from Fisher Scientific (Leicestershire, UK). Ammonium carbonate, deoxycholic acid, cholic acid, dyhydrocholic acid, chenodeoxycholic acid acid, DL-isocitric acid trisodium salt hydrate, cis-aconitic acid,  $\alpha$ -ketoglutaric acid disodium salt hydrate, sodium succinate dibasic, sodium fumarate dibasic, DL-malic acid and sodium pyruvate were all purchased from Sigma-Aldrich (Bornem, Belgium). All chemicals were of analytical-reagent grade.

### 2.2.2 Standards

All of the standards were prepared to a concentration of 10  $\mu\text{M}$  in water with the exception of the bile acids. Stock standard solutions of Deoxycholic acid, cholic acid, dehydrocholic acid and Chenodeoxycholic acid were prepared in 100 % hot ethanol. The standards were then diluted at a 1:1 ratio with  $\text{H}_2\text{O}$  and then diluted 1:100 in 100 %  $\text{H}_2\text{O}$ , to a final concentration of 10  $\mu\text{M}$ . (The structures of these compounds can be found in Fig. 2-1).

10  $\mu\text{L}$  of each sample was injected onto the column in triplicate over three days ( $n = 9$ ).

## Chapter 2

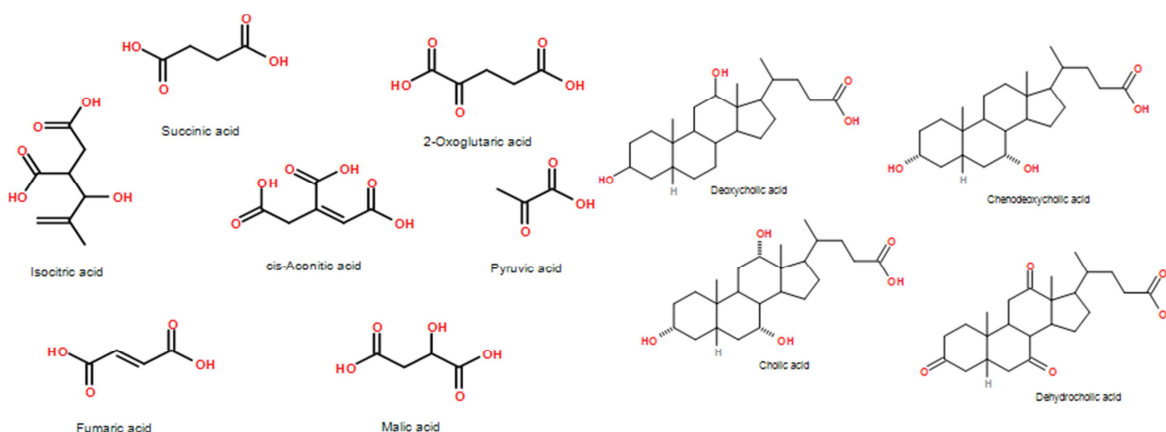


**Figure 2-1** Chemical structures of the test compounds. A selection of polar TCA intermediates (succinic acid, 2-oxoglutaric acid, isocitric acid, *cis*-aconitic acid, pyruvic acid, fumaric acid and malic acid) and nonpolar bile acids (deoxycholic acid, chenodeoxycholic acid, cholic acid and dehydrocholic acid) were utilised to determine the suitability of the system for the retention and separation of polar and nonpolar metabolites (Haggarty et al., 2015).

### 2.2.3 Beer samples

Samples of a bitter style branded ale were extracted at a ratio of 1:3:1 chloroform:methanol:beer. 250  $\mu\text{L}$  samples were dried using  $\text{N}_2$  and resuspended in 200  $\mu\text{L}$  of 10% acetonitrile in water.

10  $\mu\text{L}$  of each sample was injected onto the column in octuplicate.

To evaluate the long term reproducibility of the method, analysis of the combined method was carried out in three batches over five days, while the individual column analyses were done over a single day ( $n=23$ ).

### 2.2.4 Instrumentation

A Thermo Scientific Ultimate 3000 RSLC system (Thermo Scientific, CA, USA) was used. Column temperature was maintained at  $25^\circ\text{C}$ . The system was coupled with a Thermo Scientific Exactive Orbitrap system equipped with a HESI II interface (Thermo Scientific, Hemel Hempstead, UK).

Acquisition was carried out in positive and negative switching mode. The capillary temperature was 275 °C with a data acquisition mass range of 70-1400  $m/z$ . Thermo Xcalibur™ (version 2.2.42) was used for instrument control and data acquisition. Fragmentation for annotation of beer metabolites was performed on an identically configured Thermo Scientific Q-Exactive with a normalised collision energy of 50 and isolation width of 1 Da.

For the first separation a Hypersil GOLD (100 x 1.0 mm, 1.9  $\mu\text{m}$ ) (Thermo Scientific, Hemel Hempstead, UK) was used and the second separation was performed with a SeQuant® ZIC®-pHILIC column (150 x 4.6 mm, 5  $\mu\text{m}$ ) (Merck KGaA, Darmstadt, Germany). The two columns were coupled in series through a T-piece. The third port of the T-piece was connected to the second pump. A scheme of the instrumental set-up is given in Fig. 2-2. All metabolites were detected in negative mode except where stated.

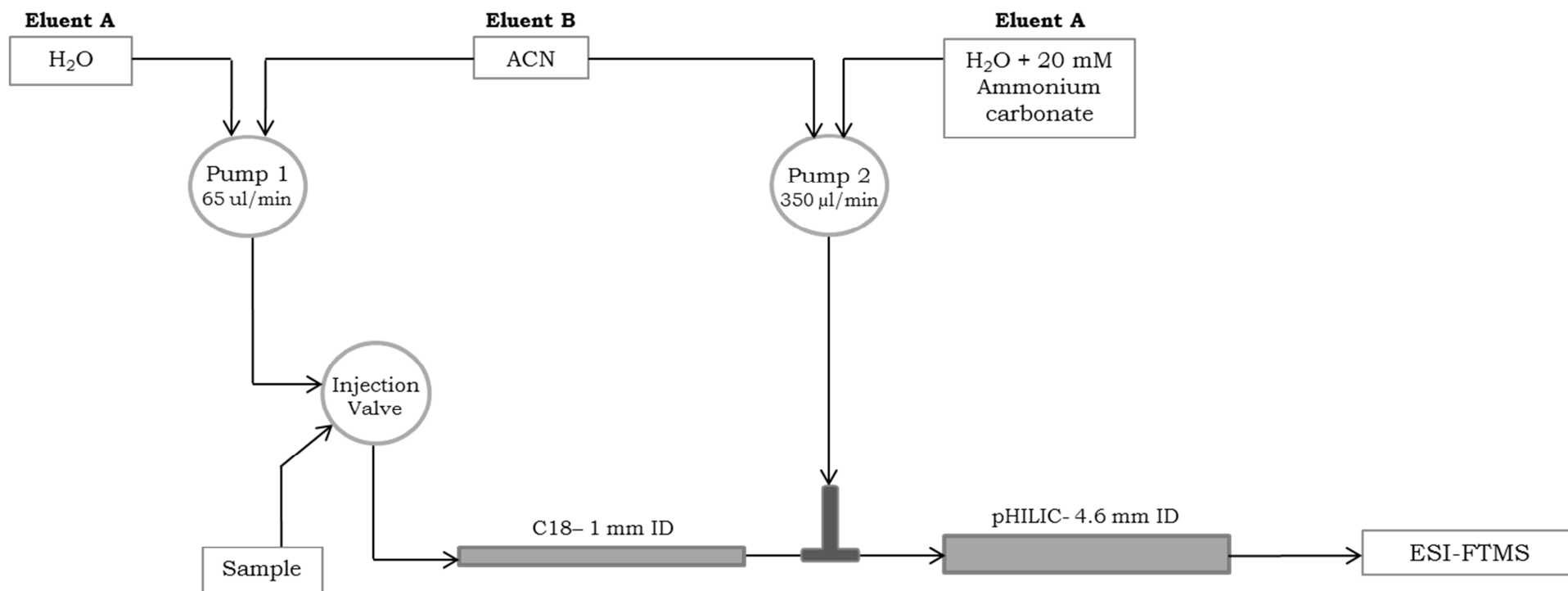


**Figure 2-2** Schematic diagram of the RPLC/pHILIC/ESI-FTMS. The first gradient pump (Pump 1), running at 65  $\mu\text{L}/\text{min}$ , delivered a high aqueous mobile phase for the analytes as they were injected onto the RP column. The second gradient pump (Pump 2) was joined via a t-piece to the system to deliver a high concentration of organic solvent (>80% ACN) before introduction of the sample to the HILIC column. Pump 2 was run at a higher flow rate of 350  $\mu\text{L}/\text{min}$  to increase the organic concentration of the eluent before the HILIC column. One injection from each sample passed through both the RP and HILIC columns before detection by the mass spectrometer. By incorporating two gradient pumps into the system individual control of the mobile phase compositions was achieved (Haggarty et al., 2015).

### 2.2.5 Chromatographic conditions

The RPLC mobile phase was a combination of LC-MS-grade water (solvent A) and acetonitrile (ACN) (solvent B). The HILIC mobile phase was a mixture of LC-MS-grade water + 20 mM ammonium carbonate, pH 9, (solvent A), ACN (solvent B) and the solvent from the RP column. The following RP gradient was applied at a rate of 65  $\mu\text{L}/\text{min}$ : a concentration of 5%B was held for 2 min and then increased to 95%B over 15min, where it was held for 5 min, followed by equilibration at 5%B, held for 15.5 min. The HILIC gradient was applied at a rate of 350  $\mu\text{L}/\text{min}$ : a 90%B was held for 5 min and then decreased to 20% B in 15 min and then decreased to 5% B and held for 5 min, followed by reconstitution of the starting conditions within 0.1 min and re-equilibration with 90%B for 12.5 min. This resulted in a total analysis time of 37.5 min. A summary of the chromatographic conditions can be found in Table 2-2.

### 2.2.6 Evaluation of reproducibility

Retention times were obtained for each peak using the Quan Browser software, part of the Thermo Xcalibur<sup>TM</sup> (version 2.2.42) suite. A total of nine replicates were used to determine retention time reproducibility for the organic and bile acid standards. As the extracted beer was a more complex sample, a total of twenty-three replicates were used to evaluate retention time reproducibility. Retention times were averaged and the standard deviation was calculated. Relative standard deviations were obtained for each compound and expressed as percentages.

**Table 2-2** Summary of the chromatographic conditions for the combined RPLC/pHILIC method (Haggarty et al., 2015). Pump 1 was running a reverse phase (RPLC) gradient through a Thermo Hypersil GOLD (100 x 1.0 mm, 1.9  $\mu\text{m}$ ) column at a flow rate of 65  $\mu\text{L}/\text{min}$ . Pump 2 was running a hydrophilic interaction liquid chromatography (HILIC) gradient through a SeQuant® ZIC®-pHILIC (150 x 4.6 mm, 5  $\mu\text{m}$ ) at a flow rate of 350  $\mu\text{L}/\text{min}$ . Solvent A consisted of water ( $\text{H}_2\text{O}$ ) for Pump 1 and  $\text{H}_2\text{O} + 20 \text{ mM}$  ammonium carbonate for Pump 2. Solvent B consisted of acetonitrile (ACN) for both Pump 1 and Pump 2.

Pump 1 (RPLC)				Pump 2 (HILIC)			
Solvent A	$\text{H}_2\text{O}$			Solvent A	$\text{H}_2\text{O} + 20 \text{ mM}$ ammonium carbonate		
Solvent B	ACN			Solvent B	ACN		
Column	Thermo Hypersil GOLD (100 x 1.0 mm, 1.9 $\mu\text{m}$ )			Column	SeQuant® ZIC®-pHILIC (150 x 4.6 mm, 5 $\mu\text{m}$ )		
Gradient	Time (min)	B%	Flow (mL/min)	Gradient	Time (min)	B%	Flow (mL/min)
	0	5	0.065		0	90	0.350
	2	5	0.065		5	90	0.350
	17	95	0.065		20	20	0.350
	22	95	0.065		20.1	5	0.350
	22.1	5	0.065		25	5	0.350
	↓	↓	0.065		25.1	90	0.350
	37.5	5	0.065		37.5	90	0.350

### **2.2.7 Extracellular-metabolite extraction**

Medium controls (50% FBS with MilliQ water) and biofilm supernatants were transferred into reaction tubes (1.5 mL, Greiner bio-one GmbH, Germany) containing ice cold chloroform:methanol:water (1:3:1 v:v:v) at a ratio of 1:40 (sample:extraction solvent). The reaction tubes were vortexed at maximum speed for 15 seconds (Vortex Genie 2, Scientific Industries, NY, USA) and stored at -80°C prior to analysis.

### **2.2.8 Intracellular-metabolite extraction**

Cell culture cover slips were removed from the wells and placed in bijoux containing ice cold 10 mM ammonium bicarbonate. The bijoux were sonicated at maximum speed for 10 minutes at 4°C (XUB5, 4.5 L, Grant Instruments, Cambridgeshire, UK). The supernatants, including the debris, were removed and placed in clean reaction tubes. The biofilm suspensions were centrifuged at 3000 rpm for 5 minutes at 4°C, the supernatants were removed, and 1 mL of a 1 mL:1 g extraction solvent (ChCl<sub>3</sub>:MeOH:H<sub>2</sub>O 1:3:1 v:v:v) : 0.1 mm acid washed glass beads (Sigma Aldrich, USA) were added to each pellet. Bead beating was carried out at 3000 rpm for 10 minutes at 4°C (Disrupter Genie, Scientific Industries, NY, USA). The samples were centrifuged at 13000 rpm for 5 minutes at 4°C, the supernatants were removed and stored at -80°C analysis.

### **2.2.9 Metabolic data analysis and statistical analysis**

Organic acid and bile acids were matched to authentic pure standards by retention time and accurate mass and can therefore be classified under the alphanumeric metabolite coding scheme as HRMS<sup>1</sup><sub>a</sub>, R<sub>ta</sub> as described in Sumner et al. (2014). Beer metabolites were matched to compounds putatively by accurate mass or accurate mass and fragment spectrum match to

the MassBank library (Horai et al. 2010) and may be classified as HRMS<sup>1</sup> or HRMS<sup>1</sup>MS<sup>2</sup><sub>PL</sub> respectively (Sumner et al. 2014).

For biofilm samples, raw mass spectrometry data was processed using our standard pipeline (Creek, Jankevics, Burgess, Breitling, & Barrett, 2012; Gloaguen et al., 2017), consisting of XCMS (C. A. Smith, Want, O'Maille, Abagyan, & Siuzdak, 2006) (for peak picking), MzMatch (Scheltema, Jankevics, Jansen, Swertz, & Breitling, 2011) (for filtering and grouping) and in-house R-scripts (for further filtering, post-processing and identification). Peaks were visualised using PeakML viewer (Scheltema et al., 2011). Core metabolite identifications were validated against a panel of unambiguous authentic pure standards (Sigma-Aldrich) using high resolution accurate mass and RT (error of 5% was allowed), and could therefore be classified as HRMS<sup>1</sup><sub>a</sub>, R<sub>ta</sub>, as described by Sumner *et al.* (2014). Additional putative identifications were assigned by accurate mass along with a RT prediction algorithm (error of 35% allowed) (Creek et al., 2011) and as such were classified as HRMS<sup>1</sup><sub>PL</sub> (Sumner et al., 2014).

Once identified and filtered, detected peak intensities were logged (base 2) and quantification was performed on sets of biological replicates by applying differential statistics to generate P values. Metabolites with apparently different levels were assessed using Bayes moderated *t*-tests (Smyth, 2004). Benjamini and Hochberg false discovery rate adjustment for multiple testing was applied (Hochberg & Benjamini, 1990) and the resulting data was used to query the KEGG database for pathway analysis (Kanehisa & Goto, 2000). For LC-MS analysis, five independent biological replicates were used.

## 2.3 Ion chromatography - mass spectrometry

### 2.3.1 Chemicals and reagents

HPLC gradient grade water was purchased from VWR (Chicago, USA). Absolute ethanol and acetonitrile were purchased from Fisher Scientific (Leicestershire, UK). All of the central carbon metabolism standards were purchased from Sigma-Aldrich (Bornem, Belgium). All chemicals were of analytical-reagent grade.

### 2.3.2 Standards

Each individual standard was prepared to a concentration of 1 mM in ultrapure *Milli-Q* water, with the exception of acetyl-CoA, CoA, succinyl-CoA, FAD, ATP and ADP which were made up to a concentration of 100  $\mu$ M.

A glycolysis mix (Table 2-3) was created by diluting the 1 mM stocks of glucose, glucose 6-phosphate, fructose 6-phosphate, dihydroxyacetone phosphate, glyceraldehyde 3-phosphate, 3-phosphoglycerate, 2-phosphoglycerate, phosphoenolpyruvate, pyruvate at a 1:10 ratio and the 1 mM stock of fructose 1,6-bisphosphate at a ratio of 1:100, resulting in a final concentration of 100  $\mu$ M for each standard and 10  $\mu$ M of fructose 1,6-bisphosphate.

A TCA mix (Table 2-4) was created by diluting 1 mM stocks of citric acid, isocitric acid, *cis*-aconitic acid, 2-oxoglutaric acid, succinic acid, fumaric acid, malic acid and oxaloacetic acid at a 1:10 ratio, resulting in a final concentration of 100  $\mu$ M of each standard.

A coenzyme and nucleoside phosphate mix (Table 2-5) was created by the addition of each of the stock solutions of nicotinamide adenine dinucleotide phosphate (NADP<sup>+</sup>), nicotinamide adenine dinucleotide (NAD<sup>+</sup>), flavin adenine dinucleotide (FAD), adenosine diphosphate (ADP), and adenosine triphosphate (ATP) at a 1:10 ratio. This resulted in a mix containing 100  $\mu$ M of NADP<sup>+</sup> and NAD<sup>+</sup>, and 10  $\mu$ M of FAD, ADP and ATP.

A total energy mix was made by diluting each of the standards at a 1:10 ratio, with the exception of fructose 1, 6-bisphosphate, which was diluted at a ratio of 1:100. This resulted in a mix containing 100  $\mu$ M of glucose, glucose 6-phosphate, fructose 6-phosphate, dihydroxyacetone phosphate, glyceraldehyde 3-phosphate, 3-phosphoglycerate, 2-phosphoglycerate, phosphoenolpyruvate, pyruvate, citric acid, isocitric acid, *cis*-aconitic acid, 2-oxoglutaric acid, succinic acid, fumaric acid, malic acid and oxaloacetic acid, NADP<sup>+</sup>, NAD<sup>+</sup>, ADP and ATP, and 10  $\mu$ M of fructose 1, 6-bisphosphate, ADP, ATP and FAD.

**Table 2-3** A list of the glycolysis standards elemental formulae, molecular weights (MW) and *m/z* values ([M-H]).

<b>Glycolysis</b>			
<b>Metabolite</b>	<b>Formula</b>	<b>MW</b>	<b>[M-H]</b>
Glucose	C <sub>6</sub> H <sub>12</sub> O <sub>6</sub>	180.0634	179.0562
Glucose-6-phosphate	C <sub>6</sub> H <sub>13</sub> O <sub>9</sub> P	260.0297	259.0225
Fructose-6-phosphate	C <sub>6</sub> H <sub>13</sub> O <sub>9</sub> P	260.0297	259.0225
Fructose-1,6-biphosphate	C <sub>6</sub> H <sub>14</sub> O <sub>12</sub> P <sub>2</sub>	339.9961	338.9889
Glyceraldehyde-3-phosphate	C <sub>3</sub> H <sub>7</sub> O <sub>6</sub> P	169.9980	168.9908
3-Phosphoglyceric acid	C <sub>3</sub> H <sub>7</sub> O <sub>7</sub> P	185.9929	184.9857
2-Phosphoglyceric acid	C <sub>3</sub> H <sub>7</sub> O <sub>7</sub> P	185.9929	184.9857
Phosphoenolpyruvic acid	C <sub>3</sub> H <sub>5</sub> O <sub>6</sub> P	167.9824	166.9752
Pyruvic acid	C <sub>3</sub> H <sub>4</sub> O <sub>3</sub>	88.0160	87.0088

**Table 2-4** A list of the TCA standards elemental formulae, molecular weights (MW) and  $m/z$  values ([M-H]).

<b>TCA cycle</b>			
<b>Metabolite</b>	<b>Formula</b>	<b>MW</b>	<b>[M-H]</b>
Citric acid	C <sub>6</sub> H <sub>8</sub> O <sub>7</sub>	192.0270	191.0198
Isocitric acid	C <sub>6</sub> H <sub>8</sub> O <sub>7</sub>	192.0270	191.0198
<i>cis</i> -Aconitic acid	C <sub>6</sub> H <sub>6</sub> O <sub>6</sub>	174.0164	173.0092
2-Oxoglutaric acid	C <sub>5</sub> H <sub>6</sub> O <sub>5</sub>	146.0215	145.0143
Succinyl-CoA	C <sub>25</sub> H <sub>40</sub> N <sub>7</sub> O <sub>19</sub> P <sub>3</sub> S	867.1313	866.1241
Succinic acid	C <sub>4</sub> H <sub>6</sub> O <sub>4</sub>	118.0266	117.0194
Fumaric acid	C <sub>4</sub> H <sub>4</sub> O <sub>4</sub>	116.0110	115.0038
Malic acid	C <sub>4</sub> H <sub>6</sub> O <sub>5</sub>	134.0215	133.0143
Oxaloacetic acid	C <sub>4</sub> H <sub>4</sub> O <sub>5</sub>	132.0059	130.9987
Acetyl-Coenzyme A (CoA)	C <sub>23</sub> H <sub>38</sub> N <sub>7</sub> O <sub>17</sub> P <sub>3</sub> S	809.1258	808.1186
Coenzyme A (CoA)	C <sub>21</sub> H <sub>36</sub> N <sub>7</sub> O <sub>16</sub> P <sub>3</sub> S	767.1152	766.108

**Table 2-5** A list of the coenzymes and nucleoside phosphates standards elemental formulae, molecular weights (MW) and  $m/z$  values ([M-H]).

<b>Coenzymes and nucleoside phosphates</b>			
<b>Metabolite</b>	<b>Formula</b>	<b>MW</b>	<b>[M-H]</b>
Nicotinamide adenine dinucleotide phosphate (NADP <sup>+</sup> )	C <sub>21</sub> H <sub>28</sub> N <sub>7</sub> O <sub>17</sub> P <sub>3</sub>	743.0755	742.0683
Nicotinamide adenine dinucleotide (NAD <sup>+</sup> )	C <sub>21</sub> H <sub>28</sub> N <sub>7</sub> O <sub>14</sub> P <sub>2</sub>	664.1170	663.1098
Flavin adenine dinucleotide (FAD)	C <sub>27</sub> H <sub>33</sub> N <sub>9</sub> O <sub>15</sub> P <sub>2</sub>	785.1571	784.1499
Adenosine diphosphate (ADP)	C <sub>10</sub> H <sub>15</sub> N <sub>5</sub> O <sub>10</sub> P <sub>2</sub>	427.0294	426.0222
Adenosine triphosphate (ATP)	C <sub>10</sub> H <sub>16</sub> N <sub>5</sub> O <sub>13</sub> P <sub>3</sub>	506.9958	505.9886

### 2.3.3 Instrumentation

A Thermo Scientific Dionex™ ICS-2100 Integrated IC System (Thermo Scientific, CA, USA) was used. The IC system was coupled to a Thermo Scientific Orbitrap Fusion™ Tribrid™ Mass Spectrometer (Thermo Scientific, CA, USA) using a HESI interface (Thermo Scientific, Hemel Hempstead, UK). The spray voltage was 2500V, with a transfer tube temperature of 333 °C. Acquisition was carried out in negative polarity mode.

The capillary temperature was 275 °C with a data acquisition mass range of 70 – 1000  $m/z$ . The analytes were detected using the Orbitrap detector with a resolution of 60 000. The ICS-2100 IC System was controlled using Thermo Chromeleon® software (version 6.80). Thermo Xcalibur™ (version 3.1.66.10) was used for mass spectrometer instrument control and data acquisition.

A Thermo Dionex™ IonPac™ AS11-HC-4 $\mu$ m (2 x 250 mm) column (Thermo Scientific, Hemel Hempstead, UK) was utilized in this study. The ICS-2100 system was coupled to the mass spectrometer via an external pump running at a flow rate of 70  $\mu$ L/min. The make-up flow consisted of 100% MeOH.

#### **2.3.4 Chromatographic conditions**

Column temperature was maintained at 35 °C. Ultrapure (18.2 M $\Omega$ ·cm at 25 °C) Milli-Q (Merck Millipore, MA, USA) water was further purified using a Thermo Scientific™ Dionex™ ICW-3000 Online Water Purifier (Thermo Scientific, CA, USA) before introduction to the ICS-2100 system. A hydroxide (OH<sup>-</sup>) mobile phase was produced using a Thermo Scientific™ Dionex™ Potassium Hydroxide Eluent Generator Cartridge (EGC 500 KOH) (Thermo Scientific, CA, USA). The following OH<sup>-</sup> gradient was applied at a rate of 230  $\mu$ L/min: an equilibration at a concentration of 1 mM was held for 7 min at the beginning of each chromatographic run. A concentration of 1 mM was held for 3 min and then increased to 31 mM over 20 min. The concentration was then increased to 36 mM over 10 min, then increased to 50 mM over 10 min and increased to 100 mM over 10 min and held 7 min, followed by a decrease to 5 mM within 0.1 min. This resulted in a total analysis time of 67.1 min. A summary of the chromatographic conditions can be found in Figure 2-3 & Table 2-6.

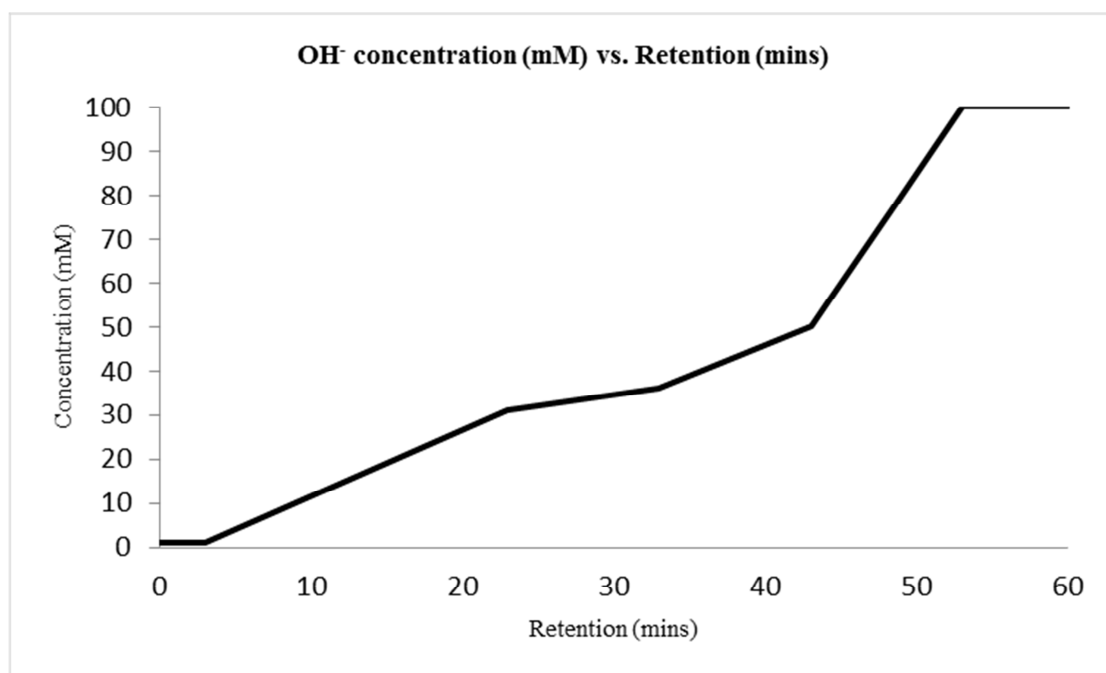


**Figure 2-3** Summary of the chromatographic conditions used for the targeted ion chromatography – mass spectrometry (ICMS) analysis of energy metabolite standards and extracted biofilm (intracellular) and spent media (extracellular) samples. A hydroxide ( $\text{OH}^-$ ) gradient increasing from 1 – 100 mM over 60 min, with a re-equilibration of 1 mM for 7 min, was carried out for each chromatographic run, resulting in a total analysis time of 67.1 min.

**Table 2-6** Summary of the chromatographic conditions used for the targeted ion chromatography – mass spectrometry (ICMS) analysis. The eluent consisted of a hydroxide ( $\text{OH}^-$ ) gradient flowing at a rate of 230  $\mu\text{L}/\text{min}$ . The column used was a Thermo Dionex™ IonPac™ AS11-HC-4 $\mu\text{m}$  (2 x 250 mm).

<b>Eluent</b>	OH (Thermo Dionex™ EGC 500 KOH)		
<b>Column</b>	Thermo Dionex™ IonPac™ AS11-HC-4 $\mu\text{m}$ (2 x 250 mm)		
<b>Gradient</b>	<b>Time (min)</b>	<b>Concentration (mM)</b>	<b>Flow (mL/min)</b>
	-7	1	0.230
	0	1	0.230
	3	1	0.230
	23	31	0.230
	33	36	0.230
	43	50	0.230
	53	100	0.230
	60	100	0.230
	60.1	5	0.230

### 2.3.5 Evaluation of reproducibility and limits of detection

Retention times for the energy metabolite standards were obtained by conducting a mass search for each individual standard peak using Thermo Scientific<sup>TM</sup> ToxID Automated Compound Screening Software (version 2.1.2.17). The average retention time for each energy metabolite was used to create an automatic processing method to screen each sample for all energy metabolites, using Quan Browser software, part of the Thermo Xcalibur<sup>TM</sup> (version 2.2.42) suite. Retention times were averaged and the standard deviation was calculated. Relative standard deviations were calculated for each compound and expressed as percentages.

The stock solution of the total energy mix was serially diluted to determine the limits of detection (LoD) for each metabolite when using the system (Table 2-7). An automatic processing method was created using the Quan Browser software (Thermo Scientific, CA, USA). The expected retention time and [M-H] for each metabolite were used to detect each analyte within the total mix dilutions. The peak areas were measured using an Xcalibur processing method and reported for each of the metabolite standards at each of the dilutions.

**Table 2-7** Summary of the energy metabolite concentrations used to determine the limits of detection (LoD) of the IC-MS system. Each metabolite's elemental formula (EF) is listed along with its final concentration (nmoles) in the total mix for each of the dilutions used (Dilution Factor).

Metabolite	EF	Dilution Factor							
		1	1/5	1/10	1/15	1/25	1/50	1/100	1/500
		Concentration (nmol)							
Glucose	C6H12O6	100000	20000	10000	6666.67	4000	2000	1000	200
Glucose-6-phosphate	C6H13O9P	100000	20000	10000	6666.67	4000	2000	1000	200
Fructose-6-phosphate	C6H13O9P	100000	20000	10000	6666.67	4000	2000	1000	200
Fructose-16-biphosphate	C6H14O12P2	10000	2000	1000	666.67	400	200	100	20
3-phosphglycerate	C3H7O7P	100000	20000	10000	6666.67	4000	2000	1000	200
2-phosphoglycerate	C3H7O7P	100000	20000	10000	6666.67	4000	2000	1000	200
Phosphoenolpyruvate	C3H5O6P	100000	20000	10000	6666.67	4000	2000	1000	200
Pyruvate	C3H4O3	100000	20000	10000	6666.67	4000	2000	1000	200
Citrate	C6H8O7	100000	20000	10000	6666.67	4000	2000	1000	200
Isocitrate	C6H8O7	100000	20000	10000	6666.67	4000	2000	1000	200
cis-Aconitate	C6H6O6	100000	20000	10000	6666.67	4000	2000	1000	200
2-Oxoglutarate	C5H6O5	100000	20000	10000	6666.67	4000	2000	1000	200
Succinate	C4H6O4	100000	20000	10000	6666.67	4000	2000	1000	200
Fumarate	C4H4O4	100000	20000	10000	6666.67	4000	2000	1000	200
Malate	C4H6O5	100000	20000	10000	6666.67	4000	2000	1000	200
Oxaloacetate	C4H4O5	100000	20000	10000	6666.67	4000	2000	1000	200
FAD	C27H33N9O15P2	100000	20000	10000	6666.67	4000	2000	1000	200
ADP	C10H15N5O10P2	10000	2000	1000	666.67	400	200	100	20
ATP	C10H16N5O13P3	10000	2000	1000	666.67	400	200	100	20

### 2.3.6 Extracellular-metabolite extraction

Medium controls (50% FBS with MilliQ water) and biofilm supernatants were transferred into reaction tubes (1.5 mL, Greiner bio-one GmbH, Germany) containing ice cold chloroform:methanol:water (ChCl<sub>3</sub>:MeOH:H<sub>2</sub>O) (1:3:1 v:v:v) at a ratio of 1:40 (sample:extraction solvent). The reaction tubes were vortexed at maximum speed for 15 seconds (Vortex Genie 2, Scientific Industries, NY, USA) and stored at -80°C prior to analysis.

### 2.3.7 Intracellular-metabolite extraction

Cell culture cover slips were removed from the wells and placed in bijoux containing ice cold 10 mM ammonium bicarbonate. The bijoux were sonicated at maximum speed for 10 minutes at 4°C (XUB5, 4.5 L, Grant Instruments, Cambridgeshire, UK). The supernatants, including the debris, were removed and placed in clean reaction tubes. The biofilm suspensions were centrifuged at 3000 rpm for 5 minutes at 4°C, the supernatants were removed, and 1 mL of a 1 mL:1 g extraction solvent (ChCl<sub>3</sub>:MeOH:H<sub>2</sub>O 1:3:1 v:v:v) : 0.1 mm acid washed glass beads (Sigma Aldrich, USA) were added to each pellet. Bead beating was carried out at 3000 rpm for 10 minutes at 4°C (Disrupter Genie, Scientific Industries, NY, USA). The samples were centrifuged at 13000 rpm for 5 minutes at 4°C, the supernatants were removed and stored at -80°C analysis.

### 2.3.8 Metabolite identification and statistical analysis

All of the energy metabolite were matched to authentic pure standards by retention time and accurate mass and can therefore be classified under the alphanumeric metabolite coding scheme as HRMS<sup>1</sup><sub>a</sub>, R<sub>ta</sub> as described by Sumner *et al.* (2014).

For biofilm samples, raw mass spectrometry data was processed using Quan Browser software, part of the Thermo Xcalibur<sup>TM</sup> (version 2.2.42) suite. Core metabolite identifications were validated against a panel of unambiguous authentic pure standards (Sigma-Aldrich) using high resolution accurate mass and RT (error of 3 ppm was allowed), and could therefore be classified as HRMS<sup>1</sup><sub>a</sub>, R<sub>ta</sub>, as described by Sumner *et al.* (2014). Detected peak intensities were logged (base 2), and quantification was performed on sets of biological replicates. For IC-MS analysis, five independent biological replicates were used with standard deviation calculated and recorded for each compound.

## **Chapter 3. *S. aureus* and *C. albicans* dual-species biofilm characterisation**

*The work presented within this chapter (sections of which have been submitted for publication) was carried out with the assistance of Ryan Kean at the University of Glasgow Dental School.*

### 3.1 Introduction

*Staphylococcus aureus* and *Candida albicans* frequently coexist within the human host as complex biofilm communities (Adam et al., 2002; Baena-Monroy et al., 2005). *S. aureus* and *C. albicans* are leading pathogens in bloodstream and systemic infections, and cause morbidity and mortality in hospitalized patients. These two organisms are of significant interest because of the escalating development of antimicrobial resistance and the increasing awareness of the involvement of polymicrobial biofilms in chronic and systemic infections (Perlroth, Choi, & Spellberg, 2007). These prokaryote and eukaryote have been shown to co-aggregate together; existing within a dynamic and interactive state (Peters, Jabra-rizk, et al., 2012; Peters, Ovchinnikova, et al., 2012; Shirtliff, Peters, & Jabra-Rizk, 2009). It appears that in an analogous manner to *C. albicans* and oral streptococci biofilms, yeast cells have the capacity to modulate the action of antibacterial agents and staphylococci, which can also affect the activity of antifungal agents in these biofilms (Adam et al., 2002). For example, it has been reported that the presence of *C. albicans* along with *S. aureus* protects the bacteria against vancomycin treatment up to concentrations as high as 1600mg/mL, which has been suggested to be a multifactorial process (Harriott & Noverr, 2009, 2010). Importantly, their interaction has been associated with enhanced pathogenic behaviour, disease severity and morbidity (Nair, Biswas, Götz, & Biswas, 2014).

The ability of these microorganisms to co-colonize or co-infect has been demonstrated in a clinical setting. In denture stomatitis patients, an archetypal polymicrobial disease, a high incidence of mixed colonization by both species has been demonstrated (Baena-Monroy et al., 2005). While not life-threatening, this is a disease of chronic inflammation, suggesting a degree of synergy between *S. aureus* and *C. albicans*. It is not uncommon to find these

two organisms preferentially isolated from sonicated vascular catheters, which is coincidental with positive blood cultures (Sherertz et al., 1990). Furthermore, mixed bacterial–fungal biofilms have been shown to be associated with a multitude of other conditions including infections of endotracheal tubes, biliary stents, silicone voice and orthopaedic prostheses and acrylic dentures (Peters, Jabra-rizk, et al., 2012). Collectively, these clinical observations give credence in the study of the interactions between these two important nosocomial bloodstream pathogens. The importance of this has already led to significant commentary on their interactions and its implications for disease (Nair et al., 2014; Shirtliff et al., 2009).

Experimentally, there have been some interesting mechanistic observations. It has been shown that *S. aureus* preferentially adheres to hyphal elements of *C. albicans*, relying on the adhesion to the agglutinin-like sequence 3 protein (Als3p) from *C. albicans* to adhere to its hyphae, though it is likely that other proteins are involved (Peters et al., 2010a; Peters, Ovchinnikova, et al., 2012). It is thought that adhesion to the hyphae, one of *C. albicans* most influential virulence factors, may assist *S. aureus* in penetrating into the host, a manner analogous to injection from a needle-stick injury. This has been demonstrated in mice studies, where in mixed infections those mice infected with *C. albicans*  $\Delta$ als3 strains along *S. aureus* were unable to invade the tongue, whereas the wild type infections demonstrated co-infection (Peters, Ovchinnikova, et al., 2012). The ramifications of this enhanced invasive capacity have been shown historically to impact mortality, where synergism between the co-infection intraperitoneally in a mouse model was shown to lead to 100% mortality, whereas mono-species infections caused no mortality whatsoever (Eunice Carlson, 1983). Whether or not the relationship between the two organisms is physical or chemical remains to be determined, although there is evidence that growth related synergy is an important factor in their co-habitation of micro-niches (Eunice Carlson & Johnson, 1985a). The

physical relationship between the organisms is important, but not fundamental, as recent studies have indicated that morphogenesis, i.e. the presence of hyphae, is not a critical factor in their pathogenic potential as demonstrated in some intricate mice studies using *C. albicans* genetically locked into the yeast state (Nash, Peters, Palmer, Fidel, & Noverr, 2014). However, these studies do suggest that the physical aspects of the interaction may be host site specific.

One key feature of this study was the implication for the role of inflammation and its role in disease outcomes (Nash et al., 2014). This could suggest that in addition to the physical cellular interactions, chemical signalling between the microorganisms may play an important additional role in alerting the host. Understanding this may be crucial in improving clinical management. Chemically mediated signalling is suggestive of quorum sensing, which could potentiate both positive and negative interactions between these two microorganisms, which inadvertently potentiates host immunity. Interestingly, *C. albicans* produces a quorum sensing molecule farnesol that has been shown to impact cell membrane integrity, viability and susceptibility to clinically important antibiotics (Jabra-Rizk, Meiller, James, & Shirliff, 2006). In the context of orthopaedic research similar data has been observed, with farnesol also eliciting negative effects on osteoblastogenesis (Unnanuntana, Bonsignore, Shirliff, & Greenfield, 2009). Therefore, this supports the idea that the interaction between the two microorganisms may have detrimental effects on the host. If the work in *Streptococcus gordonii* and *C. albicans* is extrapolated, then it can be surmised that a bidirectional relationship is likely to exist between *S. aureus* and *C. albicans* (Bamford et al., 2009).

The **aim** of this study was to test the hypothesis that *S. aureus* and *C. albicans* intimately interact with one another through chemical and protein mediated interactions. The goal was to investigate the relationship between *S. aureus*

and *C. albicans*, utilising a variety of macroscopic, microscopic and molecular techniques. The results obtained from the analysis of the polymicrobial biofilm were compared to those obtained from the individual bacterial and fungal biofilms in the hope that the differences recorded would enable elucidation of the physical and molecular interactions between these two nosocomial pathogens to be determined.

## 3.2 Material and methods

The materials and methods are the same as those described in Chapter 2.

Transcriptional analysis was attempted for a number of *S. aureus* MSCRAMM proteins. However, very low quantities of RNA were collected, which resulted in insufficient levels of cDNA production.

## 3.3 Results

### 3.3.1 Growth curves

Four different types of media were investigated to determine the optimum growth conditions for the mono-species *S. aureus* and *C. albicans* cultures and the dual-species cultures (Fig. 3-1). Trypticase soy broth (TSB) favours the growth of the co-culture and *S. aureus* (Fig. 3-1 A). There are considerably lower levels of growth of *C. albicans* in TSB, apparent after 6 hours of incubation, when the growth curves begin to plateau; where there is a significant difference ( $p = 0.002$ ) between the co-culture and *C. albicans* growth (Fig. 3-1 A). This significant difference in growth between the co-culture and *C. albicans* continues for the duration of the 24 hour incubation period ( $p < 0.0001$ ).

Brain-heat infusion is preferential for the growth of bacteria, and as such higher levels of growth were recorded for *S. aureus* and the co-culture (Fig. 3-1 B). After 24 hours of incubation the organisms appeared to still be growing at an exponential rate, signified by the absence of a curve plateau (Fig. 3-1 B). There is a significant difference in the growth profile of the *C. albicans* cultures and the co-cultures ( $p = 0.001$ ).

*C. albicans* and the co-culture grew at similar rates in the Roswell Park Memorial Institute (RPMI) media, but the media does not support the growth of *S. aureus* (Fig. 3-1 C). There was a significant difference ( $p = 0.0002$ ) between *S. aureus* and co-culture growth profiles after 8 hours of growth, when the growth began to plateau (Fig. 3-1 C). This significant difference in the growth rates of *S. aureus* and the co-culture continued for the remainder of the 24 hour incubation period ( $p < 0.0001$ ).

The levels of growth when the mono- and dual-species cultures were incubated in 50% foetal bovine serum (FBS) were lower than those recorded for TSB, BHI and RPMI (Fig. 3-1 D and A-C). However the growth levels between *S. aureus*, *C. albicans* and the co-culture were all comparable to one another, with no significant difference recorded after 10 hours of incubation, when the growth curves begin to plateau ( $p = 0.111$  for *C. aureus* vs. co-culture, and  $p = 0.216$  for *S. aureus* vs. co-culture) (Fig. 3-1 D). No significant differences in the growth levels were detected between *S. aureus*, *C. albicans* and the co-cultures ( $p = 0.117$  and  $p = 0.085$ , respectively) for the remainder of the 24 incubation (Fig. 3-1 D).

50% FBS was chosen as the culture media for further the mono- and dual-species biofilm analysis as the media equally supported the growth of the mono- and dual-species cultures.

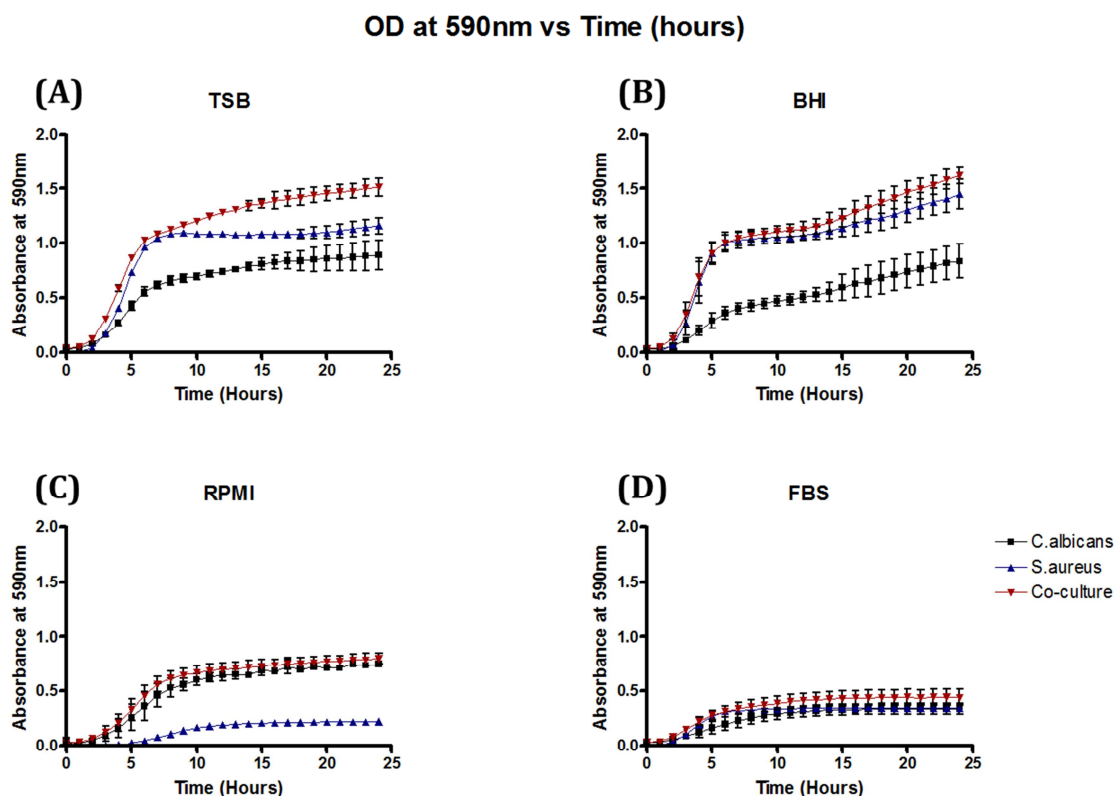


**Figure 3-1** A comparison of the growth curves of *C. albicans*, *S. aureus* and their co-culture in various media. (A) trypticase soy broth (TSB), (B) brain-heart infusion (BHI), (C) RPMI and (D) 50% foetal bovine serum (FBS). Absorbance measured at 590 nm every hour over 24 hour incubation at 37°C. Error bars  $\pm$  standard deviation (S.D). (n=3).

### 3.3.2 Biomass assay

The results obtained from the biomass assay suggest that although the level of growth between *S. aureus*, *C. albicans* and their co-culture are similar when cultured in 50% FBS, their ability to form biofilms is quite different (Fig. 3-2). FBS does not support *S. aureus* biofilm formation as a mono-species (Fig. 3-2 A and B (b)). *S. aureus* were present after 24 hours of growth, but an average absorbance of 0.057 suggested that the bacteria had formed very poor biofilms. *C. albicans* readily formed strong biofilms after 24 hours of growth, with an average absorbance of 1.120; - approximately a 20 fold increase in biomass compared to the *S. aureus* mono-species (Fig. 3-2). The dual-species biofilm displayed the greatest biomass, with an average absorbance of 1.476

(Fig. 3-2A). The biomass of the co-culture was significantly increased ( $p < 0.0001$ ) in comparison to both mono-species biofilms (Fig. 3-2 A). When the biofilms were stained using crystal violet (CV) the differences in biomass between the three cultures could be seen easily (Fig. 3-2 B).

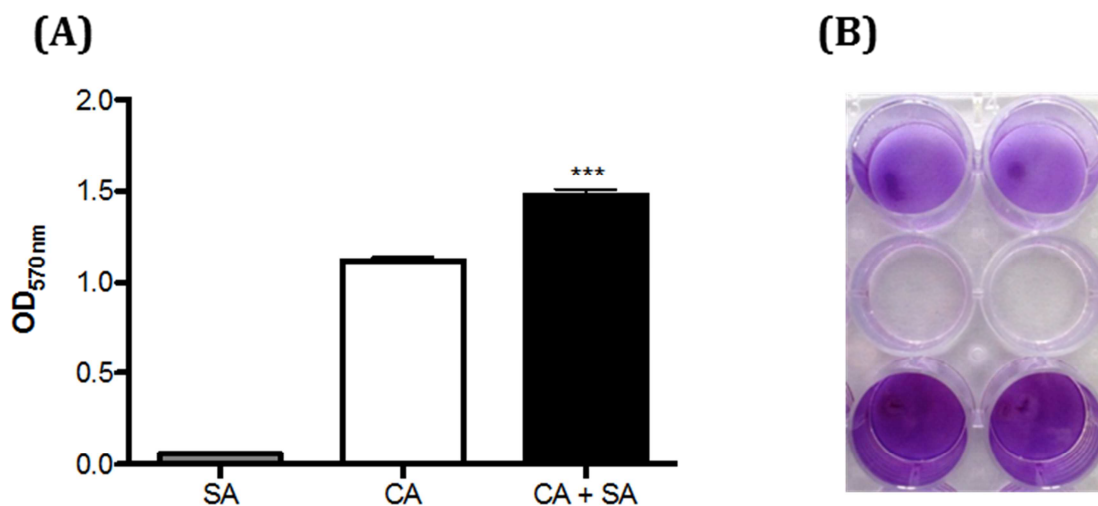


**Figure 3-2** Biomass comparison of *C. albicans*, *S. aureus* and their co-culture in 50% FBS by crystal violet (CV) staining. (A) Bar chart and (B) Macroscopic image. Well plate lay out was as follows: top row = *C. albicans*; middle row = *S. aureus*; bottom row = co-culture. CV stained and absorbance measured at 530 nm after 24 hours growth at 37°C.  $p^{***} < 0.001$ . Error bars  $\pm$  standard deviation (S.D). (n=3).

The results obtained from the CV staining assay provided a qualitative description of biomass for the mono- and dual-species biofilms. To determine the actual quantity of *S. aureus* and *C. albicans* present in the mono- and dual-species biofilms, a molecular approach was adopted comparing the colony-forming equivalents (CFE) of each mono-culture to the co-culture (Fig. 3-4).

Relative standard curves were produced for each organism using the method described in Chapter 2: Materials and methods (Graphs can be found in Appendix I). The curves displayed great linearity with linear regression

coefficients of 0.999 and 0.982 obtained for *S. aureus* and *C. albicans*, respectively (Appendix I). The CFE for each organism within the mono- and co-culture was then calculated in comparison to these standard curves.

### 3.2.2.1 Simultaneous growth

There is a significant 1.91 fold decrease in the CFE of *C. albicans* when the organism was cultured in the presence of *S. aureus* (Fig. 3-3). Conversely, a significant increase of *S. aureus* CFE was recorded, when *S. aureus* was cultured in the presence of *C. albicans* (Fig. 3-3). There was a 19.64 fold increase in *S. aureus* in the co-culture compared to the mono-species culture.

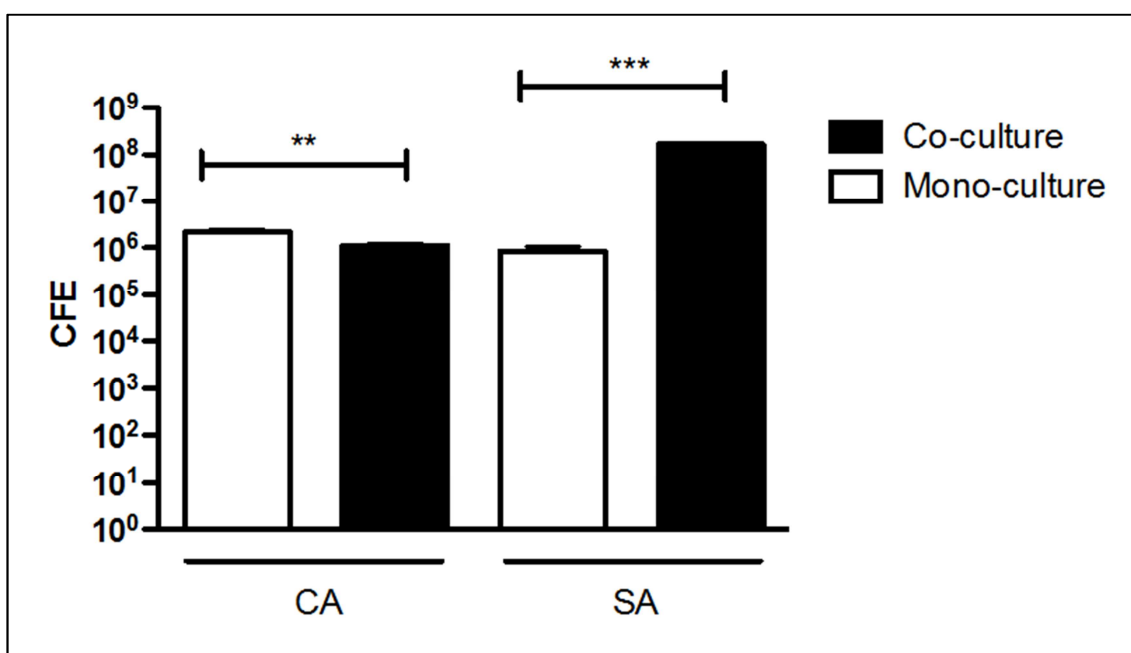


**Figure 3-3** Bar charts comparing the average colony-forming equivalents (CFE) for *C. albicans* (CA) and *S. aureus* (SA) in their mono- and co-cultures. Biofilms were grown in 50% FBS. The biofilms were washed and then sonicated in PBS to remove the biofilm from the coverslips. DNA was extracted from the samples using the fungal/bacterial DNA extraction method and quantified using qPCR, using species specific primers. Previously assembled standard curves were used for DNA quantitation.  $p^{**} < 0.01$ ,  $p^{***} < 0.001$ . Error bars  $\pm$  standard deviation (S.D). (n = 3).

### 3.2.2.2 Sequential growth

Quantitation was also carried out for the sequential growth of *C. albicans* and *S. aureus*. When *C. albicans* cells were added to a mature *S. aureus* biofilm (grown for 24 hours prior to *C. albicans* inoculation), the quantity of the fungus decreased significantly in the co-culture in comparison to its mono-species counterpart (Fig 3-4 A). There was a 2.94 fold decrease of *C. albicans* in the co-culture compared to the mono-culture after 48 hours of growth (Fig. 3-4 A). When the quantity of *S. aureus* in this co-culture was compared to the *S. aureus* mono-cultured biofilm, there was a significant 27.50 fold increase in the quantity of the bacteria (Fig.3-4 A).

The addition of *S. aureus* cells to a mature *C. albicans* biofilm resulted in a significant decrease in the number of *C. albicans* CFE; a 2.06 fold decrease compared to the *C. albicans* mono-culture (Fig. 3-4 B). The quantity of *S. aureus* in the co-culture significantly increased where a 7 fold increase in CFE was recorded compared to the *S. aureus* monoculture (Fig.3-4 B).

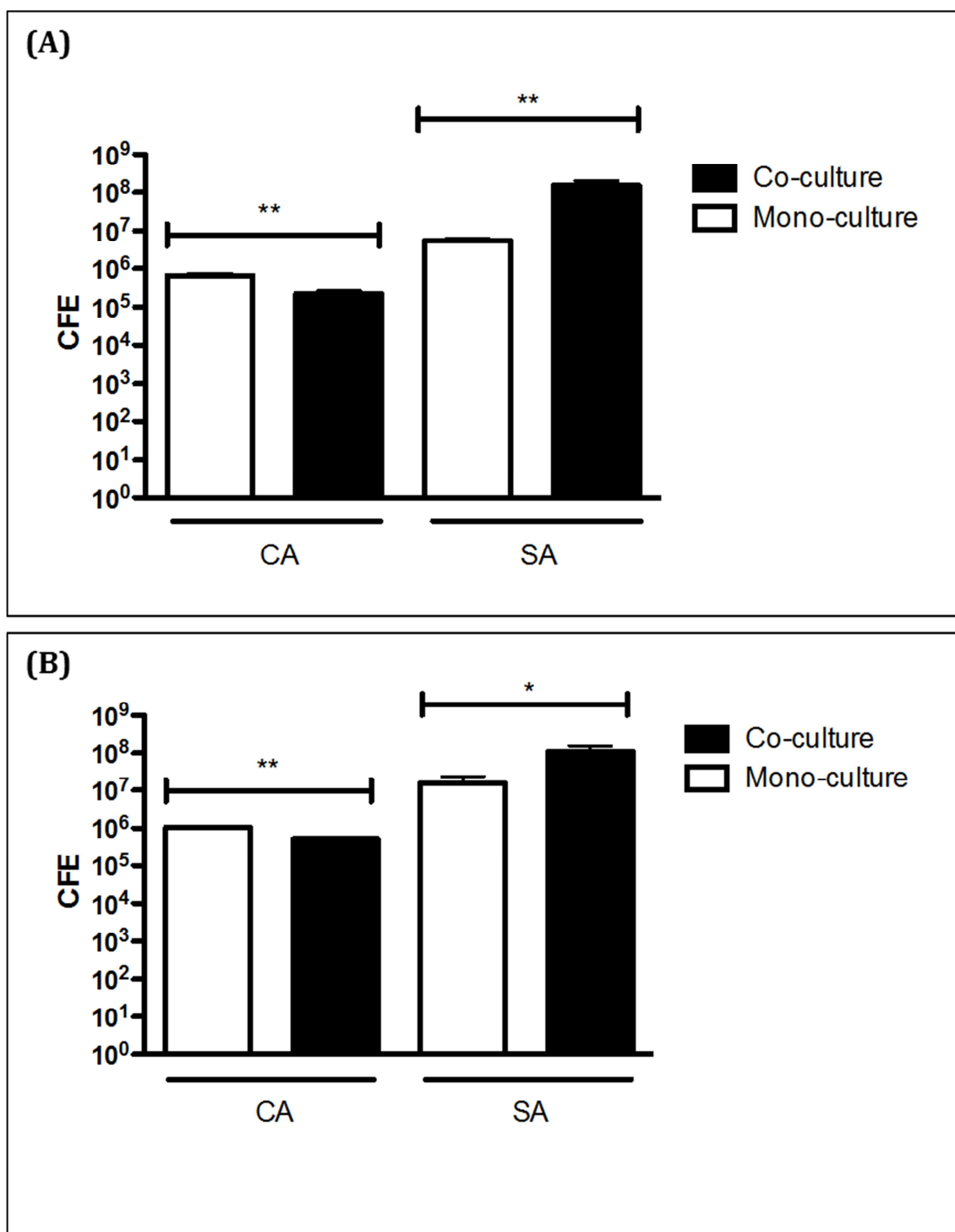


**Figure 3-4** Bar charts comparing the average colony-forming equivalents (CFE) for *C. albicans* (CA) and *S. aureus* (SA) in their mono- and co-cultures after the addition of (A) CA to a mature SA biofilm and (B) SA to a mature CA biofilm. CA (A) and SA (B) were added to the mature biofilms after 24 hours of growth and incubated for a further 24 hours. Biofilms were grown in 50% FBS. The biofilms were washed and then sonicated in PBS to remove the biofilm from the coverslips. DNA was extracted from the samples using the fungal/bacterial DNA extraction method and quantified using qPCR, using species specific primers. Previously assembled standard curves were used for DNA quantitation.  $p^* < 0.05$ ,  $p^{**} < 0.01$ . Error bars  $\pm$  standard deviation (S.D). (n = 3).

### 3.3.3 Biofilm visualisation

#### 3.3.3.1 Fluorescence microscopy

After 24 hours of growth in 50% FBS *S. aureus* produced very poor, sparsely populated biofilms when it was cultured on its own (Fig. 3-5). *C. albicans* formed a densely populated filamentous biofilm in its mono-species culture (Fig. 3-6). When the organisms were cultured together *C. albicans* formed biofilms similar to the compact, filamentous observed in its mono-culture (Fig. 3-7). Observed around these structures were large clusters of *S. aureus* populations interspersed throughout the biofilm (Fig. 3-7).

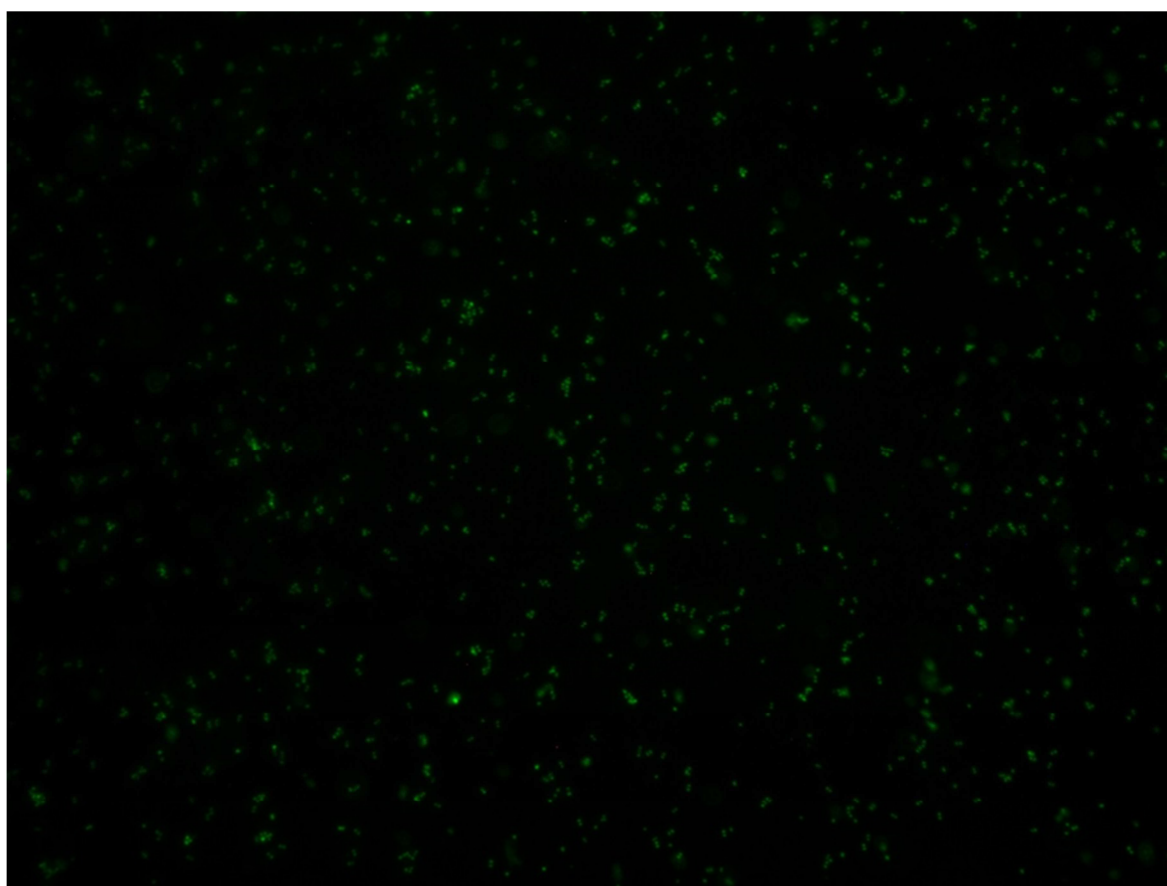


**Figure 3-5** Fluorescent images of *S. aureus* with fluorescently stained nucleic acids (green) and chitin (blue). Magnification: x40. After 24 hours of growth in 50%FBS the biofilms were washed in PBS and fixed in methanol (overnight). The biofilms were stained with fluorescent dyes and imaged using a fluorescence microscope. The SA biofilm is poorly formed, sparsely populated with bacterial cells Blue: Calcofluor white; green: SYTO9.

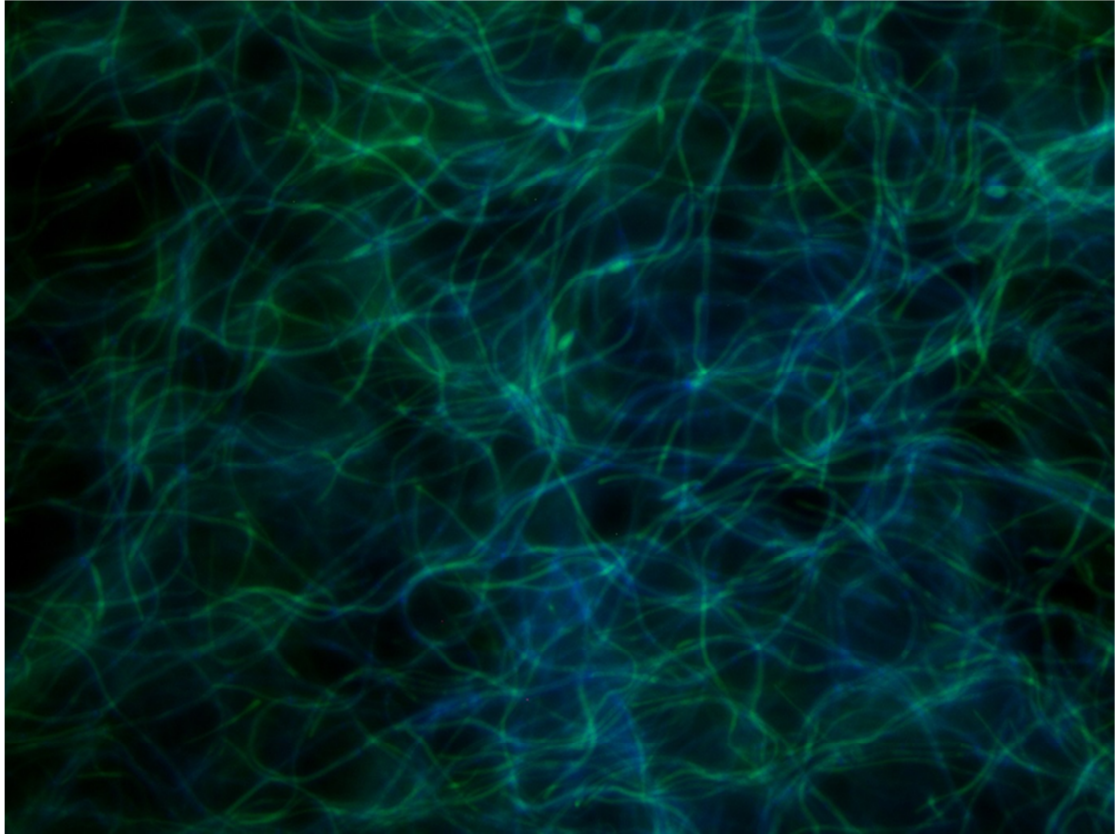


**Figure 3-6** Fluorescent images of *C. albicans* (CA), with fluorescently stained nucleic acids (green) and chitin (blue). Magnification: x40. After 24 hours of growth in 50%FBS the biofilms were washed in PBS and fixed in methanol (overnight). The biofilms were stained with fluorescent dyes and imaged using a fluorescence microscope. CA readily forms densely packed filamentous biofilms in FBS. Blue: Calcofluor white; green: SYTO9.

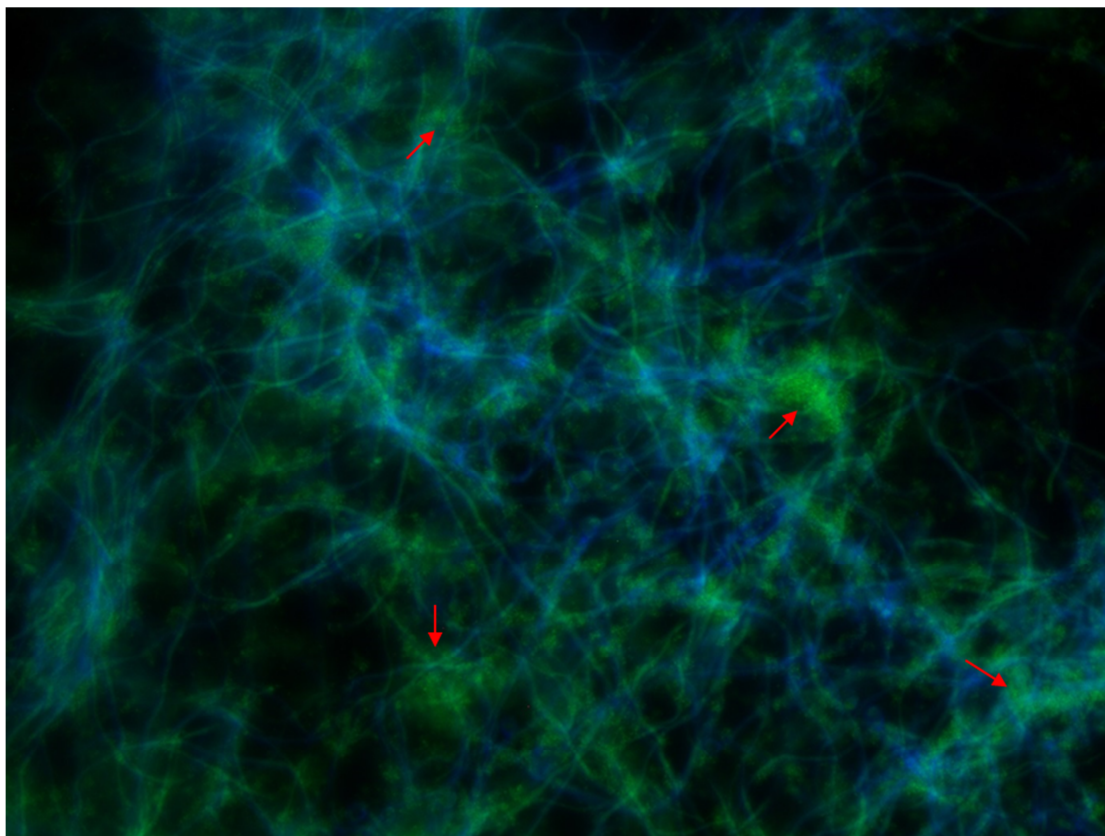


**Figure 3-7** Fluorescent images of *S. aureus* and *C. albicans* co-culture, with fluorescently stained nucleic acids (green) and chitin (blue). Magnification: x40. After 24 hours of growth in 50%FBS the biofilms were washed in PBS and fixed in methanol (overnight). The biofilms were stained with fluorescent dyes and imaged using a fluorescence microscope. SA has colonised areas on *C. albicans* with coccoid cells (arrows) in the polymicrobial biofilm. Blue: Calcofluor white; green: SYTO9.

### 3.3.3.2 Scanning electron microscopy (SEM)

SEM imaging of the *S. aureus* mono-culture confirmed that *S. aureus* was unable to form strong biofilms in FBS (Fig.3-8). The biofilms produced by the bacteria were sparsely populated with very little extracellular matrix (ECM) production (Fig. 3-8 B). As expected, *C. albicans* formed good biofilms in FBS which comprised dense networks of filamentous hyphae (Fig. 3-9).

The addition of *C. albicans* to the preformed *S. aureus* biofilms resulted in a biofilm that looked similar to the mono-species *C. albicans* biofilm (Figs. 3-9

& 3-10). The biofilm consisted of the *C. albicans* hyphal network interspersed with very few *S. aureus* (Fig. 3-10). This image suggested that the fungal biofilm could be forming over the top of the bacterial biofilm, with no interaction occurring between the two organisms.

Simultaneous co-culture of *S. aureus* and *C. albicans*, and the addition of *S. aureus* to a preformed *C. albicans*, produce almost identical biofilms. The bacteria adhere to the hyphae and ECM of the fungi (Fig. 3-11). The coccoid cells of the bacteria clustered around the filamentous structures and were coated in ECM (Fig. 3-11). It could not be determined whether the ECM was a product of the fungi, bacteria or both organisms from the SEM images. The hyphae of the *C. albicans* appeared wrinkled in comparison to the mono-species *C. albicans* hyphae (Fig. 3-9 - 11).

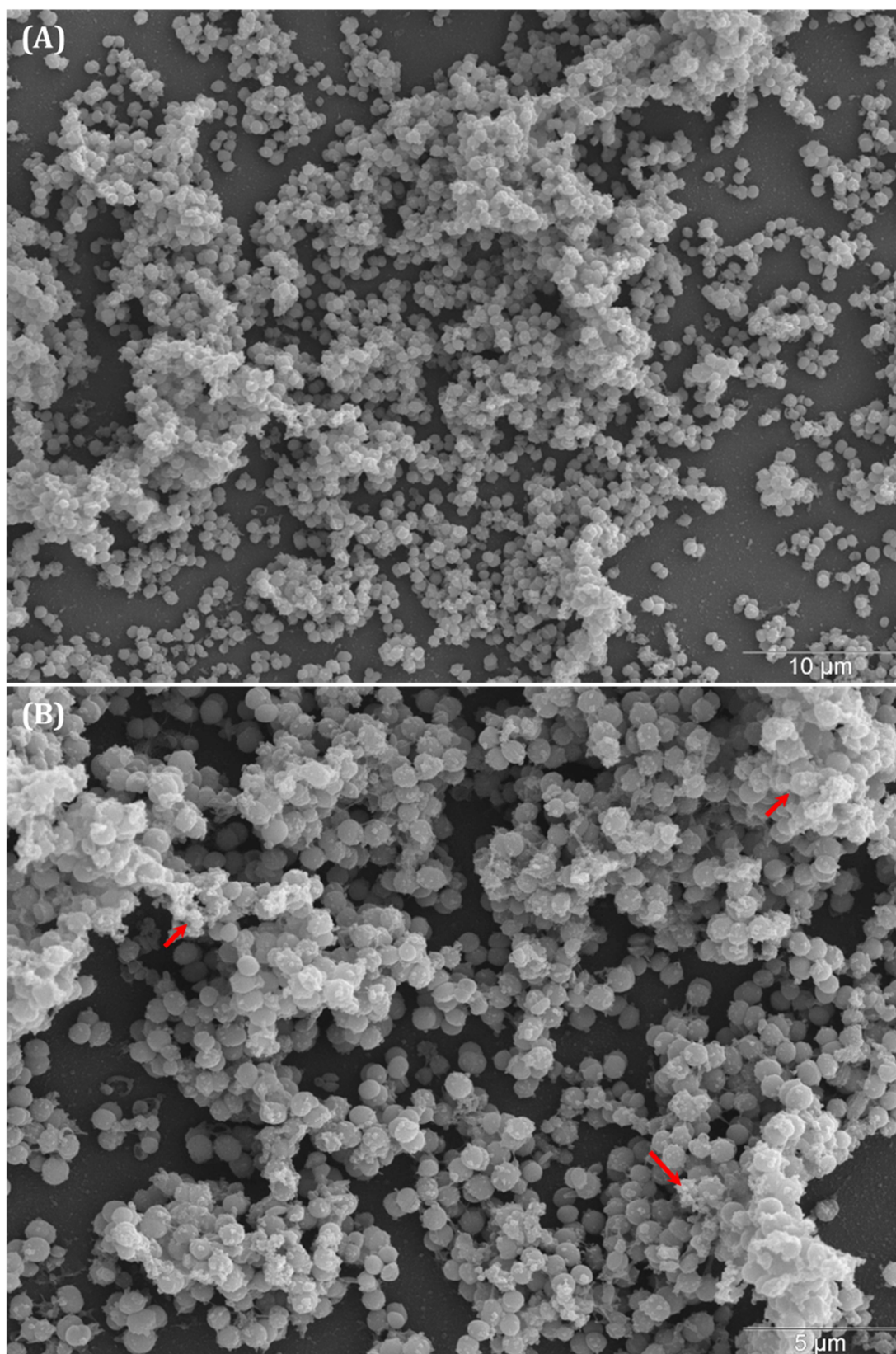


**Figure 3-8** Secondary electron images of *S. aureus* (SA) at (A) 2000x and (B) 4000x magnification. Biofilms were grown for 24 hours before being washed in PBS and fixed using aldehydes. The fixed biofilms were imaged using a JEOL JSM-6400 microscope. The SA biofilm is sparsely populated with large voids in the structure (A & B). There is little extra cellular matrix production (arrows) indicating poor biofilm development (B). Scale bars = 10 μm (A) and 5 μm (B).

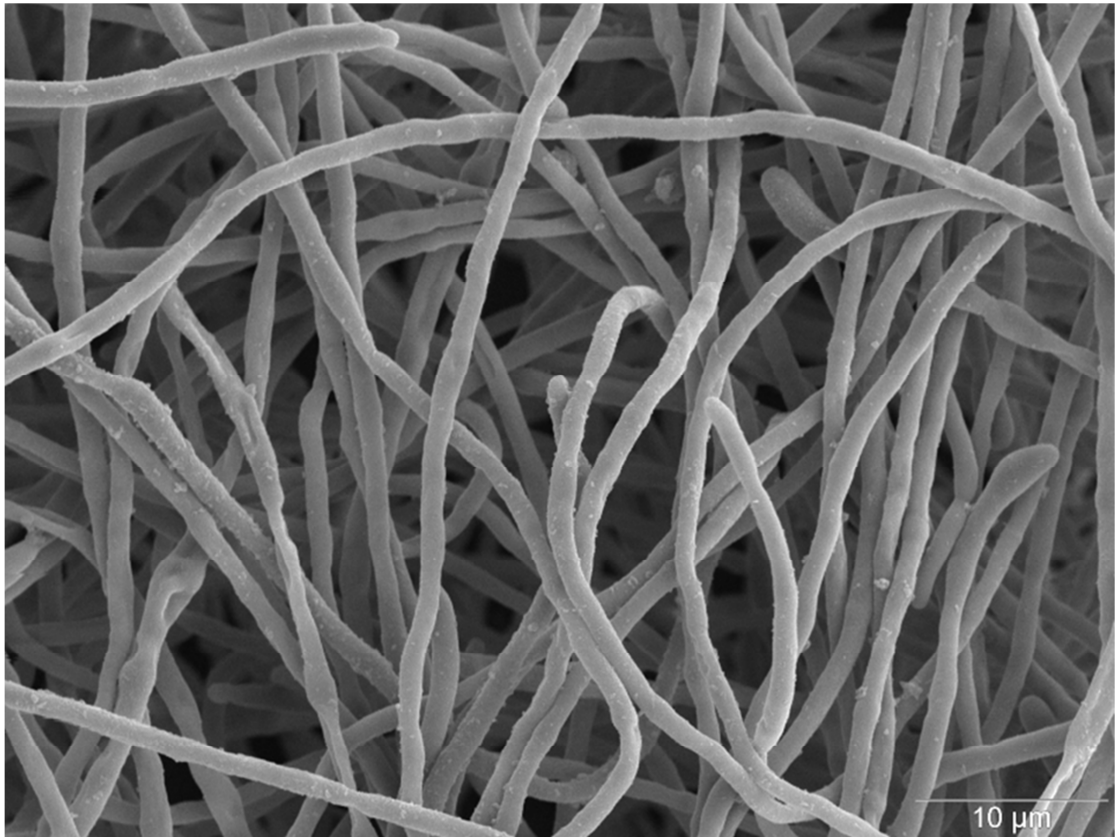


**Figure 3-9** Secondary electron images of *C. albicans* (CA). Biofilms were grown for 24 hours before being washed in PBS and fixed using aldehydes. The fixed biofilms were imaged using a JEOL JSM-6400 microscope. The biofilm is densely populated with layers of interlinking filamentous hyphae. Scale bar = 10 μm.

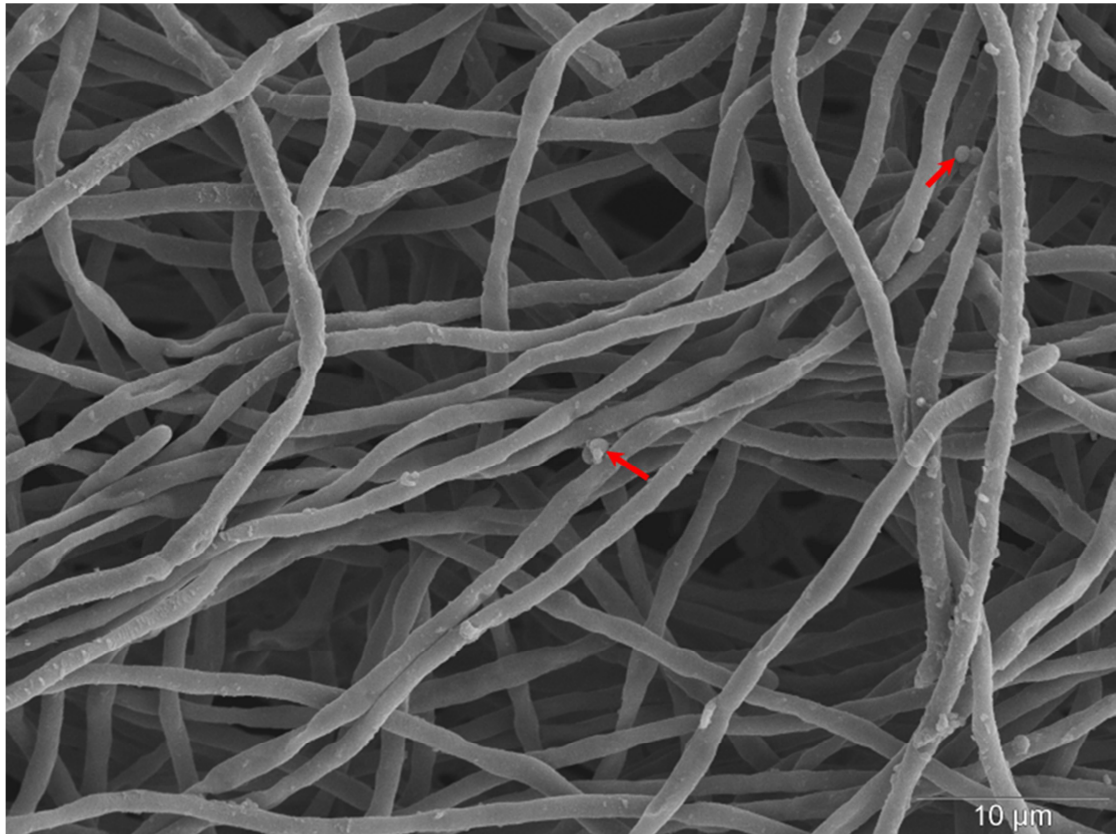


**Figure 3-10** Secondary electron images of the co-cultured biofilm. *S. aureus* was grown in 50% FBS for 24 hours. *C. albicans* was added to the mature biofilm and the co-culture incubated for a further 24 hours. The mature biofilms were washed in PBS and fixed using aldehydes. The fixed biofilms were imaged using a JEOL JSM-6400 microscope. The biofilm is mainly composed of *C. albicans* with very few *S. aureus* cells (arrows) present. Scale bar = 10 μm.

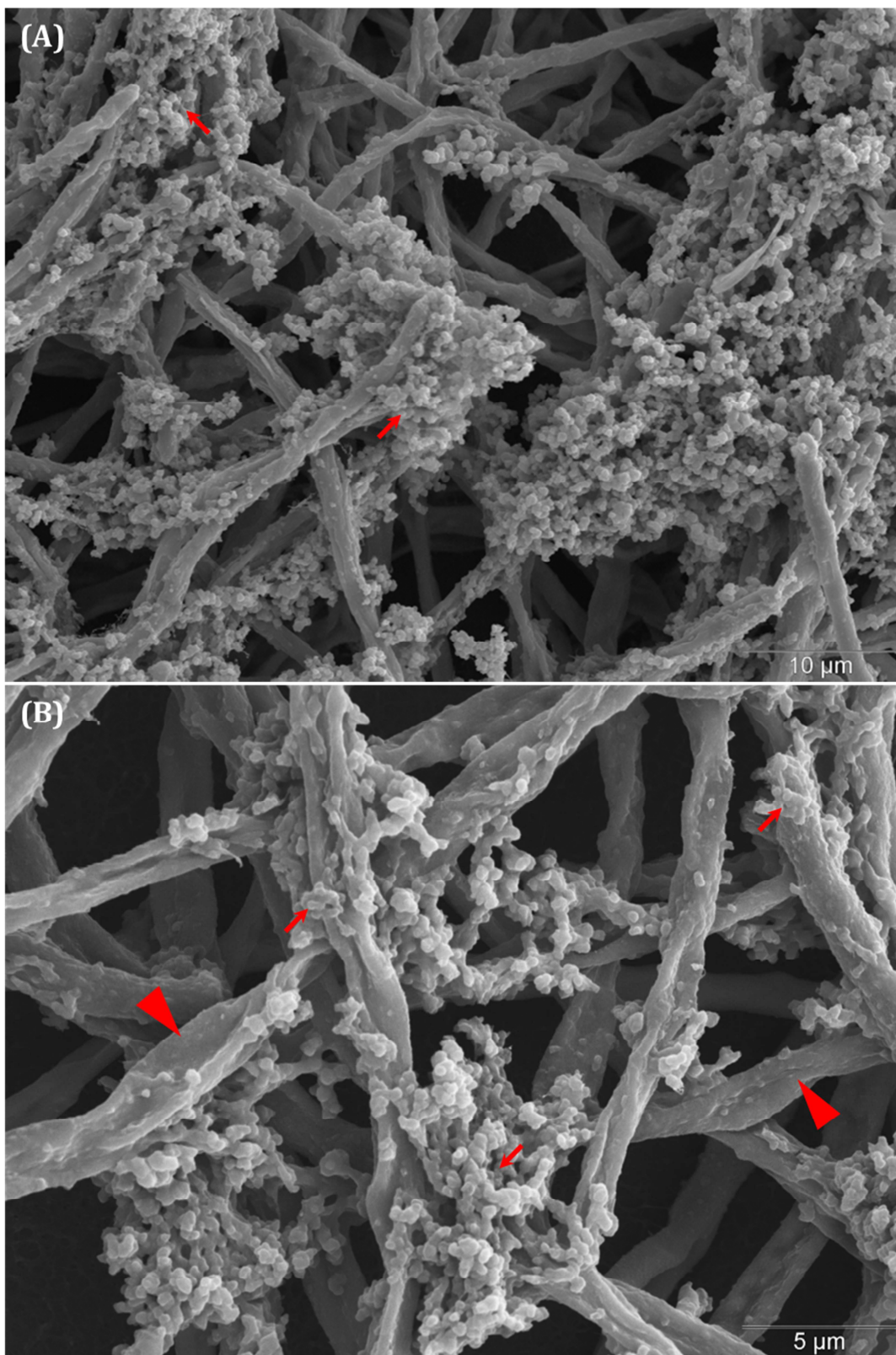


**Figure 3-11** Secondary electron images of the *S. aureus* and *C. albicans* dual-species biofilm at (A) 2000x and (B) 4000x magnification. Biofilms were grown for 24 hours before being washed in PBS and fixed using aldehydes. The fixed biofilms were imaged using a JEOL JSM-6400 microscope. The *S. aureus* coccoid cells covered in extracellular matrix (ECM) (arrows) aggregate around the hyphal structures of the *C. albicans* cells (A & B). The wrinkled hyphae (arrow heads) suggest hyphal cell damage caused by presence of *S. aureus*. Scale bar = 5 μm.

### 3.3.4 Transcriptional analysis

The previous data described the interaction between *S. aureus* and *C. albicans* in terms of their physical interaction. To determine whether *S. aureus* and *C. albicans* interact at the molecular level in the dual-species biofilm, the expression levels of two key *C. albicans* genes were evaluated (Fig. 3-12).

There was a significant increase in expression of the gene encoding the cell surface protein *Hwp1* in the co-culture compared to the *C. albicans* mono-culture (Fig. 3-12 A). There was a 1.79 fold increase in percentage expression of *Hwp1* (Fig. 3-12 A). There was an increase in the expression of the adhesion gene *Als3* (Fig. 3-12 B). Although this increase was not significant, there was 2.14 fold change in expression of this gene in the co-culture compared to the mono-culture.

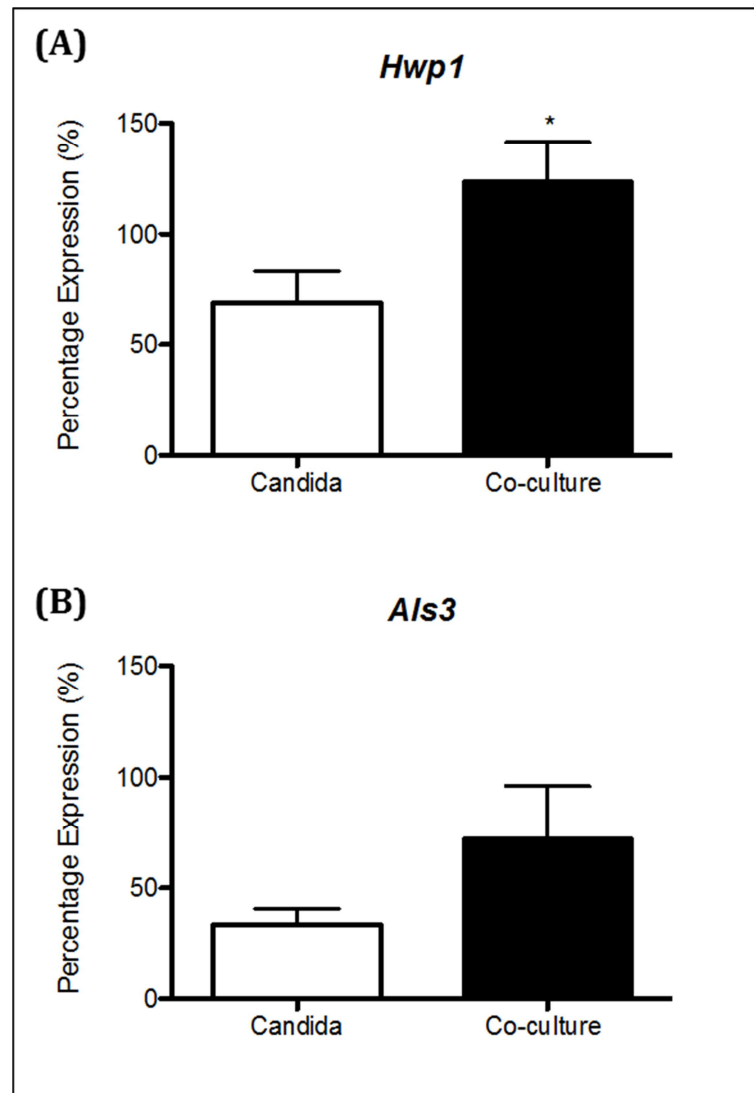


**Figure 3-12** Bar charts comparing the percentage expression of (A) *HWPI* (a filamentation protein) and (B) *ALS3* (an adhesion protein) in mono-cultured *C. albicans* compared to its co-culture with *S. aureus*. After 24 hours of growth in 50% FBS, the biofilms were washed with PBS before RNA extraction was carried out using the TRIzol® method. cDNA was synthesised and real-time PCR was used to assess the expression of the two key *C. albicans* genes. The level of expression is shown in comparison to the constitutively expressed housekeeping gene, *ACT1*. Error bars  $\pm$  standard deviation (S.D). (n=3).

### 3.4 Discussion

The aim of this study was to characterise the dual-species *S. aureus* and *C. albicans* biofilm using macroscopic, microscopic and molecular techniques to determine the physical and molecular interaction between these two nosocomial pathogens. The growth conditions were first optimised and 50% FBS chosen for the culture media due similar growth rates observed for both the mono- and dual-species cultures. This media was also more clinically relevant as the conditions were closer to those that would be present *in vivo*.

Crystal violet (CV) staining was used to determine the biomass of each of the mono- and the dual-species biofilms. The mono-species *C. albicans* and the dual-species biofilms had a high biomass, whereas the *S. aureus* mono-species failed to produce high biomass biofilms in 50% FBS. There was a significant increase in biomass observed for the co-culture suggesting that there is a synergistic increase in biomass when the bacteria and fungi are cultured together. This increase was greater even when the additive biomasses of the two mono-cultures were compared to the biomass of the polymicrobial biofilm. This result is in agreement with other co-culture studies (Peters, Ward, Rane, Lee, & Noverr, 2013).

This result was confirmed when further analysis was carried out. When fluorescence, SEM imaging and quantitation using DNA and qPCR was carried out, the biofilms produced by *S. aureus* were very poor, with large voids in the biofilm, few cell numbers and little ECM production; suggesting poor adhesion and structural stability. This result is in agreement with other *S. aureus/C. albicans* studies (Harriott & Noverr, 2009, 2010; Jey et al., 2013). Harriott et al. (2009) investigated the effect the presence of *C. albicans* had on the ability of *S. aureus* to form biofilms when grown in serum (Harriott & Noverr, 2009). They recorded that in the presence of serum, the surface was

sparsely populated and no matrix was observed; indicating a lack of biofilm formation.

When *S. aureus* and *C. albicans* were cultured together the bacteria and fungi were found interspersed throughout the biofilm. *S. aureus* appeared to form micro-colonies on the surface and they preferentially associated with the hyphal forms of *C. albicans* (Harriott & Noverr, 2009). In the images captured in this study *S. aureus* demonstrated the same preference for adherence to the *C. albicans* hyphae. This trend has been recorded in various other studies (Harriott & Noverr, 2009, 2010; Peters, Ovchinnikova, et al., 2012; Schlecht et al., 2015). Furthermore, Harriott & Noverr concluded that the ability of *S. aureus* to form polymicrobial biofilms with *C. albicans* correlated with the fungi's ability to form hyphae (Harriott & Noverr, 2010). However, this contradicts the findings from a more recent study by Nash et al. (2014) (Nash, Peters, Fidel, & Noverr, 2015; Nash et al., 2014).

Quantitation of the biofilms indicated that the number of *S. aureus* significantly increased in the polymicrobial biofilm compared to the mono-species biofilm. Conversely, the levels of *C. albicans* slightly decreased in the dual-species biofilm compared to the mono-species culture. An increase in bacterial numbers was also recorded by Harriott (Harriott & Noverr, 2009). However, Harriott recorded no change in the levels of *C. albicans* between the dual- and mono-species biofilms (Harriott & Noverr, 2009). Harriott utilized a CFU counting method for determining numbers of cells in the biofilms. The study herein utilized qPCR, which is a much more sensitive and accurate technique. This method more accurately detects differences in cell numbers using primers specific to each of the micro-organisms, which could explain the slightly contradictory findings between these two studies.

The difference in the levels of *S. aureus* recorded between the mono- and co-cultured biofilms could in part be due to the bacteria's inability to metabolise appropriate nutritional components within the sera or the carbon source being unsuitable to support subsequent growth and biofilm formation (Harriott & Noverr, 2009; Staib, Geier, & (Germany), 1971). Staib et al. (1971) showed that 37 different *S. aureus* strains could metabolize the proteolytic by-products of serum albumin produced by *C. albicans* and hence use it as a growth media, whereas undigested serum albumin was unable to support *S. aureus* growth (Staib et al., 1971). However, when Harriott investigated this using a Transwell system; in which the two organisms were separated physically, but sera components could pass freely, *S. albicans* was unable to form a strong biofilm, suggesting that cross-metabolism was not playing a key role in the polymicrobial biofilm (Harriott & Noverr, 2009). Harriott and Noverr (2010) investigated this further and found that *S. aureus* was able to form polymicrobial biofilms after being added to a *C. albicans* biofilm in which all the fungi had been killed (Harriott & Noverr, 2010). It was concluded that metabolic by-products from *C. albicans* were not required for *S. aureus* polymicrobial biofilm formation in serum (Harriott & Noverr, 2010). In the same study, when *C. albicans* biofilms were killed using formalin or heat killing, *S. aureus* were unable to form polymicrobial biofilms, suggesting that hypha-associated formalin- or heat-labile components of the *C. albicans* biofilm could be required for the attachment or biofilm formation of *S. aureus* in serum (Harriott & Noverr, 2010).

It has previously been shown that serum can interfere with the ability of bacteria to attach to abiotic surfaces (Hammond, Dertien, Colmer-Hamood, Griswold, & Hamood, 2010). Therefore, the *C. albicans* could simply be providing a physical structure for *S. aureus* attachment. Hammond et al. (2010) demonstrated that serum interfered with the attachment of *P. aeruginosa* to plastic coverslips and hence reduced or blocked biofilm

formation by the bacteria (Hammond et al., 2010). Although these results make sense with regards to host innate resistance, when Harriott tested this theory with *S. aureus* in serum, the same level of attachment was recorded for *S. aureus* grown in FBS compared to BHI (a medium which promotes *S. aureus* biofilm formation) (Harriott & Noverr, 2009). Another explanation for the increase in bacteria levels could be that *S. aureus* are using *C. albicans* as a nutrient source, through the scavenging of nutrients from the fungal cell wall, the consumption of secreted compounds or through lysis of fungal cells (D. A. Hogan & Kolter, 2002). This could also explain the lower level of fungal growth and damage to hyphae detected in the polymicrobial biofilm.

The results from this study are in agreement with the previous Harriott study. *C. albicans* facilitates the growth and promotes biofilm formation of *S. aureus* in serum, a medium that cannot support biofilm formation by *S. aureus* mono-microbial cultures and that the bacteria preferentially adhere to the hyphae of the fungi (Harriott & Noverr, 2009; Peters, Ovchinnikova, et al., 2012; Schlecht et al., 2015; Staib et al., 1971).

The reduction of the number of *C. albicans* in the polymicrobial biofilm compared to its mono-species biofilm could be the result of competition on a basic level between the bacteria and fungi. The limited amount of available nutrients could result in the bacteria out-competing the fungi, reducing fungi levels compared to the monoculture. If *S. aureus* and *C. albicans* were in competition for nutrients, the presence of the bacteria on the *C. albicans* surface may allow the bacteria to release bacterially derived antifungal compounds directly onto the fungi, which could also deplete fungi numbers (D. a Hogan, Wargo, & Beck, 2007). The *C. albicans* hyphae appear wrinkled in the polymicrobial biofilm compared to the mono-species biofilm. This could be suggestive of hyphae damage caused by the presence of *S. aureus*. As with the antagonistic relationship between *P. aeruginosa* and *C.*

*albicans*, in which the bacteria release a phenazine toxin which kills the fungi, *S. aureus* may secrete one of its many exotoxins, which could contribute to *C. albicans* cell death resulting in the fewer fungi levels recorded in this study (Dinges, Orwin, & Schlievert, 2000; Gibson, Sood, & Hogan, 2009; D. A. Hogan & Kolter, 2002; Söderquist et al., 1998). These results contradict the results recorded by Peters et al. (2010) who suggested that the relationship between *S. aureus* and *C. albicans* was entirely synergistic with no lethality to either organism (Peters et al., 2010a). However, the organisms were cultured in the *C. albicans* favouring media RPMI, so competition for nutrients may not have been as high (Peters et al., 2010a).

The trend of increased levels of *S. aureus* growth and decreased levels of *C. albicans* growth recorded for simultaneous culturing was also witnessed during sequential biofilm growth, regardless of the order in which the organisms were added to the pre-formed biofilms. The pre-formed *C. albicans* biofilm provided a biotic network of hyphae and ECM which enhanced *S. aureus* growth and promoted biofilm formation. When *C. albicans* cells were added to the poorly pre-formed *S. aureus* biofilm the same trends in bacterial and fungal cell growth were recorded. *S. aureus* is a non-flagellated, non-motile organism (Kaito & Sekimizu, 2007). The results could therefore suggest that the increase in growth of *S. aureus* within the polymicrobial biofilm isn't solely dependent on a physical interaction between the bacteria and the hyphae of the fungi. These results agree with the results obtained by Nash et al. (2014), who demonstrated that yeast-hyphal morphogenesis wasn't required for co-infection (Nash et al., 2014).

From the transcriptional analysis it was found that hyphal wall protein (*Hwp1*) was up-regulated in *C. albicans* in the polymicrobial biofilm compared to the mono-species biofilm. *Hwp1* is a key regulator in the morphological transition of *C. albicans* required for hyphal development and

also plays a role in biofilm adhesion and development (Nobile, Nett, Andes, & Mitchell, 2006; Sharkey, McNemar, Saporito-Irwin, Sypherd, & Fonzi, 1999). The up-regulation of *Hwp1* in the polymicrobial biofilm suggests that the presence of *S. aureus* within the biofilm may act as a trigger for the phenotypical transformation of *C. albicans* into its hyphal form. However, Harriott et al. (2010) concluded that although *Hwp1* was involved in polymicrobial biofilm formation, this protein was not essential to the bacterial and fungal interaction, and that it was more likely a mix of Als proteins in conjunction with *Hwp1* that was required for *S. aureus* adherence to *C. albicans* (Harriott & Noverr, 2010).

There was also a trend of increased expression of *Als3* in the polymicrobial biofilm compared to the mono-species *C. albicans* biofilm. *Als3* has been shown to mediate the adherence of *S. aureus* to *C. albicans* (Peters, Ovchinnikova, et al., 2012). Peters et al. (2012) concluded that *Als3* was required for strong adherence of *S. aureus* to the fungi's hyphae (Peters, Ovchinnikova, et al., 2012). The lack of *Als3* resulted in decreased adherence of *S. aureus* to the hyphae and an inability of the bacteria to penetrate oral epithelium compared to when the bacteria were cultured with the *C. albicans* wild type, not lacking *Als3* (Peters, Ovchinnikova, et al., 2012). Therefore, Peters concluded that *Als3* played a crucial role in the adherence process of *C. albicans* to *S. aureus*, as the hyphal adhesion acts as a receptor for the bacteria on the *C. albicans* hyphae (Peters, Ovchinnikova, et al., 2012). It is very likely that other proteins could mediate inter-species attachment and interaction, in particular the MSCRAMM (microbial surface components recognizing adhesive matrix molecules) family of *S. aureus*. Clumping factor A (ClfA) a surface-located MSCRAMM shares 3D homology with *Als3* (Edwards, 2012).

The results from this study suggest that *S. aureus* and *C. albicans* interact on a physical level and co-aggregate with one another in their polymicrobial environment. The up-regulation of two genes involved in *C. albicans* adherence and biofilm formation, indicate that the bacteria and fungi also interact at a molecular level. Although there have been a number of studies carried out to characterise the relationship and interaction between *S. aureus* and *C. albicans*, further analyses is required to fully understand the intricate relationship between these two organisms. qPCR was utilized in this study to determine the quantity of bacterial and fungal cells within the polymicrobial biofilm. Although the data generated enable the numbers to be determined, live/dead qPCR would provide a more detailed insight into the state of the biofilm. This has recently been carried out by the Ramage group (Gordon Ramage, personal communication). Particular attention should be paid to *S. aureus* and *C. albicans* surface proteins, as well as other genes which have been identified as virulence factors. This study examined the polymicrobial biofilm after 24 hours of growth, resulting in a study that focussed on a mature *S. aureus* and *C. albicans* biofilm. It is the suggestion of this author that future analysis should be carried out during initial biofilm formation, which could uncover more significant bacterial-fungal interactions in relation to attachment and subsequent biofilm formation.

**Chapter 4. Serially combined Reverse  
phase (RP)/Hydrophilic Interaction Liquid  
Chromatography (HILIC) method  
development**

## 4.1 Introduction

Small organic molecules, termed metabolites, undergo biochemical modifications during metabolic reactions which are necessary for the correct growth, maintenance and function of cells (Dettmer et al., 2007; Haggarty & Burgess, 2017). The ability of metabolomics to provide a quantitative rather than qualitative description of cellular regulation and control has led to its recognition as a powerful tool in the field of cell and systems biology (Johnson & Gonzalez, 2012; Teusink, Walsh, Van Dam, & Westerhoff, 1998). However, due to the number and complexity of metabolites in existence, it is accepted that no single analytical technique can cover the entire metabolome of even a 'simple' biological system, as the platforms selected tend to exploit specific chemical characteristics and therefore are biased towards certain classes of compounds and 'blind' to others (García-Cañaveras et al., 2016; Haggarty et al., 2015; Haggarty & Burgess, 2017).

### 4.1.1 Metabolomics techniques

LC-MS can be applied to the analysis of the majority of chemical species. Innovations in LC technology, instrumentation, and column chemistries have led to wider coverage of the metabolome.

Although there have been recent advancements in single column technologies to increase the coverage of the metabolome, including the addition of ion pairing agents and the advent of RP pentafluorophenyl (PFPP) phases that allow analysis in both reverse- and normal-phase retention (Fekete, Veuthey, & Guillarme, 2015; Lv, Palacios, Hartil, & Kurland, 2011; S. Yang, Sadilek, & Lidstrom, 2010), it is widely accepted that due to the complexity of metabolites, multiple column methods are required for optimum retention and separation of both polar and non-polar compounds (Contrepolis, Jiang, & Snyder, 2015). The coupling of columns can provide a powerful tool in the

detection of polar and non-polar metabolites, however, running two different chromatographies in parallel increases sample preparation time, as the sample buffer has to be appropriate for the solvent system used, and doubles the analysis time (Hemström & Irgum, 2006).

Traditionally, two LC methods have been implemented to improve analyte retention. Column switching utilises a 6- or a 10-port valve connected to two separate columns and pumps. The sample is loaded onto the valve and injected onto the first column and detected at the end of the run. The valve then switches to the second position and a second injection from the same sample is injected onto the 'second' system for separation and detection (Figure 4-1). This method has been successfully applied to biochemical, drug and food analysis and pesticide monitoring (Bailey & Ayling, 2013; Brabcova, Hlavackova, Satinsky, & Solich, 2013; Fernández-Ramos, Šatínský, & Solich, 2014; X. Zhang et al., 2015). In the second method, 2-dimensional liquid chromatography (2D-LC), the entire effluent is run on the first column and collected as fractions in aliquots (François, Sandra, & Sandra, 2009). The collected fractions are then either analysed in the second dimension in their entirety or specific fractions are selected for 2D analysis, termed comprehensive and heart-cutting 2D-LC, respectively (François et al., 2009). The transfer of the effluent can be carried out off-line or online using a dedicated switching valve (Figure 4-2). This method is often used in proteomics, e.g. using strong cation exchange (SCX) followed by RP, and has also been utilised in the analysis of phenolic compounds, carotenoids and bio-oils (Beelders, Kalili, Joubert, De Beer, & De Villiers, 2012; Cacciola et al., 2012; Edelmann, 2011; Le Masle et al., 2014). Many different column chemistries and lengths can be coupled using these instruments, however, the greatest coverage is witnessed when two orthogonal columns are combined (Bassanese et al., 2015; Cacciola et al., 2011; Jandera, 2008). These systems offer the user the ability to run a sample on two different stationary phases

regardless of mobile phase compatibility, with the added advantage of independent control over eluent pH and composition, gradient program, flow-rate and column temperature (Guiochon, Marchetti, Mriziq, & Shalliker, 2008). However, these methods require complicated system set-ups with expensive equipment, along with specialist knowledge and/or training meaning that these methods are often not suitable for routine use in many laboratories.

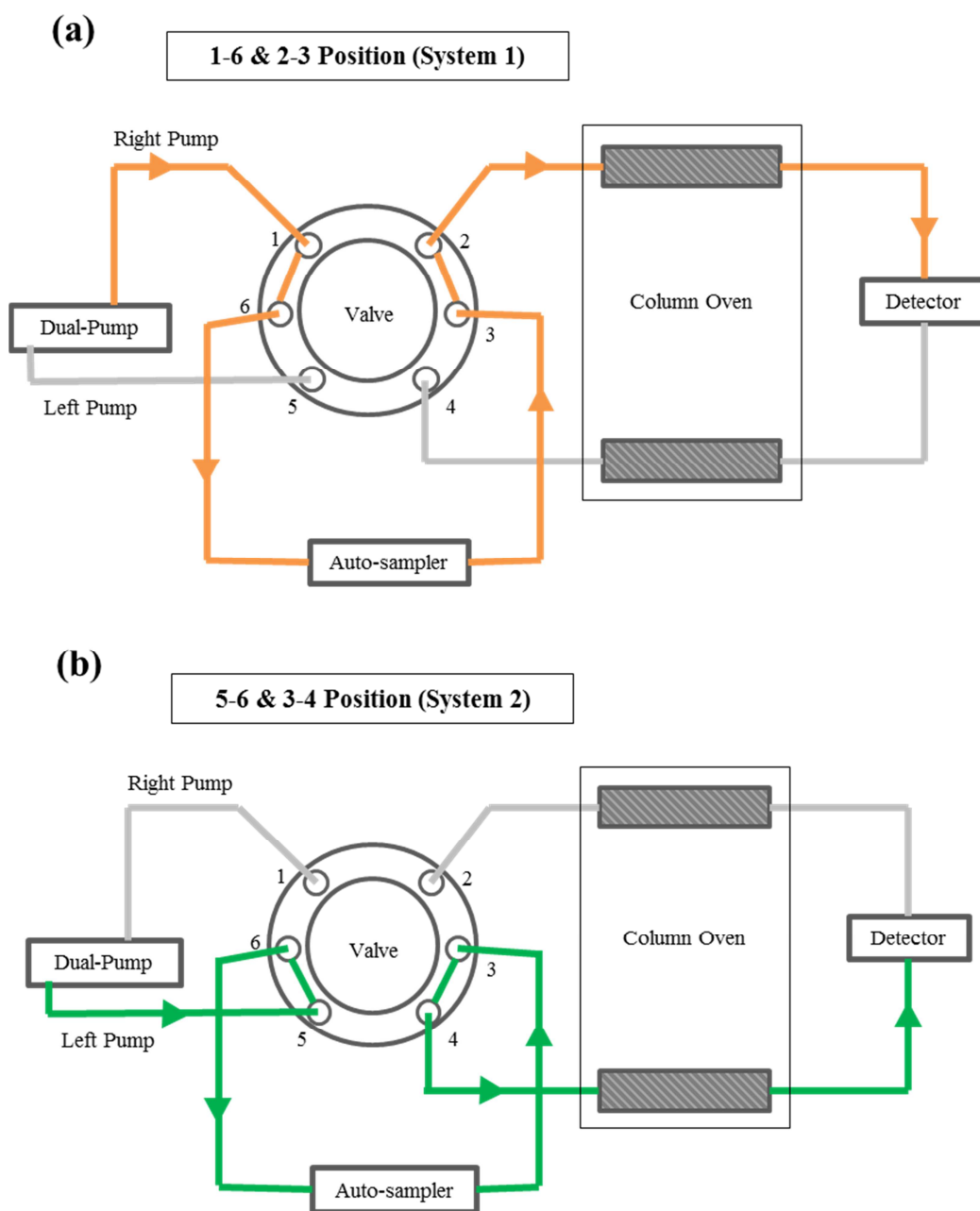


**Figure 4-1** Schematic of the novel column switching method developed by Li *et al.* (2015) that incorporates a six-port switching valve. The system shares a column oven, auto-sampler and detector. (a) In the 1-6/2-3 position the sample is injected on to the first column using the right pump (system 1). (b) When the valve switches to positions 5-6/3-4 the sample is injected on to the second column using the left pump (system 2) (Haggarty & Burgess, 2017; Y. Li *et al.*, 2015).

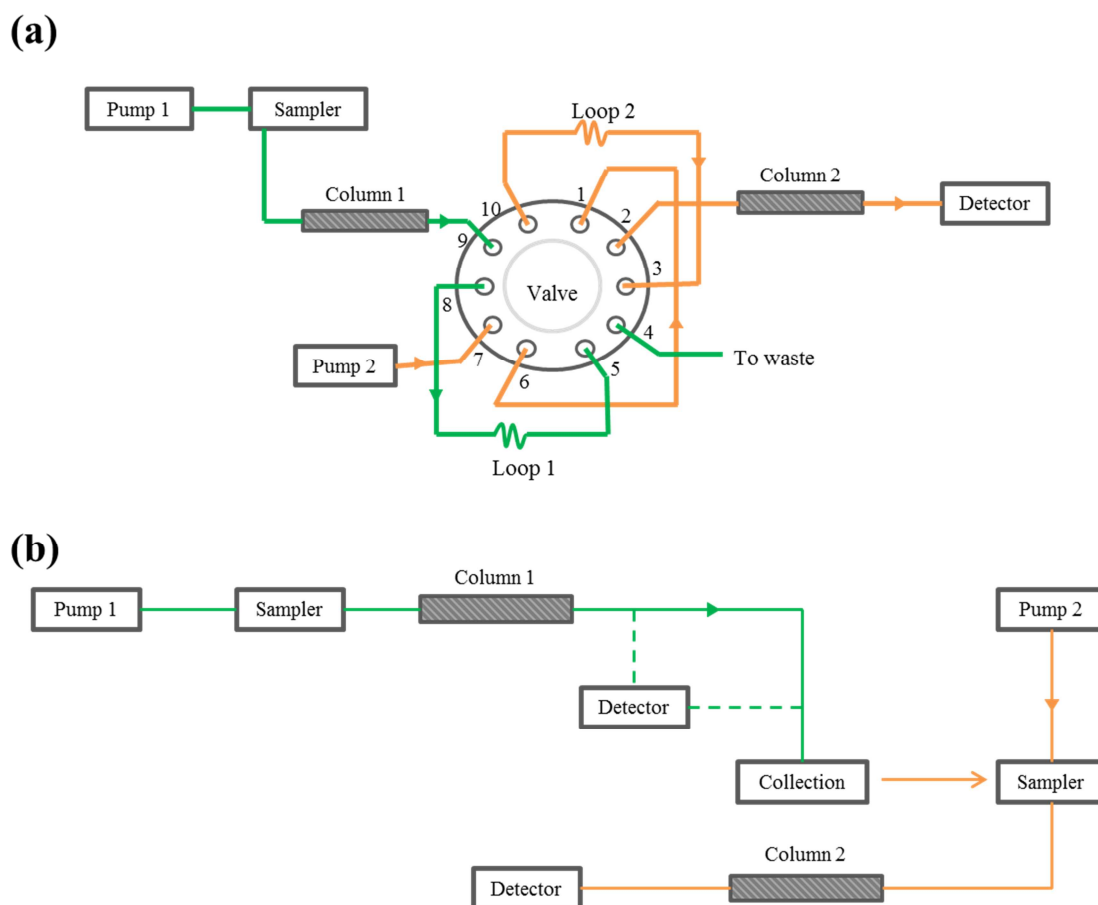


**Figure 4-2** Typical configuration for 2D-LC separations. (a) An online set-up. The sample is injected onto the first dimension and can then be collected in a sample loop before it is introduced to the second column (or dimension) by switching the valve, allowing the other loop to be concomitantly filled. (b) Off-line 2D-LC set-up. The sample is analysed in the first dimension and is then manually transferred to a second system for second dimension analysis (Z. Li, Chen, Guo, & Tang, 2016). The sample can be introduced to the column and collected in fractions, with either the analysis path running through the detector or running to the collection plate without detection.

The method of serially combining two or more columns together in tandem and running both gradients simultaneously, so that one sample injection passes through the first column and then the other in one chromatographic run, is a simple approach that has been described since the early development of LC (Benedict & Risk, 1984; Bonn, 1985; El Rassi & Horváth, 1986; Glajch, Gluckman, Charikofsky, Minor, & Kirkland, 1985; Tomellini, Hsu, & Hartwick, 1986). Various studies have been carried out previously using a variety of different stationary phase combinations; C18 columns from

different manufacturers, C18 with cyano, phenyl and amino columns, polystyrene-divinylbenzene resins and ion exchange columns, silica-based C18 columns and zirconia columns. Columns can be connected using various coupling elements including zero dead volume (ZDV) unions, like those used with Phase Optimised Liquid Chromatograph® (POPLC®) kits, ZDV finger tight couplers screwed directly to the columns, stainless steel or PEEK tubing or using a T-piece (K. Bischoff, Szuecs, & Nyiredy, 2010; X. Chen & Li, 2013; Greco, Grosse, & Letzel, 2013; Haggarty et al., 2015; Hsieh & Chen, 2005; Louw, Pereira, Lynen, Hanna-Brown, & Sandra, 2008; Ortiz-Bolsico, Torres-Lapasió, Ruiz-ángel, & García-álvarez-Coque, 2013). Although there have been numerous column chemistry couplings, columns with the most orthogonality deliver the best separation for analytes with opposing polarities (Bassanese et al., 2015; Camenzuli & Schoenmakers, 2014). The combination of HILIC and RP in parallel chromatographic runs increased the number of metabolites detected in urine and plasma by 44% and 108%, respectively, compared to using RPLC-MS alone (Contrepois et al., 2015). The difficulty of serially combining RP and HILIC columns lies in the need for diametrically opposite organic concentrations in each mobile phase at the start of each chromatographic run. Serially combining an RP column to a HILIC column with the addition of a second pump to combat mobile phase incompatibility is a less routinely described method, but has been successfully applied to the targeted separation of polar and nonpolar pharmaceuticals, phenols in wine and quaternary ammonium compounds in brain samples (Falasca, Petruzzello, Kretz, Rainer, & Zhang, 2012; Greco et al., 2013; Louw et al., 2008).

The **aim** of this research was to develop a global (untargeted) metabolomics method in which a sample can be injected onto both RP and HILIC columns in series for the analysis of polar and non-polar compounds in a single injection. This method would allow for the independent optimisation of both

columns and would remove the need for separate sample preparations or the addition of ion pairing reagents.

The practicality and the reliability of the method were investigated by the analysis of TCA intermediates and bile acid standards. Subsequently, the feasibility of the coupled method for non-targeted analysis of large nonpolar compounds and small highly polar compounds in a complex sample (beer) was evaluated.

## 4.2 Materials and methods

The materials and methods are the same as those described in Chapter 2, with the following changes:

- 1) The pHILIC column was changed from a 2 mm diameter to a 4 mm to improve retention time reproducibility.
- 2) The equilibration time for both columns was increased from 10 minutes to 12.5 minutes to combat retention time drift.
- 3) The flow rate of the second gradient pump was increased to 350  $\mu\text{L}/\text{min}$  to increase the organic content of the mobile phase at the beginning of the HILIC separation.

## 4.3 Results

### 4.3.1 Standards - Organic acids

The polar organic acids (citrate, isocitrate, *cis*-aconitate, 2-oxoglutarate, succinate, fumarate, malate and oxaloacetate) were retained on the pHILIC column between approximately 5 minutes (mins) and 15 mins (Fig. 4-3A). As expected, the organic acids were not retained when using the RPLC column

alone, with all of them coming off the column in under 1 min (Fig. 4.4B). In contrast to the RPLC, when the compounds were analysed using the RPLC/HILIC method, all of the organic acids were retained, with retention times similar to those observed when using the pHILIC column alone, between approximately 5 mins to just over 15 mins (Fig. 4-3C).

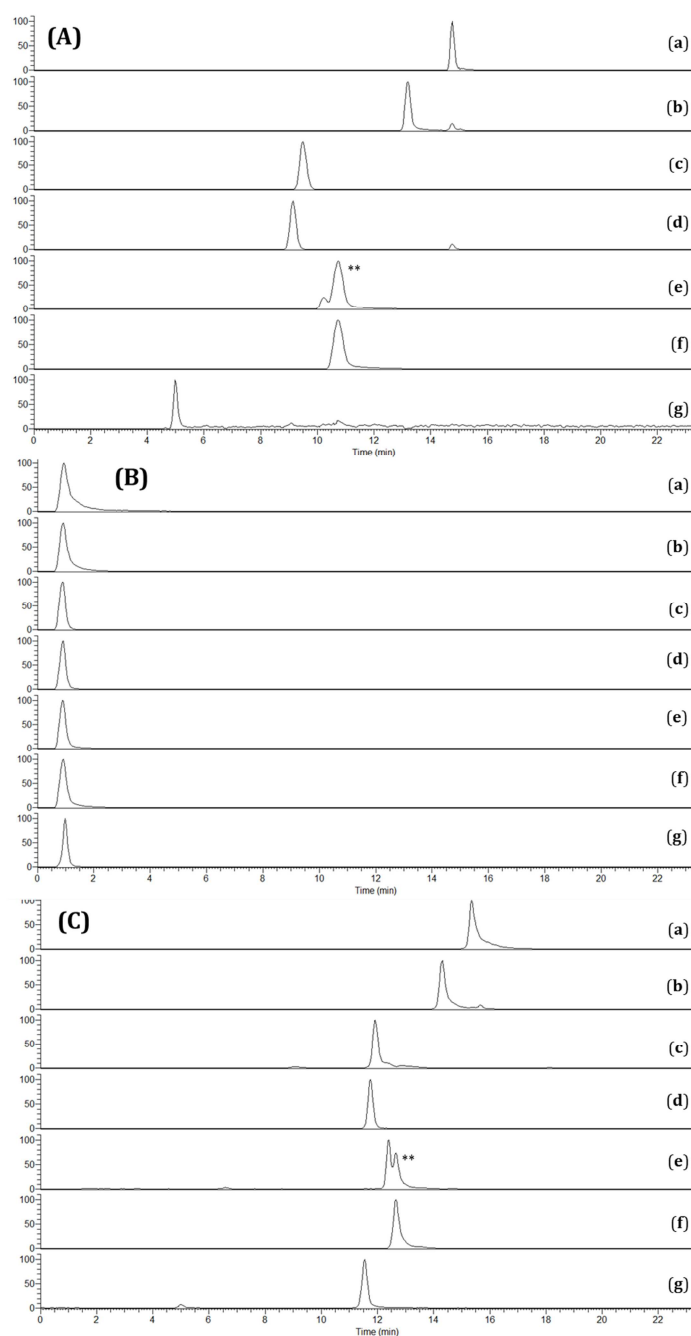


**Figure 4-3** Extracted ion chromatograms (EICs) of selected organic acids ( (a) isocitrate, (b) *cis*-aconitate, (c) 2-oxoglutarate, (d) succinate, (e) fumarate, (f) fumarate and (g) pyruvate) using (A): HILIC, (B): RPLC and (C): RPLC/HILIC separation using the same dual gradient. Detection: ESI-FTMS, negative mode. The organic acids were retained using the single HILIC method (A). None of the organic acids were retained when using the single RPLC (B). All of the polar organic acids were retained and separated using the RPLC/HILIC method (C). Note: the second component of the double peak observed for the mass of fumarate (f) on the HILIC (A) and RPLC/HILIC (C) EICs is a consequence of water loss from malate (\*\*).

The method was unable to separate the isomers citrate and isocitrate ( $m/z$  191.0198) (Fig 4-4A & B) therefore citrate was removed from the organic acid mix, before further analysis was carried out.

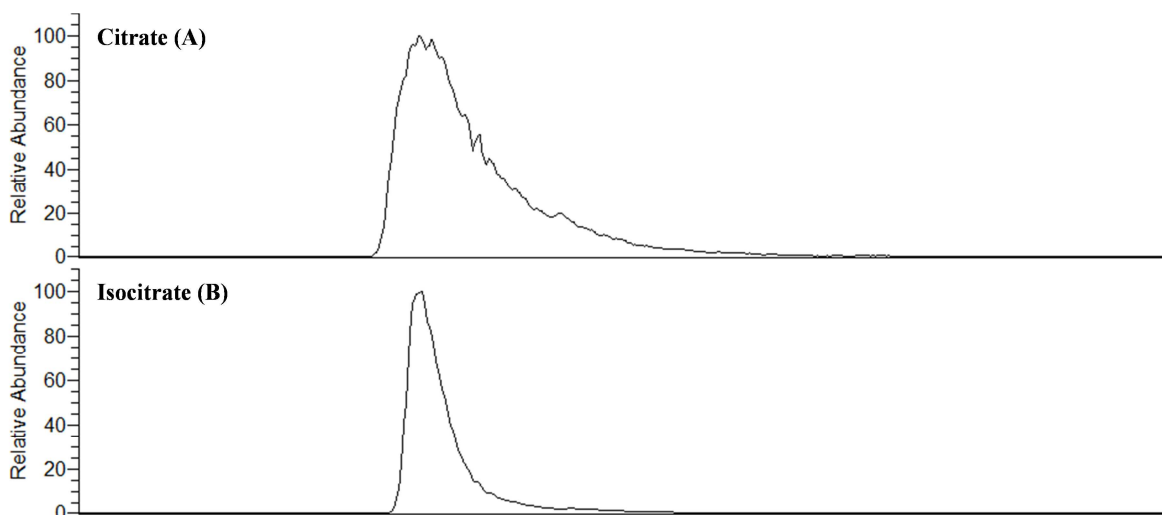


**Figure 4-4** EICs of (A): citrate and (B) isocitrate using the combined RPLC/HILIC method. Detection: ESI-FTMS, negative mode. The isomers were unable to be separated using the combined method.

When the organic acid mix was analysed, a double peak was detected at  $m/z$  115.00368 (Fig 4-3A & C). The first peak was identified as fumarate by matching both the mass and retention time (RT) to the pure standard when it was run on its own (Fig 4-3A & C, Fig 4-5A & B). The second peak was determined to be a result of water being lost from malate in the organic mix (Fig 4-6).

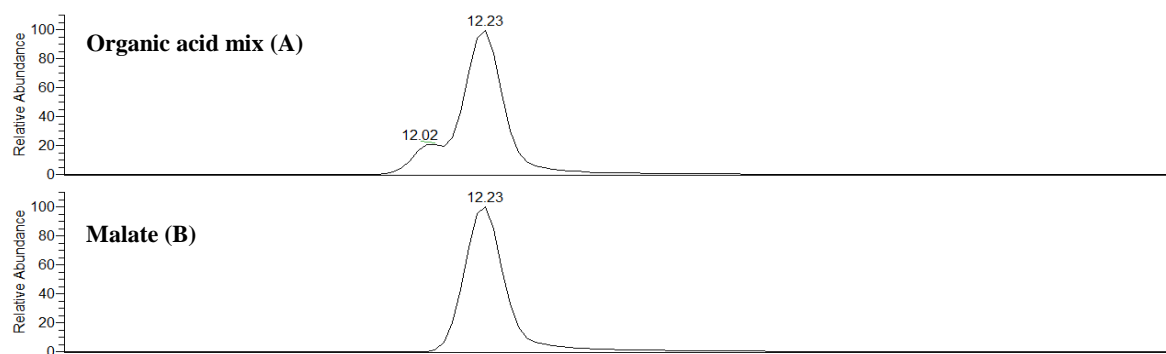


**Figure 4-5** Extracted ion chromatograms (EICs) of (A):  $m/z$  115.00368 from the organic acid mix and (B): malate ( $m/z$  133.01425). The double peak seen when a mass search was performed to detect fumarate is the result of fumarate and a water loss from malate. The first peak at RT 12.02 has a closer retention time (RT) to the pure standard of fumarate. The second peak at  $m/z$  115.00368 has the same retention time (RT) as malate (12.23 min) which reconfirmed that it was as a breakdown product of malate.

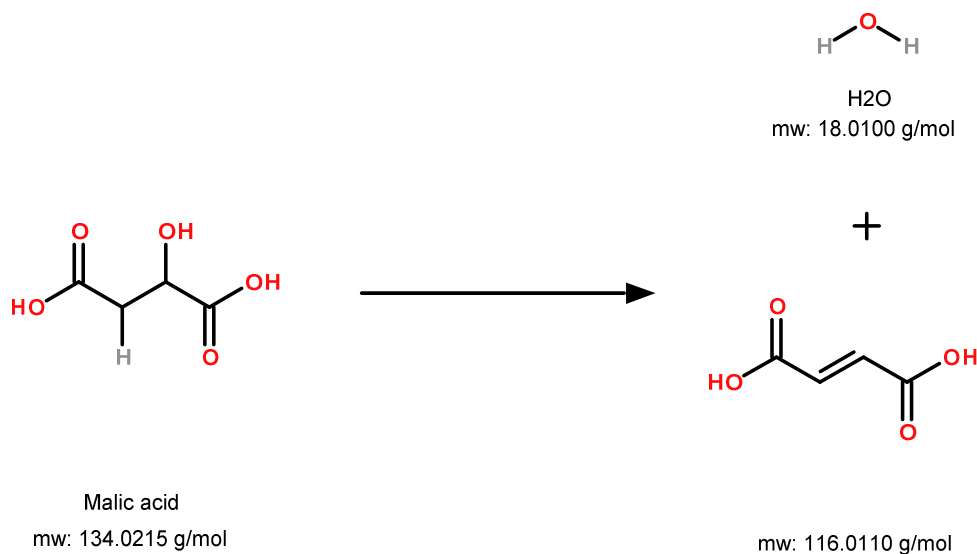


**Figure 4-6** Equation showing that water loss from malic acid, results in a compound with the same mass as fumaric acid and a water molecule. The resulting compound had the same  $m/z$  as fumarate ( $m/z$  115.0038) but a slightly different retention time (RT) as the compound is a breakdown product of malic acid, which has a different RT than fumaric acid.

#### 4.1.2 Standards - Bile acids

The non-polar bile acids deoxycholic acid, cholic acid, dehydrocholic acid and chenodeoxycholic acid were retained on the RPLC column between

approximately 16 mins and 19.5 mins (Fig. 4-7B). The bile acids were not retained very well when using the pHILIC column (Fig. 4-7B). The bile acids were retained for approximately 4 mins on the pHILIC column, possibly due to a slight polar charge on the acid group in the compounds; however, the bile acids were not able to be separated from one another using the pHILIC column alone. In contrast to the pHILIC, when the compounds were analysed using the RPLC/HILIC method, all of the bile acids were retained between 18 mins and 22 mins (Fig. 4-7C). The RTs were slightly longer than those observed for the RPLC column alone, because the addition of the second column lengthened the flow path before introduction of the compounds to the mass spectrometer.

Chenodeoxycholic acid is a synthetic bile acid with a similar structure to deoxycholic acid. The RPLC/pHILIC method was unable to separate these compounds (Fig 4-7C (a) & (d)).

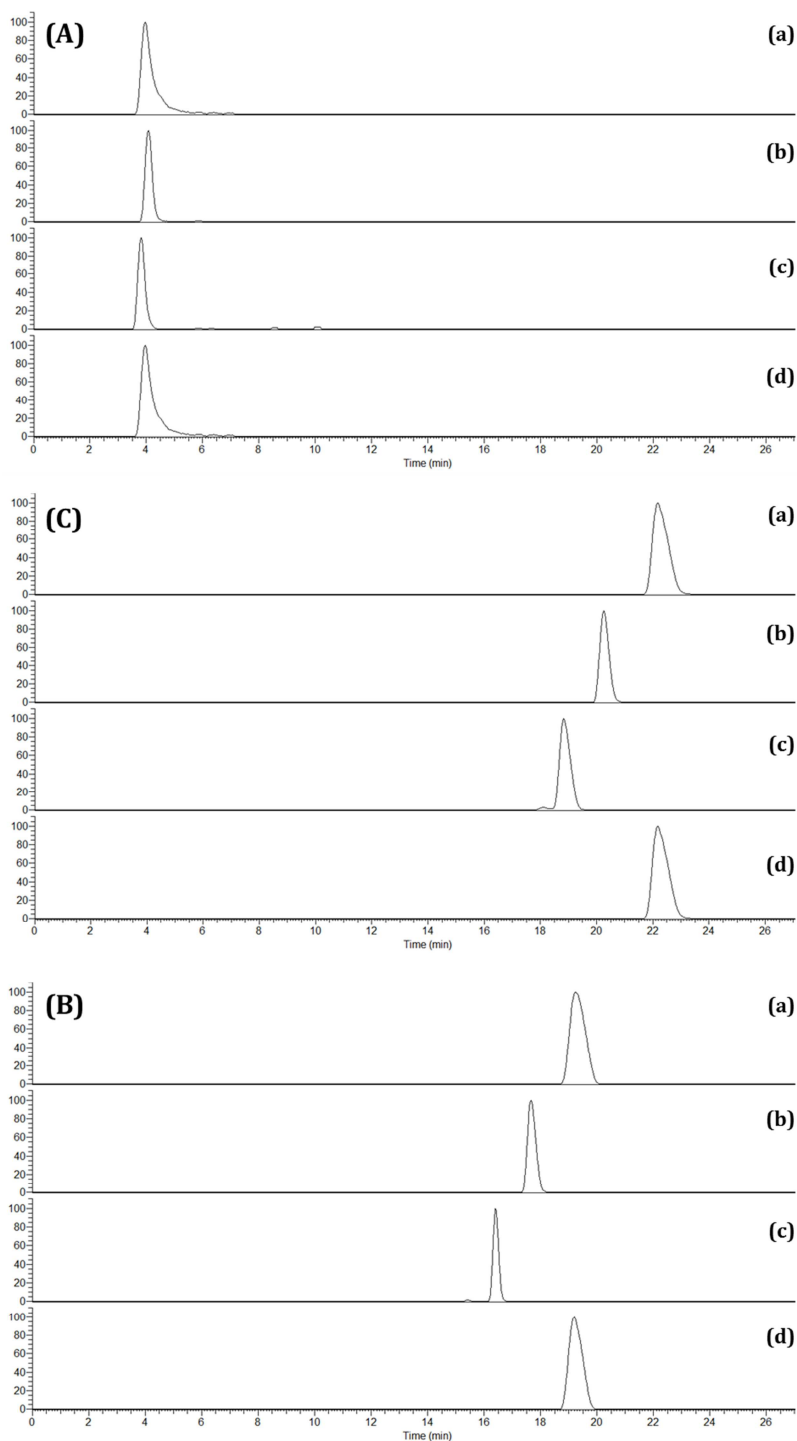


**Figure 4-7** Extracted ion chromatograms (EICs) of selected bile acids ((a) deoxycholic acid, (b) cholic acid, (c) dehydrocholic acid and (d) chenodeoxycholic acid) separated using (A): HILIC, (B): RPLC and (C): RPLC/HILIC with the same dual gradient. Detection: ESI-FTMS, negative mode. The bile acids were not retained using the single HILIC method (A). All of the bile acids were retained using the single RPLC method (B). All of the non-polar bile acids were retained and separated using the RPLC/HILIC method (C). Note: the isomers deoxycholic acid and chenodeoxycholic acid could not be separated using the RPLC/HILIC method (C).

The average retention time for each of the standards was calculated from nine separate LC-MS runs of a standards mix (Appendix II; Table 3). The RPLC/HILIC method showed good retention time reproducibility, with RSD values for each compound under 2% (Table 4-1). The combined method showed RSD values comparable to the pHILIC column on its own and better RSD values than those obtained using the single RPLC method (Table 4-1).

Although the RPLC/HILIC method was able to retain and separate both polar and non-polar standards in a mix, it was not capable of separating the isomers citrate and isocitrate ( $m/z$  191.01973) and deoxycholic acid and chenodeoxycholic acid ( $m/z$  391.28538).

**Table 4-1** Average retention times (RTs) and relative standard deviations (%RSDs) of the organic and bile acid standards. Each metabolites elemental formula (EF) was used to determine its  $m/z$  value ([M-H]).  $m/z$  values were used to establish RTs. The average RTs were calculated from nine separate standard mix injections (Appendix II). From these results the standard deviation (SDs) and relative standard deviations (%RSDs) were calculated. (n=9).

Metabolite	EF	[M-H]	HILIC			RPLC			RPLC/HILIC		
			Average	SD	%RSD	Average	SD	%RSD	Average	SD	%RSD
Isocitric acid	C6H8O7	191.01973	14.72	0.05	0.36	0.99	0.02	1.59	15.33	0.03	0.20
cis-Aconitic acid	C6H6O6	173.00916	13.14	0.05	0.40	0.93	0.05	5.68	14.27	0.06	0.43
2-Oxoglutaric acid	C5H6O5	145.01425	9.46	0.06	0.64	0.90	0.02	1.73	11.87	0.09	0.78
Succinic acid	C4H6O4	117.01933	9.08	0.07	0.76	0.93	0.02	2.58	11.70	0.09	0.80
Fumaric acid	C4H4O4	115.00368	10.17	0.08	0.79	0.90	0.02	1.73	12.37	0.07	0.58
Malic acid	C4H6O5	133.01425	10.64	0.10	0.98	0.93	0.02	2.58	12.59	0.07	0.57
Pyruvic acid	C3H4O3	87.00877	5.03	0.04	0.80	0.99	0.02	1.57	5.05	0.07	1.48
Deoxycholic acid	C24H40O4	391.28538	3.90	0.05	1.36	19.49	0.25	1.31	22.09	0.10	0.44
Cholic acid	C24H40O5	407.2803	4.04	0.05	1.31	17.62	0.18	1.03	20.20	0.06	0.32
Dehydrocholic acid	C24H34O5	401.23335	3.77	0.03	0.92	16.22	0.23	1.44	18.79	0.09	0.46
Chenodeoxycholic acid	C24H40O4	391.28538	3.90	0.05	1.36	19.43	0.27	1.38	22.09	0.10	0.44

### 4.1.3 Beer sample

Beer components, suggested from previous beer metabolome studies, were searched for using their  $m/z$  values (Frag, Porzel, Schmidt, & Wessjohann, 2012). Eight compounds in total were used; five polar metabolites (putatively identified as syringaldehyde ( $m/z$  181.05063), tyrosine ( $m/z$  182.08101), ethyl vanillin ( $m/z$  165.05572), succinic acid ( $m/z$  117.01973), and phenylalanine ( $m/z$  166.08625)) and three larger, non-polar metabolites (putatively identified as ad-/Humulone ( $m/z$  361.20205), iso-/Xanthohumol ( $m/z$  353.13945) and cohumulone ( $m/z$  347.18648)).

The small polar metabolites were retained on the pHILIC column and were not retained when using the RPLC column alone (Fig. 4-8A & B, peaks 4-8). In contrast to the RPLC, when the polar compounds were analysed using the RPLC/HILIC method, all of the selected polar beer metabolites were retained and separated (Fig. 4-8C, peaks 4-8).

The larger non-polar metabolites that were retained on the RPLC column were not retained when using the pHILIC column alone (Fig. 4-8B & A). Although iso-/xanthohumol appeared to be retained using the pHILIC column, the peak shape is incorrect and the peak elutes over 4 minutes, which is less than ideal for accurate and efficient chromatography (Fig 4-8A). In contrast to the pHILIC, when the compounds were analysed using the RPLC/HILIC method, all of the non-polar beer metabolites were retained and separated (Fig. 4-8C).

The RPLC/HILIC combined method demonstrated good RT reproducibility with RSD values of less than 1% achieved for all of the putative metabolites (Table 4-2).

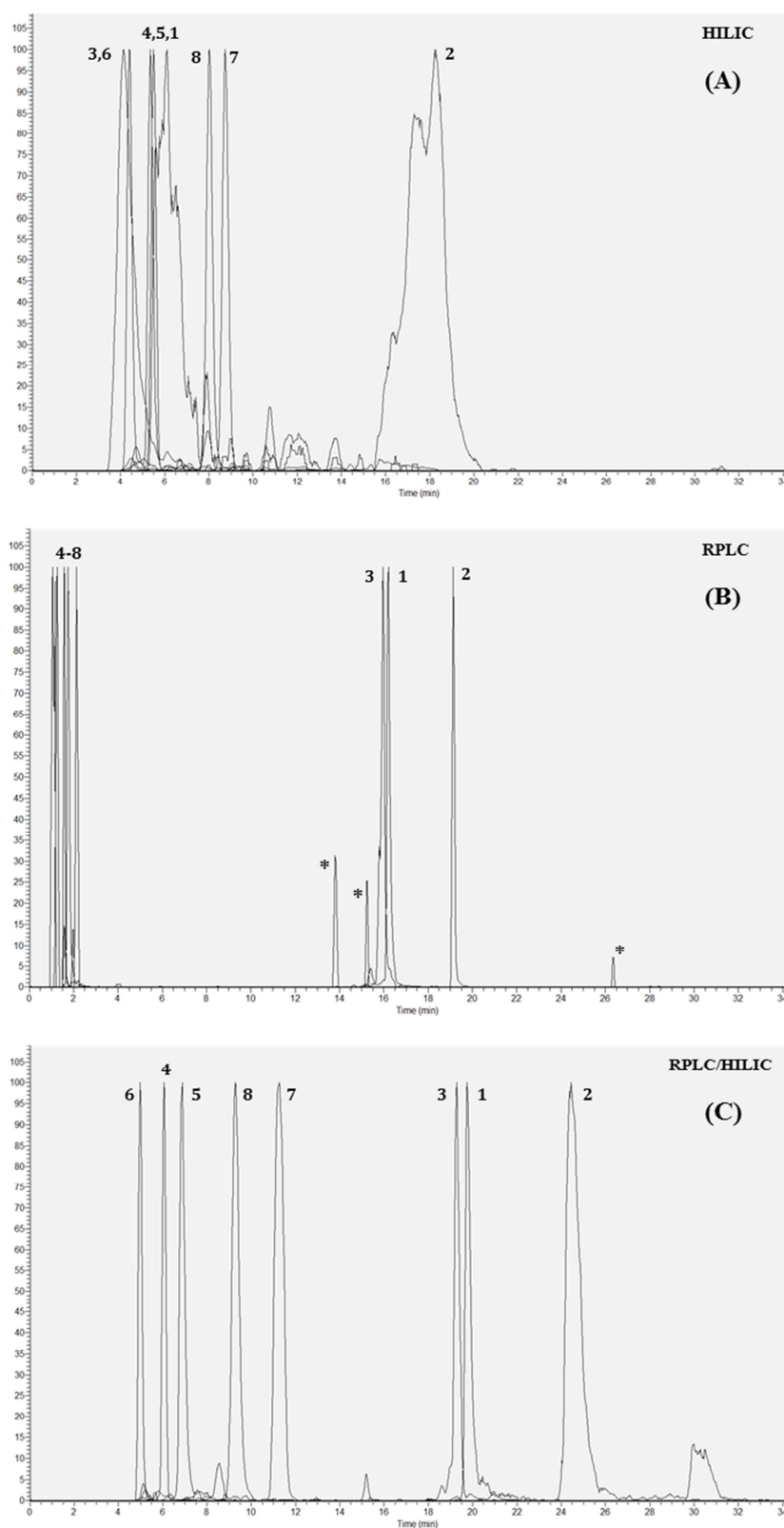


**Figure 4-8** Extracted ion chromatograms (EICs) of selected beer metabolites with annotations. (1) ad-/Humulone, (2) iso-/ Xanthohumol, (3) cohumulone, (4) syringaldehyde, (5) tyrosine (6) ethyl vanillin, (7) succinic acid, (8) phenylalanine. Detection: ESI-FTMS. Separation by (A): HILIC, (B): RPLC and (C): RPLC/HILIC. (\*) isomers with the same  $m/z$ , but different RTs as ethyl vanillin.

**Table 4-2** Average retention times (RT) and RSDs of selected beer metabolites. Each  $m/z$  value was used to determine a likely elemental formula (EF). EFs were used to putatively identify each beer metabolite.  $m/z$  values were used to establish RTs. The average RTs were calculated from twenty-three separate injections (Appendix II). From these results the standard deviation (SDs) and relative standard deviations (%RSDs) were calculated. (n=23).

Putative Metabolite	KEGG ID	EF	m/z	Metabolite ID code**	HILIC		RPLC		RPLC/HILIC	
					Average RT(mins)	%RSD	Average RT(mins)	%RSD	Average RT(mins)	%RSD
Ad-/Humulone	-/C10695	C21H30O5	361.20205	HRMS <sup>1</sup>	4.25	6.64	16.69	0.67	19.02	0.04
Iso-/Xanthohumol	-/C16417	C21H22O5	353.13945	HRMS <sup>1</sup>	18.11	2.04	19.18	0.30	23.66	0.06
Cohumulone	N/A	C20H28O5	347.18648	HRMS <sup>1</sup>	3.98	1.59	16.20	0.30	18.56	0.03
Syringaldehyde	N/A	C9H10O4	181.05063	HRMS <sup>1</sup>	5.51	0.36	1.27	0.00	5.76	0.03
Tyrosine*	C00082	C9H11NO3	182.08101	HRMS <sup>1</sup> MS <sup>2</sup> <sub>PL</sub>	11.04	0.47	1.58	1.16	11.46	0.04
Ethyl vanillin	D01086	C9H10O3	165.05572	HRMS <sup>1</sup>	4.39	0.00	1.59	1.59	4.57	0.03
Succinic acid	C00042	C4H6O4	117.01973	HRMS <sup>1</sup> MS <sup>2</sup> <sub>PL</sub>	8.78	0.87	1.12	6.84	12.03	0.05
Phenylalanine*	C00079	C9H11NO2	166.08625	HRMS <sup>1</sup> MS <sup>2</sup> <sub>PL</sub>	8.02	0.07	1.78	0.86	19.02	0.04

\*Detected in positive mode, \*\* Refers to alphanumeric coding scheme from (Sumner et al., 2014).

## 4.4 Discussion

The aim of this study was to serially combine an RPLC column and a pHILIC column for the retention and separation of both polar and nonpolar compounds within a single chromatographic run. The columns selected were a Hypersil Gold C18 RP column and a SeQuant ZIC-pHILIC column. The two columns were connected via a T-piece and two independent UP-HLC pumps were utilized, which allowed independent control over the MP gradient program for the individual columns. The gradient programs applied to each of the phases were typical for RP and HILIC analyses. The RPLC gradient starting conditions were high aqueous and low organic, rising to high organic and low aqueous and the HILIC gradient started with a high organic concentration running to low organic and high aqueous conditions. A sample was injected onto the RPLC in high aqueous conditions. The second pump, which ran at a higher flow rate of 350  $\mu\text{L}/\text{min}$ , compared to 65  $\mu\text{L}/\text{min}$  for the first pump, diluted the highly aqueous starting MP, with a high ACN MP, creating the optimum starting conditions for HILIC analysis as the sample was introduced to the pHILIC column.

Using this setup, non-polar metabolites were retained by the C18/RP stationary phase. Polar and ionic metabolites that were not retained on the RP column were then captured by the HILIC stationary phase. The gradients were then applied simultaneously to separate analytes on both columns.

This method was adapted from Louw et al. (2008) and Greco et al. (2013) who applied the RP/HILIC method to separate polar and nonpolar compounds in pharmaceuticals and polar and nonpolar phenols in wine (Greco et al., 2013; Louw et al., 2008). Louw ran a C18 2 mm ID column at a flow rate of 200  $\mu\text{L}/\text{min}$  and a HILIC 4 mm ID column at a flow rate of 1.4 mL/min. Greco suggested that the high flow rates used may affect the sensitivity of MS

detection and so used a longer C18 column, with a 3 mm ID, and a shorter HILIC column, with a 2 mm ID. They also ran at lower flow rates of 50–100 and 400  $\mu\text{L}/\text{min}$ , respectively. In the experiments described in this paper a 1 mm ID C18 and a 4 mm ID pHILIC were run at a flow rate of 65 and 350  $\mu\text{L}/\text{min}$ , respectively. Unlike Louw and Greco, the samples in this study were prepared in high aqueous solutions, the optimum conditions for initial injection onto the RP column. Ion pairing reagents were added to the RP mobile phases in both the Louw and Greco papers (and to the HILIC mobile phase in Louw et al.). In the experiments described herein, ion pairing reagents were not introduced into the RP buffers. Ion pairing reagents are usually introduced into a RP separation to mask the ionic or polar groups of compounds to encourage binding to the RP stationary phase. In this experiment this was not desirable as the HILIC column after the RP column captured and separated the ionic and polar compounds in the sample. 20 mM ammonium bicarbonate was added to the HILIC mobile phase to encourage retention of the polar and ionic compounds by increasing the pH to 9. The high dilution between the columns, achieved by the difference in flow rates, allows each of the methods to be optimised independently to suit sample requirements. The ability to inject the sample in low organic solvents onto the RPLC column and high organic solvents onto the HILIC column has allowed two very different column chemistries to be successfully coupled together.

The combined method was able to successfully retain and separate a standard mixture of polar TCA intermediates and nonpolar bile acids. Slight peak-tailing was witnessed for some of the TCA intermediates, but this had been witnessed before in standard mixes in the laboratory using the routine pHILIC method (data not shown). The method was unable to separate isomers of citrate and isocitrate and deoxycholic acid and chenodeoxycholic acid. The selected polar and non-polar metabolites extracted from beer displayed better retention and separation using the RPLC/HILIC method compared to the

individual runs. All metabolites exhibited good peak shapes and reproducibility.

Some of the limiting factors of this method include the inability to separate the isomers citrate and isocitrate. The ability of an LC system to separate isomers is important to ensure accurate metabolite concentrations are detected to enable correct conclusions to be drawn from the results. Another limiting factor in this study was that the number of metabolites detected using the RP/HILIC combined method was not compared to the number of metabolites detected when using the RP and HILIC columns individually. This comparison would have allowed the capacity of the individual columns to be compared to the combined columns. To determine the optimal combined chromatography, it would have been beneficial to have compared the performance of a variety of different HILIC and RP columns, along with different MP compositions and gradient programs (Contrepois et al., 2015).

When the combined RP/HILIC method is compared to other dual-column methods to extend the coverage of the metabolome, through the retention and separation of both polar and non-polar metabolites in a single chromatographic run, the advantages and disadvantages of this simple system can be seen (Table 4-3). Column switching and 2D-LC systems offer greater freedom when coupling columns together, as MP incompatibility is not an issue, as with the combined method, so two completely different LC methods can be used, providing greater experimental freedom. However, they require dedicated equipment that is often complex to set-up and expensive, whereas the combined method utilizes conventional laboratory equipment. The column switching and 2D-LC methods also require a level of expertise, unlike serially combining columns, which any analyst with LC experience could cope with. Unlike the combined method which requires one injection per sample, column switching requires two injections per sample, which may not be possible if the

sample volume is very low. As the gradients are run simultaneously, the combined method has a higher through-put than 2D-LC, which can have very lengthy analysis times.

A single column method that has been gaining popularity, and has the potential to exceed the combined method with regards to polar and nonpolar separation is the use of mixed-mode columns (MMCs). MMCs utilize mixes of different stationary phases, either by mixing beads with different functionalities and packing them into a column (Type I) (Walshe, Kelly, Smyth, & Ritchie, 1995), modifying a substrate at its surface with ligands of different functionalities (Type II) (R. Bischoff & McLaughlin, 1984), embedding ion exchange functionality as part of the hydrophobic ligand, 'embedded' phases (Type III) (Muentner, Stokes, Obie, & Jezorek, 1999) or having ion exchange functionality at the free end of the hydrophobic chain, 'tipped' phases (Type IV) (Nogueira, Michael, & Lindner, 2005). There are various different columns available including bimodal RPLC/cation (CEX) or anion exchange (AEX), HILIC/AEX, HILIC/CEX and trimodal RP/AEX/CEX and HILIC/AEX/CEX (K. Zhang & Liu, 2016). Different types of MMC are available. Type I and Type II columns are not widely used due to performance limitations, but Type III and IV have been commercialised for use as general-purpose columns (as alternative to C18) and for more specific analyses. As well as silica based MMCs, polymer based ones are also available. Mixed-mode separation is achieved by coating a macroporous hydrophobic polymer core with an ion exchange latex bead layer (Fontanals, Marcé, Borrull, & Cormack, 2010). As with conventional LC, MMC research has recently been moving towards the goal of separating anionic, cationic and neutral species in one chromatographic run, which has led to the development of trimodal stationary phases to provide AEX, CEX and RP separations simultaneously. The Scheizo group of columns by Imtakt

mix two types of bonded silica particles- one with C18 and CEX and one with C18 and AEX and the Obelisc N and Obelisc R by SIELC in which either

**Table 4-3** Comparison of dual- and single-column methods to separate polar and nonpolar compounds.

Method	Column Combinations and Applications	Comments
Serially combined columns	<p><i>C18/Silica (HILIC)</i>– Sugars and sulphonamides in pharmaceuticals (Louw et al., 2008)</p> <p><i>BEH C18/Silica (HILIC)</i> - arylamines and aminopyridines in pharmaceuticals (Louw et al., 2008)</p> <p><i>EC-C18/ZIC-HILIC</i> - Polar and nonpolar phenols in wine (Greco et al., 2013)</p> <p><i>C18/ZIC-pHILIC</i> - Bile acid and TCA intermediates, polar and nonpolar metabolites in beer (Haggarty et al., 2015)</p> <p><i>ZIC-HILIC/RP-amide</i> or <i>RP-amide/ZIC-HILIC</i> - Polar and nonpolar metabolites in mouse serum (Chalcraft &amp; McCarry, 2013)</p>	<p>Advantages – easy set-up, no specialist training required, no specialist equipment.</p> <p>Limitations- lack of variety and expense of column lengths. No dedicated software. MPs must be compatible. Some set-ups there is no independent control over each gradient.</p>
Column switching	<p><i>C18 x C18</i> - Carbamate and pyrethroid insecticide monitoring in water (Fernández-Ramos et al., 2014)</p> <p><i>Guard Cartridge RP-18e x C18</i> - B-carotene in food supplements (Brabcova et al., 2013)</p> <p><i>C8 x phenyl-hexyl /phenyl-hexyl</i> - Folic acid and its derivatives in human plasma (Bailey &amp; Ayling, 2013)</p> <p><i>C8 X C18</i> - Quantification of monohydroxybutenylmercapturic acid (MHBMA), N-acetyl-S-(3, 4-dihydroxybutyl) cysteine (DHBMA) and 8-Hydroxy- 2-deoxyguanosine (8-OHdG) in human urine (X. Zhang et al., 2015)</p> <p><i>BEH C18 x HSS T3</i> - Untargeted analysis of metabolites and lipids in human plasma and</p>	<p>Advantages- ability to combine two completely different LC separation platforms.</p> <p>Incompatible MPs are not an issue.</p> <p>Limitations – specialist switching interface required, expensive equipment, specialist training required, one sample is injected on to one column but does not pass through the second column- two injections are required for one full analysis.</p>

	rat livers (Y. Li et al., 2015)	
2DLC	<p><i>HILIC x C18-UHPLC</i> - analysis of a variety phenolic compounds (including monomeric flavonoids, phenolic acids, coumarins and flavan-3-ols) in unfermented and fermented rooibos samples (Beelders et al., 2012)</p> <p><i>Cyano column x C18-UHPLC</i> – Separation of carotenoids in chilli peppers (Cacciola et al., 2012)</p> <p><i>RPLC x HT-RP-UHPLC</i> (variety of silica- and non silica-based column combinations studied)– separation of standard mix of bio-oils (Le Masle et al., 2014)</p>	<p>Advantages- ability to combine two completely different LC separation platforms.</p> <p>Incompatible MPs are not an issue.</p> <p>Limitations – specialist switching interface required, expensive equipment, issues with sample dilution, specialist training required, second dimension analysis can be lengthy, creates more complexity than a 1D system so twice as likely for something to go wrong.</p>
Mixed mode columns	<p><i>RP/AEX/CEX</i> – Separation of a standard mix containing one neutral, four acidic and four basic compounds (Socia &amp; Foley, 2014)</p> <p><i>RP/AEX/CEX</i> – Separation of RNA oligonucleosides, including five isomers (Biba et al., 2013)</p> <p><i>RP/AEX/CEX x HILIC</i> – Separation of inorganic/organic anions and cations, active pharmaceutical ingredients, and carbohydrates (Kazarian et al., 2014)</p>	<p>Advantages – separation of neutral and ionic species within one analytical run, no need for specialist equipment, interaction mechanisms can be controlled by MP composition and pH.</p> <p>Limitations – complicated method development, need for dedicated columns, non-linear retention and retention time variations. To utilize all interaction mechanisms more than one MP composition has to be run- lengthening analysis time.</p>

negatively charged groups are bonded onto positively charged groups close to a silica surface using a hydrophobic chain or positively charged groups are bonded onto negatively charged groups close to a silica surface using a hydrophilic chain, respectively.

These trimodal MMCs have been used in sequential elution liquid chromatography (SE-LC), in which different groups of analytes are eluted from the column, based on their chemical characteristics (e.g. acids, bases and/or neutral compounds) using different modes of mobile phases that are selectively strong for that specific group of compounds (Little, Jeansonne, & Foley, 1991). SE-LC has been used for the separation of weak acids from weak bases from neutral compounds (Socia & Foley, 2014). A dual gradient was employed in the study, the first increasing from acidic to basic (pH 2.0 – pH 8.0) and vice versa for 30 mins and then an increasing organic gradient over 45 mins (Socia & Foley, 2014). This method not only separated ionisable analytes from neutral ones, but also acids from bases.

MMC were also used to successfully retain and separate RNA oligonucleosides (Biba et al., 2013). There was no improvement to separation compared to conventional methods when using the vendor recommended mobile phase composition, but when the MP was changed to a NaCl or NaBr salt gradient the column was able to separate oligonucleoside isomers (Biba et al., 2013).

Recently, a MMC was serially coupled to a HILIC column for the simultaneous analysis of inorganic/organic anions and cations, active pharmaceutical ingredients and carbohydrates (Kazarian et al., 2014). The sample was first injected onto the MMC where an isocratic gradient for ion exchange was applied. A dual organic/salt gradient was then applied for mixed-mode interactions. At the height of the organic mix mode gradient, the flow was switched to the HILIC column and HILIC analysis was carried out

on a second injection from the sample (Kazarian et al., 2014). This approach successfully resolved up to 23 analytes in one run with reproducible results and shows potential for use in comprehensive analysis, although this system has yet to be tested on a sample with a complex matrix (Kazarian et al., 2014).

MMCs could offer a good alternative to serially combined columns, but they have a few limitations. Dedicated columns are required for analysis and method development is considerably more complicated compared to conventional LC method development due to secondary and tertiary interactions between the analytes in the solute and stationary phases, which can also give rise to non-linear retention behaviours and retention time variations (Alvarez-Segura, Ortiz-Bolsico, Torres-Lapasio, & Garcia-Alvarez-Coque, 2015; Issaq, Gutierrez, Issaq, & Gutierrez, 2017; McLaughlin, 1989; Ordoñez, Quintana, Rodil, & Cela, 2012; K. Zhang & Liu, 2016). Another limitation, in comparison to serially combining columns is the need for more than one gradient program to take full advantage of the MMCs varied stationary phases.

The results from this study highlight the advantages of using the RPLC/HILIC method for the separation and detection of both polar and non-polar metabolites, within a complex sample, in a single run. This method could improve analytical efficiency by halving the time required for analysis and removing the need for complicated system set-ups or sample preparations. However, more method development is required to determine the optimum column combination and MP compositions, the robustness of the system and the capacity of the columns. It is also the option of this author that the effect of combining an RP and HILIC column on compounds with both charged and neutral regions should be investigated to determine how their retention will be affected by the two different phases.

**Chapter 5. Ion chromatography - mass spectrometry (IC-MS) method development for central carbon metabolism (CCM) analysis**

## 5.1 Introduction

As has been discussed previously, targeted metabolomics aims to detect a defined group of compounds. Measuring a select group of metabolites can provide a powerful insight into key areas of the metabolome which may be lost in an untargeted analysis.

Central carbon metabolism is essential to all living organisms and plays a key role in energy and biomolecule production.

### 5.1.1 Central carbon metabolism

Central carbon metabolism which encompasses glycolysis, the pentose phosphate pathway (PPP) and the tricarboxylic acid (TCA) cycle is essential and ubiquitous to all living cells (Büscher, Czernik, Ewald, Sauer, & Zamboni, 2009; Luo et al., 2007).

These metabolic networks convert incoming nutrients into energy, subunits of biopolymers, signalling molecules and in the biotechnological production of fine chemicals (e.g. amino acids and vitamins). The metabolites of CCM serve as important precursors for the anabolic biosynthetic pathways. A summary of glycolysis and the TCA cycle can be found in Figures 5-1 and 5-2, respectively. Briefly one glucose molecule is converted to two molecules of pyruvate, with a net gain of two ATP and two molecules of NADH during glycolysis (Fig. 5-1). Each pyruvate molecule is then converted to acetyl-CoA before it enters the TCA cycle. Through a number of enzyme mediated reactions each pyruvate is converted to oxaloacetate, releasing a total of four carbon dioxide ( $\text{CO}_2$ ) molecules and forming a total of six molecules of NADH, two molecules of  $\text{FADH}_2$  and two molecules of ATP (Fig. 5-2). The electrons from the NADH and  $\text{FADH}_2$  molecules produced during glycolysis

and the TCA cycle are transferred into the electron transport chain which drives the synthesis of ATP molecules through oxidative phosphorylation.

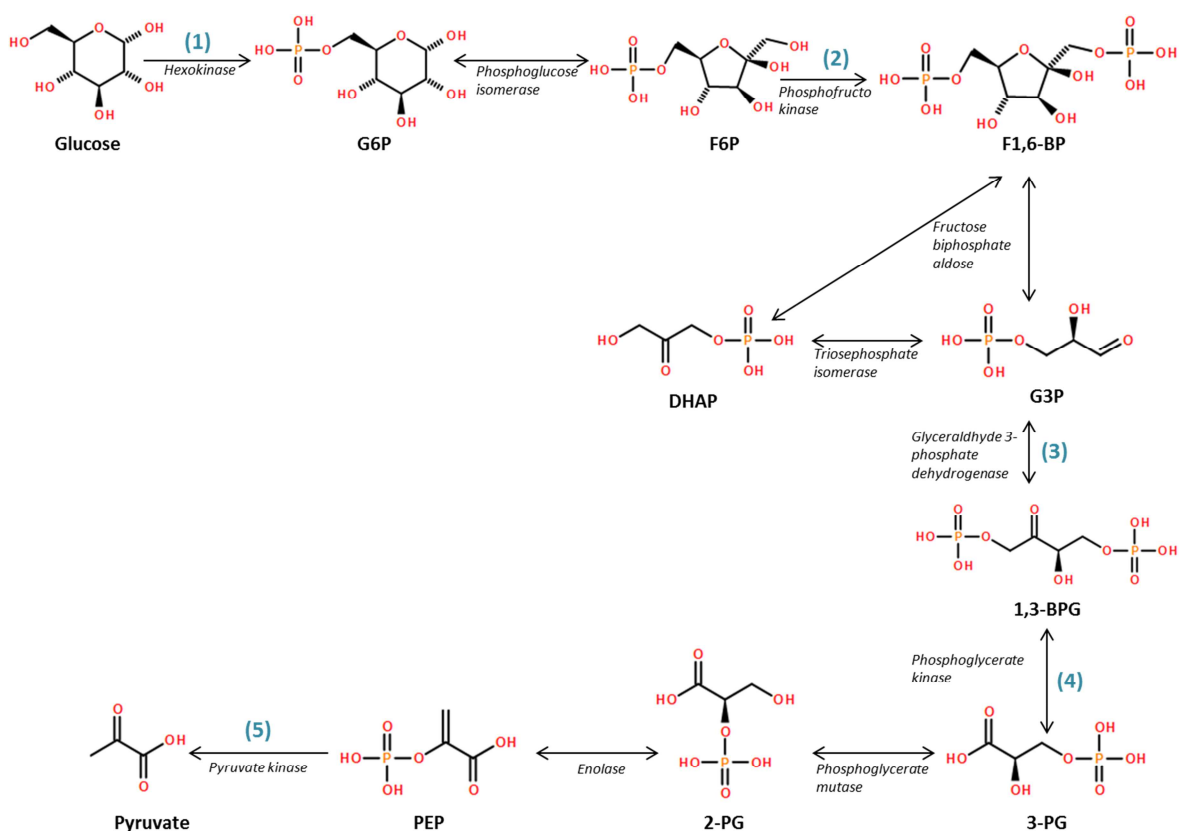


**Figure 5-1** Schematic of the glycolysis pathway. One glucose molecule is converted into two pyruvate molecules through a number of enzyme mediated chemical reactions. Glucose is converted into glucose 6-phosphate (G6P) through the transfer of a phosphate group from ATP in a reaction catalysed by hexokinase (1). Glucose 6-P is then converted into fructose 6-phosphate (F6P) in a reversible reaction catalysed by phosphoglucose isomerase. An additional phosphate group is added to fructose 6-P from another ATP molecule to produce fructose 1,6-bisphosphate (F1,6-BP) in a reaction that is mediated by phosphofructokinase (2). F1,6-BP splits into the phosphate-bearing three carbon sugars, dihydroxyacetone phosphate (DHAP) and glyceraldehyde 3-phosphate (G3P). DHAP is converted to G3P by triosephosphate isomerase to continue through the rest of the pathway, therefore this part of the pathway occurs twice. G3P loses two electrons and two protons reducing  $\text{NAD}^+$  to  $\text{NADH}$  and producing  $\text{H}^+$ , releasing energy for the attachment of a phosphate group to G3P producing 1,3-bisphosphoglycerate (1,3-BPG) (3). A phosphate group is transferred from 1,3-BPG to ADP, producing an ATP molecule and in the process converting 1,3-BPG to 3-phosphoglycerate (3-PG) in a reaction catalysed by phosphoglycerate kinase (4). 3-PG is then rearranged to form 2-phosphoglycerate (2-PG). 2-PG then loses a water molecule, forming the unstable molecule phosphoenolpyruvate (PEP). PEP readily donates a phosphate group to ADP producing another molecule of ATP in a reaction catalysed by pyruvate kinase, converting PEP to pyruvate (5). Overall glycolysis uses two molecules of ATP to produce four molecules of ATP and two molecules of  $\text{NADH}$ .

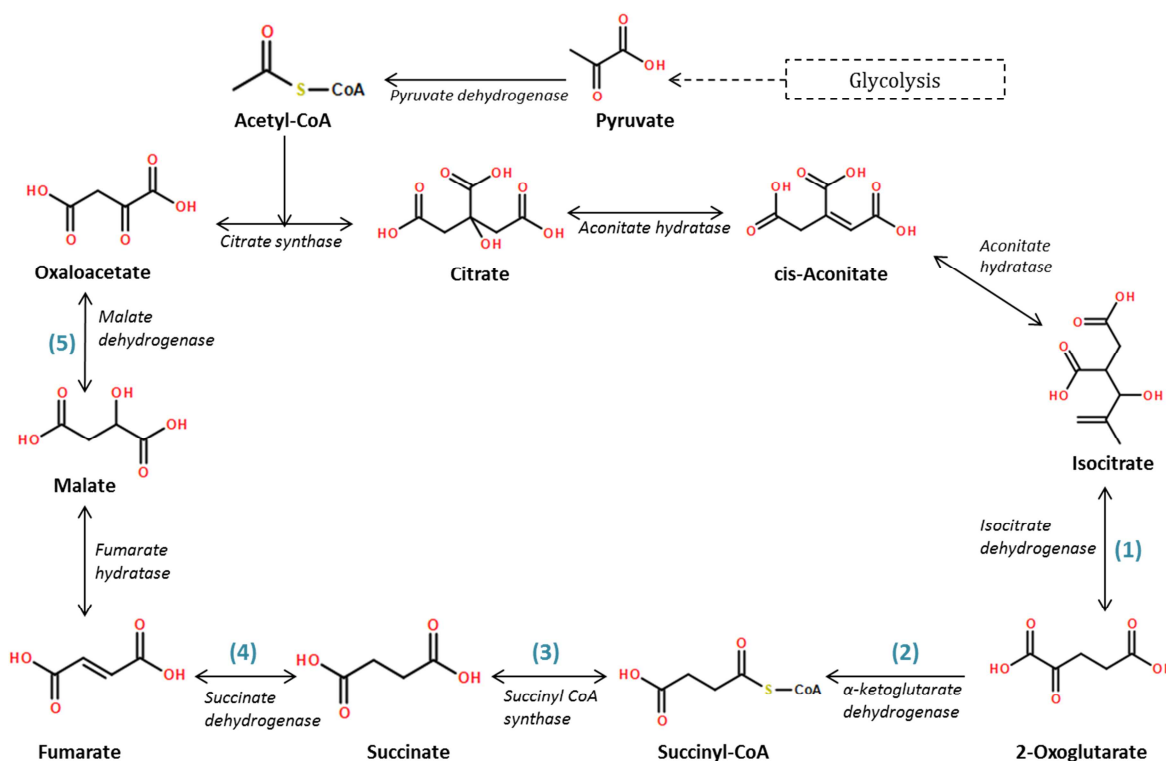


**Figure 5-2** Schematic of the tricarboxylic acid (TCA) cycle. Citrate produced from the combination of acetyl-coenzyme A (acetyl-CoA), produced by the oxidation of pyruvate, and oxaloacetate. Citrate is then rearranged in a two-step process to isocitrate in reactions catalysed by aconitate hydratase. In an oxidation reaction isocitrate loses a carbon to produce carbon dioxide ( $\text{CO}_2$ ), reducing  $\text{NAD}^+$  to  $\text{NADH}$  forming the five-carbon compound 2-oxoglutarate (1). 2-Oxoglutarate is then reduced to a four-carbon compound, releasing a molecule of  $\text{CO}_2$  and reducing  $\text{NAD}^+$  to  $\text{NADH}$  (2). Succinyl-CoA is produced from the addition of CoA to the four-carbon compound in a reaction mediated by  $\alpha$ -ketoglutarate dehydrogenase. Succinyl-CoA is unstable and the CoA is replaced by a phosphate group, which is transferred to ADP forming ATP (3), leaving succinate. Succinate is then oxidized to form fumarate. In this reaction two hydrogen atoms are transferred to FAD, producing  $\text{FADH}_2$  (4). Fumarate is converted to malate through the addition of a water molecule to the four-carbon compound. Malate is oxidised to form oxaloacetate reducing  $\text{NAD}^+$  to  $\text{NADH}$  (5). Two acetyl-CoA molecules are produced for every molecule of glucose, so overall the TCA cycle produces four molecules of  $\text{CO}_2$ , six molecules of  $\text{NADH}$ , two molecules of  $\text{FADH}_2$  and two molecules of ATP.

CCM changes dramatically with the environmental and genetic conditions a cell experiences. Due to the fundamental role that these key metabolites and pathways play in biology, there's great interest in obtaining a complete understanding of the central metabolic activity of cells as possible for the purposes of research, metabolic engineering and biotechnology (Bongaerts, Krämer, Müller, Raeven, & Wubbolts, 2001; Chassagnole, Noisommit-Rizzi,

Schmid, Mauch, & Reuss, 2002; Fiehn, 2002; Kell, 2004; Kimball & Rabinowitz, 2006; Luo et al., 2007; Nielsen & Oliver, 2005; Stitt & Fernie, 2003; Wendisch, Bott, Kalinowski, Oldiges, & Wiechert, 2006).

Each of the CCM pathways are essential for energy production, but also play key roles in other pathways. For example the TCA cycle follows glycolysis, but also for lipid metabolism, amino acid metabolism and signalling in cells (He et al., 2004; Keefer & Schuster, 1986).

The metabolites that participate in CCM include carboxylic acids, phosphorylated compounds, including sugar-phosphates (e.g. fructose 6-phosphate), phospho-carboxylic acids (e.g. PEP) and nucleotides such as ATP and NAD. These metabolites are almost entirely anionic species (Soga et al., 2002). There are various options with regards to the analytical techniques that can be adopted for targeted metabolomics. These include NMR, chromatography and MS (Lu et al., 2008; Roberts et al., 2012). Chromatography based-MS methods are often utilized in targeted metabolomics studies as they provide high sensitivity and specificity with broad dynamic range (Kimball & Rabinowitz, 2006; Rabinowitz, 2007; Rabinowitz & Kimball, 2007; Want, Nordström, Morita, & Siuzdak, 2007).

## **5.1.2 Methods to analyse central carbon metabolism (CCM)**

### **5.1.2.1 GC-MS**

GC-MS is a powerful tool in metabolomics and has been used in both targeted and untargeted analysis of small organic molecules (Fiehn, Kopka, Dörmann, et al., 2000; Fiehn, Kopka, Trethewey, & Willmitzer, 2000; Martínez & Krömer, 2016). GC-MS has been used successfully in semi-quantitative and quantitative studies of volatile compounds (Martínez & Krömer, 2016). Although GC-MS has been used in quantitative metabolomics, the

compounds analysed have to be volatile to get into the gas phase either naturally or through chemical derivatisation (Fiehn, Kopka, Dörmann, et al., 2000; Fiehn, Kopka, Trethewey, et al., 2000; Weckwerth, Loureiro, Wenzel, & Fiehn, 2004; Zamboni, Saghatelian, & Patti, 2015).

Functional groups such as hydroxyl, amine, amide, phosphate and thiol groups are problematic in GC but can be converted to more suitable alkylsilyl derivatives through silylation (Blau & Halket, 1993; Knapp, 1979). However the direct silylation of sugars results in numerous peaks being detected in the GC for each sugar, as the sugar can be found in cyclic and open structures (Blau & Halket, 1993; Knapp, 1979). To inhibit the cyclisation of sugars, a methoximation step is carried out before silylation, which results in fewer peaks for sugars. Methoximation also protects  $\alpha$ -ketoacids from decarboxylation and fixes enolizable keto groups, which facilitates identification of the original structures (Blau & Halket, 1993).

GC-MS with two-step methoximation and silylation derivatisation has been carried out for various compounds involved in CCM (Canelas, Ras, ten Pierick, van Gulik, & Heijnen, 2011; Cipollina et al., 2009; Koek, Muilwijk, Werf, & Hankemeier, 2006). GC-MS was recently used to analyse 41 metabolite standards involved in CCM (Jung & Oh, 2015). However, F16B and oxaloacetate were not detected due to low derivatization and instability, respectively and G3P and erythrose 4-phosphate (E4P) were not detected as they occurred in low concentrations. When this method was applied to the analysis of *Kluyveromyces marxianus*, a total of 25 CCM metabolites were detected and quantified (Jung & Oh, 2015). The results obtained from this study were comparable to a recent LC-MS/MS study (Rühl et al., 2012).

GC-MS is a powerful tool for quantitation studies, however the drawbacks of this method include the requirement of derivatisation of non-volatile

compounds and the incompatibility of this method for the analysis of large and heat labile molecules (Zamboni et al., 2015).

Although GC-MS provides a robust platform for the detection and quantification of small volatile organic molecules, it is generally agreed that due to the dynamic range of metabolites, liquid-based chromatographies are better suited for the targeted analysis of CCM compounds (Büscher et al., 2009).

### 5.1.2.2 CE-MS

Capillary electrophoresis (CE) separates compounds based on their intrinsic electrophoretic mobility, which is dependent on the size and charge of the analyte (Ramautar, Somsen, & de Jong, 2015). This makes CE an extremely powerful tool for the analysis of charged analytes, and as CCM compounds are almost entirely anionic, CE is well suited for their analysis (Ramautar et al., 2015; Soga et al., 2002).

Traditionally CE was coupled to UV detection, with detection limits above those that are required to detect submicromolar metabolite concentration levels that are often present in cells (Luo et al., 2007). However, the coupling of CE to MS increased the detection limits of this method by up to 100 fold (Sato, Soga, Nishioka, & Tomita, 2004). CE-MS has been used in numerous studies to separate and detect metabolites involved in CCM.

Soga et al. (2002) used sheath flow CE-MS operated in ‘negative mode’ with a cationic polymer coated capillary to separate a standard mix of 20 intermediates from glycolysis and the TCA cycle. Citrate, nucleotides and CoA compounds were detected as poorly shaped peaks, if detected at all (Soga et al., 2002). The method was then successfully applied to the analysis of *Bacillus subtilis* (Soga et al., 2002). This method could separate and detect

G3P and DHAP, but was unable to separate the isomers G6P/F6P or 2-/3-PG (Soga et al., 2002). To improve the analysis of nucleosides and CoA compounds, Soga et al. (2007) developed a pressure-assisted CE-MS (PACE-MS) method that utilized a normal fused silica-capillary (Soga et al., 2007). Silanols masked with phosphates prevented nucleosides from interacting with the capillary wall, allowing the nucleosides to be detected (Soga et al., 2007). The two CE-MS methods were then merged to create a method for the analysis of CCM compounds by sheath flow CE-MS utilizing a platinum ESI needle which improved the sensitivity and robustness of the system (Soga et al., 2009). This method was used to detect 43 anionic compounds in a standard mix and was then applied to the analysis of mouse livers (Soga et al., 2009). Although the method greatly improved the sensitivity of the CE-MS system, the RSD for the majority of the standard mixes and biological samples were above 5% (Soga et al., 2009).

Advancements in CE-MS instrumentation and interfaces has allowed large numbers of anions to be separated, without the need for derivatisation, in a sensitive and selective manner with fast analysis times (usually <25 min) (Soga et al., 2002, 2007, 2009). However, there are a number of drawbacks when using CE-MS. In comparison to GC- and LC-MS, the use of CE-MS for metabolomics studies is still relatively low and is considered the least suitable platform for the detection and quantification of CCM compounds (Büscher et al., 2009). The separation power and sensitivity of CE-MS is equal to LC and GC, but it lacks the robustness required to analyse biological samples (Büscher et al., 2009). Using some CE methods are challenging, e.g. reverse polarity methods that are required for carboxylic acid separation (W. C. Yang, Regnier, & Adamec, 2008). CE instrumentation also requires greater maintenance than both GC and LC and RT variations are greater between samples; 3%, compared to 0.5% for GC and LC (Büscher et al., 2009).

LC-MS is more time-efficient, requires less maintenance, has greater coverage and is more robust than CE-MS methods (Büscher et al., 2009).

### 5.1.2.3 LC-MS

Various LC-MS methods have been employed in CCM studies for the detection and quantification of glycolysis, TCA and PPP intermediates.

Bajad et al. (2006) compared various LC methods for the separation of 163 metabolites and found that an aminopropyl column run under HILIC conditions at pH 9.5 performed the best and was able to separate 141 compounds out of the 163 CCM standards (Bajad et al., 2006). However, the method failed to separate sugar isomers, exhibited poor performance for NADH and performed worse than GC-MS for small volatile compounds (Bajad et al., 2006).

To aid in the separation of sugar phosphates (often a challenge in LC-MS due to their high polarity and similar structures), ion-pairing agents can be added to the RPLC mobile phase (Bennett et al., 2009; Buescher et al., 2010; Kimball & Rabinowitz, 2006; Lu et al., 2010, 2014, 2008; Luo et al., 2007; Rabinowitz & Kimball, 2007). Luo et al. (2007) compared the suitability of different volatile alkylamines as ion-pairing agents for the targeted analysis of organic acids, sugar phosphates and nucleotides (Luo et al., 2007). Triethylamine (TEA), tripropylamine (TPrA), tributylamine (TBA), tripentylamine (TPeA), and trihexylamine (THA), adjusted to pH 6.8 with 5mM acetic acid were compared in the study (Luo et al., 2007). Alkylamines with shorter alkyl chains (TEA and TPrA) were unable to separate isomers. TPeA and THA, which contained long alkyl chains, exhibited very long retention times and low sensitivity due to broad peaks. TBA was considered the most suitable ion-pairing agent for RPLC-MS, although it was unable to

separate 2-/3-PG without altering the pH, resulting in a loss of organic acid retention and separation (Luo et al., 2007).

Lu et al. (2008) combined the HILIC method described by Bajad et al. and the ion-pair RPLC described by Luo et al. with negative mode ionization, which improved CCM coverage, separation and signal for negatively charged analytes (Lu, Bennett, & Rabinowitz, 2009).

TBA was used as an ion-pairing agent by Buescher et al. (2010) and Ruhl et al. (2012) for the analysis of 26 and 20 CCM compounds, respectively (Buescher et al., 2010; Rühl et al., 2012). Of the 26 glycolysis, PPP and TCA cycle intermediates, 22 were determined to be quantifiable by UHPLC-MS/MS utilizing a 25 min gradient (Buescher et al., 2010). The method had the ability to separate the isomers citrate/isocitrate, G3P/DHAP and R5P/Ru5P, but was unable to separate 2-/3-PG, and was not suitable for the quantification of oxaloacetate (Buescher et al., 2010). Although the LC-MS/MS method developed by Ruhl et al. was applied to the analysis of 20 CMM, not all of the metabolites could be detected (Rühl et al., 2012). Acetyl-CoA and oxaloacetate degraded during processing, E4P was below the detection limit, G3P and fumarate overlapped in mass and time with unknown contaminants and they had difficulty separating the isomers X5P/R5P, 2-/3-PG and citrate/isocitrate (Rühl et al., 2012).

Although the use of RPLC-MS with the aid of TBA as an ion-pairing agent enhances the separation and detection of different chemical classes involved in CCM, such as carboxylic acids, amino acids, sugar phosphates, nucleotides, and functionalized aromatics, the use of tributylamine (TBA) leads to long-term contamination of LC and MS instrumentation. Switching to a different application or polarity will require extensive and tedious cycles of

cleaning with hazardous organic solvents, although this may never fully eradicate the TBA contamination (Buescher et al., 2010).

#### 5.1.2.4 Anion Exchange Chromatography (AEX) - MS

Anion exchange chromatography (AEX) is a branch of liquid chromatography that can be used for the analysis anionic compounds, without the need for derivatization or ion-pairing agents (Bhattacharya, Fuhrman, Ingram, Nickerson, & Conway, 1995; Wunschel et al., 1997). Bhattacharya et al. (1995) applied AEX to the analysis of 23 metabolites in a single run, utilizing an IonPac AS11 (250 x 4mm) column and a CarboPac PA1 column (Bhattacharya et al., 1995). G3P, DHAP, R5P and X5P could not be detected. CoA was detected but succinyl-CoA and acetyl-CoA could not be detected and the method was unable to resolve succinate/malate, 2-oxoglutarate/G6P, 2-/3-PG (Bhattacharya et al., 1995).

Wunschel et al. (1997) used a CarboPac PA1 column with a NaOH/Na acetate gradient for the separation of sugars, sugar phosphates and sugar acids (Wunschel et al., 1997).

In the two examples above conductivity was utilized as the mode of detection. However as some analytes co-eluted it was impossible to quantify them, even if the two analytes had different structures and masses (Bhattacharya et al., 1995; Wunschel et al., 1997). The coupling of AEX to MS was unfavourable as the high ionic strength of the MP required for separation in AEX can cause the deposition of non-volatile salts at the ion source inlet of the MS. Advancements in ion chromatography instrumentation has led to the advent of an internal ion suppressor. The column outlet can be attached to a membrane suppressor. The suppressor reduces the salt concentration of the eluent by electrochemically exchanging hydroxide ions for protons, so that the eluent running through to detector is neutral (Van Dam et al., 2002). The

outlet of the detector can then be connected to the inlet of the MS. A make-up flow containing organic solvent can be run at a higher flow rate to provide the optimum conditions for ESI-MS.

The AEX-MS method developed by van Dam et al. (2002) has been utilized in other studies for the analysis of CCM compounds (Bolten, Kiefer, Letisse, Portais, & Wittmann, 2007; Kiefer, Nicolas, Letisse, & Portais, 2007; Mashego et al., 2004; Millard, Massou, Wittmann, Portais, & Létisse, 2014; Van Winden et al., 2005; Wu et al., 2005). Mashego et al. (2004) and Van Winden et al. (2005) used the method described by van Dam for the quantification of sugar phosphates in *Saccharomyces cerevisiae* (Mashego et al., 2004; Van Winden et al., 2005). Kiefer et al. (2007) and Bolten et al. (2007) used the van Dam method for the analysis of sugar phosphates and sugar phosphates and some organic acids in *Escherichia coli*, respectively (Bolten et al., 2007; Kiefer et al., 2007; Van Dam et al., 2002). The adapted van Dam method has been used to analyse non-stationary  $^{13}\text{C}$ -metabolite flux analysis in *Chlamydomonas reinhardtii* (Martzolff et al., 2012), to determine the physiological and molecular timing of the glucose to acetate transition in *E.coli* (Enjalbert, Letisse, & Portais, 2013) and for the  $^{13}\text{C}$  metabolic flux analysis in *E. coli* (Millard et al., 2014).

Although the AEX method developed by van Dam and adapted by Kiefer has been used in the successful quantification of CCM compounds in various organisms, the emphasis of these studies has been on phosphorylated sugars and only a select few organic acids (Bolten et al., 2007; Kiefer et al., 2007; Mashego et al., 2004; Millard et al., 2014; Van Winden et al., 2005; Wu et al., 2005).

The **aim** of this research was to test the suitability of a simple 60 minute AEX (IC) -MS targeted method for the analysis of CCM intermediates, including

the coenzymes. This method would allow the separation and detection of numerous classes of energy metabolites without the need for derivatisation, different analytical runs or ion-pairing agents.

The practicality and reliability of the method were investigated by the analysis of glycolysis, TCA and electron chain intermediate standards.

## 5.2 Materials and methods

The materials and methods are the same as those described in Chapter 2, with the following changes:

(1) The Thermo Scientific Dionex™ ICS-5000 first utilised in this study, was substituted for a Thermo Scientific Dionex™ ICS-2100 integrated system, as capillary IC was unsuitable for metabolomics analysis.

## 5.3 Results

Firstly, to determine the optimum conditions for metabolite detection different MP compositions were investigated to maximise ion abundance in the MS.

### 5.3.1 Make-up flow composition

Four make-up flow compositions were investigated for their use with the ICMS system: (1) no make-up flow; (2) acetonitrile (ACN); (3) methanol with 2 mM acetic acid (MeOH + ace.a) and (4) MeOH only.

Three energy metabolites were selected to determine the effects of make-up flow composition on ionisation and abundance, to aid in the selection of the most suitable make-up flow composition for the purposes of this study.

When 100  $\mu\text{M}$  of the pyruvate ( $m/z$  87.0088) standard was injected into the MS using a by-pass loop with no make-up flow the analyte abundance was lower than the abundance of one of the background ions at  $m/z$  94.9804 (Fig. 5-3A). An organic make-up flow assisted in the ionisation of analytes before entry into the MS. When the make-up flow consisted of an organic solvent (ACN, MeOH + ace.a or 100% MeOH) the abundance of pyruvate increased by at least a factor of five (Fig. 5.3B-D & Table 5.1). The highest intensity of pyruvate was achieved using 100% ACN ( $\sim 4.2\text{E}6$ ), followed by MeOH + ace.a ( $\sim 2\text{E}6$ ) and then 100% MeOH ( $\sim 1.6\text{E}6$ ). The spectra became messier with the addition of the organic make-up flows (Fig. 5-3B-D), with MeOH + ace.a (Fig. 5-3C) appearing to have more ionised species compared to ACN (Fig. 5-3B) and 100% MeOH (Fig. 5-3C).

As with pyruvate, when 100  $\mu\text{M}$  glucose ( $m/z$  179.0562) was analysed using no make-up flow, the analyte did not reach an intensity greater than the intensity recorded for the  $m/z$  94.9804 background ion (Fig. 5-4A). When ACN was used the intensity of glucose increased, but intensity was lower than the  $m/z$  94.9804 background ion (Fig. 5-4B). When MeOH + ace.a and 100% MeOH were used the intensity of the glucose ion increased to a level above the background ions (Fig. 5-4C & D). The intensity of the glucose ion was greater when MeOH + ace.a was used instead of 100% MeOH alone;  $4\text{E}6$  compared to  $1.8\text{E}6$  (Fig. 5-4C & D & Table 5-1). Fewer background ions were detected when using 100% MeOH alone, resulting in a cleaner looking spectrum (Fig. 5-4C & D).

2-Oxoglutarate ( $m/z$  145.0140) was detected at the highest intensity using ACN as the make-up flow (Fig. 5-5A),  $3\text{E}7$  compared to  $8.8\text{E}6$  and  $9.7\text{E}6$  when using MeOH + ace.a (Fig. 5-5B) and 100% MeOH (Fig. 5-5C), respectively. (Note: as the intensities of the previous analytes had not reached above the intensities of the background ions when no make-up flow was used,

it was left out of the 2-oxoglutarate analysis). 100% MeOH was taken forward as the make-flow composition for IC-MS analysis as it produced high intensity analyte ions, while resulting in cleaner spectra overall when compared to both 100% ACN and MeOH + ace.a.

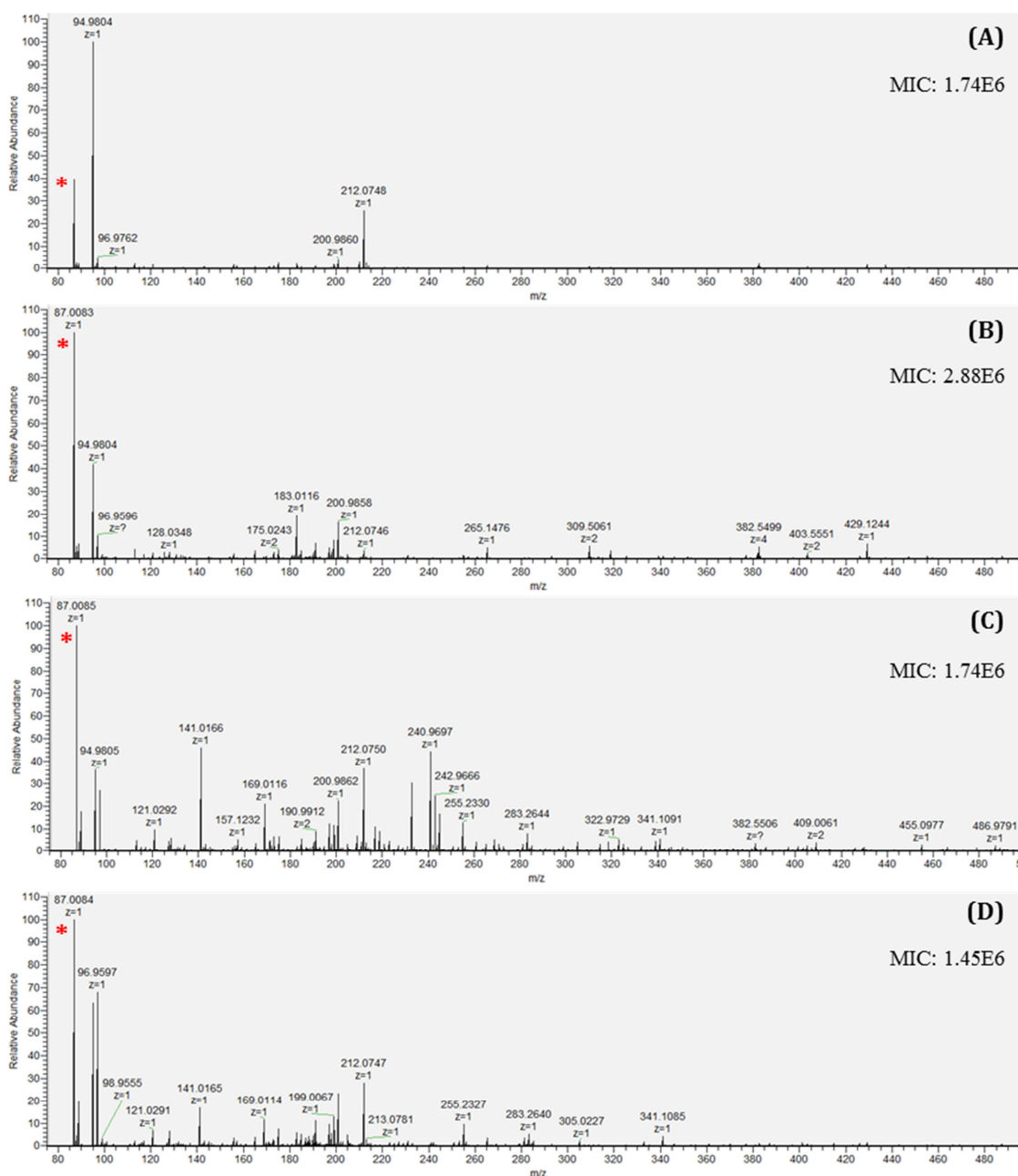


**Figure 5-3** Mass spectra of pyruvate ( $m/z$  87.0084) with **(A)** no make-up flow, **(B)** acetonitrile (ACN), **(C)** methanol with 2 mM acetic acid (MeOH + ace.a) and **(D)** 100% MeOH only. Detection: ESI-FTMS, negative mode. The analyte ion intensity did not reach a level above the background ions when no make-up flow was used **(A)**. The highest intensity and cleanest spectrum was obtained using 100% ACN **(B)**. The second highest intensity was obtained using MeOH + ace.a **(C)**. The intensity of pyruvate was similar to MeOH + ace.a **(C)** when 100% MeOH used with a cleaner spectrum **(D)**. (\*) denotes the pyruvate ion. MIC = maximum ion count.

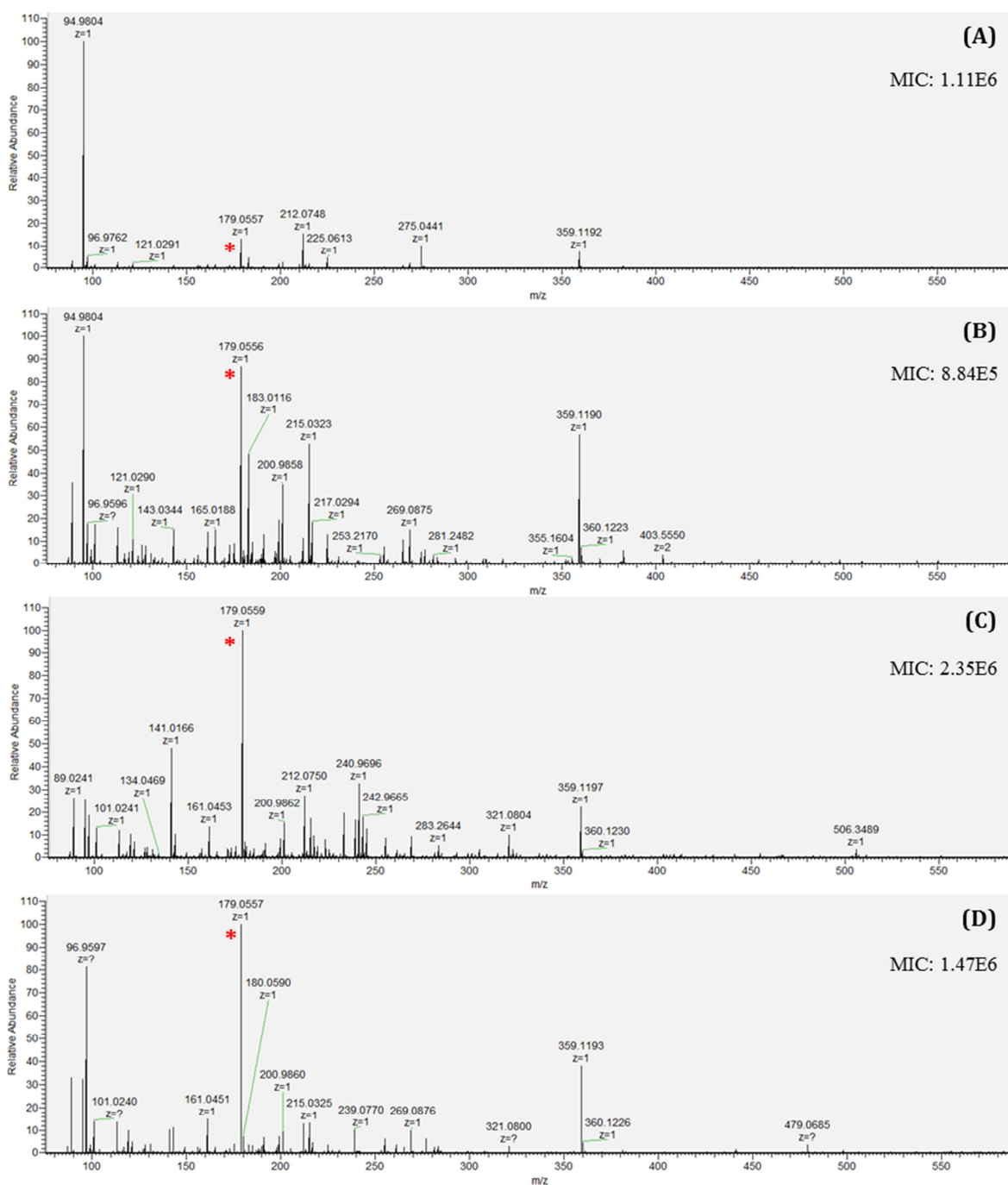


**Figure 5-4** Mass spectra of glucose ( $m/z$  179.0562) with **(A)** no make-up flow, **(B)** acetonitrile (ACN), **(C)** methanol with 2 mM acetic acid (MeOH + ace.a) and **(D)** 100% MeOH only. Detection: ESI-FTMS, negative mode. The analyte ion intensity did not reach a level above the background ions when no make-up flow was used **(A)**. The highest analyte ion intensity was achieved using MeOH + ace.a **(C)**. The second highest intensity was obtained using 100% MeOH **(D)**. The cleanest spectrum was obtained using 100% MeOH **(D)**. (\*) denotes the glucose ion. MIC = maximum ion count.

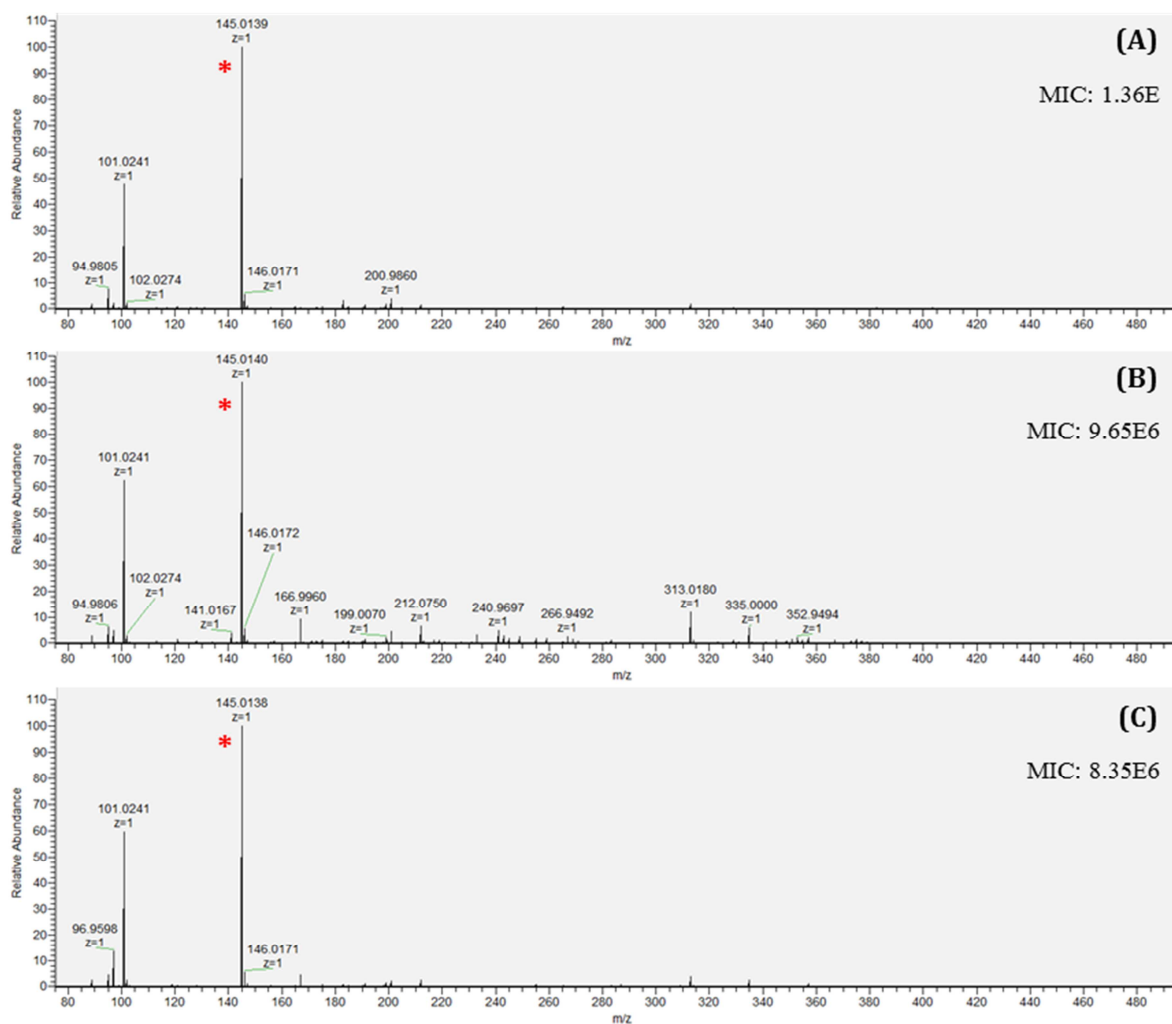


**Figure 5-5** Mass spectra of 2-oxoglutarate ( $m/z$  145.0140) with (A) acetonitrile (ACN), (B) methanol with 2 mM acetic acid (MeOH + ace.a) and (C) 100% MeOH only. Detection: ESI-FTMS, negative mode. The highest analyte ion intensity was achieved using 100% ACN (A). The second highest intensity and cleanest spectrum was obtained using 100% MeOH (C). (\*) denotes the 2-oxoglutarate ion. MIC = maximum ion count.

**Table 5-1** Ion intensities of pyruvate ( $m/z$  87.0084), glucose ( $m/z$  179.0562) and 2-oxoglutarate ( $m/z$  145.0143) using no make-up flow, acetonitrile (ACN), methanol with 2 mM acetic acid (MeOH + 2 mM a. acid) and 100% methanol (MeOH). The metabolites were injected directly into the mass spectrometer and their ion intensities were recorded.

Metabolite	Intensity			
	No make-up	ACN	MeOH + 2 mM a.acid	MeOH only
Pyruvate	751245.1	4120633.8	2000482.8	1646202.3
Glucose	163309.9	1076766	3973986.3	1753060.5
2-Oxoglutarate	-	29776066	8850457	9709970

Once MP composition was optimised, different standard mixes were analysed to optimise separation and identification using the IC-MS method.

## 5.2.2 Standards

### 5.2.2.1 Glycolysis mix

The individual standards from glycolysis were run through the IC system to determine their individual RT times before being analysed in a mix using the IC-MS method. A list of the standards, their masses and  $m/z$  values can be found in Table 5-2.

All of the glycolysis intermediates could be detected using their intact  $m/z$  values, with the exception of dihydroxyacetone (DHAP) and glyceraldehyde 3-phosphate (G3P) (Table 5-2 and Fig. 5-6). The conductivity chromatograms of DHAP and G3P had an intense peak at 28.35 and 28.32 min and a smaller peak at 9.24 and 9.47 min, respectively (Fig. 5-6). The peaks detected at 9 min for each sample had an  $m/z$  of 89.0244, which suggested that they could be the result of DHAP and G3P losing their phosphate group ( $\text{PO}_3^{2-}$ ) and one hydrogen. The presence these peaks at the beginning of the chromatographic

run suggests that the phosphate group is breaking off from the compounds in solution or as a result of the  $\text{OH}^-$  concentration in the eluent. The more intense peaks at 28 min, with an  $m/z$  value of 176.9351 could be the result of two phosphates joining together to produce diphosphate ( $\text{H}_4\text{O}_7\text{P}_2$ ). When the  $[\text{M}-\text{H}]^-$  of DHAP was searched for in the MS data, there were numerous peaks present (Fig. 5-7A). G3P produced one intense peak for  $m/z$  168.9908 at 21.51 min when its mass was searched for in the MS data (Fig 5-7B). Numerous ion peaks were present throughout the MS data for both DHAP and G3P, which could be the result of phosphate losses and bonding, water losses and the production of dimers from the monomer standards (Fig. 5-8). The presence of numerous peaks for each standard suggest that the compounds could be breaking down in the eluent or on column and then breaking down further during ionisation (Fig. 5-7 & 5-8).

The RT of DHAP could not be determined due to the number of peaks detected for the  $m/z$  of the intact compound (Figs. 5-7A). From the MS data the RT of G3P could be 21.51 min (5-7B). Fragment ions with the same  $m/z$  value as DHAP and G3P were detected in the G6P and F6P standards. The G6P fragment ion had a very similar RT to G3P, 21.70 min compared to 21.50 min. Unfortunately, the two peaks could not be resolved from one another using the IC-MS method.

As the intact ion peaks for DHAP and G3P could not be used various reporter ions were considered (Figure 5-8), however none of these were deemed suitable as they were present in almost all of the glycolysis intermediates at the same RTs.

Due to the effect that the presence of the DHAP and G3P standards had on the IC spectrum of the glycolysis mix, and the inability to find unique RTs or reporter ions, these standards were omitted from further standard mixes.

**Table 5-2** A list of the glycolysis standards elemental formulae (EF), molecular weights (MW) and  $m/z$  values ([M-H]). The table lists whether the metabolite was detected (+) or not detected (-) using the IC-MS method and, if it was detected, whether the metabolite mass chromatogram contained multiple peaks (+) or a single peak (-).

<b>Glycolysis</b>					
<b>Metabolite</b>	<b>EF</b>	<b>MW</b>	<b>[M-H]</b>	<b>Detected/Not detected</b>	<b>Multiple peaks</b>
Glucose	C6H12O6	180.0634	179.0562	+	-
Glucose-6-phosphate	C6H13O9P	260.0297	259.0225	+	-
Fructose-6-phosphate	C6H13O9P	260.0297	259.0225	+	-
Fructose-1,6-biphosphate	C6H14O12P2	339.9961	338.9889	+	-
Dihydroxyacetone phosphate	C3H7O6P	169.9980	168.9908	+	+
Glyceraldehyde-3-phosphate	C3H7O6P	169.9980	168.9908	+	+
3-Phosphoglyceric acid	C3H7O7P	185.9929	184.9857	+	-
2-Phosphoglyceric acid	C3H7O7P	185.9929	184.9857	+	-
Phosphoenolpyruvic acid	C3H5O6P	167.9824	166.9752	+	+
Pyruvic acid	C3H4O3	88.0160	87.0088	+	+

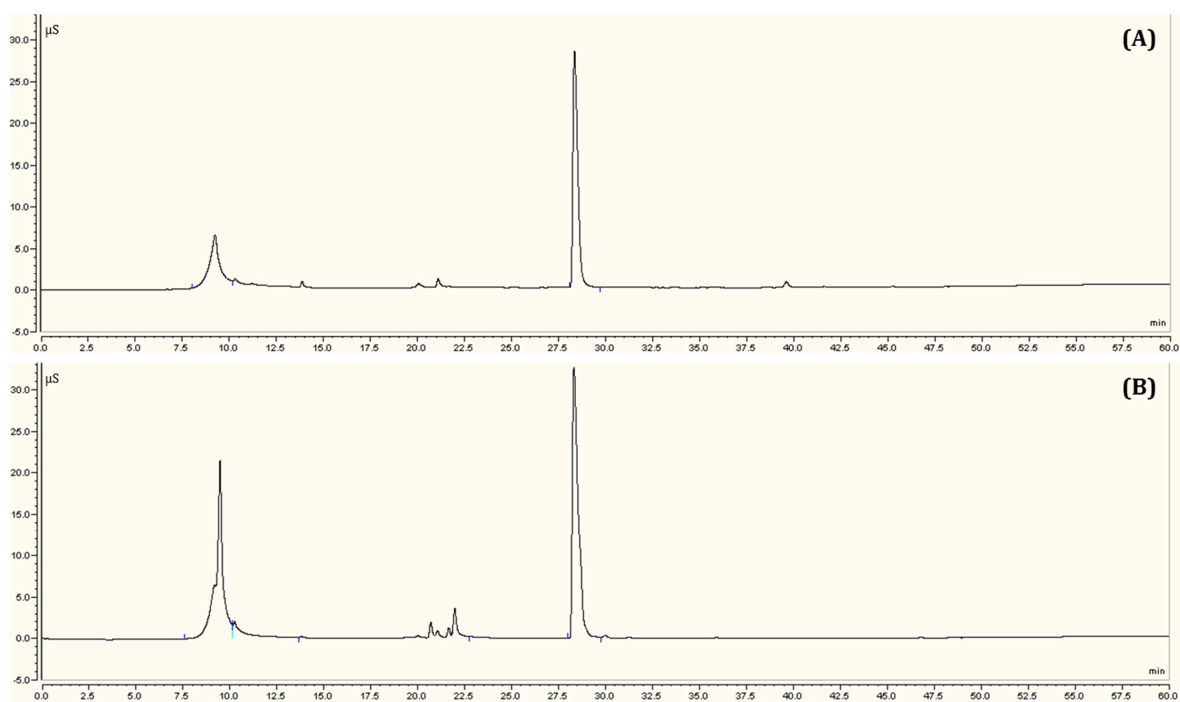


**Figure 5-6** The conductivity chromatograms of (A) dihydroxyacetone (DHAP) and (B) glyceraldehyde 3-phosphate (G3P). Detection: conductivity. Both conductivity chromatograms show a peak at approximately 9.20 min and a more intense peak at approximately 28.5 min (A & B). The presence of more than one peak suggests that the compounds may be breaking down on column or in the eluent.

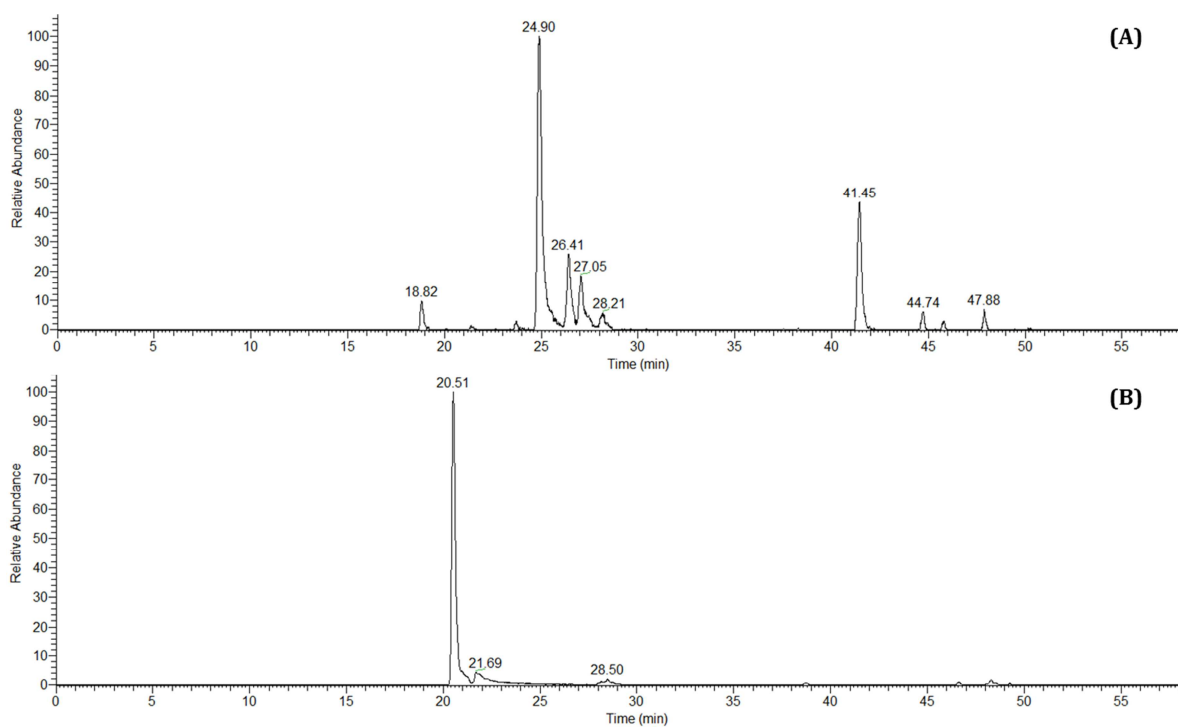


**Figure 5-7** Extracted ion chromatograms (EICs) of  $m/z$  168.9908 from the (A) dihydroxyacetone (DHAP) and (B) glyceraldehyde 3-phosphate (G3P) standards. Detection: ESI-FTMS, negative mode. Multiple peaks present when the  $m/z$  of the DHAP monomer was searched for in the individual standards run (A). When the  $m/z$  of G3P was searched for one intense peak was present at 21.51 min, with two less intense peaks at 21.69 min and 28.50 min (B). Due to the presence of multiple peaks for the same  $m/z$  value, the RT of DHAP could not be determined using the intact ion (A). 20.51 min appeared to be the most likely RT for G3P (A).

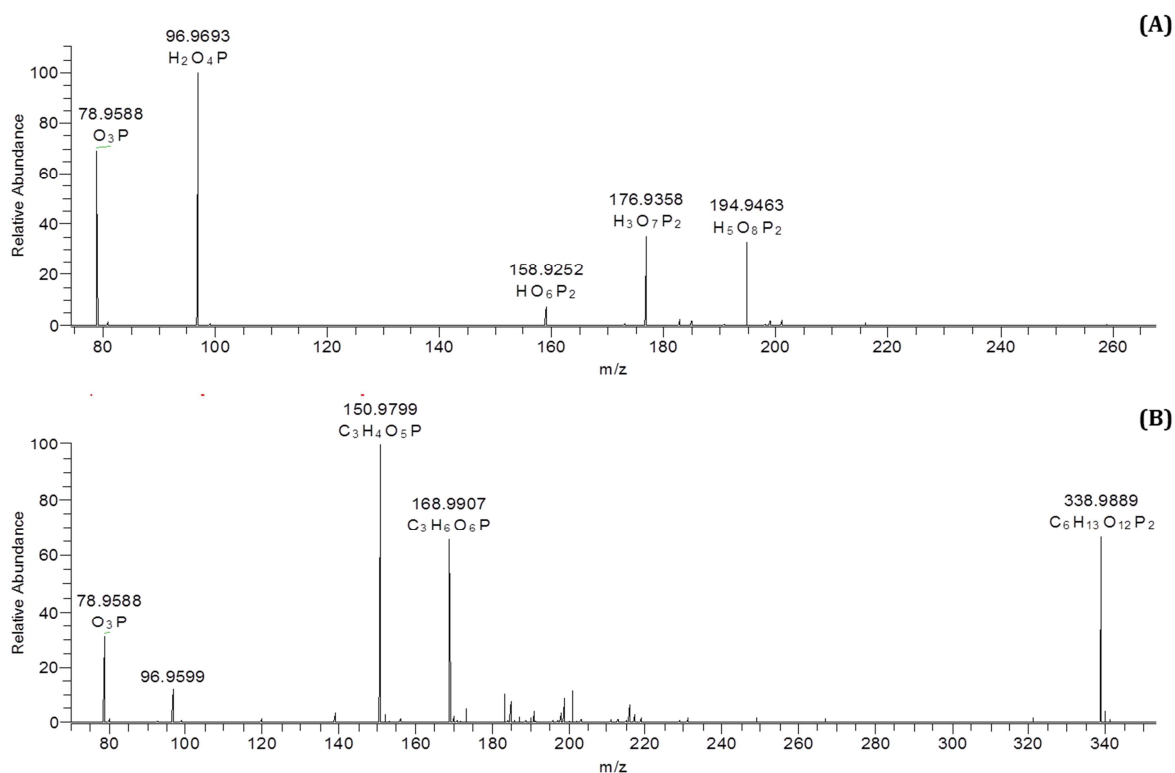


**Figure 5-8** Mass spectrometry (MS) of (A) dihydroxyacetone (DHAP) and (B) glyceraldehyde 3-phosphate (G3P) with possible elemental compositions. Detection: ESI-FTMS, negative mode. Mass tolerance : 4 ppm. Some of the ions detected for the DHAP standard included phosphate ( $m/z$  96.9693), phosphate with a water loss ( $m/z$  78.9586), pyrophosphate ( $m/z$  176.9358), pyrophosphate hydrate ( $m/z$  194.9463) and pyrophosphate with a water loss ( $m/z$  158.9252) (A). Some of the possible ions detected for G3P included the dimer of G3P ( $m/z$  338.9889), the G3P monomer ( $m/z$  168.9907), the G3P monomer with a water loss ( $m/z$  150.9799), phosphate ( $m/z$  96.9599) and phosphate with a water loss ( $m/z$  78.9588). Although there were many ions present, none of these were unique to the DHAP and G3P standards and could be detected in other glycolysis standards (data not shown).

The IC method was able to separate the sugar-phosphate isomers G6P and F6P ( $m/z$  259.0225) (Fig. 5-12(b)). However, they were unable to be completely resolved from one another. The isomers 2- and 3-phosphoglycerate ( $m/z$  184.9857) were unable to be resolved to a sufficient level to be detected as individual ions by the mass spectrometer (Figs. 5-9 & 5-12(d)). Phosphoenolpyruvate (PEP) ( $m/z$  166.9752) and pyruvate ( $m/z$  87.0088) were detected as multiple peaks in the glycolysis mix (Fig. 5-12(e) & (f)). From the individual standards runs it was determined that the correct

RT for PEP was approximately 35.10 min (Fig 5-10) and the correct RT for pyruvate was approximately 10.94 min (Fig 5-11). The second peak detected for PEP was most likely a breakdown product of 2-/3-PG (Fig. 1-12). The peaks detected at RT 29.81 min and 35.20 min for  $m/z$  87.0088 were most likely breakdown products of 2-/3-PG and PEP, respectively (Fig. 5-12).

Using the RT data from the individual standards runs all of the glycolysis metabolites were separated using the IC and their  $m/z$  values detected using the ESI-FTMS (Fig. 5-13), with the omission of DHAP and G3P, whose RTs could not be determined from the IC-MS data, and the exception of 2-/3-PG, which could be detected in the MS as one peak, but not separated by the IC.

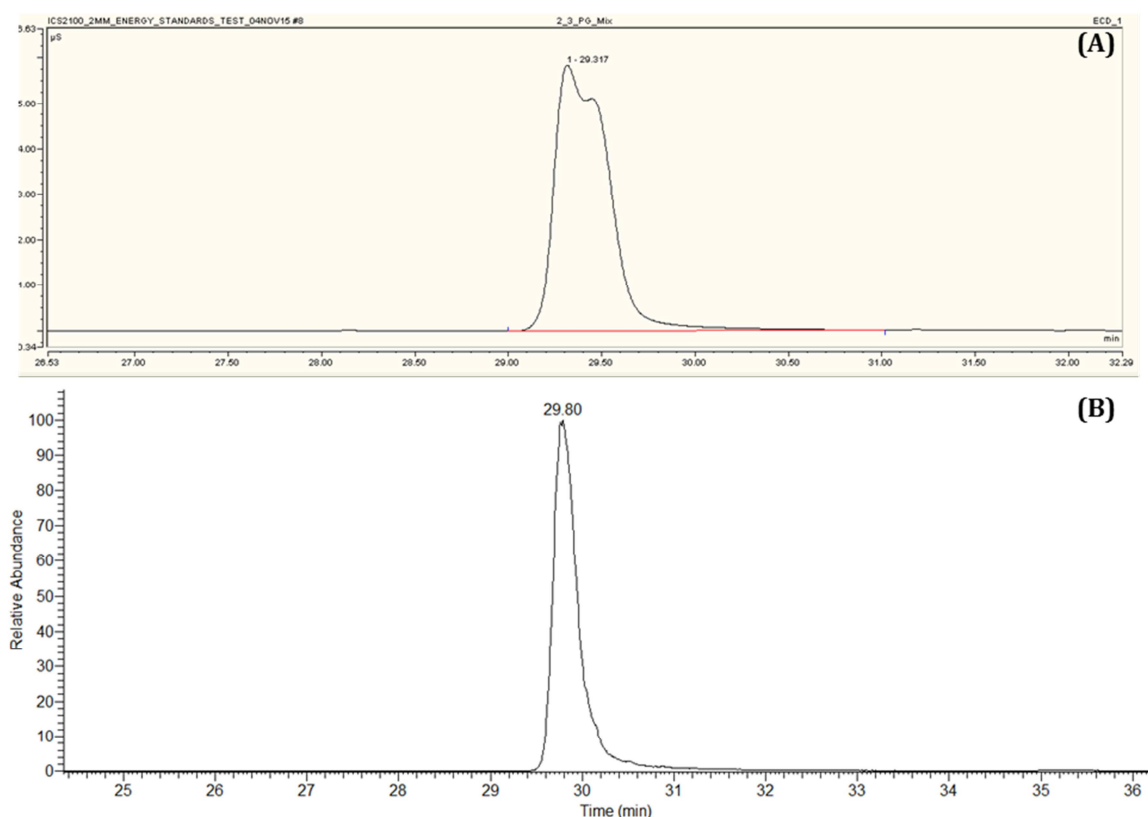


**Figure 5-9** The (A) IC conductivity chromatogram and (B) EIC from MS of 2- and 3-phosphoglycerate. Detection: ESI-FTMS, negative mode. These isomers were unable to be sufficiently separated using the IC method (A) and so were detected as one peak in the MS (B).

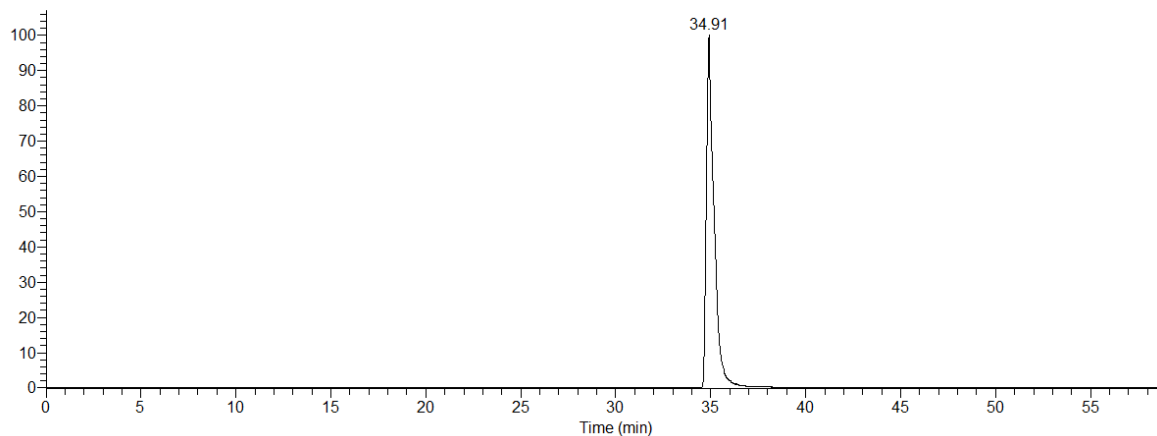


**Figure 5-10** The extracted ion chromatogram (EIC) of phosphoenolpyruvate ( $m/z$  166.9752), showing the actual RT for PEP is closer to 35 minutes rather the peak seen at 29 minutes in the glycolysis mix (Fig.5.12 (e)). Detection: ESI-FTMS, negative mode.

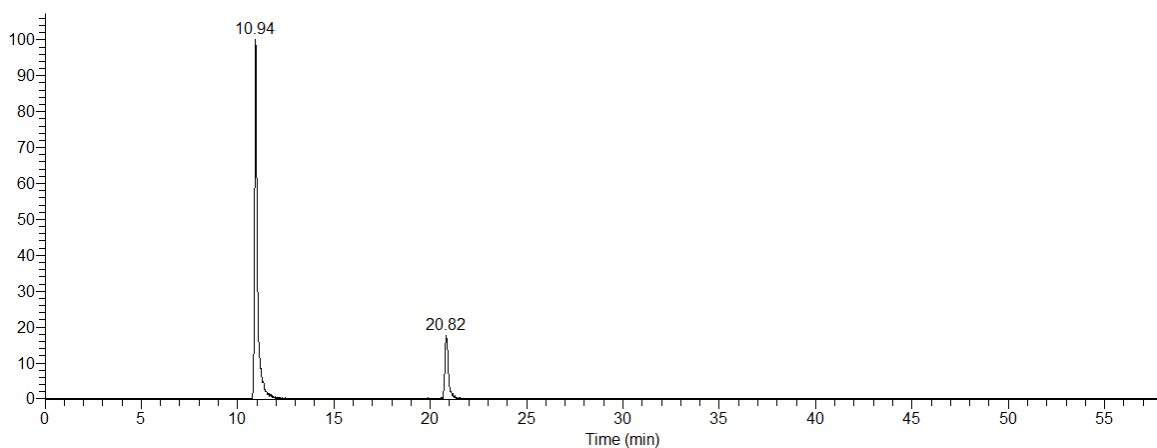


**Figure 5-11** The extracted ion chromatogram (EIC) of the pyruvate standard ( $m/z$  87.0088). Detection: ESI-FTMS, negative mode. Two peaks suggest that the standard may be contaminated. The most intense peak at a RT of 10.94 was pyruvate.

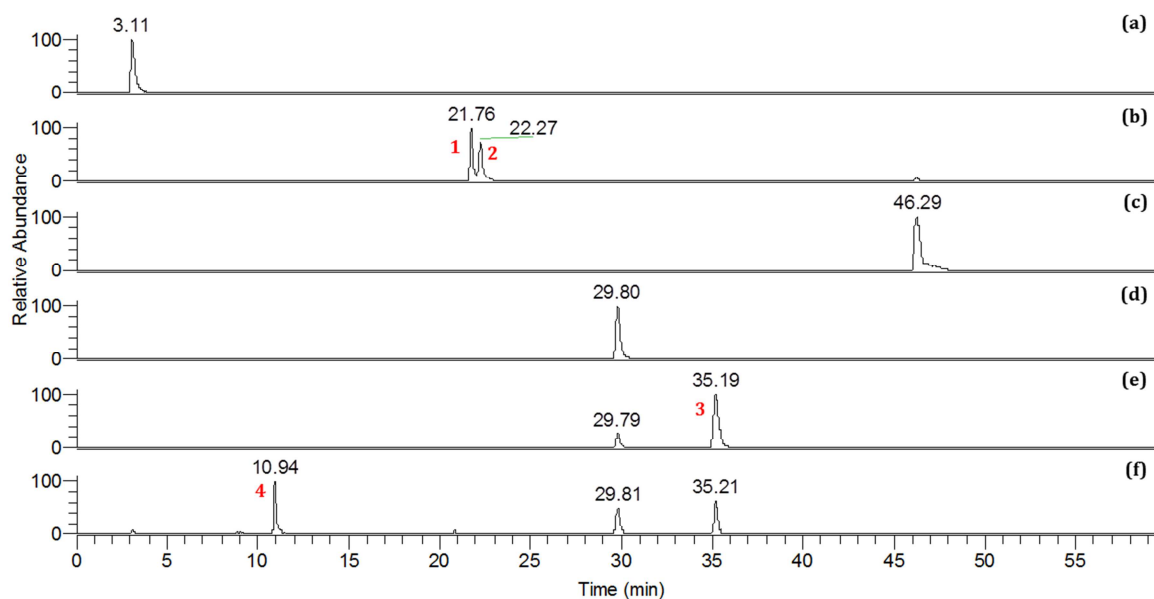


**Figure 5-12** The extracted ion chromatograms (EICs) of the glycolysis metabolites. Detection: ESI-FTMS, negative mode. (a) glucose ( $m/z$  179.0562), (b) (1) glucose 6-phosphate & (2) fructose 6-phosphate ( $m/z$  259.0225), (c) fructose 1,6-bisphosphate, (d) 2-/3-phosphoglycerate ( $m/z$  184.9857), (e) (3) phosphoenolpyruvate ( $m/z$  166.9752) and (f) (4) pyruvate ( $m/z$  87.0088). Note: dihydroxyacetone and glyceraldehyde 3-phosphate were omitted from the glycolysis mix.

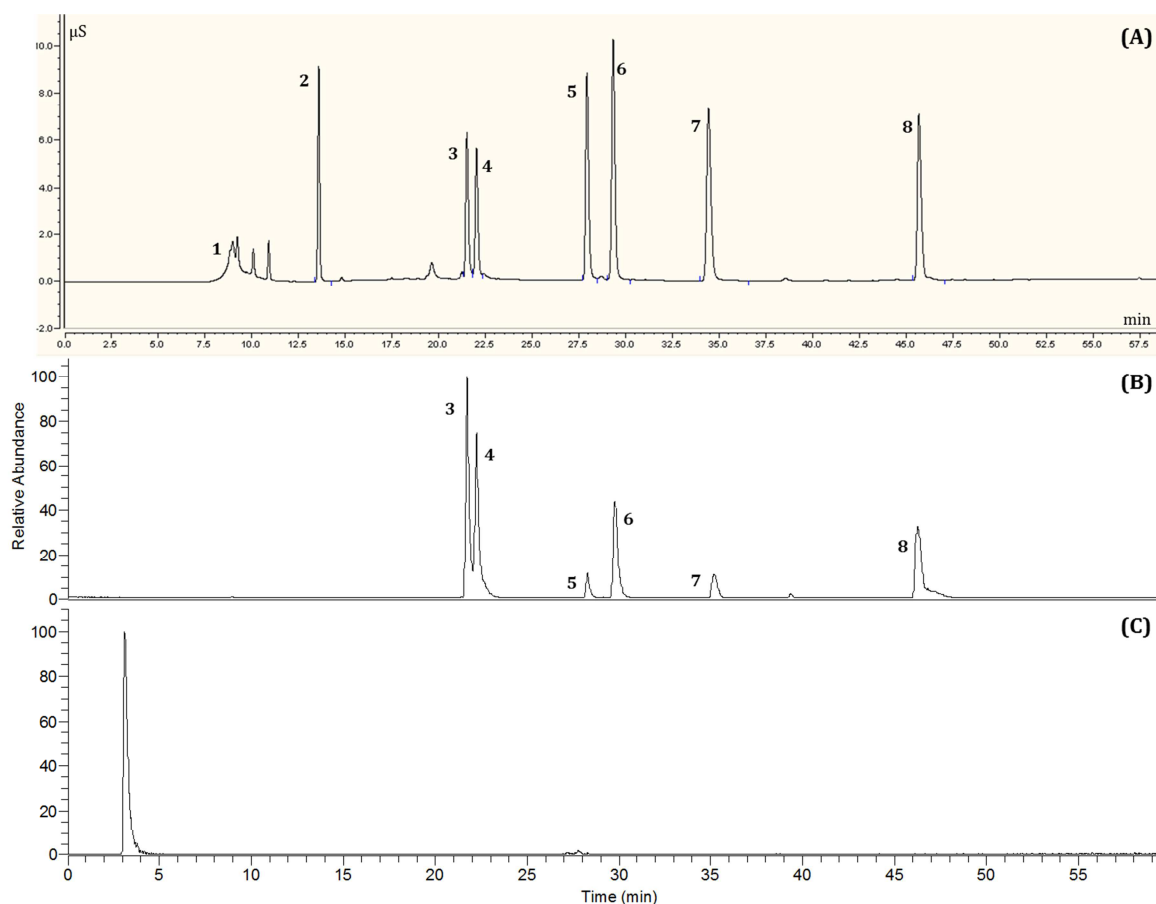


**Figure 5-13** The (A) ion conductivity (IC) chromatogram (B) mass spectrum and (C) an extracted ion chromatogram (EIC) of glucose ( $m/z$  179.0562) of the glycolysis mix. Detection: ESI-FTMS, negative mode. (1) fragment ion with a  $m/z$  89.0244 (2) unknown (not detected in MS); (3) glucose 6-phosphate; (4) fructose 6-phosphate; (5) mix of phosphate, diphosphate and pyrophosphate; (6) 2-/3-phosphoglycerate; (7) phosphoenolpyruvate; (8) fructose 1,6-bisphosphate. Mass spectrum showing the relative abundance of the ions present in the glycolysis mix (B). All of the peaks correspond to the metabolites detected in the IC (A). The presence of glucose ( $m/z$  179.05611) at a retention time (RT) of 3.11 mins, although not prominent in either the IC conductivity or MS, can be confirmed when its  $m/z$  value is searched for ( $m/z$  179.0562) using an extracted ion chromatogram (EIC) from the MS data (C).

### 5.2.2.2 The Citric Acid (TCA) cycle

The individual standards from the TCA cycle were run through the IC system to determine their individual RTs before being analysed in a mix using the IC-MS method. A list of the standards, their masses and  $m/z$  values can be found in Table 5-3.

All of the TCA intermediates could be detected using their intact  $m/z$  values (Table 5-3 and Fig. 5-20), with the exception of the coenzymes, which will be discussed later.

The isomers citrate and isocitrate ( $m/z$  191.0198), that were unable to be separated using the combined LC RPLC/pHILIC method (Fig. 5-14) were able to be baseline resolved from one another using the IC-MS method (Fig. 5-15).

Two peaks were present in the IC and MS when the *cis*-aconitate ( $m/z$  173.0092) standard was run (34.79 min and 39.02 min) consisting of a high abundance of a fragment ion with  $m/z$  129.0190, a smaller abundance of the intact standard ( $m/z$  173.0089) and another fragment ion with an  $m/z$  value of 85.0292 (Fig. 5-16). The fragment ion with  $m/z$  129.0190 could be the result of the parent ion losing a  $\text{CO}_2$  (Fig. 5-16 C). A loss of another  $\text{CO}_2$  from the  $m/z$  129.019 fragment could result in the  $m/z$  85.0292 fragment ion (Fig. 5-16 C). 35.09 min was taken as the correct RT of *cis*-aconitate as there was a higher abundance of the 173.0092 ion compared to 39.24 min. To determine which of the two peaks was *cis*-aconitate, fragmentation of each of the peaks could be carried out and the fragmentation patterns matched to a known fragmentation spectrum of *cis*-aconitate.

Succinate ( $m/z$  117.0194), fumarate ( $m/z$  115.0038) and malate ( $m/z$  133.0143) could not be separated using IC alone (Fig. 5-17 A), but were able to be distinguished from one another using the IC-MS method (Fig. 5-17 B). Succinate and malate were unable to be resolved from each other on the IC (Fig. 5-17 A), but could be detected in the MS separately using their  $m/z$  values (Fig 5-17 (B) (b) & (d)). Fumarate was separated from succinate and malate in the IC (Fig. 5-17 A), and the breakdown product from malate with

the same mass as fumarate ( $m/z$  115.0038) could be determined in the MS due to the difference in RT from fumarate (Fig. 5-17 B (b) & (c)).

Oxaloacetate ( $m/z$  130.9987) was detected as several peaks in the IC and MS (Fig. 5-18). The EIC of the oxaloacetate standard showed multiple peaks for  $m/z$  130.9987 (Fig. 5-18 B). The presence of multiple peaks in the IC and the MS could be the result of the standard breaking up in the eluent or on column. One RT could not be determined for oxaloacetate due to the presence of three intense peaks when  $m/z$  130.9987 was extracted from the mass spectrum data and the inability to identify any fragments unique to the standard. The most intense peak for  $m/z$  130.9987 was detected at 36.17 min, which could be used as the RT of oxaloacetate.

Using the RT data from the individual standards runs all of the TCA metabolites were separated using the IC-MS method (Fig. 5-19), with the exception of oxaloacetate and the co-enzymes.

**Table 5-3** A list of the TCA cycle intermediates elemental formulae (EF), molecular weights (MW) and  $m/z$  values ([M-H]). The table lists whether the metabolite was detected (+) or not detected (-) using the IC-MS method and, if it was detected, whether the metabolites mass chromatogram contained multiple peaks (+) or a single peak (-).

### TCA cycle

Metabolite	Formula	MW	[M-H]	Detected/Not detected	Multiple peaks
Citric acid	C <sub>6</sub> H <sub>8</sub> O <sub>7</sub>	192.0270	191.0198	+	-
Isocitric acid	C <sub>6</sub> H <sub>8</sub> O <sub>7</sub>	192.0270	191.0198	+	-
<i>cis</i> -Aconitic acid	C <sub>6</sub> H <sub>6</sub> O <sub>6</sub>	174.0164	173.0092	+	+
2-Oxoglutaric acid	C <sub>5</sub> H <sub>6</sub> O <sub>5</sub>	146.0215	145.0143	+	-
Succinyl-CoA	C <sub>25</sub> H <sub>40</sub> N <sub>7</sub> O <sub>19</sub> P <sub>3</sub> S	867.1313	866.1241	+	+
Succinic acid	C <sub>4</sub> H <sub>6</sub> O <sub>4</sub>	118.0266	117.0194	+	-
Fumaric acid	C <sub>4</sub> H <sub>4</sub> O <sub>4</sub>	116.0110	115.0038	+	-
Malic acid	C <sub>4</sub> H <sub>6</sub> O <sub>5</sub>	134.0215	133.0143	+	-
Oxaloacetic acid	C <sub>4</sub> H <sub>4</sub> O <sub>5</sub>	132.0059	130.9987	+	+
Acetyl-CoA	C <sub>23</sub> H <sub>38</sub> N <sub>7</sub> O <sub>17</sub> P <sub>3</sub> S	809.1258	808.1186	+	+
CoA	C <sub>21</sub> H <sub>36</sub> N <sub>7</sub> O <sub>16</sub> P <sub>3</sub> S	767.1152	766.108	+	+

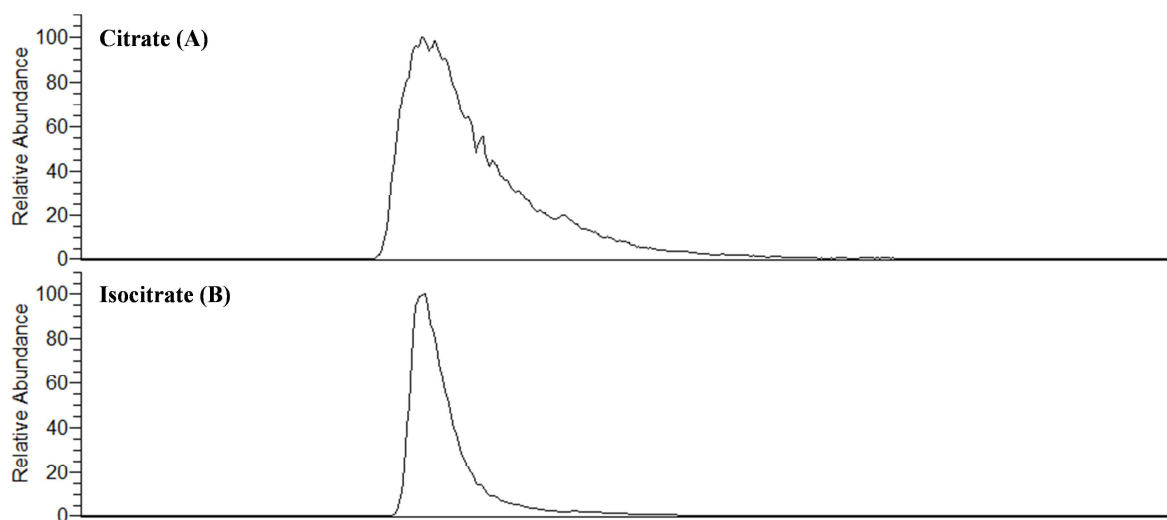


**Figure 5-14** The extracted ion chromatograms (EICs) of (A) citrate and (B) isocitrate obtained using the combined RPLC/pHILIC LCMS method. Detection: ESI-FTMS, negative mode. The isomers could not be separated for quantification using this method.

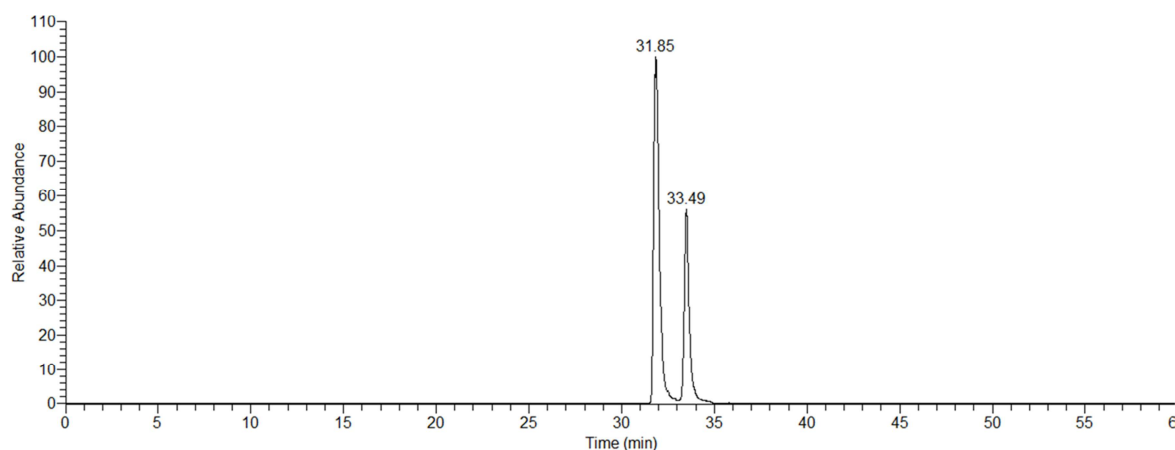


**Figure 5-15** The extracted ion chromatogram (EIC) of a citrate and isocitrate mix using the IC-MS method. Detection: ESI-FTMS, negative mode. Using the RTs from the IC data the peak at RT 31.85 min was identified as citrate and the peak at RT 33.49 min was identified as isocitrate.

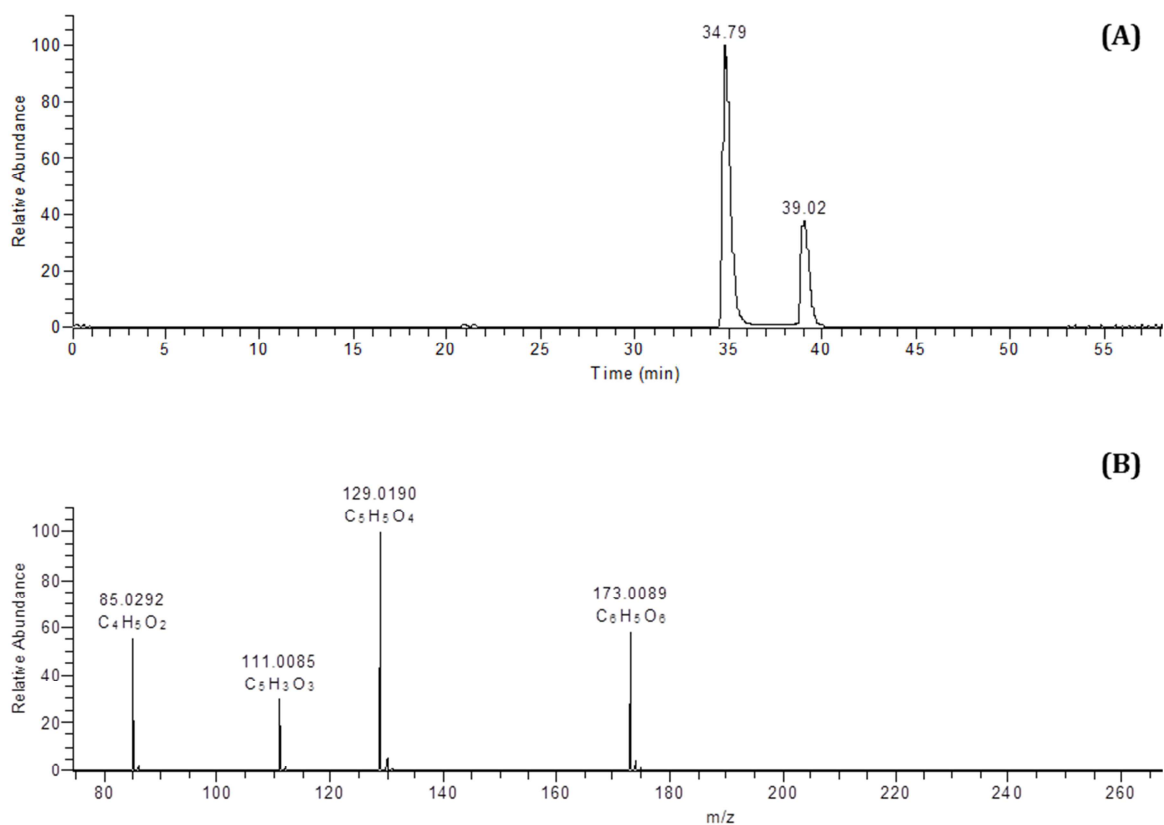


**Figure 5-16** The (A) extracted ion chromatogram (EIC) ( $m/z$  173.0092) and (B) mass spectrum (MS) of the *cis*-aconitate standard. Detection: ESI-FTMS, negative mode. When the  $m/z$  of *cis*-aconitate was searched for, two peaks were detected (A). The intact mass of *cis*-aconitate was not the most abundant ion, instead a fragment with  $m/z$  129.0190, possibly resulting from a CO<sub>2</sub> loss from the standard, was the most abundant (B). Other fragment ions included  $m/z$  111.0085 (possibly due to a water loss from  $m/z$  129.0190) and  $m/z$  85.0292 (possibly resulting from a CO<sub>2</sub> loss from the  $m/z$  129.0190 fragment) (B).

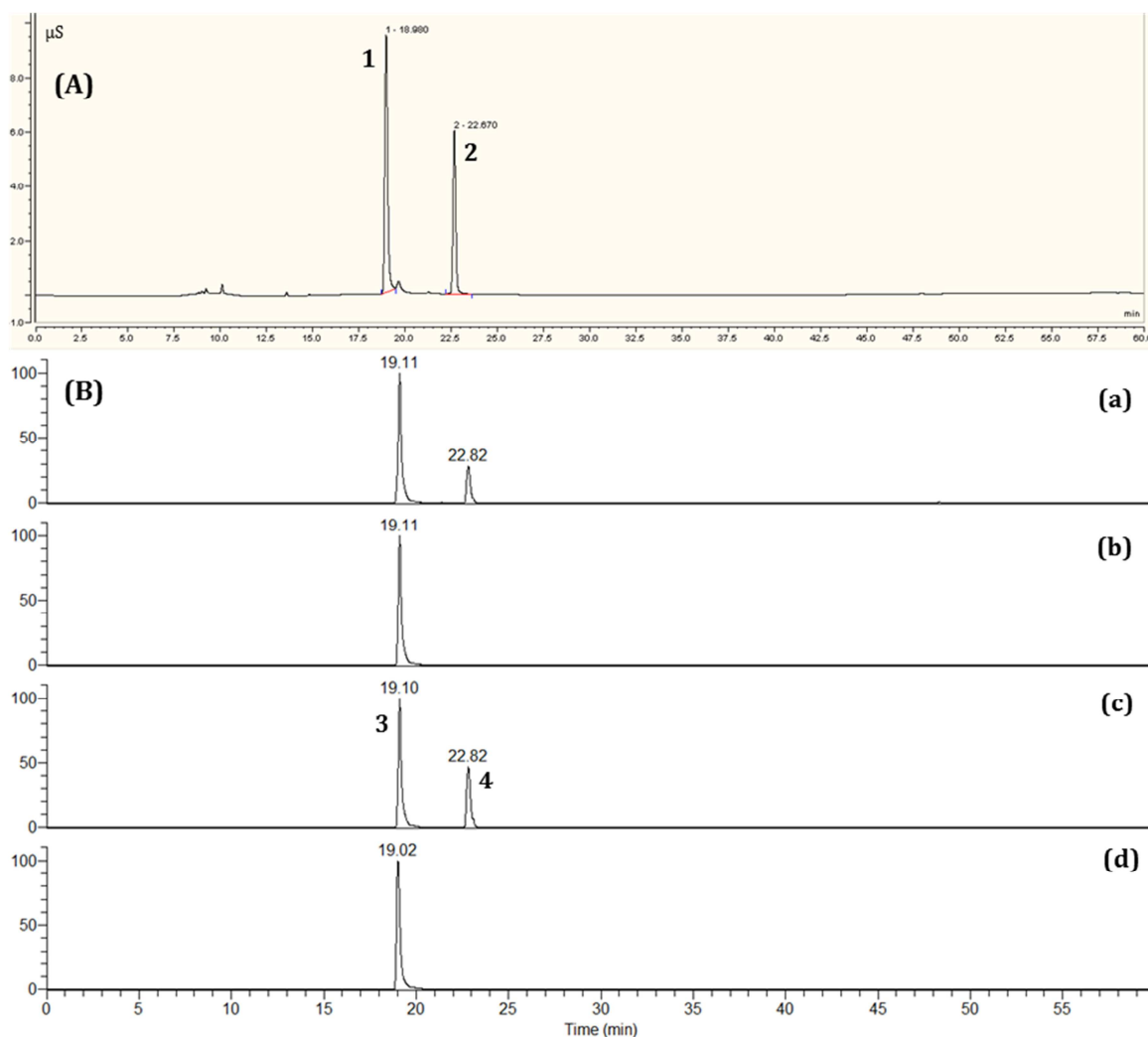


**Figure 5-17** Comparison of the (A) IC chromatogram of (1) malate & succinate and (2) fumarate and (B) the extracted ion chromatograms (EICs) of (a) the full MS of a malate, succinate and fumarate mix (b) malate ( $m/z$  133.0143), (c) fumarate ( $m/z$  115.0038) and (d) succinate ( $m/z$  117.0194). Detection: conductivity (A) and ESI-FTMS, negative mode (B). In the IC, malate and succinate co-elute at around 19 min (A; peak (1)). The mass spectrometer was used to distinguish between these two metabolites as they have different masses (B (b)&(d)). Conversely, the IC was used separate fumarate (4) and the breakdown product of malate (3), which has the same mass as fumarate (B). This enabled the correct RTs to be determined and malate, fumarate and succinate to be identified using IC-MS.

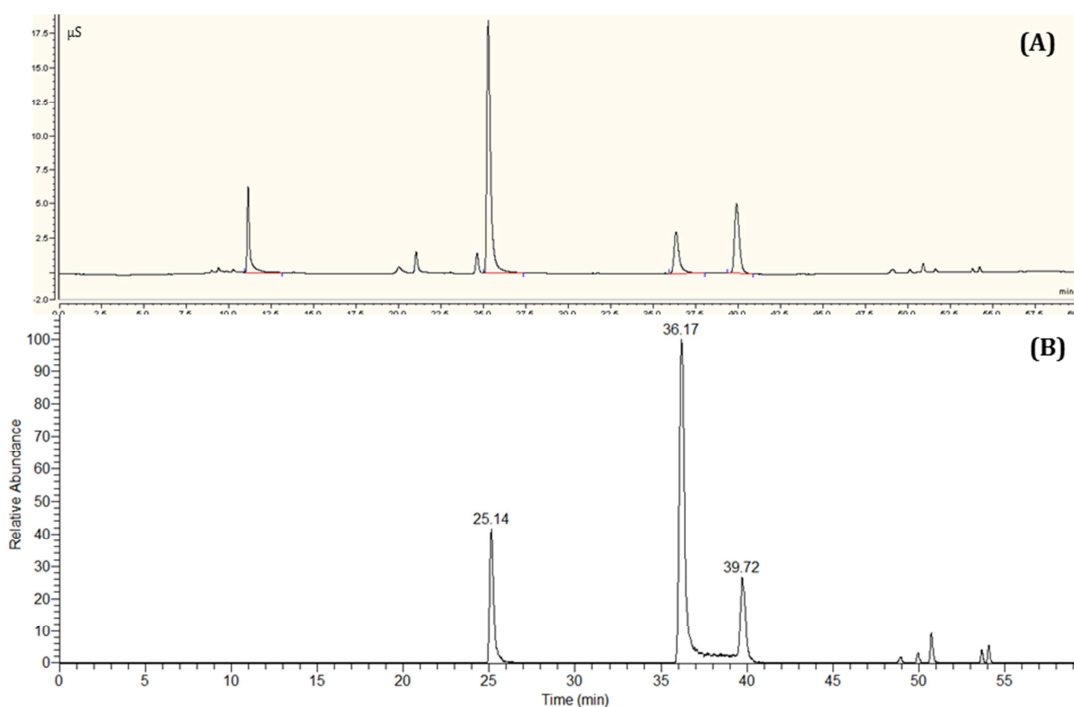


**Figure 5-18** The (A) conductivity chromatogram and (B) extracted ion chromatogram (EIC) of the oxaloacetate ( $m/z$  130.0143) standard. Detection: conductivity (A) and ESI-FTMS, negative mode (B). Multiple peaks were detected for oxaloacetate in the IC (A) and the MS (B), suggesting that the standard was contaminated or breaking up in the eluent or on column in the IC.

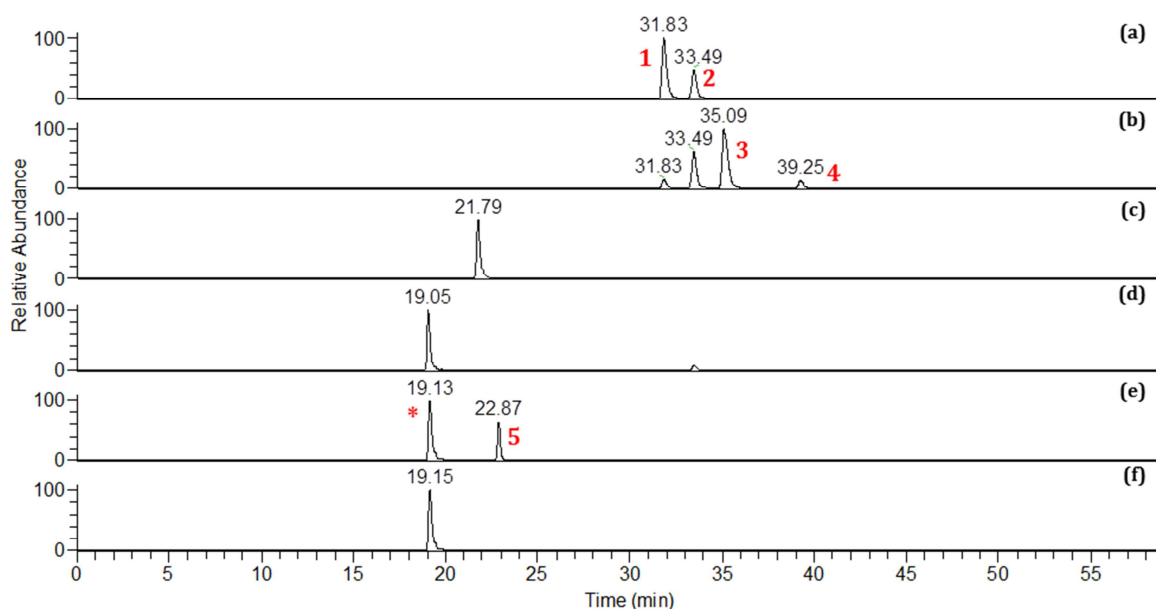


**Figure 5-19** The extracted ion chromatograms (EICs) of the individual intermediates in the TCA mix. Detection: ESI-FTMS, negative mode. (a) (1) citrate and (2) isocitrate ( $m/z$  191.0198), (b) (3 and 4) *cis*-aconitate ( $m/z$  173.0092), (c) 2-oxoglutarate ( $m/z$  145.0143), (d) succinate ( $m/z$  117.0194), (e) (5) fumarate ( $m/z$  115.0038), (f) malate ( $m/z$  133.0143). Note: \* is a breakdown product of malate (e).

### 5.2.2.3 The Co-enzymes

When coenzyme A (CoA), acetyl-CoA and succinyl-CoA standards were analysed using the IC-MS method each of the compounds produced two intense peaks at RTs of 52.7 and 57.4 min (Fig. 5-20).

The  $[M-H]^-$  of the singly charged intact masses of acetyl-CoA ( $m/z$  808.1186) and succinyl-CoA ( $m/z$  866.1241) could not be used to determine these compounds RTs. The doubly charged  $m/z$  values could not be used either,  $m/z$  403.5556 and  $m/z$  432.5583, respectively. In all three co-enzyme MS, the intense peak at 52.7 min corresponded to a small abundance of singly charged CoA ( $m/z$  766.1080) and a high abundance of doubly charged CoA ( $m/z$  382.5503). The peaks at 57.4 min corresponded to a small abundance of ions with the  $m/z$  765.1015 and  $m/z$  509.7315 and a high abundance of doubly charged  $m/z$  765.1015;  $m/z$  382.0481.

To determine whether the compounds were breaking up in the eluent or during ionisation into the MS, the mass spectra from direct infusion of the co-enzymes into the MS were compared to the mass spectra obtained when the co-enzymes were run on a 100mM  $OH^-$  isocratic gradient (Figs. 5-21 – 5-23).

Doubly charged acetyl-CoA ( $m/z$  403.5556) was the most abundant ion when the standard was injected directly into the MS (Fig. 5-21 A). When acetyl-CoA was run through the column using 100 mM  $OH^-$  the most abundant ion detected was the doubly charged CoA ( $m/z$  382.5503), with no doubly charged acetyl-CoA (Fig. 5-21 B). From the results it appeared that acetyl-CoA was being broken down in the eluent or on the column before introduction into the MS (Fig. 5-21). Regardless of the method of introduction to the MS, the most abundant ion detected in the succinyl-CoA standard was doubly charged CoA with a small amount of succinate (Fig. 5-22). When the succinyl-CoA standard was run using the  $OH^-$  gradient, succinate eluted

before the CoA fragment (Fig. 5-22 B). These results suggest that the compound is breaking up in solution. CoA was detected in its doubly charged form regardless of the method used.

The RT of CoA could be determined using its doubly charged  $m/z$  value. However the IC-MS method was not suitable for the separation and detection of the co-enzymes as the RTs of acetyl-CoA and succinyl-CoA could not be determined and the compounds readily broke down to CoA in the eluent, with identical RTs and the lack of any unique fragments.

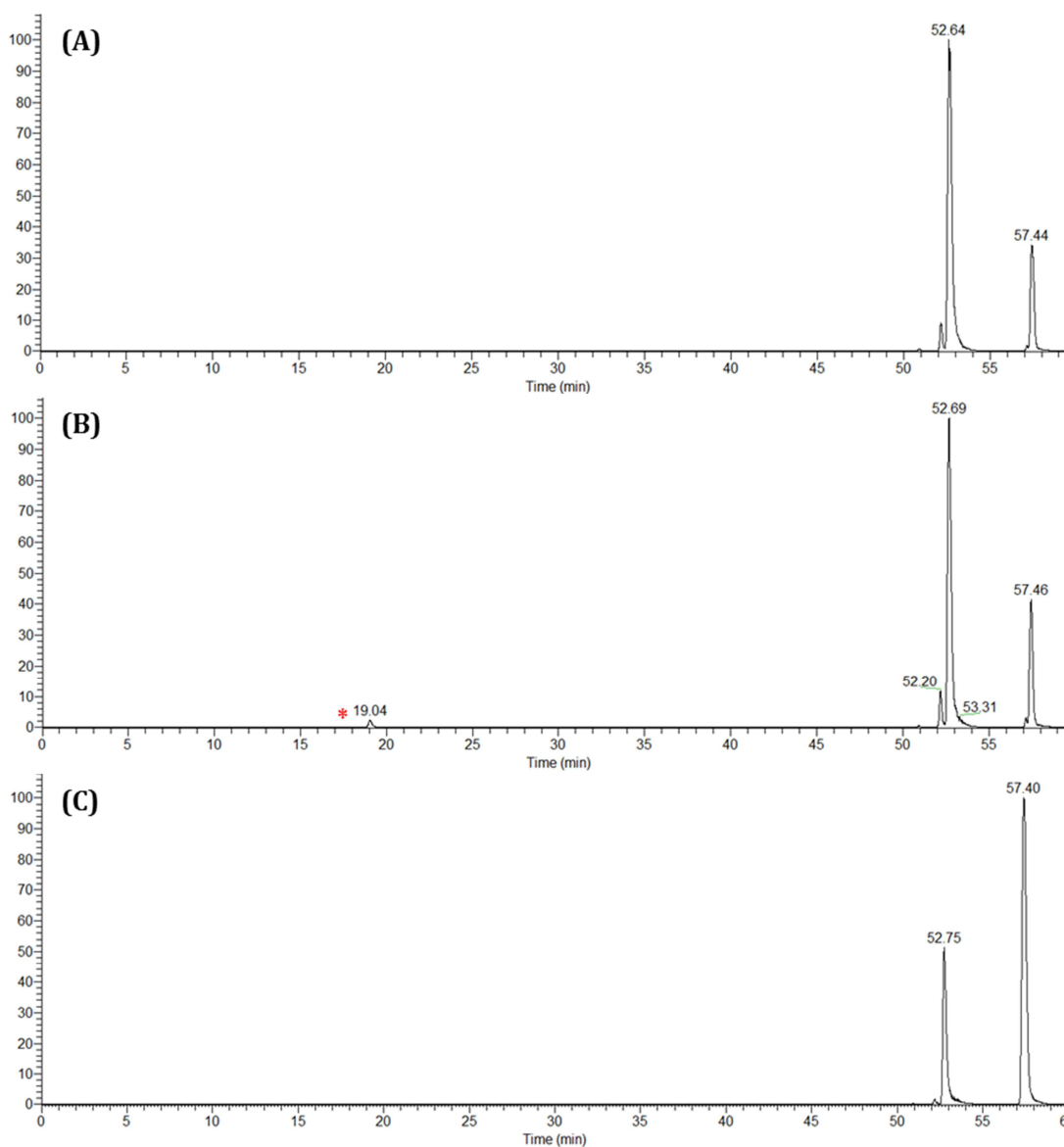


**Figure 5-20** EICs of the base peak of (A) acetyl-CoA, (B) succinyl-CoA and (C) CoA. Detection: ESI-FTMS, negative mode. Concentration: 100  $\mu$ M. Each of the standards produced an almost identical peak pattern when run on the IC-MS gradient. Succinyl-CoA and acetyl-CoA displayed the same peak intensities at each of the RTs, with a more intense peak eluting at 52.7 min (A & B). CoA had the same peak pattern, but with a more intense peak eluting at 57.4 min (C). The succinyl-CoA spectrum had a small peak at 19.04 min (marked with \*) which had  $m/z$  of 117.0194, relating to the succinate group from the compound.

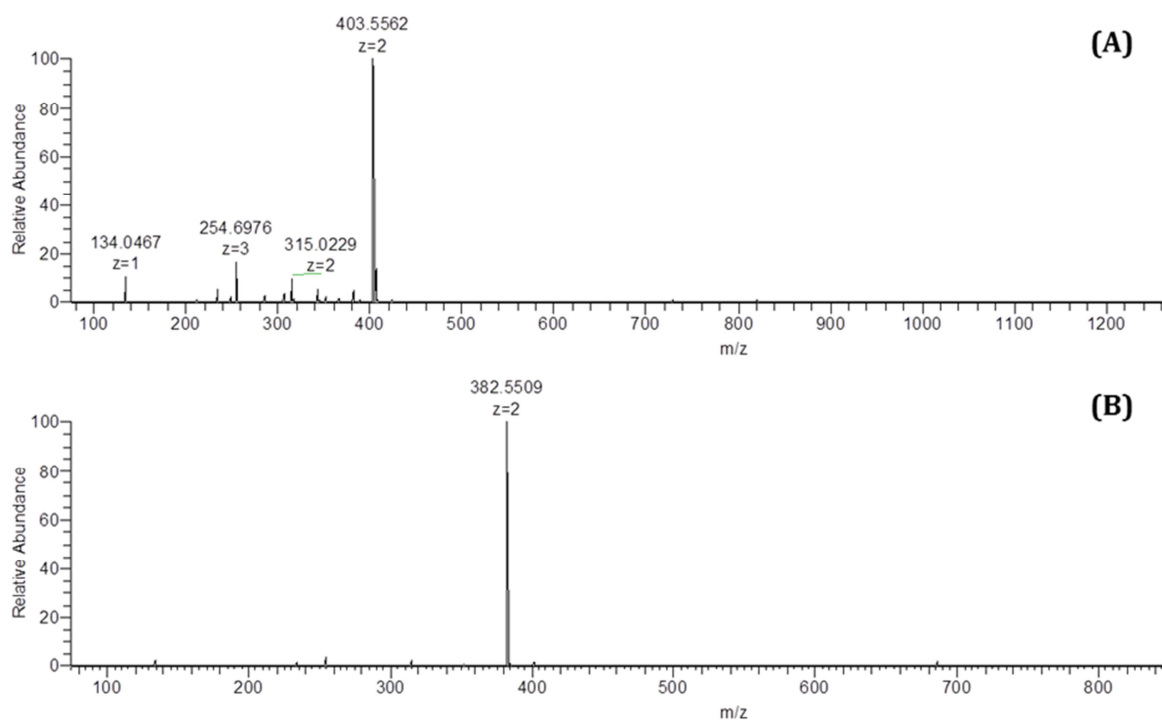


**Figure 5-21** Mass spectrum of (A) the direct injection of acetyl-CoA into the mass spectrometer and (B) acetyl-CoA injected on to the column with a 100 mM isocratic gradient. Detection: ESI-FTMS, negative mode. Concentration: 100  $\mu$ M. Double charged acetyl-CoA ( $m/z$  403.5562) was the most abundant peak when acetyl-CoA was directly injected onto the mass spectrometer (A). Double charged CoA ( $m/z$  382.5509) was the most abundant ion detected when acetyl-CoA was injected onto the column (B) suggesting that acetyl-CoA is being broken down in the eluent or on the column before introduction to the MS.

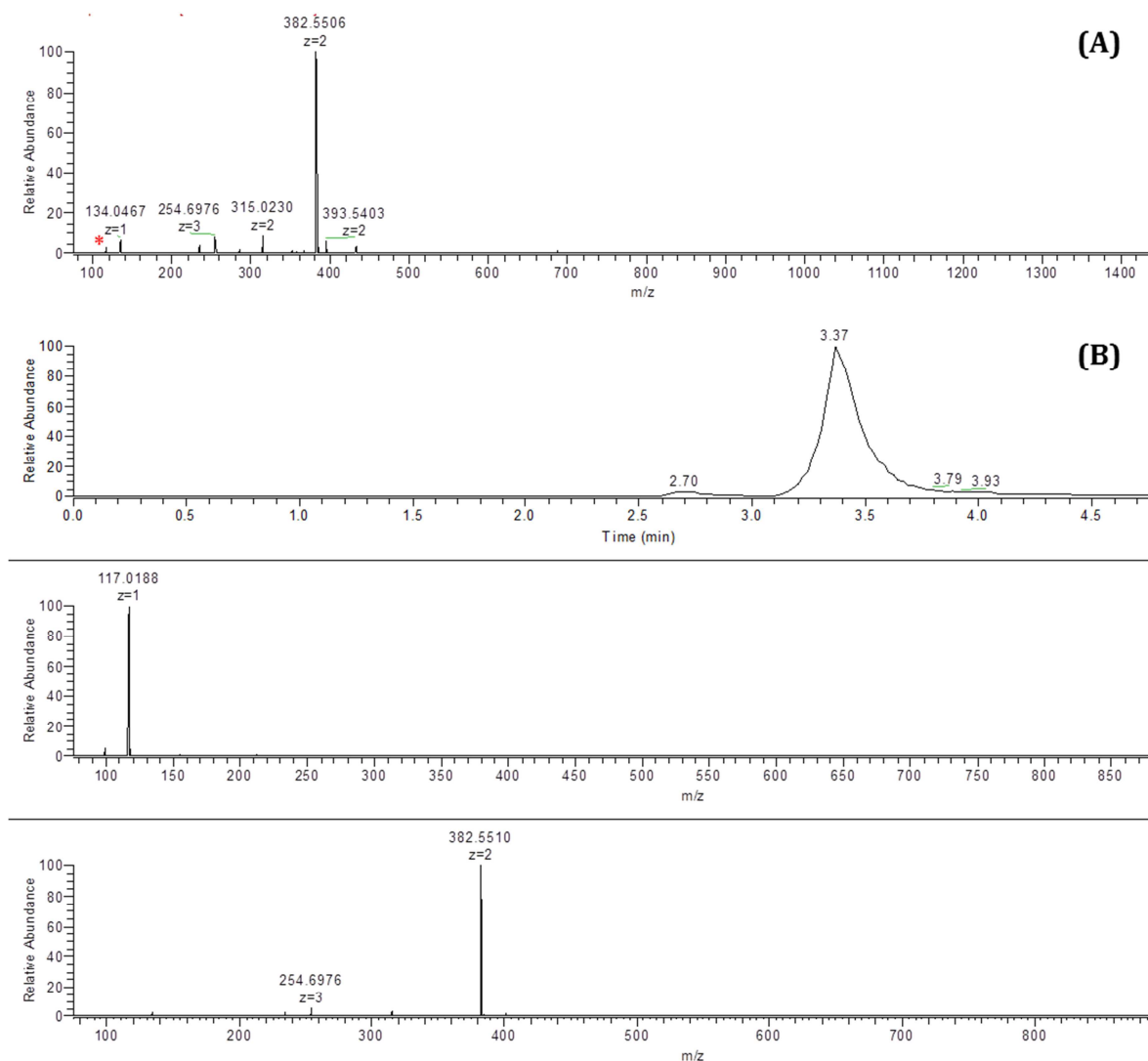


**Figure 5-22** Mass spectrum of (A) the direct injection of succinyl-CoA into the mass spectrometer and (B) succinyl-CoA injected on to the column with a 100 mM isocratic gradient. Detection: ESI-FTMS, negative mode. Concentration: 100  $\mu$ M. Double charged CoA ( $m/z$  382.5511) was the most abundant peak when succinyl-CoA was directly injected onto the mass spectrometer (A) and also when it was injected onto the column (B). Succinate ( $m/z$  117.0188) eluted first when the standard was injected onto the column (RT 2.70), followed by CoA at RT 3.37 (B). Succinate was also present when the standard was directly injected into the MS (\* $m/z$  117.0188). This suggests that the standard was degraded or that the compound was breaking up in solution.

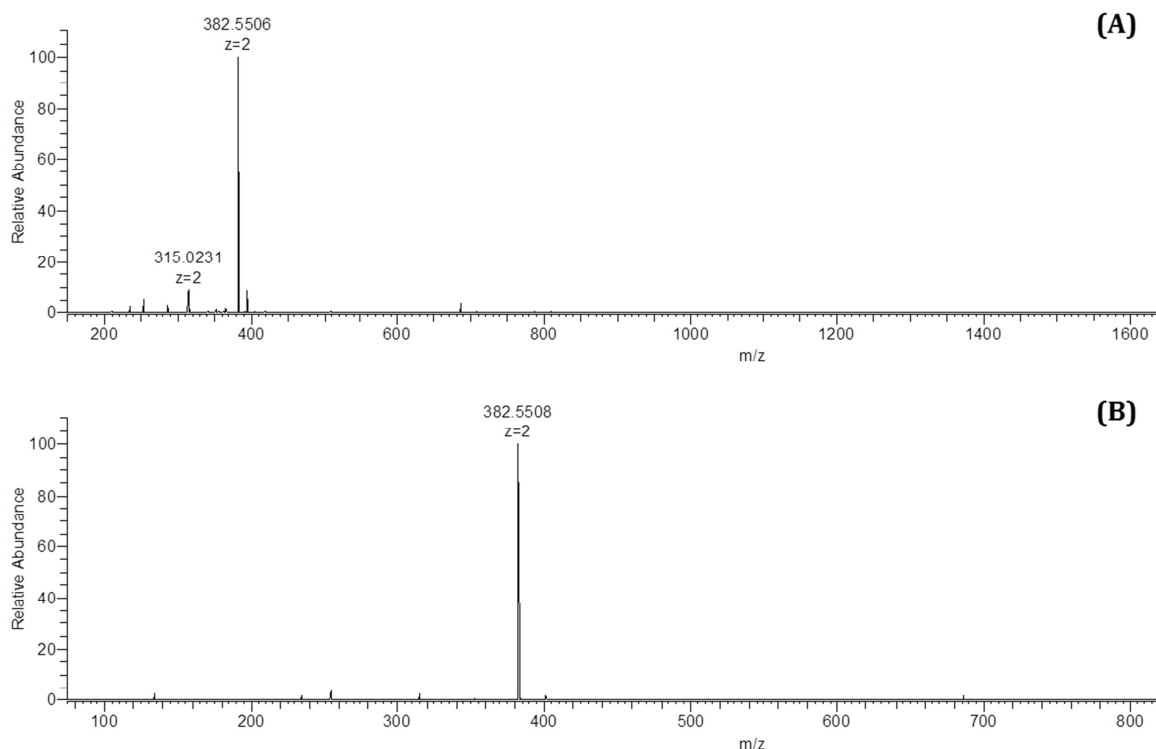


**Figure 5-23** Mass spectrum of (A) the direct injection of CoA into the mass spectrometer and (B) CoA injected on to the column with a 100 mM isocratic gradient. Detection: ESI-FTMS, negative mode. Concentration: 100  $\mu$ M. Double charged CoA ( $m/z$  382.5511) was the most abundant peak when CoA was directly injected into the mass spectrometer (A) and when the standard was injected onto the column (B).

#### 5.2.2.4 Coenzymes and nucleoside phosphates

The individual standards were run through the IC system to determine their individual RTs before being analysed in a mix using the IC-MS method. A list of the standards, their masses and  $m/z$  values can be found in Table 5-4.

ADP and FAD could be detected using their intact  $m/z$  values. ATP, when analysed using the IC-MS, produced an intense peak at 51.81 min, composed of a low intense peak, which corresponded to the intact ion ( $m/z$  505.9886) and a very intense peak that corresponded to ATP minus a phosphate group, i.e. ADP ( $m/z$  426.0222). ADP eluted at approximately 42.16 min, so the peak of the same mass eluting at 51.81 min did not interfere with the identification

of ADP (Fig. 5-24). As the  $m/z$  426.0222 peak was more intense than the  $m/z$  505.9886, this mass was used for the identification of ATP.

Although FAD could be detected by its intact  $m/z$  value, the most abundant peak at the RT was doubly charged FAD (Fig. 5-25).

The IC-MS method was not suitable for the detection of  $\text{NAD}^+$  or  $\text{NADP}^+$ .

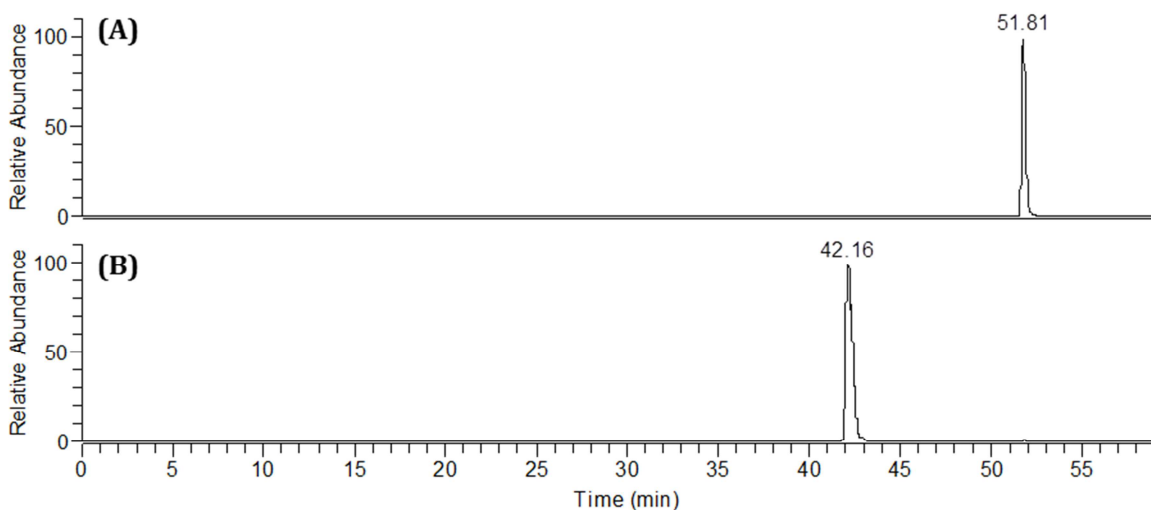


**Figure 5-24** The extracted ion chromatograms (EICs) of  $m/z$  426.0222 from the (A) adenosine triphosphate (ATP) and (B) adenosine diphosphate (ADP) standards. Detection: ESI-FTMS, negative mode. Although the peak was present in both standards, the peak at RT 51.81 min was a fragment of ATP (A) and the peak at RT 42.16 min was the ADP standard (B).

**Table 5-4** A list of the coenzymes and nucleoside phosphates intermediates elemental formulae (EF), molecular weights (MW) and  $m/z$  values ([M-H]).

<b>Coenzymes and nucleoside phosphates</b>			
<b>Metabolite</b>	<b>Formula</b>	<b>MW</b>	<b>[M-H]</b>
NADP <sup>+</sup>	C <sub>21</sub> H <sub>28</sub> N <sub>7</sub> O <sub>17</sub> P <sub>3</sub>	743.0755	742.0683
NAD <sup>+</sup>	C <sub>21</sub> H <sub>29</sub> N <sub>7</sub> O <sub>14</sub> P <sub>2</sub>	664.1170	663.1098
FAD	C <sub>27</sub> H <sub>33</sub> N <sub>9</sub> O <sub>15</sub> P <sub>2</sub>	785.1571	784.1499
ADP	C <sub>10</sub> H <sub>15</sub> N <sub>5</sub> O <sub>10</sub> P <sub>2</sub>	427.0294	426.0222
ATP	C <sub>10</sub> H <sub>16</sub> N <sub>5</sub> O <sub>13</sub> P <sub>3</sub>	506.9958	505.9886

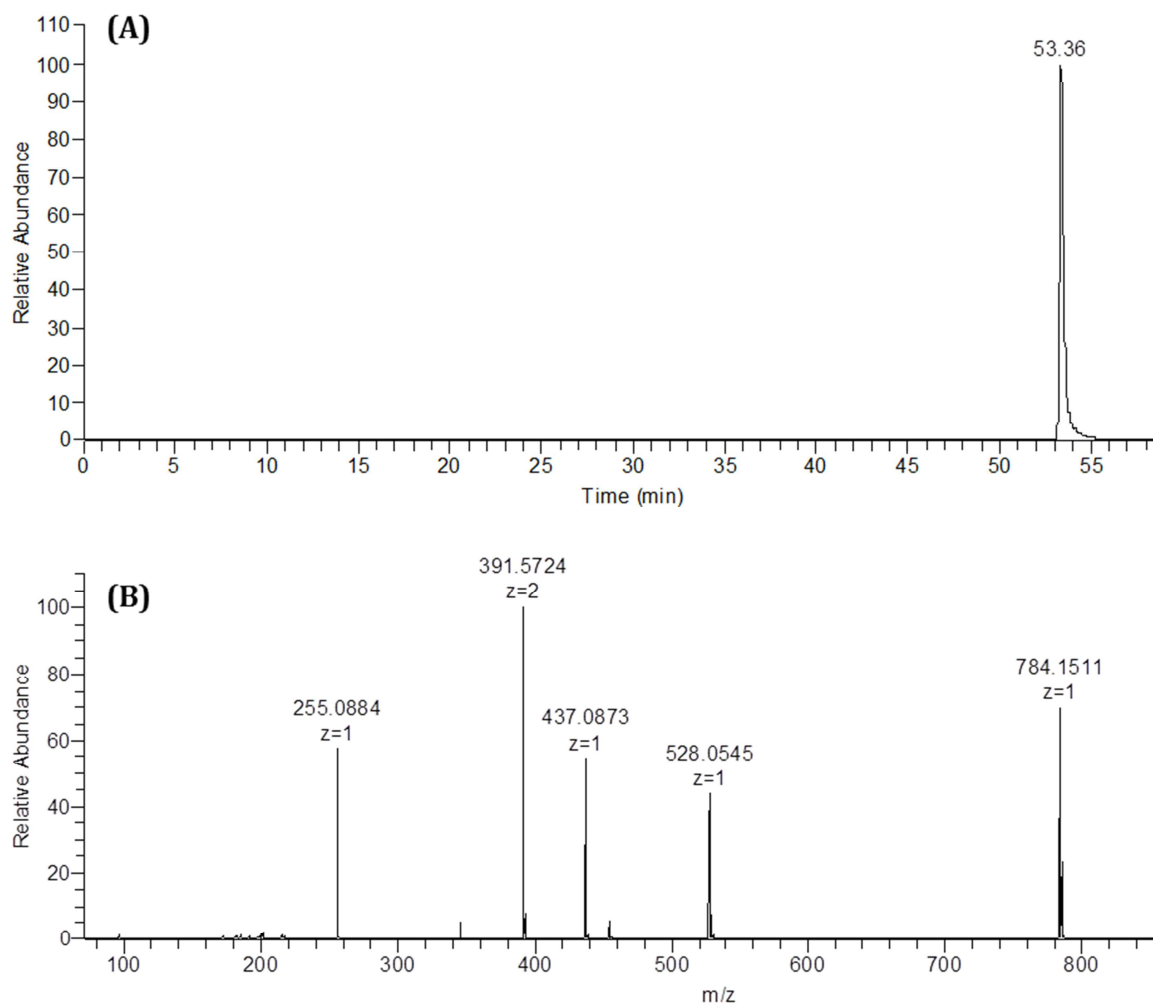


**Figure 5-25** The (A) extracted ion chromatogram (EIC) of the molecular ion of flavin adenine dinucleotide (FAD)  $m/z$  784.1499 and (B) the mass spectrum (MS) at the RT of the FAD standard (53.36 min). Detection: ESI-FTMS, negative mode. The most intense peak at 53.36 min is the doubly charged compound ( $m/z$  391.5724) (B).

Using the data from the standard mixes a total mix of all of the energy metabolites analysed in this study were able to be separated and detected using the developed IC-MS method, with the exception of DHAP, G3P, oxaloacetate, acetyl-CoA, succinyl-CoA,  $\text{NAD}^+$  and  $\text{NADP}^+$  (Fig. 5-26).

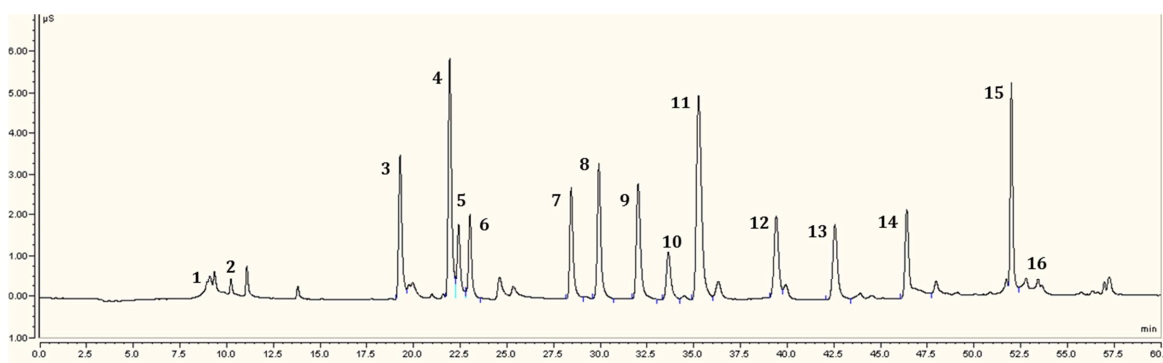


**Figure 5-26** IC conductivity chromatogram of the total mix of the energy metabolism standards using IC-MS. (1) Fragment ion with a  $m/z$  89.0244; (2) pyruvate; (3) malate and succinate (same RT but different mass); (4) 2-oxoglutarate and glucose 6-phosphate (similar RT, different mass); (5) fructose 6-phosphate; (6) fumarate; (7) mix of phosphate, diphosphate and pyrophosphate; (8) 2-/3-phosphoglycerate; (9) citrate; (10) isocitrate; (11) phosphoenolpyruvate and *cis*-aconitate (similar RT, different mass); (12) *cis*-aconitate; (13) ADP; (14) fructose 1,6-bisphosphate; (15) ATP; (16) FAD.

To determine the robustness of the system, the RT reproducibility and the limits of detection of the IC-MS system were calculated.

### 5.2.2.5 Reproducibility

The IC-MS method showed good retention time reproducibility, with RSD values for all of the detectable compounds under 1%, with the exception of fructose 1,6-bisphosphate whose RSD value was 1.03% (Table 5-5).

**Table 5-5** The average retention times (RTs), standard deviations (SD) and relative standard deviations (%RSDs) of each detectable energy metabolism standard. (n=3).

Metabolite	Retention Time (mins)			Average RT (mins)	SD	%RSD
	1	2	3			
Glucose	3.15	3.17	3.11	<b>3.14</b>	0.03	0.97
Glucose-6-phosphate	21.66	21.71	21.75	<b>21.71</b>	0.04	0.21
Fructose-6-phosphate	22.25	22.22	22.36	<b>22.28</b>	0.07	0.33
Fructose-16-biphosphate	46.24	45.44	46.28	<b>45.99</b>	0.47	1.03
3-phosphglycerate	29.72	29.43	29.78	<b>29.64</b>	0.19	0.63
2-phosphoglycerate	29.72	29.61	29.78	<b>29.70</b>	0.09	0.29
Phosphoenolpyruvate	35.06	34.91	35.20	<b>35.06</b>	0.14	0.41
Pyruvate	10.83	10.93	10.94	<b>10.90</b>	0.06	0.56
Citrate	31.84	31.86	31.85	<b>31.85</b>	0.01	0.03
Isocitrate	33.47	33.49	33.48	<b>33.48</b>	0.01	0.03
cis-Aconitate	35.09	35.12	35.07	<b>35.09</b>	0.03	0.07
2-Oxoglutarate	21.78	21.79	21.79	<b>21.79</b>	0.01	0.03
Succinate	19.05	19.07	19.04	<b>19.05</b>	0.02	0.08
Fumarate	22.87	22.87	22.86	<b>22.87</b>	0.01	0.03
Malate	19.15	19.15	19.13	<b>19.14</b>	0.01	0.06
FAD	53.46	53.45	53.36	<b>53.42</b>	0.05	0.10
ADP	42.38	42.40	42.14	<b>42.31</b>	0.14	0.34
ATP	51.81	51.84	51.79	<b>51.81</b>	0.03	0.05

### 5.2.2.6 Limits of Detection

Using the IC-MS method, the detectable sugar-phosphates and organic acids could be detected at concentrations of lower than 2 pmol, with the exception of PEP, which could be detected to a concentration of 10 pmol (Table 5-6). F16B, ADP and ATP could be detected to concentrations of lower than 0.2 pmol (Table 5-7).

The detection response was linear for glucose, G6P, F6P, citrate, isocitrate, *cis*-aconiate, 2-oxoglutarate, succinate, fumarate and malate over a range of 2 – 200pmol (Table 5-6 and Fig. 5-27). The detection response was linear for 2/3-phosphoglycerate from 2 – 1000 pmol (Table 5-6) and phosphoenolpyruvate from 10 – 1000 pmol (Table 5.6), with all linear regression coefficients  $\leq 0.99$  (Table 5-6). The range of linearity for F16B, ADP and ATP was 0.2 – 100 pmol (Table 5-7 and Fig. 5-28), with linear regression coefficients  $\leq 0.98$  (Table 5-7).

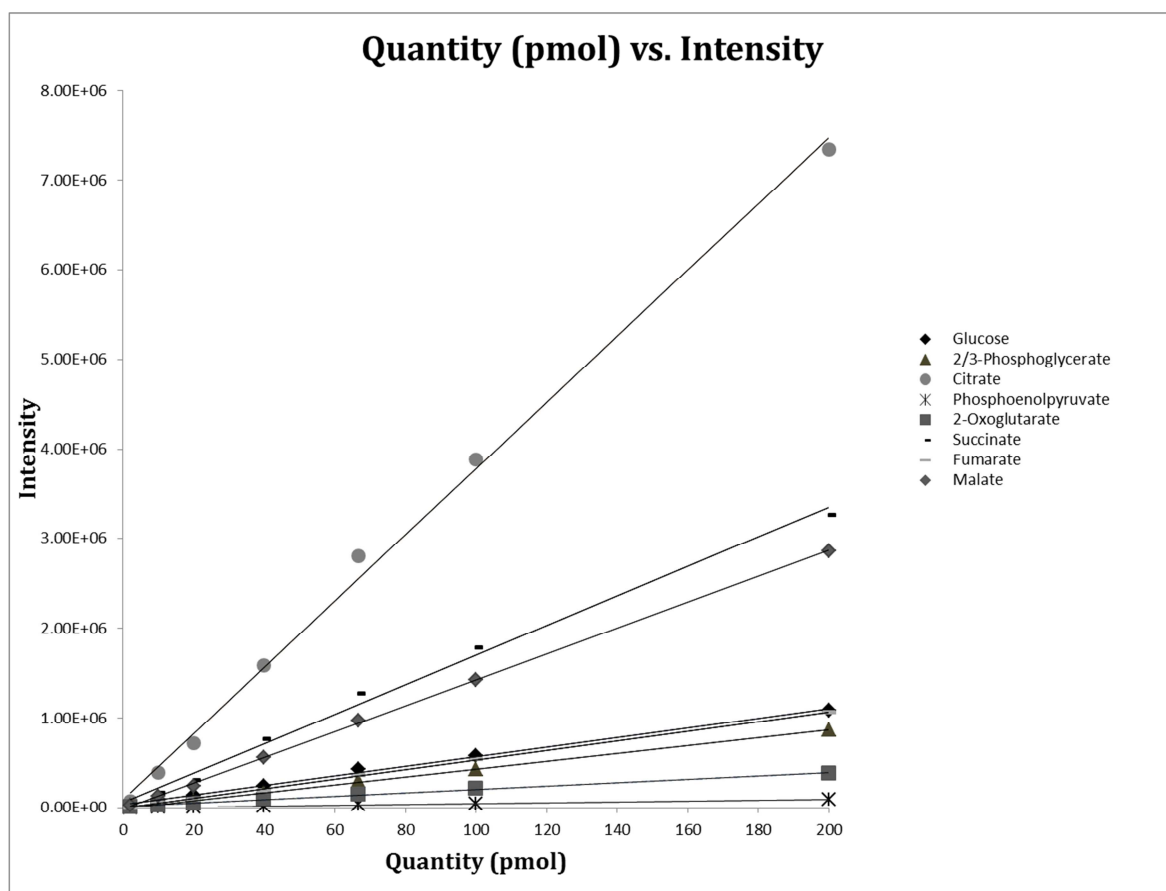


**Figure 5-27** Graph illustrating the peak areas detected for a selection of energy metabolites. The graph shows the peak areas detected for glucose, 2/3-phosphoglycerate, citrate, phosphoenolpyruvate, 2-oxoglutarate, succinate, fumarate and malate ranging from 2 – 200 pmol. A list of the  $R^2$  values can be found in Table 5-6.

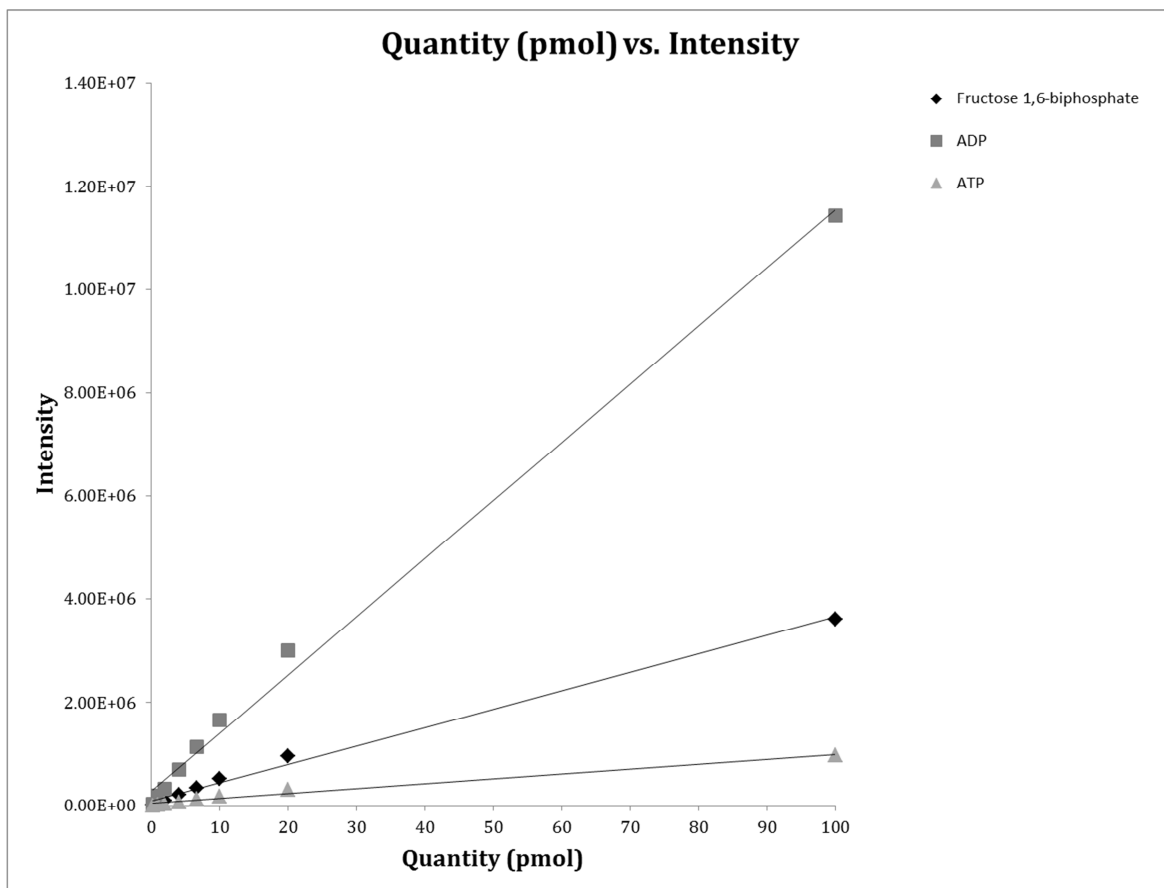


**Figure 5-28** Graph illustrating the peak areas detected for fructose 1,6-bisphosphate, ADP and ATP ranging from 200 fmol – 100 pmol. A list of the  $R^2$  values can be found in Table 5-7.

**Table 5-6** A list of the elemental formulae (EF), peak areas and linear regression coefficients ( $R^2$ ) for the energy metabolites at 2 pmol - 1nmol.

Metabolite	EF	Quantity (pmol)								$R^2$ (2-200 pM)	$R^2$ (2-1000 pM)
		1000	200	100	66.7	40	20	10	2		
		Intensity									
Glucose	C6H12O6	2.61E+06	1.09E+06	5.79E+05	4.33E+05	2.45E+05	1.36E+05	7.20E+04	1.85E+04	0.9962	0.9520
Glucose 6-P	C6H13O9P	2.40E+07	1.25E+07	7.56E+06	5.09E+06	3.13E+06	1.56E+06	8.63E+05	1.67E+05	0.9881	0.8868
Fructose 6-P	C6H13O9P	2.25E+07	1.10E+07	6.37E+06	4.49E+06	2.60E+06	1.25E+06	7.16E+05	1.41E+05	0.9908	0.9104
2/3-PG	C3H7O7P	3.15E+06	8.73E+05	4.30E+05	2.95E+05	1.69E+05	6.94E+04	3.50E+04	6.82E+03	0.9996	0.9935
PEP	C3H5O6P	3.45E+05	9.29E+04	4.26E+04	3.25E+04	1.49E+04	7.81E+03	2.93E+03	-	0.9967	0.9946
Citrate	C6H8O7	1.50E+07	7.34E+06	3.89E+06	2.81E+06	1.59E+06	7.21E+05	3.94E+05	7.64E+04	0.9970	0.9130
Isocitrate	C6H8O7	1.44E+07	7.19E+06	3.87E+06	2.74E+06	1.56E+06	6.96E+05	3.86E+05	2.13E+04	0.9964	0.9062
<i>cis</i> -Acon	C6H6O6	4.88E+06	2.14E+06	1.15E+06	8.06E+05	4.78E+05	2.08E+05	1.18E+05	7.35E+04	0.9973	0.9412
2-Oxo	C5H6O5	7.64E+05	3.79E+05	2.14E+05	1.43E+05	8.78E+04	4.32E+04	2.47E+04	4.76E+03	0.9956	0.9080
Succinate	C4H6O4	6.64E+06	3.27E+06	1.78E+06	1.28E+06	7.71E+05	3.11E+05	1.65E+05	3.32E+04	0.9945	0.9093
Fumarate	C4H4O4	2.31E+06	1.07E+06	5.44E+05	3.60E+05	1.97E+05	9.47E+04	5.40E+04	1.04E+04	0.9994	0.9302
Malate	C4H6O5	5.80E+06	2.86E+06	1.43E+06	9.74E+05	5.62E+05	2.38E+05	1.30E+05	2.33E+04	0.9996	0.9133

**Table 5-7** A list of the elemental formulae (EF), peak areas and linear regression coefficients ( $R^2$ ) for the energy metabolites at 200 fmol – 100 pmol.

Metabolite	EF	Quantity (pmol)								$R^2$ Value
		100	20	10	6.7	4	2	1	0.2	
		Intensity								
Fructose 1,6-biphosphate	C6H14O12P2	3616549	955527	526981	332416	211887	96852	44952	10911	0.9952
ADP	C10H15N5O10P2	11429135	3002949	1661896	1147555	705999	330488	184087	35715	0.9955
ATP	C10H16N5O13P3	978058	313324	172271	121838	63300	28840	15635	3427	0.9832

### 5.3 Discussion

The aim of this study was to develop a targeted IC-MS method for the separation and detection of various energy metabolism standards within a sample in a single chromatographic run. The column selected was a Thermo Dionex™ IonPac™ AS11-HC-4 $\mu$ m (2 x 250 mm). The metabolites were detected on the Dionex™ ICS-2100 Integrated IC System using a conductivity detector. The ICS-2100 system was coupled to an Orbitrap Fusion™ Tribrid™ Mass Spectrometer (Thermo Scientific) via an external pump running at a flow rate of 70  $\mu$ L/min. The make-up flow consisted of 100% MeOH. The gradient applied was an increasing OH<sup>-</sup> concentration from 1 mM to 100 mM over 60 min, at a flow rate of 230  $\mu$ L/min. There was a 7 min step at the beginning of each chromatographic run to allow the conductivity detector to equilibrate before the next run, resulting in a total run time of 67 min.

This method was adapted from methods first described by Bhattacharya et al. (1995) and Groussac et al. (2000). Bhattacharya utilized an IonPac AS11 column (250 x 4mm) in a 40 min run, at an alkaline pH, with UV and conductivity detection for the analysis of 33 metabolites, however many metabolites were not retained, resolved and/or detected (acetate, pyruvate, G3P, DHAP, R5P, X5P, succinate/malate, 2-oxoglutarate/G6P, 2-/3-PG and CoA derivatives) (Bhattacharya et al., 1995). To improve and simplify this method, Groussac employed the AS11 column with a 0.5 – 35 mM NaOH gradient over 30 min with a flow rate of 2 mL/min and conductivity detection for the analysis of a selection of organic acids (Groussac, Ortiz, & Francois, 2000). A CarboPac PA1 (4 x 250 mm) column with a NaOH/Na-acetate gradient running from 0 – 500 mM over 75 min, holding for 10 min and then returning to the initial starting conditions until 95 min at a flow rate of 1

mL/min with pulsed amperometry detection (PAD) was used for the analysis of sugar-phosphates (Groussac et al., 2000).

Van Dam et al. (2002) coupled the AEX to an MS to aid in the detection of co-eluting compounds that could not be distinguished from one another using conductivity detection or PAD (Van Dam et al., 2002). The flow rates employed for the AEX analysis by Bhattacharya, Groussac and van Dam were too high for MS pairing, so to counteract this van Dam used a flow splitter to lower the flow rate to  $\sim 100 \mu\text{L}/\text{min}$  (Van Dam et al., 2002). These methods have been adapted by various other groups for the analysis of various organic acids and phosphorylated compounds in bacteria and fungi (Bolten et al., 2007; Kiefer et al., 2007; Martzloff et al., 2012; Millard et al., 2014; Van Dam et al., 2002), almost all using the method that Kiefer et al. (2007) adapted from van Dam (Kiefer et al., 2007).

Kiefer ran an AS11 (4 x 250 mm) column at a flow rate of  $350 \mu\text{L}/\text{min}$ . The mobile phase consisted of Eluent A: 0.1: MeOH and Eluent B: 20% MeOH. Eluent B was increased from 0% to 8% over 25 min, held for 40 min, decreased to 0% and held for 5 min. The KOH concentration was increased in a step gradient from 0.5 mM to 40 mM over 65 min, decreased to 0.5 mM and held for 5 min, to give a total analysis time of 70 min. In the experiments described herein a 4mm AS11 column was run at a lower flow rate of  $230 \mu\text{L}/\text{min}$ . Unlike Kiefer, the mobile phase in this study consisted of an increasing  $\text{OH}^-$  concentration without the addition of a second MeOH containing eluent. MeOH can be used to enhance the separation of the organic acids succinate, malate, fumarate and 2-oxoglutarate (Groussac et al., 2000), but as the MS can distinguish between these compounds using their masses, the addition of the organic solvent was considered unnecessary. It is unclear whether van Dam and Kiefer ran make-up flows in their analyses. In the

experiments described in this study, a make-up flow consisting of 100% MeOH was selected to enhance metabolite ionisation into the MS inlet.

Many of the studies utilizing various adaptations of the AEX method are aimed at a specific group or selection of CCM compounds (Bolten et al., 2007; Kiefer et al., 2007; Martzloff et al., 2012; Millard et al., 2014; Van Dam et al., 2002). In this study glycolysis, TCA and ETC intermediates were separated using the IC-MS method.

The IC-MS method was able to successfully retain and separate a standard mixture of glycolysis intermediates with the exception of DHAP and G3P. The DHAP and G3P standards produced numerous fragment ions when analysed using IC-MS. DHAP and G3P have been unable to be detected in previous studies (Bhattacharya et al., 1995; Groussac et al., 2000). This could be the result of chemical decomposition of the compounds due to hydrolysis of the phosphodiester bond by OH<sup>-</sup> ions (Bhattacharya et al., 1995). Unique fragment ions that could be used for the identification of these compounds could not be determined from the MS data, so DHAP and G3P were unable to be identified within the mix using this method.

All of the TCA intermediates were detected and succinate, fumarate and malate were distinguished from each other with the use of high-resolution accurate mass MS. For reasons that are not understood *cis*-aconitate and oxaloacetate were detected as numerous peaks. The peaks were composed of fragment ions and a small abundance of the intact standards. It is unclear whether this decomposition was a product of the eluent conditions or whether weak collision induced dissociation (CID) was taking place in the ionisation source or interface (Luo et al., 2007). The difficulty in the detection of oxaloacetate has been encountered in other studies, using different analytical platforms (Buescher et al., 2010; Jung & Oh, 2015; Rühl et al., 2012).

The IC-MS method demonstrated good separation for the isomers citrate/isocitrate and G6P/F6P, however was unable to separate 2-/3-PG. The inability to separate 2-/3-PG is a common occurrence throughout energy metabolism analysis (Bajad et al., 2006; Soga et al., 2002). Soga et al. (2002) developed a CE-MS method for the analysis of energy metabolites, however were unable to separate 2-/3-PG (Soga et al., 2002, 2009). Bajad et al. (2006) developed an LC-MS/MS method, however never tested its performance for the separation of 2-/3-PG or G6P/F6P (Bajad et al., 2006). The method was unable to separate other sugar phosphate isomers (including F6P/other sugar isomers that were not G6P) (Bajad et al., 2006). GC-MS is particularly useful in the separation of sugar-phosphates, using known fragmentation patterns for the identification and quantitation of structural isomers, and has also been utilized to separate 2-/3-PG (Jung & Oh, 2015).

Of the coenzymes, FAD, ADP and ATP could be detected. CoA, succinyl-CoA and acetyl-CoA could not be distinguished from each other using the IC-MS method. Succinyl- and acetyl-CoA broke down in the eluent during the chromatography procedure to produce one peak that corresponded to CoA. This is in agreement with other IC studies (Bhattacharya et al., 1995; Groussac et al., 2000; Rühl et al., 2012). Bajad et al. (2006) developed a HILIC LC-MS/MS method that enabled the detection and differentiation of CoA, succinyl-CoA and acetyl-CoA (Bajad et al., 2006).

The method showed good RT reproducibility with most of the metabolites having RSD values of <1%. The reproducibility of this method is comparable to those of LC- and GC-MS and greater than the reproducibility of CE-MS (Büscher et al., 2009; Soga et al., 2009).

A selection of sugars, sugar phosphates and organic acids could easily be detected down to concentrations lower than 2 pmol. Phosphoenolpyruvate

could be detected to a concentration of 10 pmol. Fructose 1,6-bisphosphate, ADP and ATP could all be detected to concentrations of lower than 0.2 pmol. F16B, ADP and ATP displayed linearity over a range of 0.2 – 100 pmol and PEP had a range of linearity over 10 – 1000 pmol. All of the remaining standards displayed good linearity over a range of 2 – 200 pmol. The lower limits of detection are better than the detection limits achieved by Bhattacharya and are comparable to the LoDs recorded by van Dam for sugar-phosphates (however further dilutions would need to be analysed to determine the lowest amount that can be detected) (Bhattacharya et al., 1995; Van Dam et al., 2002). The lower detection limits achieved in this study were greater than those achieved using LC/TOF-MS (200 pmol) and were comparable to GC/TOF-MS (2.5 pmol), with some compounds comparable to the LoDs achieved using CE/TOF-MS (0.2 pmol) (Büscher et al., 2009).

Overall the IC-MS method performed well. Almost all of the CCM intermediates were detectable within a 60 min analysis, without the need for ion-pairing agents or derivatisation. The limitations of the method surround the high OH<sup>-</sup> concentration in the eluent, which causes hydrolysis of the phosphodiester bonds of a number of compounds. The IC-MS method is suitable for the analysis of organic acids, some sugar-phosphates, ADP, ATP, FAD and CoA. It may not be suitable for the analysis of DHAP, G3P or CoA derivatives without the consideration of lowering the concentration of the OH<sup>-</sup> ions in the eluent. However, the presence of OH<sup>-</sup> may cause hydrolysis even at very low concentrations. The effect the lower concentration of OH<sup>-</sup> would have on the retention of the sugar-phosphates and nucleosides would need to be determined as these compounds require higher concentrations to elute from the column. 2-/3-PG were unable to be separated. The addition of MeOH could possibly aid in their separation, although this would need to be investigated.

When this method is compared to other chromatography-MS methods the advantages and limitations of this system can be seen. GC-MS offers better separation of sugar-phosphates and volatile compounds; however lengthy derivatisation steps are sometimes required for non-volatile compounds and GC is unsuitable for the analysis of large, labile compounds. Samples are prepared and injected onto the IC column, without the need for derivatisation. LC-MS offers a wide coverage with a wide dynamic range. However, the need for non-volatile organic ion-pairing agents, e.g. TBA, can lead to contamination of MS instrumentation and LC may not be suitable for the detection of low abundance metabolites. Ion-pairing agents are not required in IC-MS and the sensitive instrumentation has a LoD of  $\leq 2$  pmol for most CCM compounds. CE-MS has been gaining popularity in recent years and is well suited for the analysis of polar compounds and metabolites that are in low abundance. However, the CE-MS system lacks the robustness required to analyse biological samples and the instrumentation requires a lot of maintenance. CE-MS reproducibility can also be poor, with large retention time drifts between samples and batches. IC instrumentation requires very little maintenance and has demonstrated highly reproducible results.

Sample derivatisation before LC-MS analysis offers an alternative to TBA ion-pairing RPLC and has the potential to perform better than IC-MS for the analysis of CCM compounds (D. Kloos et al., 2012; Tan, Lu, Dong, Zhao, & Kuo, 2014). Kloos et al (2012) carried out derivatisation of TCA intermediates using *N*-methyl-2-phenylethylamine and carried out LC-MS analysis in positive mode (D. Kloos et al., 2012). The intermediates were separated with an analysis time of 10 mins and the method was successfully applied to the targeted analysis of  $^{13}\text{C}$  labelled heart tissue. However, only a select number of TCA intermediates were chosen, not the full complement (D. Kloos et al., 2012). A more in-depth LC-MS/MS analysis was carried out for the separation and quantification of all of the TCA intermediates by Tan et

al (2014) (Tan et al., 2014). Derivatisation was carried out using *O*-benzylhydroxylamine (*O*-BHA) with the samples run on a C18 column and analysed in positive mode (Tan et al., 2014). A run time of 8 min was implemented for most analytes, although this had to be increased to 17 min, with the use of a different C18 column, for the separation of methylmalonate/succinate and maleate/fumarate (Tan et al., 2014). This method showed improved sensitivity, broader coverage with a faster analysis time when compared to the commonly used HILIC and RP/ion-pairing LC-MS/MS methods without derivatisation (Tan et al., 2014). Although this method has not been applied to wider CCM studies, Tan et al (2014) suggest that the method can be adapted for other common organic acids and biological matrices (Tan et al., 2014).

The results from this study highlight the advantages of using the IC-MS method for the separation and detection of CCM intermediates within a single chromatographic run. This method could detect and separate the majority of the CCM compounds selected in this study and has the capability to be set up as a simple routine method in a laboratory. However, more investigation is required to determine the fate of DHAP and G3P in the eluent and also at the ionisation source. More method development should be carried out utilizing different columns and chromatographic conditions, to determine whether the analytical platform is suitable for the detection of CoA derivatives and the separation of 2-/3-phosphoglycerate. The IC-MS method should also be applied to the analysis of the pentose phosphate pathway intermediates. This would allow the method to be tested for wider coverage of CCM. It is the opinion of this author that the IC-MS method developed in this study would be a good method to adopt for ease of use, sample preparation and instrument robustness. However, CCM coverage of the method is limited and more development is required to investigate the applicability of the method for the detection of all central carbon intermediates. At the moment, GC-MS would

be a preferable method for greater CCM coverage and it will be interesting to see if LC-MS/MS with derivatisation has the potential to surpass GC-MS in relation to CCM coverage.

**Chapter 6. Metabolomics analysis of *S. aureus* and *C. albicans* mono- and dual-species biofilms**

## 6.1 Introduction

The **aim** of this study was to apply the IC- and LC-MS methods developed during this research (Chapter 4 & 5) to the analysis of mono- and dual-species *S. aureus* and *C. albicans* biofilms. It was hypothesised that analysis of the biofilms using IC-MS would highlight differences in central carbon metabolism (CCM) between the mono-species *S. aureus*, *C. albicans* and dual species biofilms. It was hoped that any differences in CCM would enable the behaviour of the microorganisms in their dual-species biofilm to be elucidated.

Similarly, it was hypothesised that the application of the LC-MS method to the analysis of the mono- and dual-species biofilms would uncover significant differences in a number of metabolic pathways. Unlike the IC-MS method, it was hoped that the untargeted method would generate a number of different hypotheses and aid in directing possible future analyses to investigate the intricate relationship between *S. aureus* and *C. albicans* in their dual-species biofilm.

## 6.2 Materials and methods

The materials and methods are the same as those described in Chapter 2, with the following changes:

(1) Issues with the RPLC/pHILIC instrumentation and the metabolomics data quality led to the standard pHILIC method being utilised in place of the RPLC/pHILIC combined method.

## 6.3 Results

The mono- and dual-species biofilms were analysed using the developed IC-MS and LC-MS methods, previously described in Chapters 3 & 4. Method evaluation was carried out prior to data interpretation to determine system performance and applicability to the biofilm samples. After method evaluation, the intracellular data was analysed to determine its biological significance. Due to the sheer volume of data generated from the untargeted LC-MS analysis, data interpretation was limited to three significantly changing pathways.

### 6.3.1 Targeted analysis - IC-MS method

#### 6.3.1.1 Method evaluation

Energy intermediates were identified in the intracellular and extracellular biofilm samples using their known RT and  $m/z$  values (Table 6-1).

A Thermo™ Xcalibur™ processing method was created for automated peak detection and integration. The presence or absence of analyte peaks not detected using this processing method were confirmed manually using Quan Browser in the Thermo™ Xcalibur™ software suite. To be considered present in a sample, the metabolite peak had to have a minimum intensity of 5.0E3. Overall, peak area was utilized in relative abundance comparisons in place of highest intensities, as intensities assume peak symmetry and not all of the peaks were symmetrical. The peaks produced during IC-MS analysis were jagged. Although this was expected noise due to the nature of ESI, during processing, peak smoothing was employed as it allowed for the presence of artefacts and enabled more accurate peak area comparisons to be carried out. However, a symptom of peak smoothing is peak broadening. This phenomenon has to be taken into account when analysing analytes in this

way. For an analyte to be considered present within a sample group, it had to be detected in at least 60% of the individual samples within that group. A summary of the presence or absence of each energy metabolite within each of the samples is listed in Table 6-1.

Glucose was detected in all of the sample groups (Table 6-1). From glycolysis, none of the phosphorylated compounds were detected in the media, with the exception of 2-/3-phosphoglycerate, which was detected in two individual *S. aureus* samples, although overall it was considered absent from the sample group. All of the glycolysis intermediates were detected in all of the intracellular sample groups (Table 6-1). Pyruvate was detected in all sample groups except from the fresh media and *C. albicans* spent media samples (Table 6-1). Of the TCA intermediates, citrate, 2-oxoglutarate, succinate and malate were detected in all of the sample groups. Isocitrate was detected in all but one of the sample groups: - the *S. aureus* intracellular group. *cis*-Aconitate was detected in the all of the spent media samples, but not in the fresh media or any of the intracellular sample groups (Table 6-1). Fumarate was only present in both *C. albicans* sample groups and the fresh media.

When applied to analysis of a complex sample, the IC-MS method displayed good retention time reproducibility with all of the selected compounds achieving RSD values under 1%, with the exception of glucose, which had an RSD value of 4.29% (Table 6-2) A list of the individual RTs used to calculate the average RTs, SDs and RSDs can be found in Appendix III.

**Table 6-1** A list of detected (+) and undetected (-) energy intermediates in *C. albicans* (CA), *S. aureus* (SA), dual-species (CASA) biofilms and fresh media (FM) using the targeted IC-MS method. The number of + corresponds to the number of samples each metabolite was detected in. A negative sign (-) indicates that the metabolite was not detected in any of the replicates within a sample group. The metabolite had to be detected in at least 3/5 samples (+++) to be considered present within a sample group.

Metabolite	Detected/not detected in media				Detected/not detected in cells		
	CA	SA	CASA	FM	CA	SA	CASA
Glucose	+++++	+++++	+++	+++++	+++++	+++++	++++
Glucose-6-phosphate	-	-	-	-	+++++	++++	++++
Fructose-6-phosphate	-	-	-	-	+++++	+++	++++
Fructose-16-biphosphate	-	-	-	-	++++	+++	++++
2-/3-phosphglycerate	-	++	-	-	+++++	++++	+++++
Phosphoenolpyruvate	-	-	-	-	+++++	+++	++++
Pyruvate	-	++++	+++	-	+++	+++	+++
Citrate	+++++	+++++	+++++	+++++	+++++	+++++	+++++
Isocitrate	+++++	+++++	+++++	++++	+++++	+	++++
<i>cis</i> -Aconitate	+++++	+++++	++++	++	++	-	+
2-Oxoglutarate	+++++	+++++	++++	++++	+++++	+++	+++
Succinate	+++++	+++++	+++++	+++++	+++++	+++++	+++++
Fumarate	+++++	+	-	+++	+++++	-	++
Malate	+++++	+++++	+++++	+++++	+++++	++++	+++++
FAD	-	-	-	-	-	-	-
ADP	-	+	++	+	+++++	+++++	+++++
ATP	-	+++	+++	+++	+++++	+++++	+++++
Double charged FAD	-	-	-	-	-	-	-

**Table 6-2** The elemental formulae (EF),  $m/z$  values ([M-H]), expected retention times (RTs), average RTs, standard deviations (SDs) and relative standard deviations (RSDs) of the energy metabolism intermediates detected in the biofilm samples. (n=9).

Metabolite	EF	[M-H]	Expected RT	Average RT	SD	%RSD
Glucose	C6H12O6	179.0562	3.14	3.27	0.14	4.29
Glucose-6-phosphate	C6H13O9P	259.0225	21.74	21.54	0.03	0.12
Fructose-6-phosphate	C6H13O9P	259.0225	22.10	22.01	0.02	0.08
Fructose-16-biphosphate	C6H14O12P2	338.9889	45.85	45.91	0.02	0.03
2-/3-phosphglycerate	C3H7O7P	184.9857	29.61	29.33	0.07	0.23
Phosphoenolpyruvate	C3H5O6P	166.9752	35.06	34.73	0.08	0.24
Pyruvate	C3H4O3	87.0088	10.80	10.86	0.07	0.67
Citrate	C6H8O7	191.0198	31.78	31.55	0.02	0.06
Isocitrate	C6H8O7	191.0198	33.43	33.11	0.03	0.10
cis-Aconitate	C6H6O6	173.0092	35.02	34.83	0.13	0.38
2-Oxoglutarate	C5H6O5	145.0143	21.76	21.59	0.02	0.08
Succinate	C4H6O4	117.0194	19.06	18.88	0.04	0.19
Fumarate	C4H4O4	115.0038	22.86	22.64	0.02	0.08
Malate	C4H6O5	133.0143	19.14	18.94	0.03	0.15
ADP	C10H15N5O10P2	426.0222	42.31	41.97	0.02	0.06
ATP	C10H16N5O13P3	505.9886	51.81	51.67	0.02	0.03

Although the RT reproducibility of the instrument was robust in relation to the analysis of complex biological samples, the complexity of the samples and presence of multiple structural isomers had a negative effect on peak resolution (Fig. 6-1). Most of the analytes were detected as one peak, however multiple peaks were present when the  $m/z$  of glucose, G6P and F6P were searched for in the IC-MS data (Fig. 6-1). The presence of multiple peaks could be a consequence of the open and closed ring forms of these compounds. It could also be a consequence of structural isomers with chemical properties similar to glucose and the hexose-phosphates. Glucose belongs to a group of monosaccharides, which contain 6 carbon atoms with the chemical formula  $C_6H_{12}O_6$ , known as hexoses. Hexoses can be classed as aldohexoses or ketohexoses depending on whether there is an aldehyde at position one or a ketone at position two (Fig. 6-2). The aldohexoses have four chiral centres for a total of 16 possible aldohexose stereoisomers and the ketohexoses have three chiral centres and therefore eight possible stereoisomers. The naturally occurring aldohexoses and ketohexoses all share the same chemical structures and masses. As well as this, the hexoses can have a D or L configuration depending on the orientation of the hydroxyl group at position five (Fig. 6-3). These 6-carbon sugars can form cyclic hemiacetals. The formation of cyclic hexoses causes the symmetric carbon at position one to become asymmetric. This means that acyclic (or open ring) hexoses yield two cyclic isomers (anomers) denoted by ' $\alpha$ -' and ' $\beta$ -' (Fig. 6-4). The acyclic and cyclic forms are present in nature in equilibrium, the ring can spontaneously open and close, allowing rotation around the C1 bond, yielding either the  $\alpha$ - or  $\beta$ -configuration through a reaction process termed mutarotation. It is likely that the complex samples contain a mix of the hexose stereoisomers and anomers, which results in multiple peaks obtained in the IC (Fig. 6-1).

Unfortunately the analyte peaks were not baseline resolved, making quantitation inaccurate. Manual peak integration aided in identifying the analyte peaks, however the lack of resolution interfered with quantitation. To combat the effects of anomers derivatisation, such as those employed before GC analysis, could be investigated to determine their suitability to stop the interconversion of the acyclic and cyclic forms of the hexoses, as well as other monosaccharides within the samples.

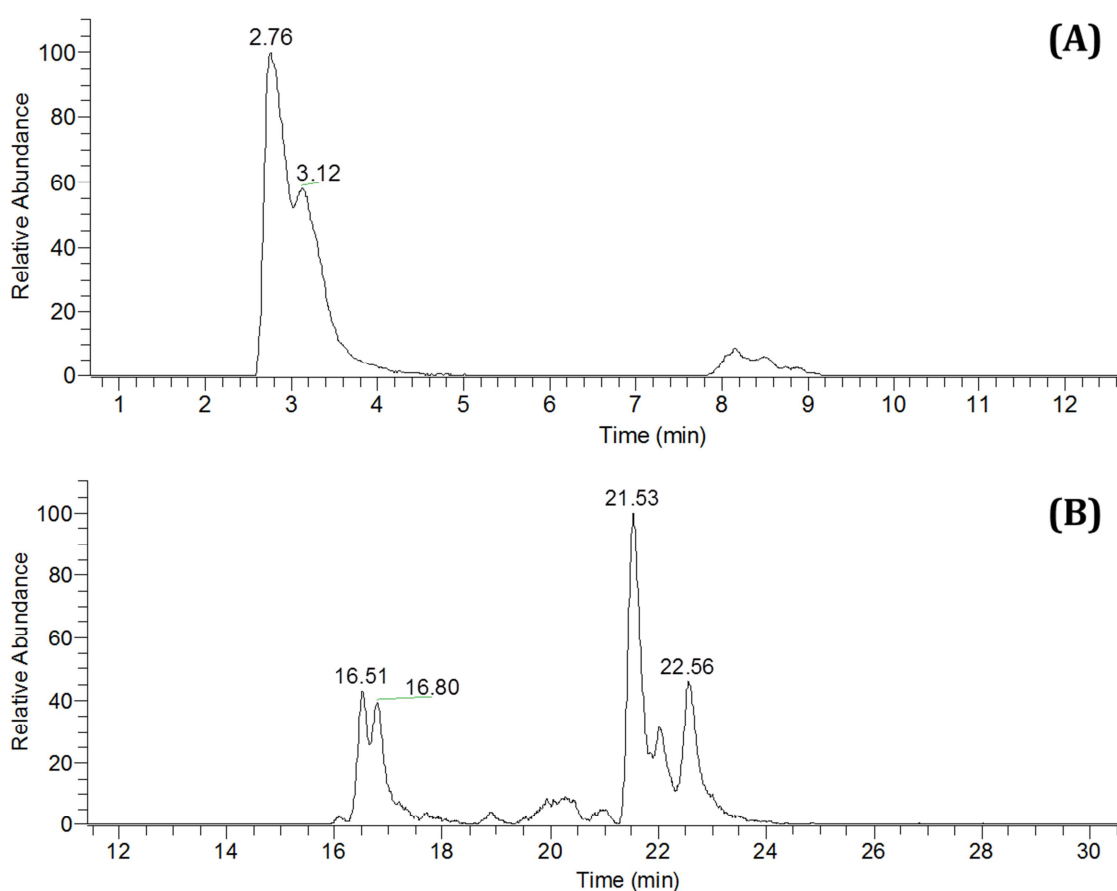


**Figure 6-1** Extracted ion chromatograms (EICs) of (A) glucose ( $m/z$  179.0562) and (B) G6P and F6P ( $m/z$  259.0225). 24 hour biofilms were washed in PBS and metabolites extracted using chloroform:methanol:water (1:3:1 v:v). Intracellular metabolites were extracted using a 4°C bead beating method. Extracellular metabolites were extracted with a ratio of 1:40 supernatant:extraction buffer at 4°C. Detection: ESI-FTMS, negative mode. Mass tolerance: 4 ppm. Two peaks were detected at  $m/z$  179.0562 (A). The peak at RT 3.12 was glucose. The peak at RT 2.76 was an isomer of glucose. Multiple peaks present when  $m/z$  259.0225 was searched for in the sample run (B). Peaks at RT 21.53 and 22.02 pertain to G6P and F6P, respectively. Due to an inability to baseline resolve multiple peaks with the same mass, quantitation was not accurate.

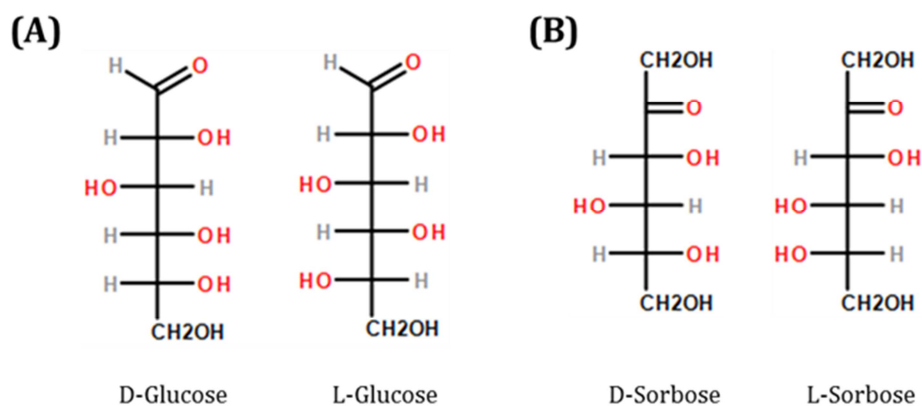


**Figure 6-2** Schematic diagrams of the stereoisomers of (A) glucose and (B) sorbose in D- and L- configurations.

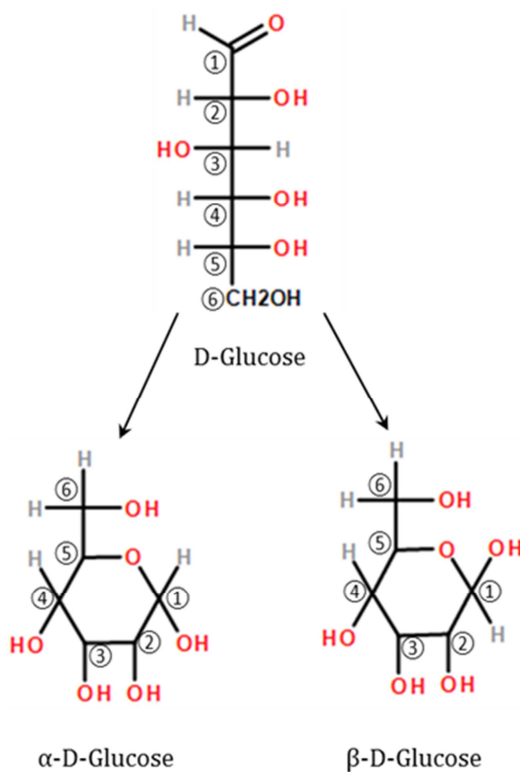


**Figure 6-3** Schematic diagram of the ring configuration of  $\alpha$ - and  $\beta$ -D-glucose.

Another phenomenon observed was peak tailing (Fig. 6-4). Peak tailing occurs when there is excessive dead volume in the system or solute

adsorption takes place on column. Peak tailing interferes with quantitation by affecting peak symmetry. Again, manual peak integration was utilized to try and minimise the effect of tailing on the relative quantitation of the analytes.

Metabolite comparisons were carried out for the intracellular and extracellular biofilm samples with the acknowledgement that further optimisation of this IC-MS method would be desirable.

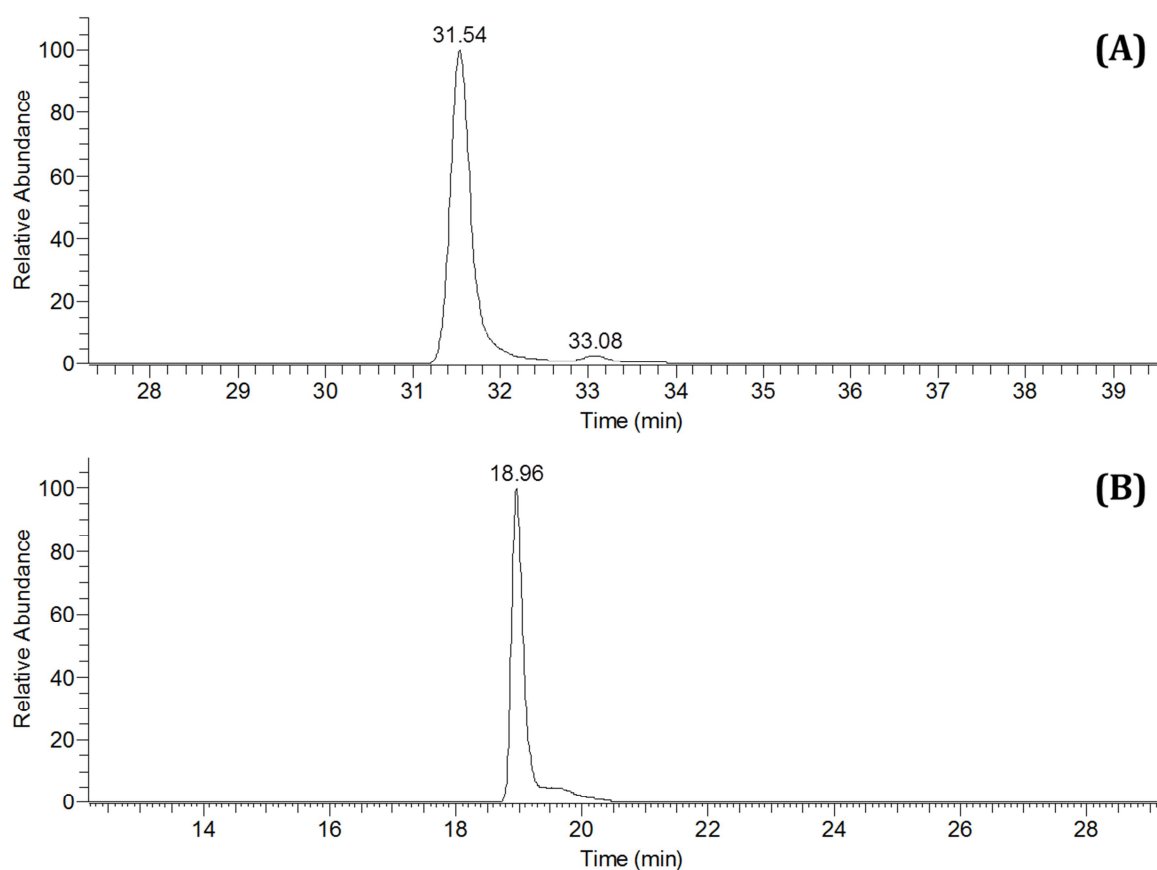


**Figure 6-4** EICs of (A) citrate and isocitrate ( $m/z$  191.0198) and (B) succinate ( $m/z$  117.0194). 24 hour biofilms were washed in PBS and metabolites extracted using chloroform:methanol:water (1:3:1 v:v:v). Intracellular metabolites were extracted using a 4°C bead beating method. Extracellular metabolites were extracted with a ratio of 1:40 supernatant:extraction buffer at 4°C. Detection: ESI-FTMS, negative mode. Mass tolerance: 4 ppm. Peak tailing was observed in numerous chromatograms. This phenomenon is undesirable as it interferes with quantitation accuracy and resolution of analyte peaks.

### 6.3.1.2 Data analysis

When the intracellular data was analysed, some of the energy metabolites were not detected in the *S. aureus* mono-species samples (Table 6-1 & Fig. 6-5). The absence of these metabolites could be a result of the low cell number and biomass obtained when the bacteria were grown in FBS. It could be argued that the absence of isocitrate, *cis*-aconitate and fumarate were due to metabolite abundances being lower than the detection limits of the instrument.

Many of the metabolites were detected at a lower abundance in the *S. aureus* mono-species compared to the dual species biofilm, with the exception of pyruvate, succinate and ADP (Fig. 6.5). When the *C. albicans* mono-species was compared to the dual-species biofilm metabolite abundances were similar (Fig. 6-5).

A heat map was created for the comparison of the spent media metabolites (Table 6-3). The metabolites were first compared to abundances detected in the fresh media before being compared to each other.

A positive value indicated that the analyte was found in a higher abundance in the sample spent media compared to the fresh media. A positive value could suggest that the analyte was being secreted by the cells or was being produced due to the breakdown of a larger compound. A negative value was indicative of higher analyte abundance in the fresh media compared to the spent media. This could suggest that the analyte was being taken up by the cells or that the metabolite was being broken down in the media.

Similar abundances of glucose, citrate, iso-citrate, *cis*-aconitate and succinate were detected in all three sample groups (Table 6-3). Glucose, citrate, iso-citrate and succinate abundances were similar to those detected in the fresh media. *cis*-Aconitate was found at a higher abundance in all of the sample groups compared to the fresh media. 2-Oxoglutarate was detected at similar abundances in *C. albicans* and the fresh media, whereas higher abundances of this metabolite were detected in *S. aureus* and the dual-species spent media compared to fresh media. Pyruvate was found in a higher abundance in the *S. aureus* spent media compared to the *C. albicans* and dual-species spent media (Table 6-3). Fumarate was found in lower abundances in the *S. aureus* and dual-species spent media compared to the fresh media. Similar abundances of fumarate were detected in the *C. albicans* spent media and fresh media.

Malate was found in similar abundances in the fresh media and the fungal spent media. The *S. aureus* mono-species and the dual-species biofilms had similar abundances of malate to each other, but lower abundances of malate compared to the fresh media. ADP was found at a lower abundance in all three sample groups when compared to fresh media. Far less ADP was detected in the *C. albicans* mono-species media compared to both the *S. aureus* and the dual-species spent media (Table 6-3).

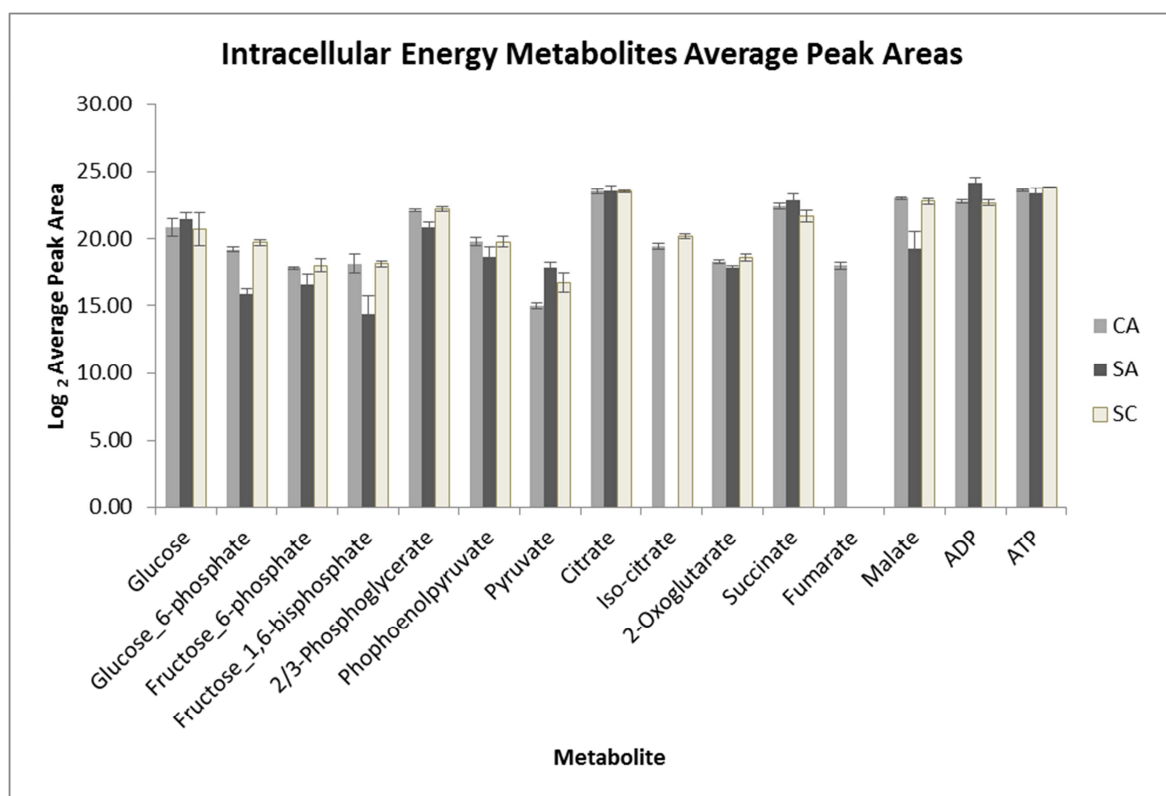


**Figure 6-5** Bar chart comparing the average peak areas calculated for each of the intracellular energy metabolites detected in *C. albicans* (CA), *S. aureus* (SA) and the dual-species biofilm (SC). 24 hour biofilms were washed in PBS and intracellular metabolites extracted using chloroform:methanol:water (1:3:1 v:v:v) in conjunction with a 4°C bead beating method. Detection: ESI-FTMS, negative mode. Mass tolerance: 4 ppm. Error bars  $\pm$  standard deviation (SD). (n=5).

**Table 6-3** Heat map comparison of the energy metabolites detected in the spent media of the *C. albicans* (CAM), *S. aureus* (SAM) and the dual species (SCM) biofilms. Data was normalised between each sample group using total useable signal. For each metabolite, average peak areas from each sample group were compared to fresh media (MO).  $\text{LogFC} = \log_2(\text{Sample peak area}/\text{fresh media})$ . Positive values indicate that the spent media contained more of the metabolite than the fresh media and a negative value indicates that the spent media contained less of the metabolite than the fresh media. (n=5).

Metabolite	LogFC CAM/MO	LogFC SAM/MO	LogFC SCM/MO	Metabolite ID code*
Glucose	-0.41	-0.54	-0.87	R <sub>ta</sub> HRMS <sub>a</sub> <sup>1</sup>
Pyruvate	-0.51	1.90	0.34	R <sub>ta</sub> HRMS <sub>a</sub> <sup>1</sup>
Citrate	0.06	0.06	0.20	R <sub>ta</sub> HRMS <sub>a</sub> <sup>1</sup>
Iso-citrate	0.60	0.38	0.57	R <sub>ta</sub> HRMS <sub>a</sub> <sup>1</sup>
<i>cis</i> -Aconitate	1.02	1.53	1.04	R <sub>ta</sub> HRMS <sub>a</sub> <sup>1</sup>
2-Oxoglutarate	0.55	1.32	1.56	R <sub>ta</sub> HRMS <sub>a</sub> <sup>1</sup>
Succinate	0.10	0.56	0.56	R <sub>ta</sub> HRMS <sub>a</sub> <sup>1</sup>
Fumarate	0.55	-1.24	-3.11	R <sub>ta</sub> HRMS <sub>a</sub> <sup>1</sup>
Malate	0.29	-1.14	-1.95	R <sub>ta</sub> HRMS <sub>a</sub> <sup>1</sup>
ADP	-8.26	-3.80	-2.01	R <sub>ta</sub> HRMS <sub>a</sub> <sup>1</sup>

\* Refers to alphanumeric coding scheme from (Sumner et al., 2014).

## 6.3.2 Untargeted analysis - RPLC/HILIC method

### 6.3.2.1 Method evaluation

To ensure the optimum LC-MS method was employed for the analysis of the *S. aureus* and *C. albicans* mono- and dual-species biofilms, the combined RPLC/pHILIC method was compared to the standard pHILIC method routinely used within the metabolomics laboratory. Less than half of the number of metabolites were detected using the RPLC/pHILIC method compared to the pHILIC method (Table 6-4). The peak shapes obtained using the RPLC/pHILIC method were poorer than those obtained using the pHILIC method (Fig. 6-6). When the ToxID™ reports were consulted, a lot of peak splitting was observed (Fig. 6-7). Peak splitting is a symptom of poor

chromatography and can arise from different problems. As a significant number of peaks were splitting, it appeared that the problem occurred before separation. The most common reasons for peak splitting are a blocked frit or a void at the head of the column.

**Table 6-4** Comparison of the RPLC/pHILIC combined and the routine pHILIC methods. Comparisons took into consideration the number of intracellular, and extracellular (secretome) metabolites detected, identified and the number of KEGG pathways the annotated and identified metabolites mapped onto.

	Intracellular metabolome		Secretome	
	RPLC/pHILIC	pHILIC	RPLC/pHILIC	pHILIC
<b>Metabolites Detected</b>	1151	3368	1465	3661
<b>Metabolites Identified</b>	39	67	49	68
<b>KEGG Metabolite Pathways</b>	175	186	180	208

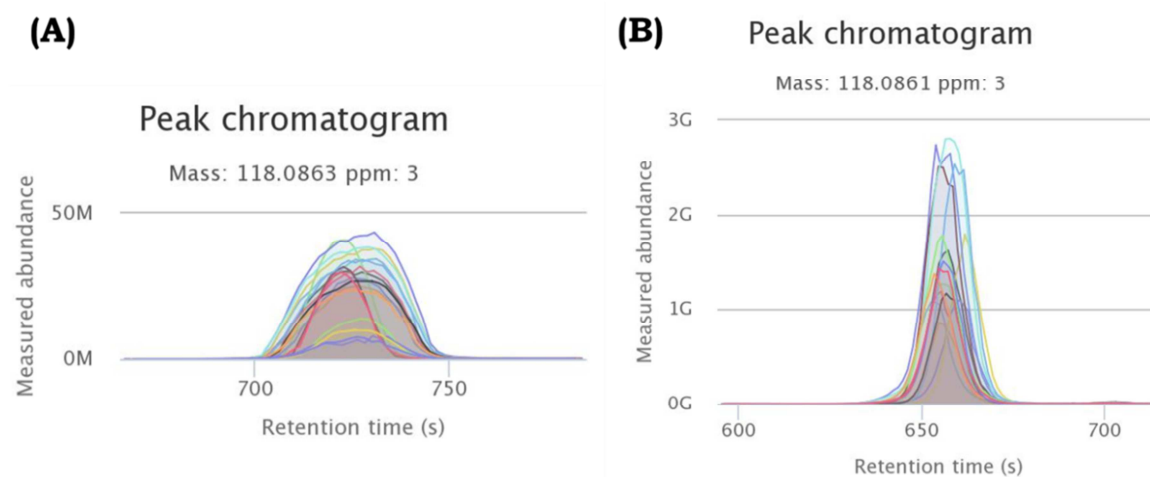


**Figure 6-6** An example of the peak shapes obtained using (A) the RPLC/pHILIC combined method and (B) the standard pHILIC method. The standard pHILIC method resulted in peaks that resembled the normal-Gaussian-shaped peak (B). The peak shape obtained using the combined RPLC/pHILIC columns resulted in broader peaks that deviated from this 'ideal' chromatography peak. Detection: ESI-FTMS, negative mode.

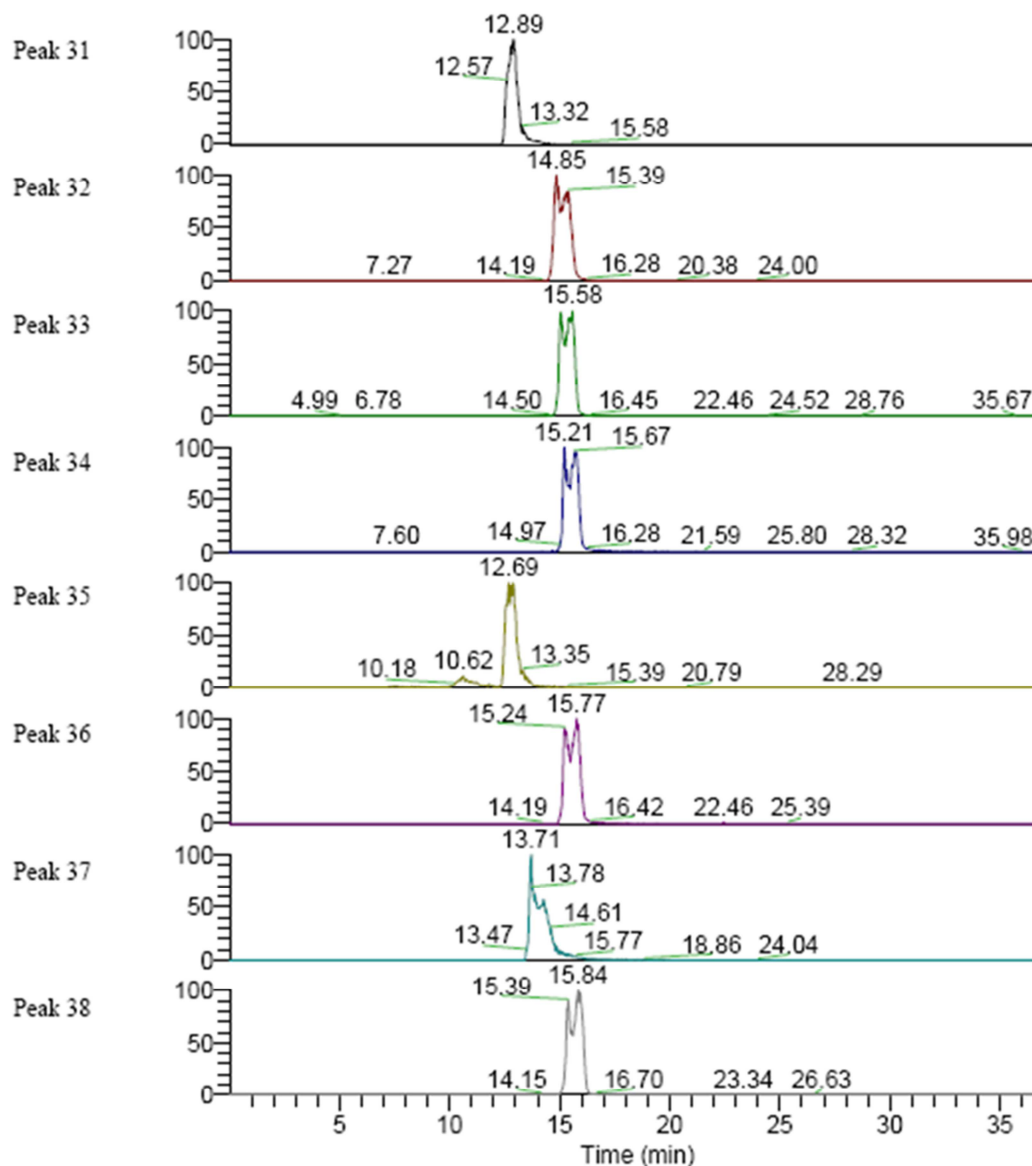


**Figure 6-7** An example of peak splitting observed using the RPLC/pHILIC combined method.

These three observations, coupled with the difficulties encountered maintaining the backpressure of the system within the maximum limits of the HPLC pumps led to the standard pHILIC method being utilized for the analysis of the bacterial and fungal biofilms. The pHILIC method is an established method, which has been optimised and perfected over a number of years. It was therefore concluded that more information could be gained using this method compared to the RPLC/pHILIC method. It should be emphasised

here that the RPLC/pHILIC method displays a great deal of potential for the separation and detection of polar and nonpolar analytes, however this method requires a great deal of development to determine the best column combinations, mobile phase compositions and the effect linking two column chemistries has on analyte separations in complex samples.

### 6.3.2.2 Purine metabolism

Fifteen metabolites were detected from the purine metabolism pathway. Six of these were identified and seven were annotated (or putatively identified). 5-amino-4-imidazole carboxylate was detected at similar levels in blank LC-MS runs compared to those detected in sample runs and therefore was omitted from purine metabolism analysis.

Overall, the relative abundance of purine metabolites were higher in the co-culture biofilm compared to the *S. aureus* mono-species biofilm (Table 6-5), with exception of L-glutamine, adenosine monophosphate (AMP) and xanthosine (Table 6-5 & Fig. 6-8). The abundances of L-glutamine, AMP and xanthosine were higher in the *S. aureus* biofilm than both the mono-species *C. albicans* and the dual-species biofilms (Table 6-5 & Fig. 6-8). AMP, 3'AMP and deoxyguanosine monophosphate (dGMP) are structural isomers of each other. Although AMP was identified using a standard it was unknown whether 3'AMP and dGMP were separated from AMP. A slightly higher abundance of xanthosine was detected in the *S. aureus* mono-species biofilm, but this was not considered a significant difference (Table 6.5 & Fig. 6.8 C). Significantly higher abundances of hypoxanthine, adenosine, deoxyguanosine, xanthine, uric acid and (R/S)(-/+)-allantoin were detected in the co-culture compared to the *S. aureus* mono-species biofilm (Table 6-5 & Fig. 6-8). Higher abundances of adenine and sulphate were detected in the dual-species biofilm compared to the bacterial mono-species biofilm,

although the differences were not significant at a p-value of 0.05 (Table 6-5). These results suggested that purine metabolism was up-regulated in the dual-species biofilm compared to the *S. aureus* mono-species biofilm.

When the abundances of the detectable purine metabolites in *C. albicans* were compared to the co-culture, many of the metabolites had similar relative abundances (Table 6-5). Similar abundances of L-glutamine, adenine, uric acid, sulphate and (R/S)(-/+)-allantoin were detected in the dual-species and *C. albicans* biofilms (Table 6-5). A significantly higher abundance of hypoxanthine was detected in the *C. albicans* mono-species biofilm compared to both the *S. aureus* mono-species and the dual-species biofilms (Table 6-5). Higher abundances of adenosine, deoxyguanosine, AMP, 3'AMP, dGMP and xanthine were detected in *C. albicans* compared to the co-culture, although these differences were not considered significant. A slightly higher abundance of xanthosine was detected in the co-culture compared to the *C. albicans* mono-culture, although this difference was not considered significant (Table 6-5). With the exception of xanthosine, L-glutamine and adenine, overall lower abundances of purine metabolites were detected in the dual-species biofilm compared to *C. albicans* biofilm (Table 6-5). Although many of the differences recorded were not significant, they did suggest a trend of decreased purine metabolism in the co-culture compared to the *C. albicans* mono-species biofilms.

**Table 6-5** Heat map comparison of the intracellular metabolite abundances detected in the *C. albicans* (CAC), *S. aureus* (SAC) and the dual species (SCC) biofilms. The elemental formulae (EF), metabolite identification and log-fold changes (logFC) of the identified and annotated metabolites from the purine metabolism pathway are listed. LogFC = log<sub>2</sub> (dual-species/mono-species). (n = 5).

Metabolite	EF	LogFC SCC/CAC	LogFC SCC/SAC	Metabolite ID code*
L-Glutamine	C5H10N2O3	0.27	-1.06	R <sub>ta</sub> HRMS <sub>a</sub> <sup>1</sup>
Adenine	C5H5N5	0.52	0.91	R <sub>ta</sub> HRMS <sub>a</sub> <sup>1</sup>
Hypoxanthine	C5H4N4O	-1.74	1.82	R <sub>ta</sub> HRMS <sub>a</sub> <sup>1</sup>
Adenosine	C10H13N5O4	-0.93	1.9	R <sub>ta</sub> HRMS <sub>a</sub> <sup>1</sup>
AMP	C10H14N5O7P	-0.74	-1.18	R <sub>ta</sub> HRMS <sub>a</sub> <sup>1</sup>
Xanthine	C5H4N4O2	-0.61	2.11	R <sub>ta</sub> HRMS <sub>a</sub> <sup>1</sup>
Deoxyguanosine	C10H13N5O4	-0.93	1.9	HRMS <sup>1</sup>
3'-AMP	C10H14N5O7P	-0.74	-1.18	HRMS <sup>1</sup>
dGMP	C10H14N5O7P	-0.74	-1.18	HRMS <sup>1</sup>
Urate	C5H4N4O3	-0.28	1.75	HRMS <sup>1</sup>
Sulphate	H2SO4	-0.1	0.7	HRMS <sup>1</sup>
(R/S)-Allantoin	C4H6N4O3	-0.43	1.31	HRMS <sup>1</sup>
Xanthosine	C10H12N4O6	0.94	-0.56	HRMS <sup>1</sup>

\* Refers to alphanumeric coding scheme from (Sumner et al., 2014).

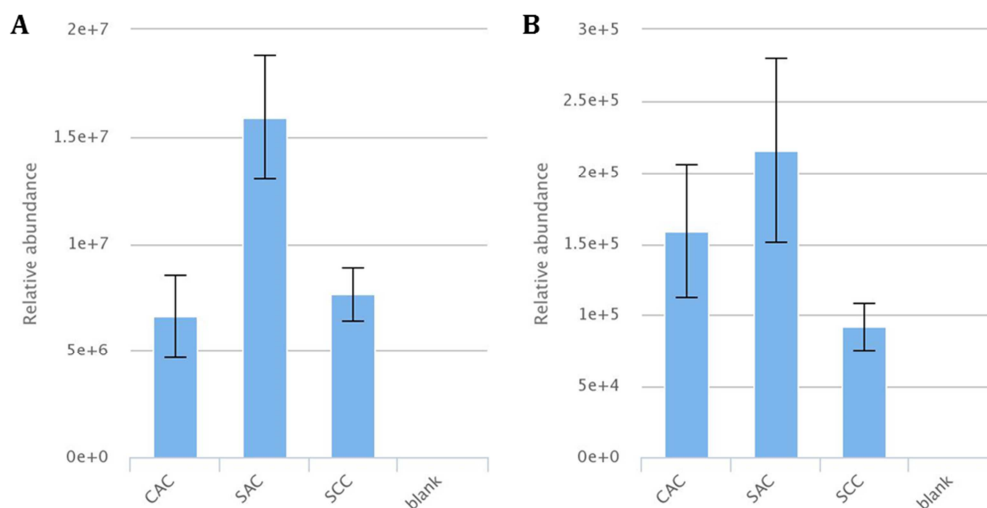


**Figure 6-8** Bar charts comparing the relative abundance of intracellular (A) L-glutamine and (B) adenosine monophosphate (AMP) detected in the mono-species *C. albicans* (CAC), *S. aureus* (SAC) and their co-culture (SCC). The biofilms were cultured in 50% FBS for 24 hours. Mature biofilms were washed twice in PBS. Metabolites were extracted according to the established protocol in ice-cold chloroform:methanol:water (1:3:1, v:v:v). Higher levels of L-glutamine and AMP were detected in the mono-species *S. aureus* compared *C. albicans* and the co-culture. Similar levels of L-glutamine were detected in *C. albicans* and the co-culture (A). More AMP was detected in the *C. albicans* compared to the co-culture (B). Analysis: HPLC-ESI-FTMS. Polarity mode: pos/neg switching. Mass tolerance: 4 ppm. Error bars  $\pm$  standard deviation (SD). (n=5).

### 6.3.2.3 Pyrimidine metabolism

Twenty-two metabolites from pyrimidine metabolism were detected in the intracellular biofilm samples. Of these, eight metabolites were identified from in-house standards and the remaining fourteen were annotated from their masses.

Uridine diphosphate (UDP)-glucose, deoxyuridine and ureidopropionic acid were detected in the co-culture and *C. albicans* mono-species biofilms, but not in *S. aureus* mono-species biofilms (Fig. 6-9 A-C). *S. aureus* lacks the enzyme to incorporate UDP-glucose into the cell so the absence of this compound in the intracellular metabolome of the bacteria was expected. Uridine, thymidine, uracil and pseudouridine were all detected at significantly higher levels in the co-culture compared to *S. aureus* (Fig. 6-9 D-F). 3-Hydroxypropanoate was detected at a higher abundance in the dual-species biofilm compared to the *S. aureus* biofilm; however, this difference was not significant. L-Glutamine, orotate and 3-ureidoisobutyrate were detected at significantly higher abundances in the *S. aureus* biofilm compared to the dual-species biofilm (Fig. 6-10). The remaining metabolites were detected at similar abundances in both cultures. The trend was towards higher abundances in the co-culture, with the exception of cytosine, 5-methylcytosine and 5-methylbarbiturate (Table 6-6). The levels of detectable metabolites from pyrimidine metabolism suggested that pyrimidine metabolism was up-regulated in the dual-species biofilm compared to the mono-species *S. aureus* biofilm (Table 6-6).

Methylmalonate, deoxyuridine, thymidine, uridine and pseudouridine were all detected at higher intensities in the mono-species fungal biofilm compared to the dual-species biofilm (Table 6-6). Although not considered significant, UDP-glucose,  $\beta$ -alanine, ureidopropionic acid and 3-Hydroxypropanoate

were detected at higher intensities in the *C. albicans* biofilm compared to the co-culture (Table 6-6). 3-Amino-isobutanoic acid and 3-oxoproanoate, which were detected at similar levels in the *S. aureus* mono-species and the dual-species biofilms, were detected at significantly lower levels in the mono-species *C. albicans* biofilm (Table 6-6). The remaining metabolites were detected at similar levels in the dual-species and *C. albicans* mono-species biofilms (Table 6-6). Although some of the metabolites were detected at similar abundances the significantly lower levels of deoxyuridine, uridine and thymidine detected in the co-culture compared to the mono-species *C. albicans* could suggest that pyrimidine synthesis is down-regulated in the dual-species biofilm compared to when *C. albicans* is cultured in a mono-species biofilm.

**Table 6-6** Heat map comparison of the intracellular metabolite abundances detected in the *C. albicans* (CAC), *S. aureus* (SAC) and the dual species (SCC) biofilms. The elemental formulae (EF), metabolite identification and log-fold changes (logFC) of the identified and annotated metabolites from the pyrimidine metabolism pathway are listed. LogFC =  $\log_2$  (dual-species/mono-species). (n = 5).

Metabolite	EF	LogFC	LogFC	Metabolite ID code*
		SCC/CAC	SCC/SAC	
L-Glutamine	C5H10N2O3	0.27	-1.06	R <sub>ta</sub> HRMS <sub>a</sub> <sup>1</sup>
UDP-glucose	C15H24N2O17P2	-0.68	15.52	R <sub>ta</sub> HRMS <sub>a</sub> <sup>1</sup>
Methylmalonate	C4H6O4	-0.97	0.13	R <sub>ta</sub> HRMS <sub>a</sub> <sup>1</sup>
beta-Alanine	C3H7NO2	-0.74	0.39	R <sub>ta</sub> HRMS <sub>a</sub> <sup>1</sup>
Deoxyuridine	C9H12N2O5	-2.81	14.64	R <sub>ta</sub> HRMS <sub>a</sub> <sup>1</sup>
Thymidine	C10H14N2O5	-2.82	9.13	R <sub>ta</sub> HRMS <sub>a</sub> <sup>1</sup>
Uridine	C9H12N2O6	-2.22	12.26	R <sub>ta</sub> HRMS <sub>a</sub> <sup>1</sup>
Orotate	C5H4N2O4	0.3	-0.96	R <sub>ta</sub> HRMS <sub>a</sub> <sup>1</sup>
3-Ureidoisobutyrate	C5H10N2O3	0.27	-1.06	HRMS <sup>1</sup>
3-Aminoisobutyric acid	C4H9NO2	1.16	0.39	HRMS <sup>1</sup>
Ureidopropionic acid	C4H8N2O3	-0.75	16.16	HRMS <sup>1</sup>
3-Hydroxypropanoate	C3H6O3	-0.87	0.81	HRMS <sup>1</sup>
Dihydrouracil	C4H6N2O2	-0.09	0.05	HRMS <sup>1</sup>
Cytosine	C4H5N3O	-0.13	-0.22	HRMS <sup>1</sup>
5-Methylcytosine	C5H7N3O	0.04	-0.08	HRMS <sup>1</sup>
Pseudouridine	C9H12N2O6	-1.75	7.25	HRMS <sup>1</sup>
3-Oxopropanoate	C3H4O3	1.44	0.37	HRMS <sup>1</sup>
Uracil	C4H4N2O2	-0.03	0.99	HRMS <sup>1</sup>
Barbiturate	C4H4N2O3	0.02	0.2	HRMS <sup>1</sup>
Malonate	C3H4O4	-0.05	0.01	HRMS <sup>1</sup>
5,6-Dihydrothymine	C5H8N2O2	0.66	0.19	HRMS <sup>1</sup>
5-Methylbarbiturate	C5H6N2O3	-0.04	-0.21	HRMS <sup>1</sup>

\* Refers to alphanumeric coding scheme from (Sumner et al., 2014).

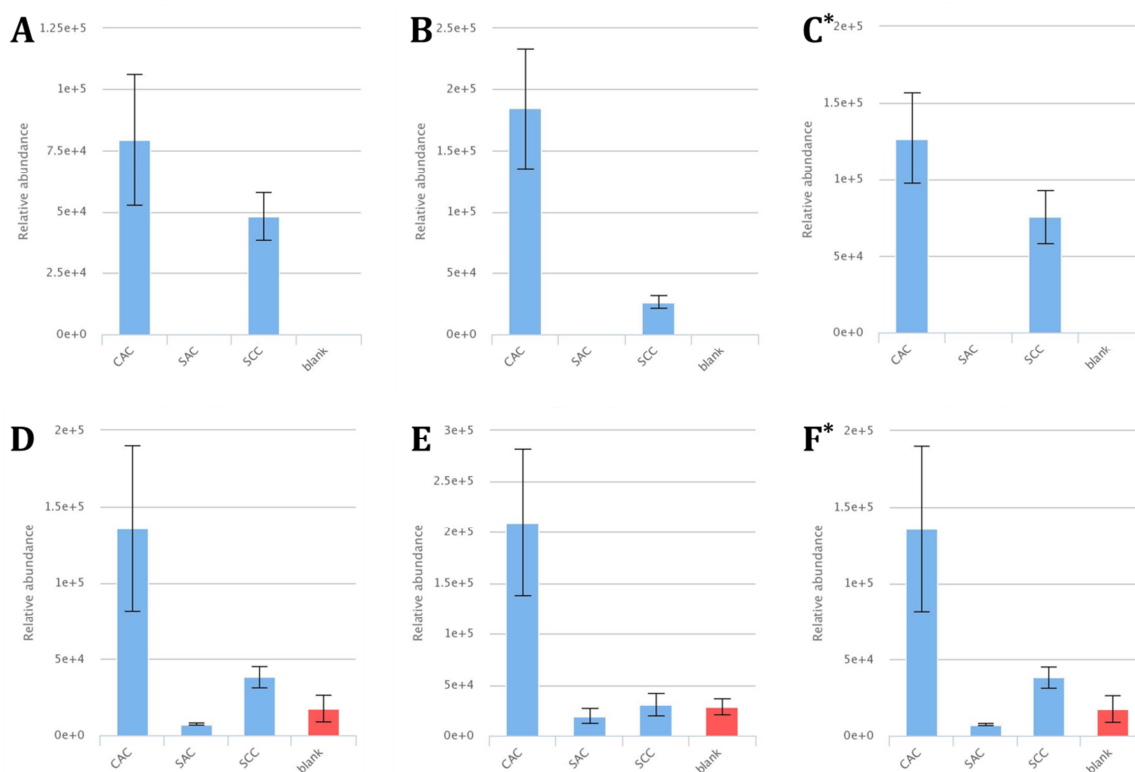


**Figure 6-9** Bar charts comparing the relative abundance of intracellular (A) uridine diphosphate (UDP)-glucose; (B) deoxyuridine; (C) ureidopropionic acid; (D) uridine; (E) thymidine and (F) pseudouridine detected in the mono-species *C. albicans* (CAC), *S. aureus* (SAC) and their co-culture (SCC). The biofilms were cultured in 50% FBS for 24 hours. Mature biofilms were washed twice in PBS. Metabolites were extracted according to the established protocol in ice-cold chloroform:methanol:water (1:3:1, v:v:v). UDP-glucose, deoxyuridine and ureidopropionic acid were not detected in the mono-species *S. aureus*, but were detected in the co-culture and *C. albicans* (A-C). Slightly higher levels of UDP-glucose and ureidopropionic acid were detected in the *C. albicans* compared to the co-culture (A & C). Significantly higher levels of deoxyuridine were detected in *C. albicans* compared to the dual-species biofilm (B). Lower levels of uridine, thymidine and pseudouridine were detected in *S. aureus* compared to *C. albicans* and the co-culture (D-E). Higher levels of uridine, thymidine and pseudouridine were detected in *C. albicans* and the co-culture (D-E). Analysis: HPLC-ESI-FTMS. Polarity mode: pos/neg switching. Mass tolerance: 4 ppm. Error bars  $\pm$  standard deviation (SD). (n=5). (Note: \* indicates putative identification).

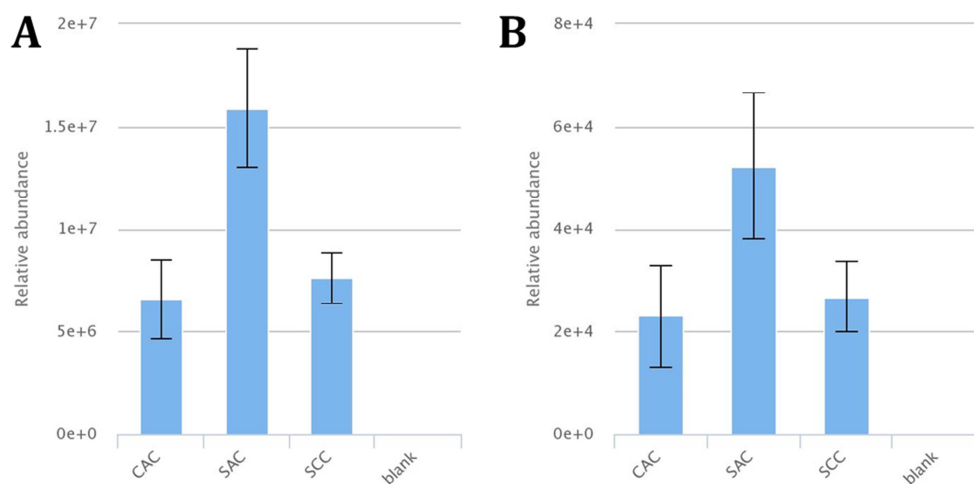


**Figure 6-10** Bar charts comparing the relative abundance of intracellular (A) L-glutamine and (B) orotate detected in the mono-species *C. albicans* (CAC), *S. aureus* (SAC) and their co-culture (SCC). Significantly higher levels of L-glutamine and orotate were detected in the mono-species *S. aureus* compared *C. albicans* and the co-culture (A & B). Similar levels of L-glutamine and orotate were detected in *C. albicans* and the co-culture (A & B). Analysis: HPLC-ESI-FTMS. Polarity mode: pos/neg switching. Mass tolerance: 4 ppm. Error bars  $\pm$  standard deviation (SD). (n=5).

### 6.3.2.4 Cysteine and methionine metabolism

Fifteen metabolites from cysteine and methionine metabolism were detected using LC-MS (Table 6-7). Of these, six were identified to known standards and eleven were annotated using mass alone.

5'Methylthioadenosine, glutathione, s-adenosyl-L-homocysteine, L-methionine and S-adenosyl-L-methionine were not detected in *S. aureus*, but were detected in *C. albicans* and the co-culture (Fig. 6-11). L-Aspartate, O-succinyl-L-homoserine and L-homoserine were detected at higher abundances in the *S. aureus* monoculture compared to both the *C. albicans* monoculture and the co-culture (Fig. 6-12). Similar levels of O-acetylserine, pyruvic acid and L-alanine were detected in *S. aureus* and the co-culture (Table 6-7).

Higher abundances of L-alanine, glutathione, S-adenosyl-L-homocysteine and L-methionine were detected in the *C. albicans* monoculture compared to the co-culture (Fig. 6-11 B-D). Similar levels of 5'methyladenosine, S-adenosyl-L-methionine, L-aspartate, sulphate and O-acetylserine were detected in the co-culture and *C. albicans* (Table 6-7 and Fig. 6-11 A & E). O-succinyl-L-homoserine was detected at a higher abundance in the co-culture compared to *C. albicans* (Table 6-7 & Fig. 6-12 15 C). The difference was recorded as a logFC of 12.03, but in the bar chart comparing the abundance of O-succinyl-L-homoserine found in each of the mono-species and dual-species biofilms the levels appeared similar (Table 6-7 & Fig. 6-13 A). However, when the individual mono-species *C. albicans* samples were examined, the metabolite was only detected in one of them (Fig. 6-13 B). Therefore, although the abundances in bar chart look similar between the co-culture and *C. albicans*, the results from the individual *C. albicans* samples agree with the logFC listed in the table (Table 6-7 & Fig. 6-13).

L-cystathionine was present at a lower abundance in the co-culture compared to both of the mono-species biofilms (Table 6-7 & Fig. 6-14A). O-acetyl-L-homoserine and 3-sulfinyl-L-alanine were detected at higher abundances in the co-culture compared to both the *S. aureus* and *C. albicans* mono-species cultures (Table 6-7 & Fig. 6-14 B & C).

**Table 6-7** Heat map comparison of the intracellular metabolite abundances detected in the *C. albicans* (CAC), *S. aureus* (SAC) and the dual species (SCC) biofilms. The elemental formulae (EF), metabolite identification and log-fold changes (logFC) of the identified and annotated metabolites from the cysteine and methionine metabolism pathway are listed. LogFC =  $\log_2$  (dual-species/mono-species). (n = 5).

Metabolite	EF	Mass	logFC		Metabolite ID code*
			SCC/CAC	SCC/SAC	
5'Methylthioadenosine	C11H15N5O3S		0.24	23.27	R <sub>ta</sub> HRMS <sup>1</sup> <sub>a</sub>
S-Adenosyl-L-homocysteine	C14H20N6O5S		-1.84	16.99	R <sub>ta</sub> HRMS <sup>1</sup> <sub>a</sub>
L-Methionine	C5H11NO2S		-0.92	18.43	R <sub>ta</sub> HRMS <sup>1</sup> <sub>a</sub>
L-Aspartate	C4H7NO4		-0.38	-1.24	R <sub>ta</sub> HRMS <sup>1</sup> <sub>a</sub>
L-Alanine	C3H7NO2		-0.74	0.39	R <sub>ta</sub> HRMS <sup>1</sup> <sub>a</sub>
L-Cystathionine	C7H14N2O4S		-9.57	-9.69	R <sub>ta</sub> HRMS <sup>1</sup> <sub>a</sub>
O-Acetyl-L-serine	C5H9NO4		0.53	-0.51	HRMS <sup>1</sup>
Glutathione	C10H17N3O6S		-1.66	17.75	HRMS <sup>1</sup>
S-Adenosyl-L-methionine	C15H22N6O5S		0.03	18.47	HRMS <sup>1</sup>
O-Acetyl-L-homoserine	C6H11NO4		0.85	0.82	HRMS <sup>1</sup>
Pyruvate	C3H4O3		1.44	0.37	HRMS <sup>1</sup>
Sulphate	H2SO4		-0.1	0.7	HRMS <sup>1</sup>
O-Succinyl-L-homoserine	C8H13NO6		12.03	-3.34	HRMS <sup>1</sup>
L-Homoserine	C4H9NO3		0.38	-0.87	HRMS <sup>1</sup>
3-Sulfinyl-L-alanine	C3H7NO4S		0.79	0.63	HRMS <sup>1</sup>

\* Refers to alphanumeric coding scheme from (Sumner et al., 2014).

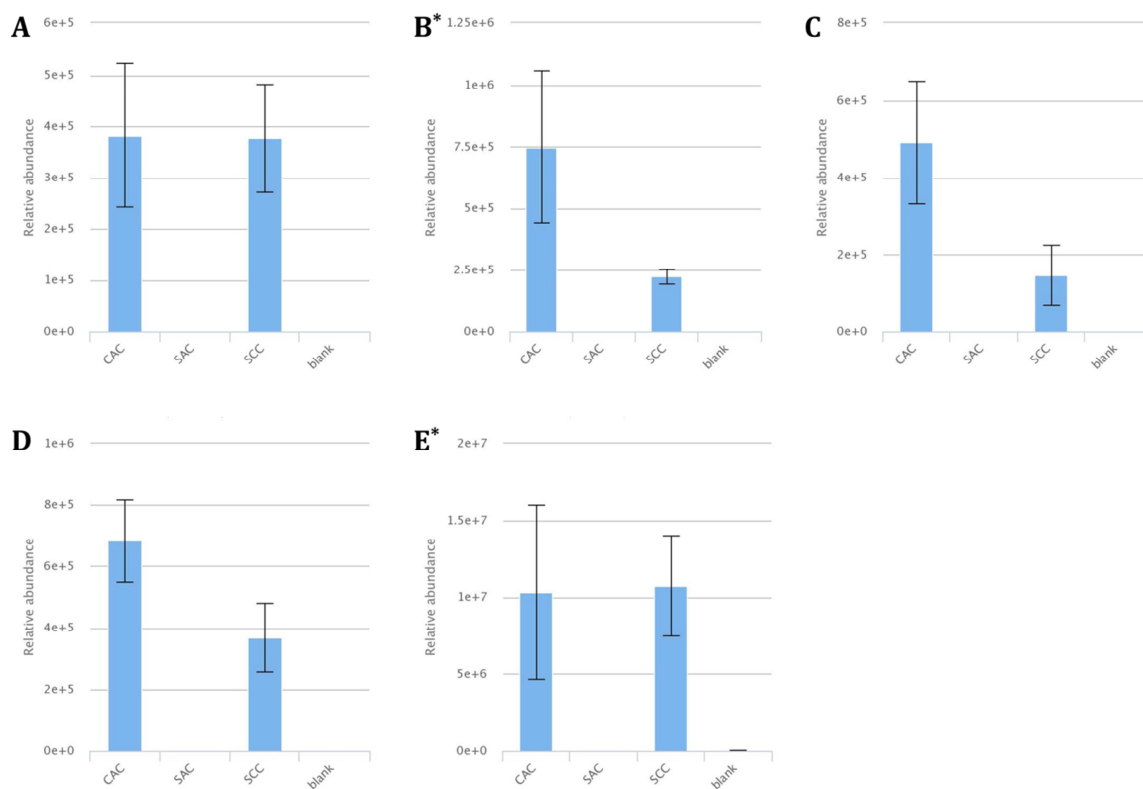


**Figure 6-11** Bar charts comparing the relative abundance of intracellular (A) 5'-methylthioadenosine; (B) glutathione; (C) S-adenosyl-L-homocysteine; (D) L-methionine and (E) S-adenosyl-L-methionine detected in the mono-species *C. albicans* (CAC), *S. aureus* (SAC) and their co-culture (SCC). The biofilms were cultured in 50% FBS for 24 hours. Mature biofilms were washed twice in PBS. Metabolites were extracted according to the established protocol in ice-cold chloroform:methanol:water (1:3:1, v:v:v). None of the metabolites were detected in the *S. aureus* mono-species biofilm. Similar abundances of 5'-methyladenosine and S-adenosyl-L-methionine were detected in the co-culture and the *C. albicans* mono-species biofilm (A & E). Higher abundances of glutathione, S-adenosyl-L-homoserine and L-methionine were detected in *C. albicans* compared to the co-culture (B, C & D). Analysis: HPLC-ESI-FTMS. Polarity mode: pos/neg switching. Mass tolerance: 4 ppm. Error bars  $\pm$  standard deviation (SD). (n=5). (Note: \* indicates putative identification).

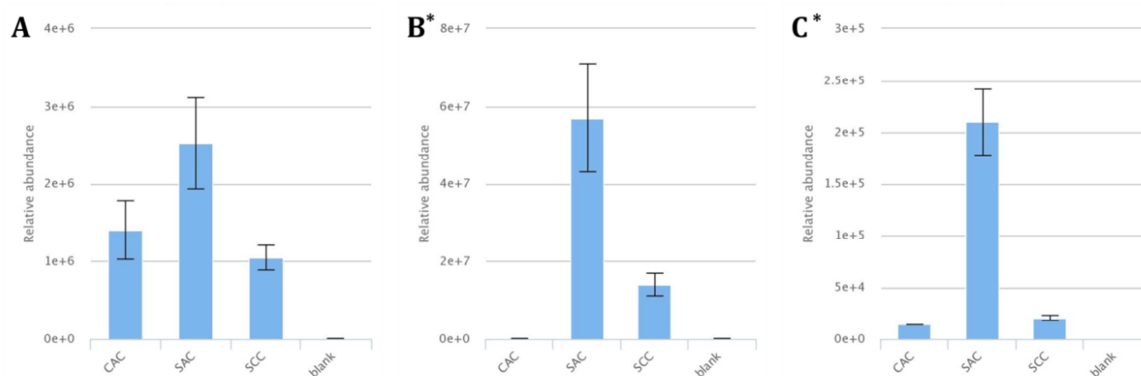


**Figure 6-12** Bar charts comparing the relative abundance of intracellular (A) L-aspartate; (B) L-homoserine and (C) O-succinyl-L-homoserine detected in the mono-species *C. albicans* (CAC), *S. aureus* (SAC) and their co-culture (SCC). The biofilms were cultured in 50% FBS for 24 hours. Mature biofilms were washed twice in PBS. Metabolites were extracted according to the established protocol in ice-cold chloroform:methanol:water (1:3:1, v:v:v). Higher abundances of the metabolites were detected in the *S. aureus* mono-species biofilm compared to both the *C. albicans* mono-species biofilm and the dual-species biofilm. Similar abundances of L-aspartate were detected in the co-culture and *C. albicans* biofilms (A). Higher abundances of L-homoserine and O-succinyl-L-homoserine were detected in the co-culture compared to the *C. albicans* biofilm (B & C). Analysis: HPLC-ESI-FTMS. Polarity mode: pos/neg switching. Mass tolerance: 4 ppm. Error bars  $\pm$  standard deviation (SD). (n=5). (Note: \* indicates putative identification).

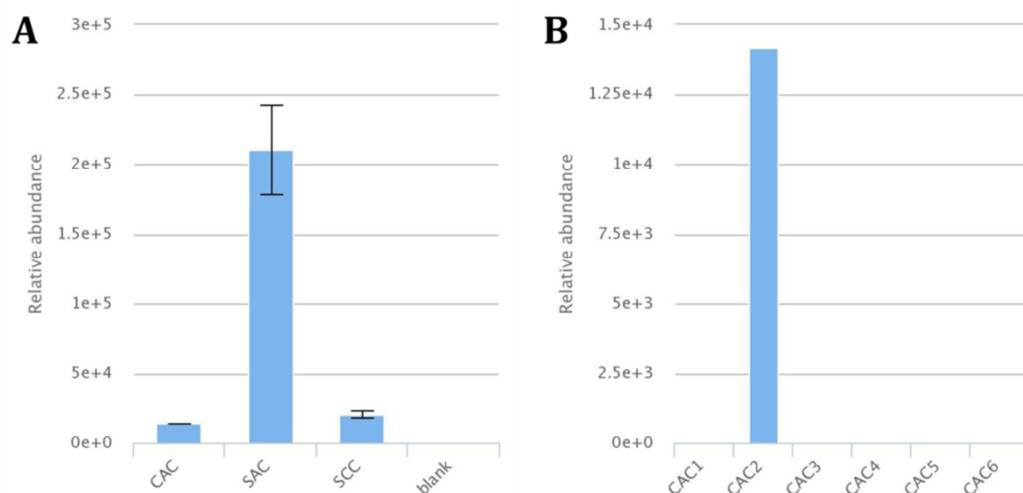


**Figure 6-13** Bar charts comparing the relative abundance of O-succinyl-L-homoserine detected in (A) the mono-species *C. albicans* (CAC), *S. aureus* (SAC) and their co-culture (SCC) and (B) the individual *C. albicans* samples. The relative abundance of O-succinyl-L-homoserine look similar in the co-culture compared to the *C. albicans* mono-species (A). However, this metabolite was only present in one of the individual *C. albicans* samples (B). Analysis: HPLC-ESI-FTMS. Polarity mode: pos/neg switching. Mass tolerance: 4 ppm. Error bars  $\pm$  standard deviation (SD). (n=5).

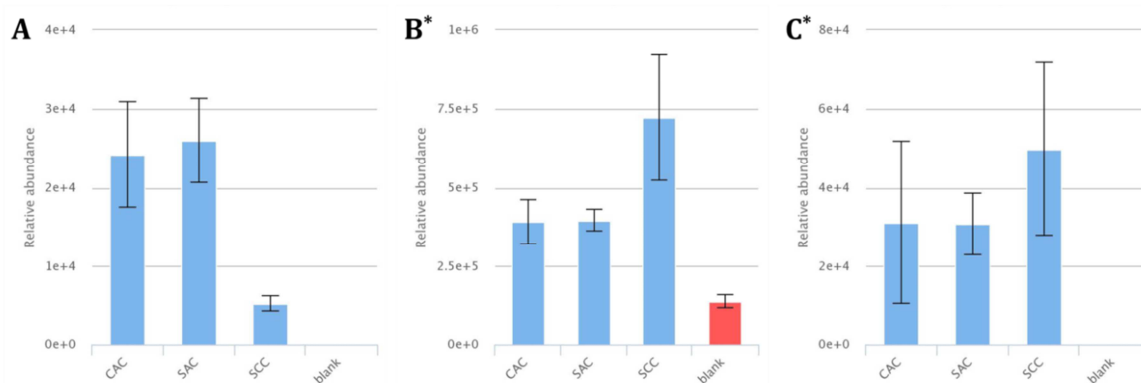


**Figure 6-14** Bar charts comparing the relative abundance of intracellular (A) L-cysthionine; (B) O-acetyl-L-homoserine and (C) 3-sulfino-L-alanine detected in the mono-species *C. albicans* (CAC), *S. aureus* (SAC) and their co-culture (SCC). The biofilms were cultured in 50% FBS for 24 hours. Mature biofilms were washed twice in PBS. Metabolites were extracted according to the established protocol in ice-cold chloroform:methanol:water (1:3:1, v:v:v). L-cysthionine was detected at a significantly lower abundance in the co-culture compared to both mono-species biofilms (A). Relatively higher abundances of O-acetyl-L-homoserine and 3-sulfino-L-alanine were detected in the dual-species biofilm compared to the mono-species biofilms (B & C). Analysis: HPLC-ESI-FTMS. Polarity mode: pos/neg switching. Mass tolerance: 4 ppm. Error bars  $\pm$  standard deviation (SD). (n=5). (Note: \* indicates putative identification).

## 6.4 Discussion

The aim of this research was to apply the previously developed targeted IC-MS and untargeted RPLC/pHILIC methods to the analysis of *S. aureus* and *C. albicans* mono- and dual-species biofilms. It was hoped that the metabolomics data generated from these analyses would enable the relationship between *S. aureus* and *C. albicans* within the dual-species biofilm to be explored in further detail. Greater understanding of this relationship could highlight potential drug targets for the treatment of *S. aureus/C. albicans* cross-infections.

### 6.4.1 IC-MS

The IC-MS method was applied to the analysis of *S. aureus* and *C. albicans* mono- and dual-species biofilms. Although the samples were analysed successfully using the IC-MS method, and the method displayed good RT reproducibility, the presence of structural isomers and peak tailing made quantitation difficult. As well as this, many metabolites were not detected in the cellular *S. aureus* mono-species. This made any intracellular comparisons tricky, as the absence of these metabolites could be because the analyte intensities were lower than the detection limits of the instrument. The low analyte intensities could be a result of the very low biomasses obtained when *S. aureus* was cultured in serum in isolation. It has been shown previously that sera does not facilitate *S. aureus* growth or biofilm formation (Harriott & Noverr, 2009; Peters, Ovchinnikova, et al., 2012; Schlecht et al., 2015; Staib et al., 1971). This problem was encountered previously in this study, during biofilm characterisation (Chapter 3). RNA analysis was carried out on a selection of important *S. aureus* biofilm genes (ClfB, FnbA, Sas6 and SasF). Although extractions were carried out numerous times and attempts were made for extraction optimisation, the quantity of RNA collected from the *S. aureus* samples were too low to synthesise cDNA. Therefore, if intracellular metabolites exist at low abundances, low biomass and/or cell number would make analyte detection difficult.

With the omission of the *S. aureus* mono-species, overall the intracellular metabolite abundances were similar between *C. albicans* and the dual-species biofilm. However, for unknown reasons fructose 1,6-bisphosphate and fumarate were not detected in the dual-species culture.

The biofilms were cultured for 24 hours before metabolite extractions were carried out. Yeater et al. (2007) carried out gene expression analysis during *C.*

*albicans* biofilm formation and identified the upregulation of different cellular processes at different developmental stages (Yeater et al., 2007). Glycolysis, pyruvate metabolism and energy production were upregulated during biofilm formation at 6 and 12 hours, but not at 48 hours. At the mature biofilm stage, genes relating to energy conservation were upregulated. These observations could corroborate the data generated from this research. After 24 hours of growth the microorganisms within the mature biofilms could reach an equilibrium with regards to energy metabolism. This could explain why few differences were recorded between the sample groups. Carrying out a targeted analysis during the early stages of biofilm formation may provide better insight into the behaviour of *S. aureus* and *C. albicans* within their mono- and dual-species biofilms.

Further to this, metabolic flux analysis (MFA), that is the *in vivo* reaction rates of enzymes, could provide a better insight into the metabolic activity of *S. aureus* and *C. albicans* within their mono- and dual-species biofilms (Sauer, 2006). Fluxes are time-dependant motions of metabolites through a metabolic network (Sauer, 2006). Fluxes are mapped through computer model-based interpretation of measurable quantities (Sauer, 2006). Commonly  $^{13}\text{C}$ -labelled substrates are used, e.g.  $^{13}\text{C}_6$ -glucose.  $^{13}\text{C}$  MFA is based on carbon labelling experiments (Marx, De Graaf, Wiechert, Eggeling, & Sahm, 1996). The  $^{13}\text{C}$ -labelled substrate is fed to a population of cells and the labelled carbon atoms are distributed over a metabolic network, which can then be measured by NMR or MS (Marx et al., 1996). Labelling patterns are detected within metabolic intermediates which directly relate to the distribution of fluxes (Marx et al., 1996; Sauer, 2004, 2006; Wiechert, 2001). Network distribution of fluxes are then reconstituted from measured  $^{13}\text{C}$  data and can show the rate at which metabolites are anabolically or catabolically distributed within a network. Using MFA, differences in rate of metabolic activity and the fate of intermediates within CCM could be determined for *S.*

*aureus* and *C. albicans* in their mono- and dual-species biofilms. Tracking fluxes would enable temporal changes in the behaviour of the bacteria and fungi to be observed.

However, the IC-MS method would have to be improved to ensure baseline separation of glucose and sugar phosphate isomers before any further analysis could be carried out. Method optimisation options include altering the mobile phase gradient, testing different columns and investigating the suitability of the addition of organic solvents to aid in peak separation.

Next, untargeted RPLC/pHILIC-MS analysis was carried out on the extracted biofilm samples.

#### **6.4.2 LC-MS**

The RPLC/pHILIC combined method was applied to the analysis of *S. aureus* and *C. albicans* mono- and dual-species biofilms. Although the samples were analysed successfully using the combined method, when the results were compared to those obtained using a pHILIC method far fewer metabolites were detected. 3368 intracellular and 3661 extracellular metabolites were detected when the pHILIC method was used compared to 1151 intracellular and 1465 extracellular when the RPLC/HILIC combined method was utilized. More metabolites were identified using the pHILIC method compared to the RPLC/pHILIC method. 67 intracellular metabolites were identified using the pHILIC method compared to 39 for the combined method, and 68 extracellular metabolites compared to 49, respectively. The significant decrease in the number of metabolites detected, coupled with the poorer peak-shapes witnessed, led to mono-column pHILIC method being utilized in place of the RPLC/pHILIC dual-column method.

### 6.4.2.1 Biochemical interpretation

The intracellular analysis of the mono- and dual-species biofilms indicated that 51 identified metabolites and 241 annotated metabolites were significantly changing between the *S. aureus* mono-species biofilm and the dual-species biofilm. 26 identified metabolites and 183 annotated metabolites were significantly changing between the *C. albicans* mono-species biofilm and the dual-species biofilm. Relative abundances of individual metabolites in isolation are unable to provide a clear picture of the metabolic state of a sample, therefore to enable accurate interpretation of the data, metabolic pathways were visualised in place of individual metabolites.

Due to the key roles that purine and pyrimidine metabolism play in RNA, protein and DNA synthesis, as well as energy production, these two pathways were analysed first.

#### 6.4.2.1.1 Comparison of purine metabolism in *S. aureus* and the dual-species biofilm

The relative abundances of the detected metabolites involved in purine metabolism were higher in the co-culture compared to the *S. aureus* biofilm, with the exception of L-glutamine, adenosine monophosphate (AMP), deoxyguanosine monophosphate (dGMP) and xanthosine (Fig. 6-15). Glutamine plays an important role in the production of purines and pyrimidines. It donates nitrogen atoms that form the N-9 and N-3 of the purine ring and participates in the amination of xanthine monophosphate (XMP) to form guanosine monophosphate (GMP). The higher levels of glutamine, coupled with the lower levels of other purine metabolites within the pathway could suggest lower levels of purine synthesis. However, the presence of higher abundances of AMP, dGMP and xanthosine in the *S. aureus* mono-species compared to the co-culture conflict with this conclusion.

The higher levels of AMP detected in *S. aureus* could suggest up-regulation of either ATP or dATP synthesis in the bacterial monoculture compared to the co-culture. AMP is an intermediate in the conversion of inosine monophosphate (IMP) to adenosine triphosphate (ATP) through the purine nucleotide cycle (Fig. 6-16). In the presence of guanosine triphosphate (GTP), IMP reacts with aspartate to form adenylosuccinate, which is then cleaved to form AMP and fumarate. AMP can be phosphorylated to ADP which can be used to produce adenosine triphosphate (ATP). ATP can be used for energy by the cell as well as being utilized in RNA synthesis. ADP can also be reduced to deoxyadenosine diphosphate (dADP) in a reaction mediated by ribonucleotide reductase. dADP is then phosphorylated to form deoxyadenosine triphosphate (dATP) which can be used for the synthesis of DNA. The higher abundance of AMP could suggest that the bacteria are altering their metabolism to favour energy production.

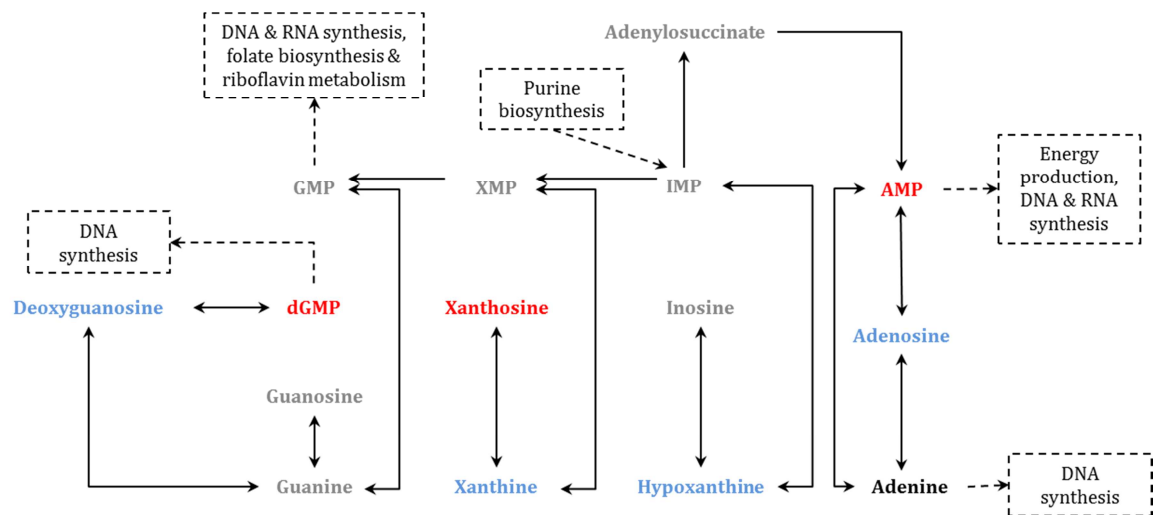


**Figure 6-15** Schematic diagram depicting identified and annotated metabolites within the purine metabolism pathway in relation to known *S. aureus* enzymes. Colour code: grey = undetected, red = higher abundance detected in *S. aureus* mono-species, blue = higher abundance detected in dual-species biofilm, black = found in equal abundance in both *S. aureus* and dual-species biofilms. Inosine monophosphate (IMP) is produced from a reaction pathway that begins with 5'phospho-alpha-D-ribose-1-diphosphate. L-Glutamine is utilized in the next reaction to produce ribosylamine 5-phosphate. After a number of reactions IMP is produced. Adenosine monophosphate (AMP) can be synthesised from IMP through the conversion of IMP to adenylosuccinate. AMP can then be converted to adenine, either directly or through conversion to adenosine, which in turn is converted to adenine. Adenine can then be utilized for DNA synthesis. AMP can also be converted to ADP and ATP, which are utilized in energy production, as well as DNA and RNA synthesis. IMP can also be converted to xanthosine monophosphate (XMP), which in turn is converted to guanosine monophosphate (GMP). GMP can undergo various reactions for its conversion to metabolites that can be incorporated into DNA synthesis, RNA synthesis, riboflavin metabolism and folate biosynthesis. GMP can also be converted to guanine. Guanine can then be reduced to form deoxyguanosine. Deoxyguanosine is phosphorylated to produce deoxy-GMP (dGMP), which can then be utilized in DNA synthesis. Higher abundances of adenosine monophosphate (AMP), xanthosine and deoxyguanosine monophosphate (dGMP) were detected in the *S. aureus* mono-species biofilm compared to the dual-species biofilm. Higher abundances of deoxyguanosine, xanthine, hypoxanthine and adenosine were detected in the co-culture compared to *S. aureus*. There was a similar abundance of adenine detected in both the *S. aureus* mono-species and dual-species biofilms.

Biosynthesis of polymers is one of the most energy demanding processes in bacteria (Mongodin, Climo, Rosato, Gill, & Archer, 2003). In vancomycin resistant bacteria metabolic alterations directed metabolism towards increased production of AMP compared to their vancomycin susceptible counterparts (Mongodin et al., 2003). The up-regulation of AMP production was explained

through the increase in cell-wall volume of the resistant bacteria. Precursor metabolites used in substrate-level phosphorylation in the generation of ATP were likely utilized in polymer biosynthesis for cell wall construction. An increase in AMP would allow ATP production through AMP phosphorylation, thereby alleviating the need to utilize other metabolites, which could be used in polymer biosynthesis, in ATP generation (Mongodin et al., 2003). The *S. aureus* present in the mono-species biofilm could be directing their metabolism towards AMP production for ATP generation in a bid to save precursor metabolites for different processes.

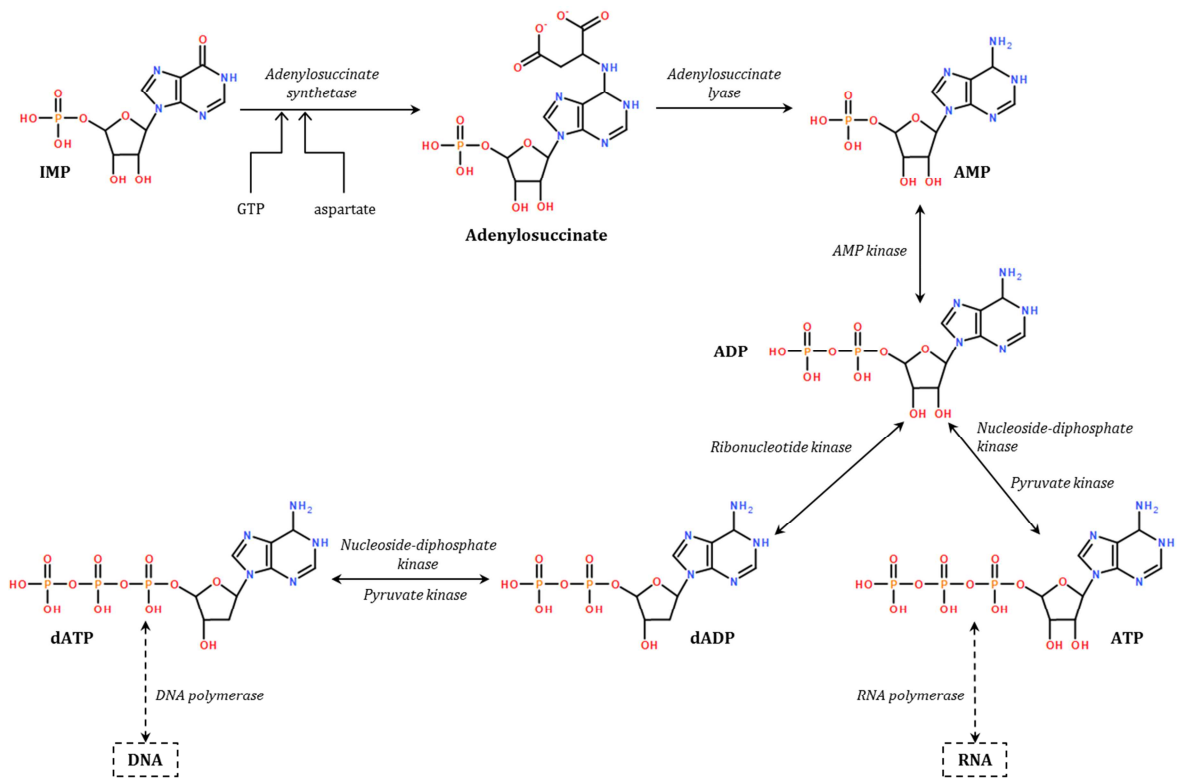


**Figure 6-16** Adenosine triphosphate (ATP) and deoxyadenosine triphosphate (dATP) synthesis from inosine monophosphate (IMP). In the presence of guanosine triphosphate (GTP) and aspartate, IMP is converted to adenylosuccinate in an irreversible reaction mediated by adenylosuccinate synthetase. Adenylosuccinate is cleaved to produce adenosine monophosphate (AMP) and fumarate through the action of adenylosuccinate lyase. Adenosine diphosphate is synthesised by through the transfer of a phosphate group from ATP to AMP by AMP kinase. ADP can then be converted into ATP, through the addition of a phosphate group, or it can be converted to deoxyadenosine diphosphate (dADP) by ribonucleotide kinase. dADP can then be converted to dATP, by the addition of a phosphate group. ATP and dATP can be utilised in the synthesis of RNA and DNA, respectively.

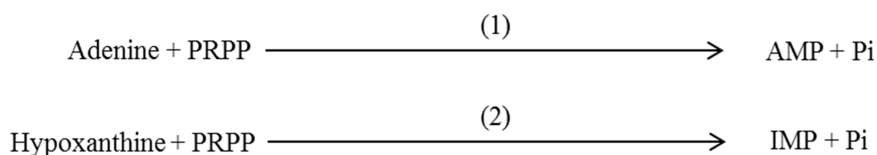
Another explanation for higher AMP abundance could be that the bacteria have entered a starvation state due to nutrient depletion in the media (Khakimova, Ahlgren, Harrison, English, & Nguyen, 2013; Potrykus, Murphy, Philippe, & Cashel, 2011). The stringent response in bacteria involves alarmones e.g. guanosine tetra- or penta-phosphate ((p)ppGpp), which are activated in response to a shortage of amino acids. Alarmones regulate gene expression at the transcription level. (p)ppGpp inhibits RNA synthesis and therefore causes a decrease in translation, which enables bacteria to conserve the levels of the remaining amino acid pools. The stringent response also causes up-regulation in amino acid biosynthesis pathways and other genes involved in the stress response. The higher levels of AMP detected in the bacterial mono-species could be due to the stringent response in *S. aureus* halting RNA synthesis, as AMP plays a key role in the synthesis of metabolites for utilization in RNA synthesis (Fig. 6-16). Unfortunately, none of the other metabolites involved in this part of the metabolic pathway were detected, so it is unclear whether the bacteria shifted towards AMP production in the mono-species compared to the dual-species biofilm or whether the increased abundance of AMP was as a result of the stringent response due to environmental stress.

It could be argued that the results from the comparison of purine metabolism in the bacterial mono-species and the dual-species biofilms points to the latter of these two conflicting conclusions. The poor biofilm formation and lower numbers of bacteria detected in the mono-species *S. aureus* biofilm compared to the dual-species biofilm during biofilm characterisation support the opinion that the increased abundance of AMP detected in the *S. aureus* mono-species is a result of the stringent response of the bacteria to the culturing conditions. Defective purine biosynthesis caused decreased biofilm formation and virulence in persistent infections such as endocarditis (Ge et al., 2008). In *S. aureus* purine biosynthesis has been associated with survival in stressed

conditions, such as vancomycin and daptomycin treatment and it has been speculated that purine biosynthesis plays a crucial role in *S. aureus* biofilm formation (Keer, Smeulders, & Williams, 2001; D. Mack et al., 2004; Mongodin et al., 2003). Purine biosynthesis plays a crucial role in *S. aureus* persists in response to rifampicin treatment and genes involved in purine biosynthesis have also been shown to be important for antibiotic and stress tolerance in *S. aureus* (Yee, Cui, Shi, Feng, & Zhang, 2015).

As well as this, the down-regulation of other purine metabolism intermediates could suggest lower levels of DNA synthesis and ATP production. This explanation is in agreement with the presence of fewer number of *S. aureus* in the mono-species compared to the co-culture recorded during biofilm characterisation, as DNA is required for replication.

The lower levels of adenine and hypoxanthine detected in *S. aureus* compared to the co-culture and the mono-species *C. albicans* (Fig. 6-15) are suggestive of *S. aureus* utilising purine ‘salvage pathways’ (Fig. 6-17). AMP and IMP can be synthesised from the transfer of phosphoribosyl pyrophosphate (PRPP) to adenine and hypoxanthine by adenine phosphoribosyl transferase (PTR) and hypoxanthine-guanine PTR, respectively (Fig. 6-17). The higher levels of AMP detected in the *S. aureus* mono-species (Fig. 6-15) could be a result of the bacteria utilizing adenine to synthesis AMP. Recycling free purine bases from degraded nucleic acids and nucleotides through salvage pathways requires less ATP than energy-intensive *de novo* pathways and could be employed by the bacteria as an ATP saving method of purine biosynthesis.



Where: PRPP = phosphoribosyl pyrophosphate  
 (1) = adenine phosphoribosyl transferase  
 (2) = hypoxanthine-guanine phosphoribosyl transferase  
 AMP = adenosine monophosphate  
 IMP = inosine monophosphate  
 P<sub>i</sub> = inorganic phosphate

**Figure 6-17** Salvage pathways for purines. Adenosine monophosphate (AMP) and inosine monophosphate (IMP) can be salvaged from adenine and hypoxanthine through the transfer of phosphoribosyl pyrophosphate (PRPP) using specific phosphoribosyl transferases (PTRs).

#### 6.4.2.1.2 Comparison of purine metabolism in *C. albicans* and the dual-species biofilm

In contrast to the results obtained for *S. aureus*, when *C. albicans* was compared to the co-culture almost all of the purine metabolism intermediates were detected at lower abundances in the dual-species biofilm, with the exception of adenine and xanthine (Fig. 6-18). Overall, this suggests down-regulation in purine metabolism when *C. albicans* is cultured with *S. aureus* compared to when the fungi is cultured in isolation. This result was unexpected due the important role purine metabolism plays in the virulence of various microorganisms (Ge et al., 2008; Keer et al., 2001; J. K. Kim et al., 2014; Mongodin et al., 2003; Yee et al., 2015). Although purine metabolism may enhance biofilm formation in *S. aureus*, it may not be identical in *C. albicans*. In a recent study, low (LBF) and high (HBF) biofilm forming *C. albicans* phenotypes were compared to determine the differences in gene expression between the two phenotypes (Rajendran et al., 2016). It was determined that purine metabolism was up-regulated in LBF compared to

HBF (Rajendran et al., 2016). In another study, down-regulation of purine metabolism was found to be involved in the morphological change in *C. albicans* from yeast cells to its hyphal form (T. li Han, Cannon, & Villas-Bôas, 2012). Therefore, down regulation of purine metabolism in the dual-species biofilm compared to the *C. albicans* mono-species biofilm may indicate higher biofilm formation. These results would be in agreement with the significant increase in biomass noted in the dual-species biofilm compared to both mono-species biofilms when the samples were characterised using CV staining methods.

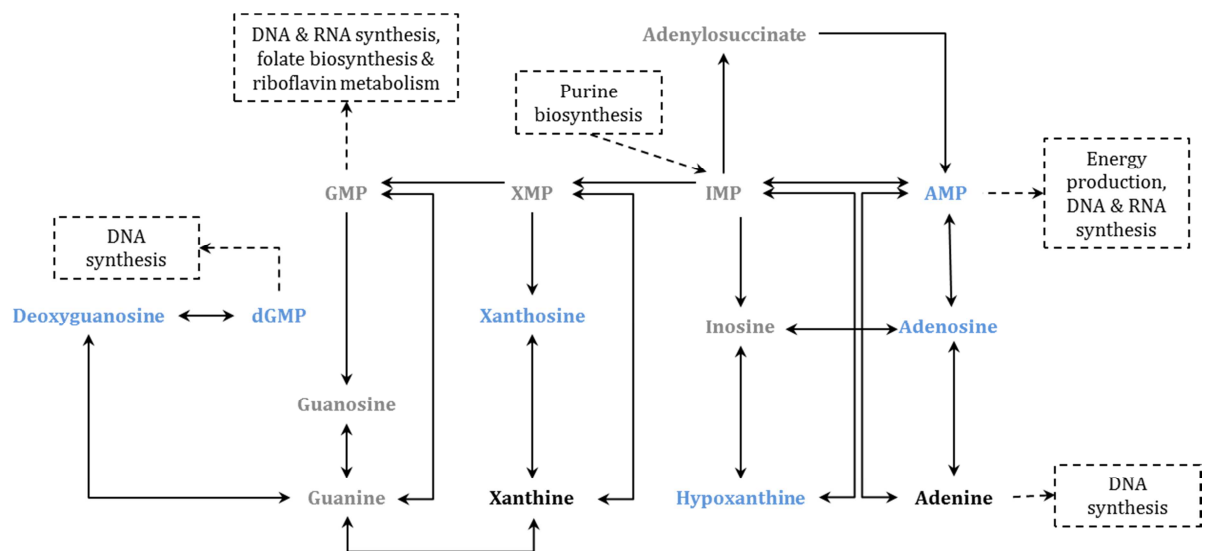


**Figure 6-18** Schematic diagram of the purine metabolism pathway in relation to known *C. albicans* enzymes. Colour code: grey = undetected, red = higher abundance detected in the dual species biofilm, blue = higher abundance detected in *C. albicans*, black = found in equal abundance in both *C. albicans* and dual-species biofilms. The reaction pathways for purine metabolism in *C. albicans* are similar to those seen in *S. aureus* with some differences. *C. albicans* possess enzymes for the direct conversion of inosine monophosphate (IMP) to adenosine monophosphate (AMP), IMP to inosine, inosine to adenosine, xanthosine monophosphate (XMP) to xanthosine, guanosine monophosphate (GMP) to guanosine and hypoxanthine to guanine. All of the detected metabolites within the purine metabolism pathway were down-regulated in the dual-species biofilm compared to the *C. albicans* mono-species biofilm, with the exception of adenine and xanthine, which were detected at similar abundances in both the dual- and mono-species biofilms.

Only 15 metabolites were detected out of a possible 92, resulting in 17.39% coverage of this pathway. More metabolites in this pathway would have to be detected for precise conclusions to be drawn. To determine whether the increased abundance of AMP in the *S. aureus* biofilm is a result of stringent response to harsh environmental conditions, efforts should be made to detect purine intermediates involved in AMPs conversion to ADP, dADP and ATP. The detection of IMP, XMP, GMP along with guanosine could help elucidate whether salvage pathways are being utilised in the mono-species bacterial biofilm. The detection of intermediates involved in initial purine biosynthesis would enable conclusion to be drawn as to whether purine metabolism is being up- or down-regulated in each of the three samples.

Next pyrimidine metabolism pathways were analysed.

#### **6.4.2.1.3 Comparison of pyrimidine metabolism in *S. aureus* and the dual-species biofilm**

Overall, detectable pyrimidine metabolites were found in a lower abundance in the mono-species *S. aureus* biofilm when compared to abundances detected in the co-culture. However, from the metabolites that were detected a difference was observed in the abundance of metabolites involved in *de novo* pyrimidine biosynthesis. These metabolites were detected at a higher abundance in the *S. aureus* biofilm than the dual-species biofilm (Fig. 6-19). UDP-glucose is utilized in the synthesis of uracil monophosphate (UMP) in pyrimidine biosynthesis. According to KEGG pathways both *S. aureus* and *C. albicans* lack the enzyme to synthesize UMP from UDP-glucose. The lack of UDP-glucose detected in the intracellular metabolome of the bacteria is in agreement with this.

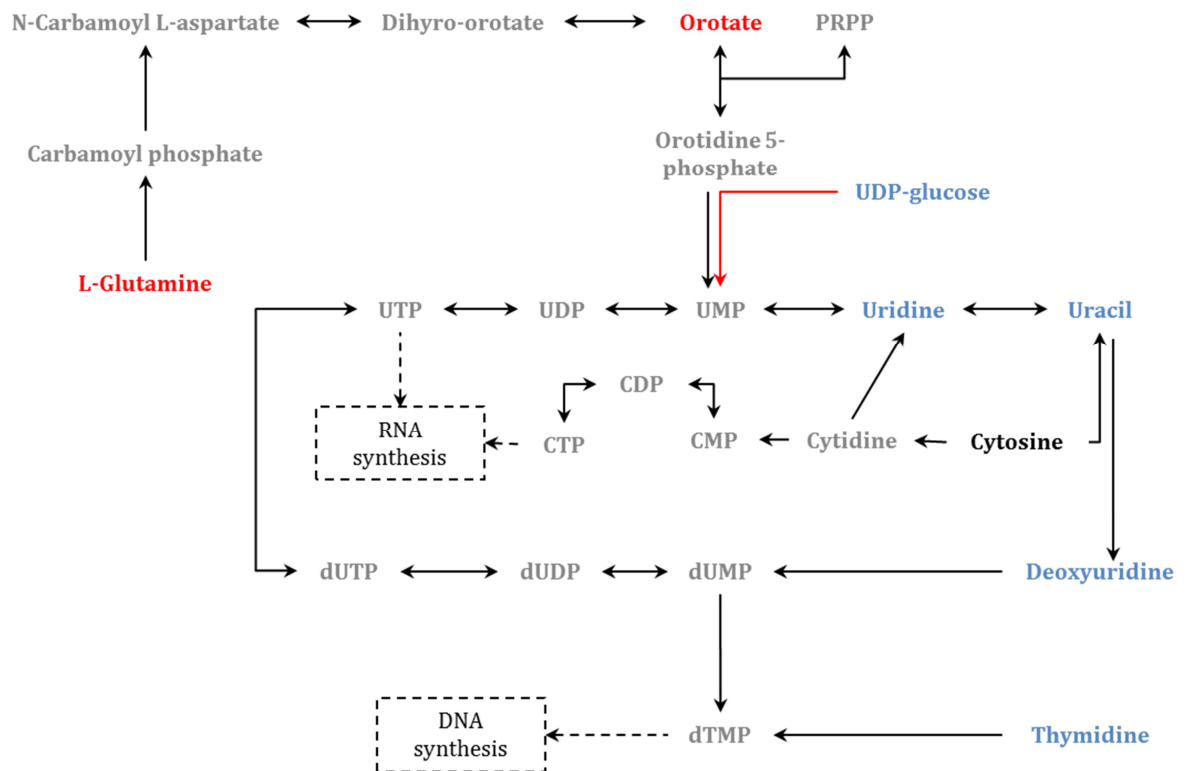


**Figure 6-19** Schematic diagram depicting identified and annotated metabolites within the pyrimidine metabolism pathway in relation to known *S. aureus* enzymes. Colour code: grey = undetected, red = higher abundance detected in *S. aureus* mono-species, blue = higher abundance detected in dual-species biofilm, black = found in equal abundance in both *S. aureus* and dual-species biofilms. Orotate and L-glutamine were detected at a higher abundance in the *S. aureus* mono-species. Cytosine was detected at a similar level in the bacterial mono-species and the dual-species biofilm. UDP-glucose, uridine, uracil, deoxyuridine and thymidine were detected at a higher abundance in the co-culture compared to the bacterial mono-species.

The higher levels of L-glutamine and orotate detected in the *S. aureus* mono-species compared to both the *C. albicans* mono-species and the dual-species biofilms could be indicative of up-regulation of the *de novo* pyrimidine biosynthesis pathway in the bacterial mono-species (Figs. 6-19 & 6-20). Up-regulation of *de novo* biosynthesis could be a result of growing the bacteria in 50% FBS. Purine and pyrimidine biosynthesis are critical for bacterial growth in blood (Samant et al., 2008). The inactivation of nucleotide biosynthesis

genes in *E. coli*, *Salmonella enterica* & *Bacillus anthracis* prevented bacterial growth in human serum, and Mei et al. (1997) demonstrated the importance of nucleotide biosynthesis for the survival and replication of *S. aureus* in blood (Mei, Nourbakhsh, Ford, & Holden, 1997). The pyrimidine *de novo* biosynthetic pathway has a higher energy cost than salvage pathways, so up-regulation of this pathway over less costly salvage pathways could suggest that *S. aureus* is unable to utilize salvage pathways when grown in sera. The need for *S. aureus* to synthesise pyrimidines *de novo* could result in lower energy production and fewer available metabolite precursors for the synthesis of components required for biofilm formation, which could result in the poor biofilms observed when *S. aureus* is grown in 50% FBS (Harriott & Noverr, 2009; Peters, Ovchinnikova, et al., 2012; Schlecht et al., 2015; Staib et al., 1971). Another possible reason for higher abundances of the *de novo* pathway metabolites in *S. aureus* could be that the accumulation of energetically costly metabolites is a result of *S. aureus* starvation (Link, Fuhrer, Gerosa, Zamboni, & Sauer, 2015). Using real-time metabolome profiling, Link et al. (2015) demonstrated that *E. coli* maintained AMP abundance during starvation. The higher abundance of *de novo* intermediates, lack of salvage pathway intermediates and poor biofilm formation could be the manifestation of the lack of metabolisable nutrients in the growth media.

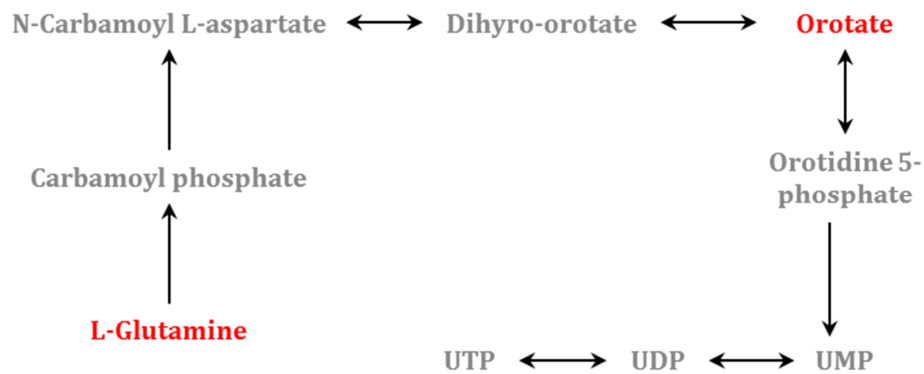


**Figure 6-20** Schematic diagram of pyrimidine biosynthetic *de novo* pathway in *S. aureus*. Colour code: grey = undetected, red = higher abundance detected in *S. aureus* mono-species, blue = higher abundance detected in dual-species biofilm, black = found in equal abundance in both *S. aureus* and dual-species biofilms. Higher abundances of L-glutamine and orotate were detected in the *S. aureus* mono-species compared to the dual-species biofilm.

#### 6.4.2.1.4 Comparison of pyrimidine metabolism in *C. albicans* and the dual-species biofilm

When *C. albicans* was compared to the dual-species biofilm, similar abundances of L-glutamine and orotate were detected. This suggests similar levels of pyrimidine *de novo* biosynthesis. Higher abundances of the metabolites involved in pyrimidine salvage pathways were detected in the *C. albicans* compared to the dual-species biofilm. Nucleotide biosynthesis is required for antifungal resistance (Banerjee, Burkard, & Panepinto, 2014). The inactivation of *de novo* pyrimidine biosynthesis affects the ability of the yeast *Cryptococcus neoformans* to grow at 37°C (de Gontijo et al., 2014). Upregulation of salvage pathways requires less energy than *de novo* biosynthesis, which would enable the fungi to drive metabolism towards other pathways. These observations substantiate the results obtained from the biofilm characterisation. The results suggest that *C. albicans* is able to maintain pyrimidine metabolite pools in sera compared to *S. aureus*. The increased numbers of *S. aureus* detected in the dual-species biofilm could be

due, in part, to the increased availability of UMP precursors, either those required for *de novo* biosynthesis or free bases utilised in salvage pathways, provided through cross-feeding from *C. albicans*.

22 metabolites in this pathway were detected out of a possible 66, which resulted in 36.36% coverage. More metabolites would have to be detected for any conclusions to be drawn.

As there appeared to be some significant changes occurring in these pathways, cysteine and methionine metabolism were also analysed.

#### **6.4.2.1.5 Comparison of methionine metabolism in *S. aureus* and the dual-species biofilm**

Although the majority of the metabolites detected within cysteine and methionine metabolism were at a higher abundance in the dual-species biofilm compared to the *S. aureus* mono-species biofilm, the majority of those involved in methionine biosynthesis were found in a higher abundance in the bacterial mono-species biofilm, with the exception of L-methionine, S-adenosyl-L-methionine (SAM) and O-acetyl-homoserine (Fig. 6-21). Many microorganisms produce methionine through *de novo* biosynthesis. To generate methionine staphylococci employ the trans-sulfuration pathway (Fig. 6-21) (Rodionov, Vitreschak, Mironov, & Gelfand, 2004).

L-methionine and SAM were absent from the bacterial mono-species samples (Fig. 6-21). The increased abundance of methionine biosynthesis intermediates and the absence of methionine and SAM from this pathway could suggest that culturing *S. aureus* in sera results in the inhibition of the end-point of this pathway (Fig. 6-21).

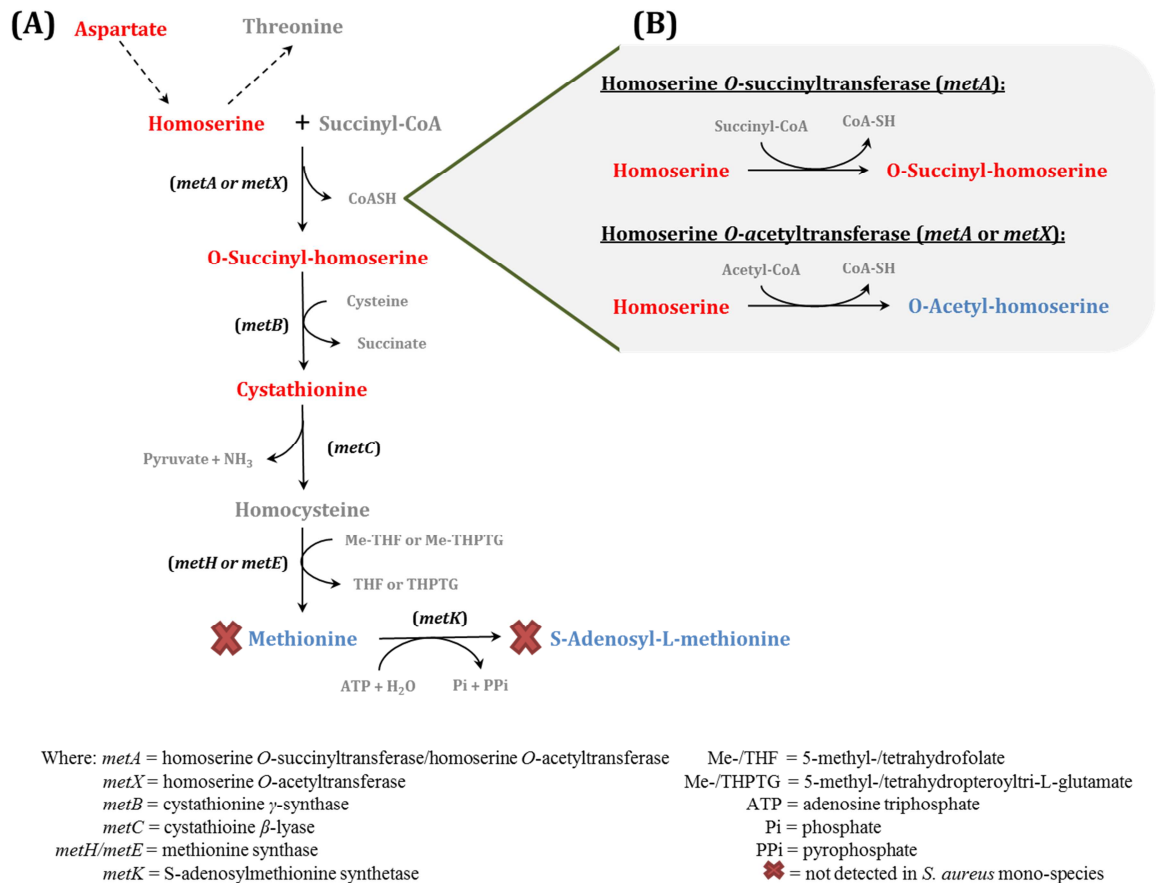


**Figure 6-21** Schematic diagram depicting identified and annotated metabolites within the (A) methionine and S-adenosyl-L-methionine (SAM) biosynthetic pathway and (B) the alternative reactions for the O-acylation of homoserine in relation to known *S. aureus* enzymes. Colour code: grey = undetected, red = higher abundance detected in *S. aureus* mono-species, blue = higher abundance detected in dual-species biofilm. Aspartate, homoserine, O-succinyl-L-homoserine and cystathionine were detected at a higher abundance in the bacterial mono-species biofilm (A). Methionine and SAM were not detected in the *S. aureus* mono-species biofilm, but were present in the dual-species biofilm (A). *S. aureus* Newman strain possesses the *metA* gene encoding both homoserine O-succinyltransferase and homoserine O-acetyltransferase (B).

Methionine and its chemical derivatives have important functions in the cell (Schoenfelder et al., 2013). For example (formyl-)methionine is the universal N-terminal amino acid of nearly all proteins and plays a crucial role in the initiation of protein biosynthesis. SAM serves as a methyl donor in a number of metabolic and biosynthetic processes, which include methylation, SAM radical-mediated vitamin synthesis, and propylamine group transfer in

polyamine synthesis (Parveen & Cornell, 2011). Intracellular SAM is utilized in the methylation of nucleic acids and proteins in both eukaryotes and prokaryotes, a product of which is S-adenosyl-L-homocysteine (SAH) (Parveen & Cornell, 2011). Following methylation, the products are detoxified and recycled to homocysteine, which in its turn is reused for methionine/SAM synthesis (Schoenfelder et al., 2013). SAM is also utilized in the synthesis of polyamines and acylhomoserine lactones, although acylhomoserine lactones are only produced by Gram negative bacteria (Parveen & Cornell, 2011; Schoenfelder et al., 2013). 5'-methylthioadenosine (MTA), produced during polyamine synthesis is again metabolized to methionine through the methionine salvage pathway (Parveen & Cornell, 2011; Schoenfelder et al., 2013). S-adenosyl-L-homocysteine and 5'-methylthioadenosine were not detected in the *S. aureus* mono-species. Staphylococci lack both the methionine salvage and polyamine synthesis pathways (Schoenfelder et al., 2013). The absence of the polyamine synthesis pathway can explain the lack of MTA detected in the *S. aureus* mono-species. The absence of SAH could suggest an inability of the bacteria to synthesise macromolecules, which in turn could be a symptom of the inactivation of methionine and SAM biosynthesis. The inability of *S. aureus* to synthesise macromolecules due to deficiencies in methionine biosynthesis is in agreement with the failure of mono-cultured *S. aureus* to form strong biofilms in serum.

Methionine abundance may not be a limiting factor under normal growth conditions (Schoenfelder et al., 2013). However, when methionine supply is limited, e.g. during host colonization, or exposure to antimicrobials, *de novo* methionine biosynthesis becomes crucial (Chaffin, Taylor, Skerrett, & Rubens, 2012; Pietiäinen et al., 2009; Schoenfelder et al., 2013). Furthermore, a recent study highlighted the critical role that methionine biosynthesis plays in *S. aureus* colonization (Krismer et al., 2014). *S. aureus* depended heavily

on *de novo* synthesis of methionine during growth in a synthetic nasal media (SNM3) and its biosynthesis was up-regulated in this media compared to when it was cultured in basic media (Krismer et al., 2014). Mutants defective in methionine biosynthesis exhibited reduced colonisation capabilities in cotton rat models when compared to a parental Newman's strain (Krismer et al., 2014). Recently the methionine biosynthesis pathway has been highlighted as a potential staphylococcal 'Achilles Heel' (Ochsner et al., 2005; Schoenfelder et al., 2013).

Interestingly, the methyl group donator methyl-tetrahydrofolate (Me-THF) and resulting THF are crucial for pyrimidine synthesis, specifically this co-factor is utilized in the conversion of uridine monophosphate to thymidine monophosphate (Fig. 6-22). Due to its role in DNA, RNA and amino acid biosynthesis, the bacterial THF synthesis pathway is already a target for various antibacterial drugs, e.g. sulfonamides (such as sulfamethoxazole) and diaminopyrimidines (such as trimethoprim). The results from this study could suggest that the inactivation of one of the pathways (most likely pyrimidine synthesis) is having an inhibitory knock-on effect for the other. However, further research would be required to investigate this.

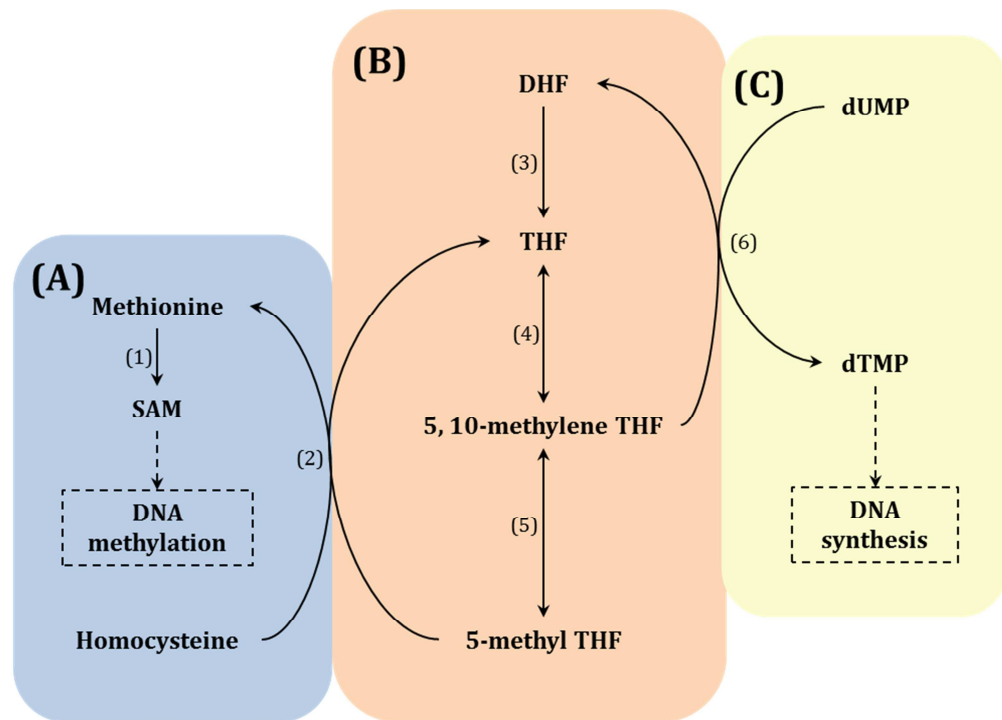


**Figure 6-22** A simple diagram highlighting the relationship between the (A) methionine, (B) tetrahydrofolate and (C) pyrimidine synthesis pathways. (1) S-adenosylmethionine synthetase; (2) methionine synthase; (3) dihydrofolate reductase; (4) serine hydroxymethyltransferase; (5) methylenetetrahydrofolate reductase and (6) thymidylate synthase (adapted from Crider 2012).

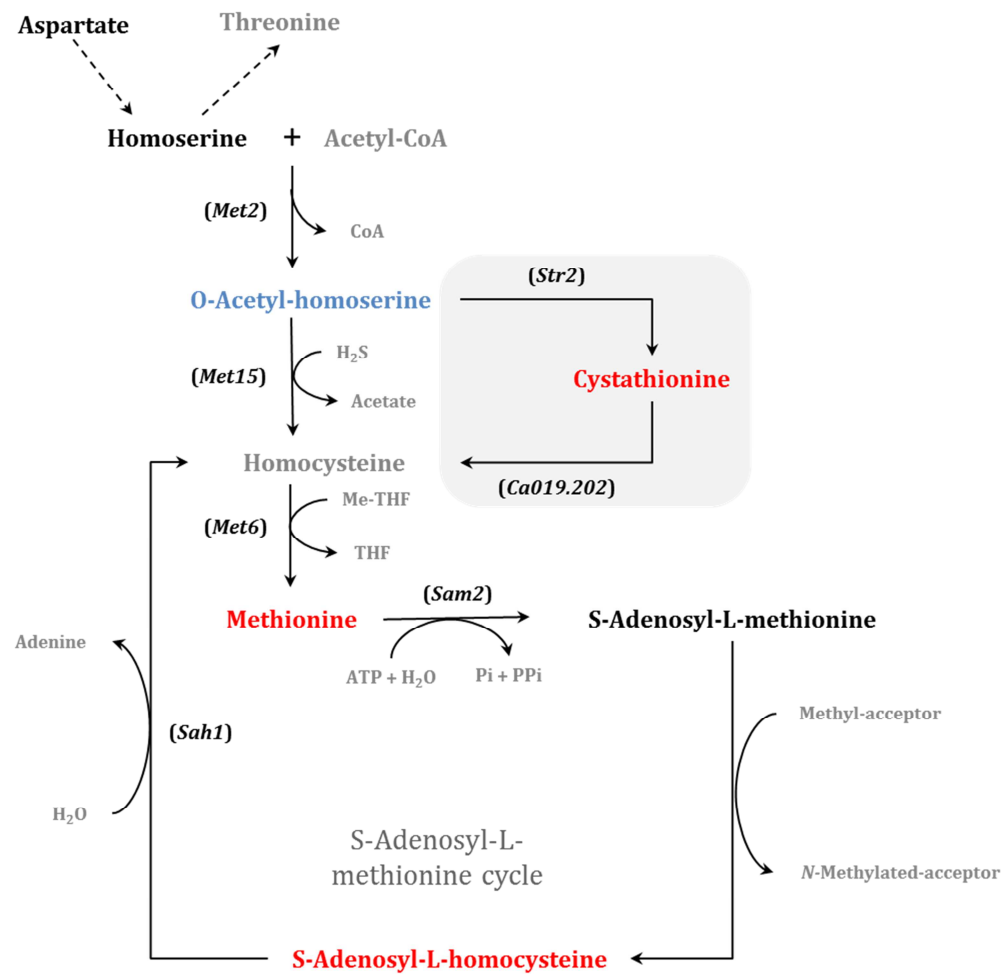
#### 6.4.2.1.6 Comparison of methionine metabolism in *C. albicans* and the dual-species biofilm

The absence of *O*-succinyl-L-homoserine from the fungal mono-species biofilm was expected as *C. albicans* lacks the *metA* gene encoding *O*-succinyltransferase, so only has the ability to acylate homoserine to *O*-acetyl-L-homoserine (<http://www.candidagenome.org>) (Fig. 6-23). In fungi, L-homoserine is *O*-acetylated through the action of L-homoserine transacetylase. The sulphur atom is then introduced in one of two ways- either through the action of *O*-acetylhomoserine(thiol)-lyase to give homocysteine, or through the conversion of *O*-acetyl-homoserine and cysteine to L-cystathionine, which is then converted to L-homocystiene. This two-step reaction is mediated by cystathionine  $\gamma$ -synthase and cystathionine  $\beta$ -lyase, respectively. The final

step is the S-methylation of L-homocysteine to form methionine in a reaction that is catalysed by methionine synthase (Fig. 6-23). Methionine can then be converted to SAM and utilized in methylation reactions. SAH can be converted back to L-homocysteine in the S-adenosyl-L-methionine cycle, in a reaction catalysed by S-adenosyl-L-homocysteine hydrolase (Fig. 6-23).

Methionine biosynthesis is essential for the survival of pathogenic fungi in a human host during infection (Jastrzębowska & Gabriel, 2015). Deletion of different genes within the methionine biosynthetic pathway cause an inability of fungi to produce methionine (Jastrzębowska & Gabriel, 2015). *Met6* inhibition causes accumulation of the toxic intermediate L-homocysteine, which interferes with ergosterol biosynthesis, an important cell membrane component (Hatanaka, Ariga, Nagai, & Katsuki, 1974; McCammon & Parks, 1981; Parks & Casey, 1995). Inactivation of *Met2* resulted in attenuated virulence of *Cryptococcus neoformans* in a mouse model, inhibited sexual development and reduced virulence in *Fusarium graminearum* (Y. K. Han, Lee, Han, Yun, & Lee, 2004; Nazi et al., 2007). Inhibition of *Str2* in the fungal plant pathogens *F. graminearum* and *Magnaporthe grisea* resulted in a significant reduction of virulence (Balhadere, Foster, & Talbot, 1999; Fu, Wu, Jiang, Wang, & Ma, 2013). *F. graminearum* also exhibited hypersensitivity to specific fungicides (Fu et al., 2013).

When the *C. albicans* mono-species was compared to the dual-species biofilm the higher abundances of SAH and MTA could be suggestive of fungal regulation of methionine/SAM metabolism through the utilisation of salvage and recycling pathways (Parveen & Cornell, 2011).



Where: *Met2* = homoserine transacetylase

*Met15* = acetylhomoserine aminocarboxypropyltransferase

*Met6* = methionine synthase

*Sam2* = methionine adenosyltransferase

*Str2* = cystathionine  $\gamma$ -synthase

*Ca019.202* = cystathionine  $\beta$ -lyase

*Sah1* = S-adenosyl-L-homocysteine hydrolase

Me-/THF = 5-methyl-/tetrahydrofolate

ATP = adenosine triphosphate

Pi = phosphate

PPi = pyrophosphate

**Figure 6-23** Schematic diagram depicting identified and annotated metabolites within the (A) methionine and S-adenosyl-L-methionine (SAM) biosynthetic pathway. Colour code: grey = undetected, red = higher abundance detected in *C. albicans* mono-species, blue = higher abundance detected in dual-species biofilm. Aspartate, homoserine and Sam were detected at similar abundances in the fungal mono- and dual species biofilms. Methionine, cystathionine and S-adenosyl-L-homocysteine were detected at a higher abundance in the *C. albicans* mono-species. O-acetyl-homoserine was detected at a higher abundance in the dual-species biofilm.

A common observation was the significantly lower abundance of L-cystathionine in the dual-species biofilm compared to both the fungal and

bacterial mono-species biofilms. As well as its role as an intermediate in the biosynthesis of methionine (Figs 6-21 & 6-23), it is also an intermediate in the conversion of methionine to cysteine, through the reverse transsulfuration pathway (Fig. 6-24) (Guédon & Martin-Verstraete, 1997).

#### **6.4.2.1.7 Cysteine and the reverse transsulfuration pathway**

Cysteine plays a crucial role in cellular physiology, and its biosynthesis is the primary pathway for sulphur incorporation into the cell (Guédon & Martin-Verstraete, 1997). As well as being a precursor for methionine, cysteine is also a precursor for thiamine, biotin, lipoic acid, CoA and co-enzyme M (CoM). It is involved in the biogenesis of [Fe-S] clusters, is found at the catalytic site of several enzymes and forms disulphide bonds in proteins, which aid in folding and assembly. As well as this, cysteine-derived proteins such as glutathione and thioredoxine help protect cells against oxidative stress.

There are two major cysteine biosynthetic pathways in microorganisms; - the thiolation pathway and the reverse transsulfuration pathway (Guédon & Martin-Verstraete, 1997). The thiolation pathway directly incorporates sulphide or thiosulfate into O-acetyl-serine, whereas in the transsulfuration pathway L-homocysteine is converted to cysteine with cystathionine as an intermediate.

Many microorganisms employ this pathway, including *B. subtilis*, *Klebsiella aerogenes*, *P. aeruginosa*, *M. tuberculosis* and *S. cerevisiae*, which enable them to utilise methionine as a sole sulphur source (Seiflein & Lawrence, 2001; Sekowska & Danchin, 1999; Thomas & Surdin-Kerjan, 1997; Vermeij & Kertesz, 1999; Wheeler et al., 2005). Methionine is converted to SAM, which in turn is converted to SAH during methylation reactions. SAH is then degraded to L-homocysteine either by SAH hydrolase or by SAH

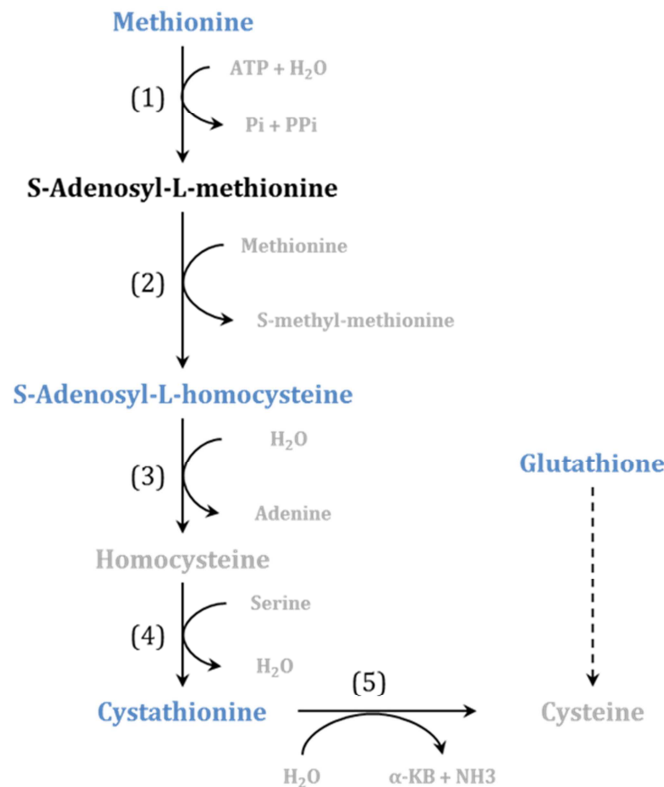
nucleosidase and an S-ribosyl-homocysteine in a two-part reaction (Guédon & Martin-Verstraete, 1997). L-homocysteine is then converted to cysteine through the reverse transsulfuration pathway. Cystathionine  $\beta$ -synthase catalyses the condensation reaction of L-homocysteine and serine to cystathionine, which in turn is converted to ammonia,  $\alpha$ -ketobutyrate and cysteine via another condensation reaction, this time catalysed by cystathionine  $\gamma$ -lyase (Guédon & Martin-Verstraete, 1997).

Glutathione is a cysteine containing tripeptide ( $\gamma$ -glu-cys-gly) which can be used as a sulphur source in many organisms. Glutathione can be taken up by the cell and broken down to cysteine, glycine and glutamate in sequential reactions catalysed by  $\gamma$ -glutamyltranspeptidase, aminopeptidases A, B, and N and dipeptide D (Suzuki, Hashimoto, & Kumagai, 1993; Suzuki, Kamatani, Kim, & Kumagai, 2001).

With the exception of cystathionine, none of the detectable metabolites within the reverse transsulfuration pathway were present in the *S. aureus* mono-species. This could suggest that the bacterial pools of these metabolites were depleted after 24 hours of growth in the media. It could also suggest that *S. aureus* lack the genes encoding the enzymes required for this pathway. Glutathione was also absent from the bacterial mono-species, again this could either suggest that the bacteria lack the enzymes for glutathione uptake and metabolism.

In stark contrast to these findings, all of the metabolites involved in the reverse transsulfuration pathway were detected in the *C. albicans* mono-species (Fig. 6-24). Glutathione was also detected in the fungal mono-species biofilm. Although all of these metabolites were detected in the dual-species biofilm, they were detected at lower abundances, suggesting that these pathways are down-regulated when *C. albicans* is cultured with *S. aureus*. It

could be argued that suppression of this pathway is indicative of antagonistic behaviour towards one (or both) of these microorganisms. Cystathionine  $\gamma$ -synthase inactivation could account for the lower abundance of cystathionine detected in the dual-species biofilm.



Where: (1) = methionine adenosyltransferase  
 (2) = methionine S-methyltransferase  
 (3) = adenosylhomocysteinase  
 (4) = cystathionine  $\beta$ -synthase  
 (5) = cystathionine  $\gamma$ -lyase  
 $\alpha\text{-KB}$  =  $\alpha$ -ketobutyrate

**Figure 6-24** Schematic diagram of the reverse transsulfuration pathway for the conversion of methionine to cysteine. Colour code: grey = undetected, red = higher abundance detected in dual-species biofilm, blue = higher abundance detected in *C. albicans*, black = similar abundance detected in both *C. albicans* and dual-species biofilms.

### 6.4.3 Conclusions

Overall, results from the LC-MS analysis were able to detect numerous differences between the *S. aureus* and *C. albicans* mono- and dual-species biofilms. The differences detected within individual pathways are suggestive of a difference in behaviour when the microorganisms are cultured with one another. The absence of a large portion of essential metabolites within purine, pyrimidine, cysteine and methionine pathways is indicative of the bacteria struggling to proliferate and form strong biofilms in sera. In agreement with the results obtained during biofilm characterisation, *C. albicans* facilitates *S. aureus* growth in sera. The LC-MS analysis has highlighted some of the pathways that could be examined in further detail to determine their role and importance in the formation of a healthy dual-species biofilm.

All of the pathways were down-regulated in the dual-species biofilm compared to the *C. albicans* mono-species biofilm. This could indicate that the presence of *S. aureus* within the biofilm is having an adverse effect on the *C. albicans*. This conclusion would corroborate some of the observations made during biofilm characterisation. Lower *C. albicans* cell numbers and the presence of 'crinkled' hyphae support the notion that *S. aureus* may behave antagonistically towards the fungi. This observation is in partial agreement with a study carried out by Peters et al. (2010), which documented the upregulation of proteins related to stress response in both *S. aureus* and *C. albicans* when the microorganisms were cultured with each other compared to when they were cultured in isolation (Peters et al., 2010b). However, further analysis would have to be carried out to confirm this hypothesis.

## **Chapter 7.      General discussion**

Microorganisms within their microenvironment do not exist in isolation, but rather within complex polymicrobial biofilm communities (Brogden et al., 2005). Within these communities' bacteria, fungi, parasites and/or viruses interact both directly and indirectly with one other. Cross-feeding, signalling and physical interactions influence behaviour, growth, virulence and survival of the organisms within these biofilms (De Sordi & Mühlischlegel, 2009; Anton Y Peleg et al., 2010). In recent years, increasing attention has been paid to the influence of polymicrobial interactions on antimicrobial resistance, virulence and disease outcomes, however relatively little is known about the subtle changes caused to the metabolic pathways.

*S. aureus* and *C. albicans* are human commensals that are found on the skin and in other areas around the body, including the GI and reproductive tracts (Achkar & Fries, 2010; Ganguly & Mitchell, 2011; Kennedy & Volz, 1985; Kumamoto, 2002, 2011; Wertheim et al., 2005). Often these microorganisms exist on/in the host without causing any harm. However, this prokaryote and eukaryote can exhibit pathogenicity towards healthy and immunocompromised individuals, causing a plethora of infections and disease that can often be very severe and/or life-threatening (Calderone & Fonzi, 2001; Rex et al., 2004; Wisplinghoff et al., 2004). In addition, *S. aureus* and *C. albicans* form polymicrobial biofilms that increase antimicrobial resistance and pathogenicity (Eunice Carlson, 1983; Eunice Carlson & Johnson, 1985a, 1985b; Dahlén et al., 2009; Ekwempu et al., 1981; Harriott & Noverr, 2009, 2010; S. a. Klotz et al., 2007; Siegman-Igra et al., 1988; A. J. Smith et al., 2003; Valenza et al., 2008).

Although *S. aureus* and *C. albicans* polymicrobial biofilms are of clinical importance, their interactions within their micro-environment are not well understood. Therefore, the overall aim of this research was to develop and apply novel metabolomics methods to the analysis of a dual species *S.*

*aureus*/*C. albicans* biofilm to provide further insight into the interaction between this bacteria and fungi.

We first carried out microscopic and molecular characterisation of the dual-species biofilm.

### **7.1 *S. aureus* and *C. albicans* biofilm characterisation**

A variety of macroscopic, microscopic and molecular techniques were utilised to investigate the interaction between *S. aureus* and *C. albicans*. Culture conditions were optimised.

The results obtained were mainly in agreement with other studies that have been carried out; *C. albicans* facilitates the growth of *S. aureus* in serum (a medium that doesn't support *S. aureus* biofilm development) and *S. aureus* preferentially adhere to the hyphal elements of the *C. albicans* (Harriott & Noverr, 2009, 2010; Jey et al., 2013; Peters et al., 2013). In addition, a significant increase in the number of *S. aureus* was recorded as well as a decrease in the number of *C. albicans*. Furthermore, an increase in the expression of two proteins involved in biofilm formation in *C. albicans* was observed. An interesting observation was the presence of 'crinkled' hyphae which could suggest that the relationship between the bacteria and fungi is not mutually synergistic as has previously been suggested, although Peters et al. (2010) did observe an increase in the expression of proteins related to stress response in both micro-organisms (Peters et al., 2010a).

Biofilm characterisation enabled optimisation of culture conditions, aided in biofilm visualisation and the determination of the spatial distribution within the biofilm, and offered an insight into the behaviour of *S. aureus* and *C. albicans*.

The limitations of this analysis included an inability to carry out successful RNA extraction of *S. aureus* MSCRAMM genes, the cell counts carried out using qPCR did not take into account whether the cells were viable or not and only the mature biofilm was analysed.

For the biofilm characterisation a more in-depth analysis should be carried out. Live/dead staining would enable the state of the microorganisms within the dual species biofilm to be determined. *S. aureus* RNA extractions were unsuccessful; therefore an optimised method to study gene expression in *S. aureus* would be beneficial. The biofilms that were analysed had been allowed to mature for 24 hours. Sequential microscopic and molecular studies characterising early, intermediate and late stage biofilms could lead to a deeper understanding of how the nature of the relationship between *S. aureus* and *C. albicans* progresses from initial attachment. Genes involved in biofilm formation were targeted during this study. It could be of benefit to investigate the regulation of other known virulence genes, and perhaps genes related to stress response in both organisms or toxin production in *S. aureus*.

## **7.2 Serially combined Reverse phase (RP)/Hydrophilic Interaction Liquid Chromatography (HILIC) method development**

A combined RPLC/HILIC method was then developed to allow the separation and detection of polar and nonpolar metabolites in one analytical run.

Overall the method worked well and the chromatographic system was able to separate polar and nonpolar standards and compounds within a complex sample. The RPLC/HILIC system presented reproducible results with low RSDs.

However, the system was unable to separate the isomers citrate and isocitrate in the standard mix and there were some difficulties regarding the back pressure of the system. This could have been due to a blockage in the tubing

or on the C<sub>18</sub> column. Other limitations surrounded optimisation of the method. Due to time constraints, instrument down-time and the cost of running the MS, the effects of MP composition on the selectivity, retention, efficiency and resolution of analytes were never investigated. The flow rates were optimised so that the correct dilution between the columns could be achieved, but alternative flow rates (that would still result in the correct dilution factor but that could possibly lead to improved resolution) were not considered.

### **7.3 Ion chromatography - mass spectrometry (IC-MS) method development for central carbon metabolism (CCM) analysis**

A targeted IC-MS was also developed for the analysis of intermediates involved in CCM.

Good separation of almost all of the glycolysis intermediates (with the exception of DHAP/G3P and 2-/3-PG) and TCA intermediates (with the exception of oxaloacetate) was achieved. The system exhibited great RT reproducibility and wide ranging LoD.

The IC system employed was unsuitable for the analysis of the co-enzymes, NADH or NADPH. The high OH<sup>-</sup> concentration in the eluent could be responsible for the breakdown of the co-enzymes on column; however this high hydroxide concentration is required for the elution of ADP and ATP. Altering the pH or column may hold the key to utilizing IC-MS to analyse these compounds, but unfortunately the instrument was removed from the laboratory before any alternative chromatographic conditions could be investigated.

Overall the IC results had significant impact on Thermo Scientific's marketing of capillary flow ICMS for metabolomics.

Although IC-MS was able to separate numerous CCM intermediates, due to the complexity of the samples' peak resolution was poor. Method development to improve peak separation could be carried out. The IC instrument utilised in this study had an integrated eluent generator. This was beneficial in relation to instrument maintenance and system set-up. However, it meant that only the hydroxide concentration of the eluent could be varied. Using a system which offers greater control over the MP composition could enable separation optimisation through manipulation of the MP components and additives.

Another option could be to use a more established targeted method that encompasses the pentose phosphate pathway as well as the other pathways targeted in this study. Although GC-MS involves a lot more sample preparation, it could provide wider coverage as well as better quantitation. Derivatisation before LC-MS analysis could also offer a powerful method for CCM analysis.

Analysing the biofilms from initial attachment over a time-course could provide a better understanding of central carbon metabolism in these microorganisms. Flux analysis could be carried out to follow the movement of metabolites through metabolic networks. Feeding *S. aureus* and *C. albicans* heavy labelled glucose would enable differences in the fate of glucose within each of the microorganisms to be determined. However, as both microorganisms metabolise glucose studying the dual species culture in this way may prove problematic as it will be impossible to distinguish which organism has utilised the glucose in which way.

Another possibility to improve this targeted analysis could be through the optimisation of a metabolite extraction method that targets energy metabolites such as organic acids and sugar-phosphates.

## 7.4 Metabolomics analysis of *S. aureus* and *C. albicans* mono- and dual-species biofilms

The developed IC-MS and RPLC/HILIC methods were then applied to the analysis of *S. aureus* and *C. albicans* dual-species biofilms.

The application of the IC-MS method was by the complexity of the microbial samples. The presence of sugar isomers resulted in poor resolution of peaks, making quantitation difficult. The absence of metabolites from the *S. aureus* mono-species culture also complicated comparisons as it was unclear whether this was as a result of metabolite concentration being below the limits of detection of the instrument or that they were absent as a result of the culture conditions. When *S. aureus* was removed from the comparison the metabolite concentrations between *C. albicans* and the co-culture were similar with the exception of fumarate and fructose 1,6-bisphosphate.

The RPLC/HILIC method also performed poorly when applied to the analysis of the biofilm samples. Poor peak shapes, lower number of metabolites detected and issues with column backpressure compared to the routine pHILIC method employed in the laboratory led to the utilisation of the routine pHILIC method in place of the serially combined method.

The untargeted metabolomics analysis uncovered numerous differences between the *S. aureus* and *C. albicans* mono- and dual-species cultures. From the data three pathways were chosen due to significant changes present between each of the cultures.

Overall, the results obtained from this study suggest that *S. aureus* is unable to metabolise components within sera for the biosynthesis of purine and pyrimidines that are essential for the formation of strong biofilms (Keer et al., 2001; D. Mack et al., 2004; Mongodin et al., 2003). Furthermore, many of the metabolites involved in methionine biosynthesis were detected in a higher

abundance in the *S. aureus* mono-species, with the exception of L-methionine and SAM. This could suggest that there is some sort of biochemical ‘block’ within this pathway which is affecting the production of these two key metabolites, which are required for the biosynthesis of macromolecules. Me-THF which plays key roles in both methionine and pyrimidine biosynthetic pathways could be linked to the impairment of both of these pathways in mono-culture, which could lead to the formation of weak biofilms observed when *S. aureus* is cultured in sera alone.

In contrast, the presence of the *S. aureus* resulted in the down-regulation of purine, pyrimidine and methionine biosynthetic pathways. This suggests that the presence of the bacteria may have a detrimental effect on *C. albicans* within the dual-species culture. Although the fungi support *S. aureus* growth and development, the bacteria could be secreting some kind of toxin directly onto the fungi or into the environment that causes damage to the fungi while allowing the bacteria to thrive.

From the results obtained during Chapter 3 and 6 it could be suggested that the presence of *C. albicans* within the dual-species culture either presents an opportunity for *S. aureus* to metabolise components directly from the surface of fungal hyphae, which could explain the presence of damaged hyphae in the co-culture, or *C. albicans* could be secreting a compound into the environment that *S. aureus* can metabolise.

The detection of proteins related to stress response by Peters et al. (2010) corroborates this theory and could suggest that the increased pathogenicity exhibited by *S. aureus* and *C. albicans* dual infections are in fact a consequence of competition between these two opportunistic pathogens rather than a mutualistic relationship leading to increased virulence (Peters et al., 2010c). Although the RPLC/HILIC was not robust enough for biofilm analysis, optimisation of the method could provide improved results. Van

Deemter plots could be used to determine optimum flow rates for each of the columns individually, which could then be adjusted to ensure the optimum dilution between both columns when they serially combined. Different MP compositions could also be examined, including the possible addition of buffers to one of the MPs. The back pressure of the system was unstable at times and often went beyond the limits of the pumps. This appeared to be an issue with the C<sub>18</sub> column. Different RPLC columns could be tested to ensure optimum column capacity and orthogonality. Another reason for the system going over pressure could be the presence of particulates within the samples. Either the use of filtration vials or filtration of the samples before injection in the LC could eliminate this issue.

The routine pHILIC method employed did detect numerous metabolites; however coverage of a lot of the pathways was not ideal. The lack of detected metabolites within pathways made data interpretation quite difficult and speculative. Optimisation of the serially combined method is one option to improve this. Another option is to carry out two optimised metabolite extractions; one for the polar metabolites and one for non-polar metabolites. These could then be run on a truly reverse phase system and HILIC system, respectively. The data could then be integrated and analysed. This would complicate sample preparation and data analysis but, through optimisation of each approach, coverage of the metabolome would increase which would ensure as many metabolites as possible were identified between the two separate chromatographic runs.

The biological interpretation highlighted a number of interesting differences between the mono- and dual-species cultures. It could be beneficial to investigate the importance of different pathways within each of the microorganisms. *S. aureus* could be cultured with mutant strains of *C. albicans* which exhibit deficiencies in different regulators of purine, pyrimidine, methionine or cysteine biosynthesis. Strains deficient in

regulators of the reverse-transsulfuration pathway could also provide an insight into the relationship between *S. aureus* and *C. albicans*. The results obtained as part of this study pointed to a possible link of THF and the inability of *S. aureus* to synthesis L-methionine and SAM. To investigate this further metabolomics analysis could be carried out on a mutant strain defective in THF biosynthesis grown in a biofilm promoting medium. The folate and THF biosynthetic pathways could be targeted in *C. albicans* to determine how it affects the dual-species biofilm.

## 7.5 Future work

The work presented herein has made progress towards our understanding of the inter-kingdom interactions of *S. aureus* and *C. albicans*. The results from this research have highlighted a number of studies that could be carried out to elucidate the intimate relationship between these two pathogenic microorganisms.

Gram positive bacteria often utilize small peptides as signalling molecules. Numerous dipeptides were putatively identified during this study (data not shown) but as many had the same mass they could not be distinguished from one another and could not be identified. Therefore peptidomics could be utilised in further studies in an effort to identify potential signalling molecules.

In relation to peptidomics, a multi-omics approach could be employed that encompasses proteomics, genomics and transcriptomics. This could provide a more complete picture of the interaction of *S. aureus* and *C. albicans*.

The extraction method utilised in the study of the dual-species biofilm did not distinguish between *S. aureus*, *C. albicans* and ECM. Method optimisation should be carried out prior to metabolomics to separate the bacteria from the fungi and both of these organisms from the ECM. Separating out the

organisms before analysis would enable changes within the individual organisms to be detected.

The work presented here only looked at one laboratory strain of *S. aureus* and *C. albicans*. A natural progression from the results obtained in this study would be to carry-out further analyses on clinical strains of *S. aureus* and *C. albicans*.

Finally, this study adopted a multi-omics approach. Unlike traditional studies that perhaps analyse a single organism using more than one omics approach, in this study multiple organisms were analysed using a single omics approach. The approach of analysing polymicrobial communities through analysing each component in isolation and then in the presence of the other provides greater insight into how the presence of one organism influences the other.

Historically microorganisms have been studied in isolation to gain an understanding of their behaviour. It is now widely accepted that a significant number of infections are the product of multi-species colonisation. The importance of the interaction between different microorganisms within a host is becoming more influential in clinical thinking and it is becoming increasingly important in our understanding of what constitutes a normal flora, the changes which lead to morbidity, the changes found as a result of morbidity and possible interventions to the dynamic interaction between the microorganisms found in those circumstances. It is apparent that the composition of different polymicrobial communities and the interactions between specific microbes present within these communities play a crucial role in disease severity and outcomes. Although progress has been made towards understanding how microorganisms within these communities interact, there is still a very long way to go in determining the species specific interactions through which clinically important microorganisms influence one

another. Metabolomics provides a methodology with which to directly probe how microbial interactions influence behaviour, virulence and host response.

Although metabolomics offers a way to directly measure the influence of one or more organisms on another, the incorporation of other omics techniques such as proteomics, genomics, peptidomics, lipidomics and transcriptomics would provide an explanation of these interactions on every molecular level. Investigating polymicrobial infections using a truly multi-omics technique would enable comprehensive understanding of the intricacies of these interactions. Uncovering specific interactions could highlight potential drug targets or enable clinicians to embark on novel therapeutic strategies, thus providing a platform with which to tackle the substantial threat posed by increasing antimicrobial resistance, virulence, mortality and morbidity exhibited by multi-species infections.

# Appendices

Please see attached files.

## References

- Achkar, J. M., & Fries, B. C. (2010). Candida infections of the genitourinary tract. *Clinical Microbiology Reviews*, 23(2), 253–273. <https://doi.org/10.1128/CMR.00076-09>
- Adam, B., Baillie, G. S., & Douglas, L. J. (2002). Mixed species biofilms of *Candida albicans* and *Staphylococcus epidermidis*, 51, 344–349.
- Ahadi, E., & Konermann, L. (2011). Ejection of solvated ions from electrosprayed methanol/water nanodroplets studied by molecular dynamics simulations. *Journal of the American Chemical Society*, 133(24), 9354–9363. <https://doi.org/10.1021/ja111492s>
- Al-Fattani, M. A., & Douglas, L. J. (2006). Biofilm matrix of *Candida albicans* and *Candida tropicalis*: Chemical composition and role in drug resistance. *Journal of Medical Microbiology*, 55(8), 999–1008. <https://doi.org/10.1099/jmm.0.46569-0>
- Alpert, A. . (1990). Hydrophilic-interaction chromatography for the separation of peptides, nucleic acids and other polar compounds. *Journal of Chromatography*, 499, 177–196.
- Alvarez-Segura, T., Ortiz-Bolsico, C., Torres-Lapasio, J. R., & Garcia-Alvarez-Coque, M. C. (2015). Serial versus parallel columns using isocratic elution: A comparison of multi-column approaches in mono-dimensional liquid chromatography. *Journal of Chromatography A*, 1390, 95–102. <https://doi.org/10.1016/j.chroma.2015.02.058>
- Anderson, J. B. (2005). Evolution of antifungal-drug resistance: mechanisms and pathogen fitness. *Nat.Rev.Microbiol.*, 3(1740–1526 (Print)), 547–556. <https://doi.org/10.1038/nrmicro1179>
- Andes, D. R., Safdar, N., Baddley, J. W., Playford, G., Reboli, A. C., Rex, J. H., ... Kullberg, B. J. (2012). Impact of treatment strategy on outcomes in patients with candidemia and other forms of invasive candidiasis: A patient-level quantitative review of randomized trials. *Clinical Infectious Diseases*, 54(8), 1110–1122. <https://doi.org/10.1093/cid/cis021>
- Arbeit, R. D., Karakawa, W. W., Vann, W. F., & Robbins, J. B. (1984). Predominance of two newly described capsular polysaccharide types among clinical isolates of *Staphylococcus aureus*. *Diagnostic Microbiology and Infectious Disease*, 2(2), 85–91. [https://doi.org/http://dx.doi.org/10.1016/0732-8893\(84\)90002-6](https://doi.org/http://dx.doi.org/10.1016/0732-8893(84)90002-6)
- Archer, N. K., Mazaitis, M. J., Costerton, J. W., Leid, J. G., Powers, M. E., & Shirtliff, M. E. (2011). *Staphylococcus aureus* biofilms: properties, regulation, and roles in human disease. *Virulence*, 2(5), 445–459. <https://doi.org/10.4161/viru.2.5.17724>
- Baena-Monroy, T., Moreno-Maldonado, V., Franco-Martínez, F., Aldape-Barrios, B., Quindós, G., & Sánchez-Vargas, L. O. (2005). *Candida albicans*, *Staphylococcus aureus* and *Streptococcus mutans* colonization in patients wearing dental prosthesis. *Medicina Oral, Patología Oral Y Cirugía Bucal*. <https://doi.org/10488958> [pii]
- Bailey, S. W., & Ayling, J. E. (2013). Differential coulometric oxidation following post column-switching high pressure liquid chromatography for fluorescence measurement of unmetabolized folic acid in human plasma. *Journal of Chromatography A*, 1315,

86–91. <https://doi.org/10.1016/j.chroma.2013.09.027>

- Bajad, S. U., Lu, W., Kimball, E. H., Yuan, J., Peterson, C., & Rabinowitz, J. D. (2006). Separation and quantitation of water soluble cellular metabolites by hydrophilic interaction chromatography-tandem mass spectrometry. *Journal of Chromatography A*, *1125*(1), 76–88. <https://doi.org/10.1016/j.chroma.2006.05.019>
- Balhadere, P. V, Foster, A. J., & Talbot, N. J. (1999). Identification of pathogenicity mutants of the rice blast fungus *Magnaporthe grisea* by insertional mutagenesis. *Mol. Plant Microbe Interact.*, *12*(2), 129–142. <https://doi.org/10.1094/MPMI.1999.12.2.129>
- Bamford, C. V, d’Mello, A., Nobbs, A. H., Dutton, L. C., Vickerman, M. M., & Jenkinson, H. F. (2009). *Streptococcus gordonii* modulates *Candida albicans* biofilm formation through intergeneric communication. *Infection and Immunity*, *77*(9), 3696–704. <https://doi.org/10.1128/IAI.00438-09>
- Banerjee, D., Burkard, L., & Panepinto, J. C. (2014). Inhibition of nucleotide biosynthesis potentiates the antifungal activity of Amphotericin B. *PLoS ONE*, *9*(1), 1–12. <https://doi.org/10.1371/journal.pone.0087246>
- Bassanese, D. N., Holland, B. J., Conlan, X. A., Francis, P. S., Barnett, N. W., & Stevenson, P. G. (2015). Protocols for finding the most orthogonal dimensions for two-dimensional high performance liquid chromatography. *Talanta*, *134*(May), 402–408. <https://doi.org/10.1016/j.talanta.2014.11.037>
- Beelders, T., Kalili, K. M., Joubert, E., De Beer, D., & De Villiers, A. (2012). Comprehensive two-dimensional liquid chromatographic analysis of rooibos (*Aspalathus linearis*) phenolics. *Journal of Separation Science*, *35*(14), 1808–1820. <https://doi.org/10.1002/jssc.201200060>
- Benedict, C. R., & Risk, M. (1984). Determination of urinary and plasma dihydroxyphenylalanine by coupled-column high-performance liquid chromatography with C8 and C18 stationary phases. *Journal of Chromatography*, *317*, 27–34.
- Bennett, B., Kimball, E., & Gao, M. (2009). Absolute metabolite concentrations and implied enzyme active site occupancy in *Escherichia coli*. *Nature Chemical ...*, *5*(8), 593–599. <https://doi.org/10.1038/nchembio.186.Absolute>
- Bertesteanu, S., Triaridis, S., Stankovic, M., Lazar, V., Chifiriuc, M. C., Vlad, M., ... Grigore, R. (2014). Polymicrobial wound infections: Pathophysiology and current therapeutic approaches. *International Journal of Pharmaceutics*, *463*(2), 119–126. <https://doi.org/10.1016/j.ijpharm.2013.12.012>
- Bhattacharya, M., Fuhrman, L., Ingram, A., Nickerson, K. W., & Conway, T. (1995). Single-run separation and detection of multiple metabolic intermediates by anion-exchange high-performance liquid chromatography and application to cell pool extracts prepared from *Escherichia coli*. *Analytical Biochemistry*, *232*(1), 98–106. <https://doi.org/10.1006/abio.1995.9954>
- Biba, M., Jiang, E., Mao, B., Zewge, D., Foley, J. P., & Welch, C. J. (2013). Factors influencing the separation of oligonucleotides using reversed-phase/ion-exchange mixed-mode high performance liquid chromatography columns. *Journal of*

*Chromatography A*, 1304, 69–77. <https://doi.org/10.1016/j.chroma.2013.06.050>

- Bien, J., Sokolova, O., & Bozko, P. (2011). Characterization of Virulence Factors of *Staphylococcus aureus*: Novel Function of Known Virulence Factors That Are Implicated in Activation of Airway Epithelial Proinflammatory Response. *Journal of Pathogens*, 2011, 1–13. <https://doi.org/10.4061/2011/601905>
- Bischoff, K., Szuvecs, Z., & Nyiredy, S. (2010). Elements for separating substances by distributing between a stationary and mobile phase, and method for production of a separating device, (19).
- Bischoff, R., & McLaughlin, L. W. (1984). Nucleic acid resolution by mixed-mode chromatography. *Journal of Chromatography A*, 296(C), 329–337. [https://doi.org/10.1016/S0021-9673\(01\)96427-1](https://doi.org/10.1016/S0021-9673(01)96427-1)
- Blau, K., & Halket, J. M. (1993). *Handbook of Derivatives for Chromatography*. (K. Blau & J. M. Halket, Eds.) (2nd ed.). Chichester, U.K: John Wiley & Sons Ltd.
- Blow, N. (2008). Biochemistry 's new look. *Nature*, 455(October), 697–700. <https://doi.org/10.1038/455697a>
- Bolten, C. J., Kiefer, P., Letisse, F., Portais, J.-C., & Wittmann, C. (2007). Sampling for metabolome analysis of microorganisms. *Analytical Chemistry*, 79(10), 3843–9. <https://doi.org/10.1021/ac0623888>
- Bongaerts, J., Krämer, M., Müller, U., Raeven, L., & Wubbolts, M. (2001). Metabolic engineering for microbial production of aromatic amino acids and derived compounds. *Metabolic Engineering*, 3(4), 289–300. <https://doi.org/10.1006/mben.2001.0196>
- Bonn, G. (1985). High-performance liquid chromatographic elution behaviour of oligosaccharides, monosaccharides and sugar degradation products on series-connected ion-exchange resin columns using water as the mobile phase. *Journal of Chromatography A*, 322(C), 411–424. [https://doi.org/10.1016/S0021-9673\(01\)97707-6](https://doi.org/10.1016/S0021-9673(01)97707-6)
- Boyd, G. E., Adamson, A. W., & Myers, L. S. (1947). The Exchange Adsorption of Ions from Aqueous Solutions by Organic Zeolites. II. Kinetics 1. *Journal of the American Chemical Society*, 69(11), 2836–2848. <https://doi.org/10.1021/ja01203a066>
- Brabcova, I., Hlavackova, M., Satinsky, D., & Solich, P. (2013). A rapid HPLC column switching method for sample preparation and determination of  $\beta$ -carotene in food supplements. *Food Chemistry*, 141(2), 1433–1437. <https://doi.org/10.1016/j.foodchem.2013.04.063>
- Brogden, K. A., Guthmiller, J. M., & Taylor, C. E. (2005). Human polymicrobial infections. *Lancet*, 365(9455), 253–255. [https://doi.org/10.1016/S0140-6736\(05\)17745-9](https://doi.org/10.1016/S0140-6736(05)17745-9)
- Buescher, J. M., Moco, S., Sauer, U., & Zamboni, N. (2010). Ultrahigh performance liquid chromatography-tandem mass spectrometry method for fast and robust quantification of anionic and aromatic metabolites. *Analytical Chemistry*, 82(11), 4403–4412. <https://doi.org/10.1021/ac100101d>

- Buffo, J., Herman, M. a, & Soll, D. R. (1984). A characterization of pH-regulated dimorphism in *Candida albicans*. *Mycopathologia*, 85(1–2), 21–30. <https://doi.org/10.1007/BF00436698>
- Büscher, J. M., Czernik, D., Ewald, J. C., Sauer, U., & Zamboni, N. (2009). Cross-platform comparison of methods for quantitative metabolomics of primary metabolism. *Analytical Chemistry*, 81(6), 2135–2143. <https://doi.org/10.1021/ac8022857>
- Cacciola, F., Delmonte, P., Jaworska, K., Dugo, P., Mondello, L., & Rader, J. I. (2011). Employing ultra high pressure liquid chromatography as the second dimension in a comprehensive two-dimensional system for analysis of *Stevia rebaudiana* extracts. *Journal of Chromatography A*, 1218(15), 2012–2018. <https://doi.org/10.1016/j.chroma.2010.08.081>
- Cacciola, F., Donato, P., Giuffrida, D., Torre, G., Dugo, P., & Mondello, L. (2012). Ultra high pressure in the second dimension of a comprehensive two-dimensional liquid chromatographic system for carotenoid separation in red chili peppers. *Journal of Chromatography A*, 1255, 244–251. <https://doi.org/10.1016/j.chroma.2012.06.076>
- Cakir, T., Patil, K. R., Onsan, Z. iIsen, Ulgen, K. O., Kirdar, B., & Nielsen, J. (2006). Integration of metabolome data with metabolic networks reveals reporter reactions. *Molecular Systems Biology*, 2, 50. <https://doi.org/10.1038/msb4100085>
- Calderone, R., & Fonzi, W. (2001). Virulence factors of *Candida albicans*. *Trends in Microbiology*, 9(7), 327–35. [https://doi.org/10.1016/S0966-842X\(01\)02094-7](https://doi.org/10.1016/S0966-842X(01)02094-7)
- Camenzuli, M., & Schoenmakers, P. J. (2014). A new measure of orthogonality for multi-dimensional chromatography. *Analytica Chimica Acta*, 838, 93–101. <https://doi.org/10.1016/j.aca.2014.05.048>
- Canelas, A. B., Ras, C., ten Pierick, A., van Gulik, W. M., & Heijnen, J. J. (2011). An in vivo data-driven framework for classification and quantification of enzyme kinetics and determination of apparent thermodynamic data. *Metabolic Engineering*, 13(3), 294–306. <https://doi.org/10.1016/j.ymben.2011.02.005>
- Carlson, E. (1982). Synergistic effect of *Candida albicans* and *Staphylococcus aureus* on mouse mortality. *Infection and Immunity*, 38(3), 921–924.
- Carlson, E. (1983). Effect of Strain of *Staphylococcus aureus* on Synergism with *Candida albicans* Resulting in Mouse Mortality and Morbidity. *Infection and Immunity*, 42(1), 285–292.
- Carlson, E., & Johnson, G. (1985a). Protection by *Candida albicans* of *Staphylococcus aureus* in the Establishment of Dual Infection in Mice, 50(3).
- Carlson, E., & Johnson, G. (1985b). *Staphylococcus aureus* in the establishment of Protection by *Candida albicans* of *Staphylococcus aureus* in the Establishment of Dual Infection in Mice, 50(3), 655–659.
- Cauda, R. (2009). *Candidaemia* in patients with an inserted medical device. *Drugs*, 69 Suppl 1(0012–6667 (Print)), 33–38. <https://doi.org/10.2165/11315520-000000000-00000>

- Chaffin, D. O., Taylor, D., Skerrett, S. J., & Rubens, C. E. (2012). Changes in the *Staphylococcus aureus* transcriptome during early adaptation to the lung. *PLoS ONE*, *7*(8). <https://doi.org/10.1371/journal.pone.0041329>
- Chalcraft, K. R., & McCarry, B. E. (2013). Tandem LC columns for the simultaneous retention of polar and nonpolar molecules in comprehensive metabolomics analysis. *Journal of Separation Science*, *36*(21–22), 3478–3485. <https://doi.org/10.1002/jssc.201300779>
- Chandra, J., Kuhn, D. M., Mukherjee, P. K., Hoyer, L. L., McCormick, T., Ghannoum, M. A., ... Mitchell, J. S. F. and A. P. (2001). Genetic Control of *Candida Albicans* Biofilm Development. *National Review of Microbiology*, *9*(18), 109–118. <https://doi.org/10.1128/JB.183.18.5385>
- Chassagnole, C., Noisommit-Rizzi, N., Schmid, J. W., Mauch, K., & Reuss, M. (2002). Dynamic modeling of the central carbon metabolism of *Escherichia coli*. *Biotechnology and Bioengineering*, *79*(1), 53–73. <https://doi.org/10.1002/bit.10288>
- Chavakis, T., Wiechmann, K., Preissner, K. T., & Herrmann, M. (2005). *Staphylococcus aureus* interactions with the endothelium. The role of bacterial “Secretable Expanded Repertoire Adhesive Molecules” (SERAM) in disturbing host defense systems. *Thrombosis and Haemostasis*, *95*(4), 715–9. <https://doi.org/10.1160/TH05-05-0306>
- Chen, J., Zhao, X., Fritsche, J., Yin, P., Schmitt-Kopplin, P., Wang, W., ... Xu, G. (2008). Practical approach for the identification and isomer elucidation of biomarkers detected in a metabolomic study for the discovery of individuals at risk for diabetes by integrating the chromatographic and mass spectrometric information. *Analytical Chemistry*, *80*(4), 1280–1289. <https://doi.org/10.1021/ac702089h>
- Chen, X., & Li, X. (2013). Extracorporeal shock wave therapy could be a potential adjuvant treatment for orthopaedic implant-associated infections. *Journal of Medical Hypotheses and Ideas*, *7*(2), 54–58. <https://doi.org/10.1016/j.jmhi.2013.03.002>
- Cipollina, C., ten Pierick, A., Canelas, A. B., Seifar, R. M., van Maris, A. J. A., van Dam, J. C., & Heijnen, J. J. (2009). A comprehensive method for the quantification of the non-oxidative pentose phosphate pathway intermediates in *Saccharomyces cerevisiae* by GC-IDMS. *Journal of Chromatography B: Analytical Technologies in the Biomedical and Life Sciences*, *877*(27), 3231–3236. <https://doi.org/10.1016/j.jchromb.2009.07.019>
- Clarke, S. R., & Foster, S. J. (2006). *Surface Adhesins of Staphylococcus aureus*. *Advances in Microbial Physiology* (Vol. 51). [https://doi.org/10.1016/S0065-2911\(06\)51004-5](https://doi.org/10.1016/S0065-2911(06)51004-5)
- Contrepolis, K., Jiang, L., & Snyder, M. (2015). Optimized Analytical Procedures for the Untargeted Metabolomic Profiling of Human Urine and Plasma by Combining Hydrophilic Interaction (HILIC) and Reverse-Phase Liquid Chromatography (RPLC)–Mass Spectrometry. *Molecular & Cellular Proteomics*, *14*(6), 1684–1695. <https://doi.org/10.1074/mcp.M114.046508>
- Cornely, O. A., Bassetti, M., Calandra, T., Garbino, J., Kullberg, B. J., Lortholary, O., ... Ullmann, A. J. (2012). ESCMID guideline for the diagnosis and management of *Candida* diseases 2012: Non-neutropenic adult patients. *Clinical Microbiology and Infection*, *18*(SUPPL.7), 19–37. <https://doi.org/10.1111/1469-0691.12039>

- Costerton, J. W., Lewandowski, Z., Caldwell, D. E., Korber, D. R., & LappinScott, H. M. (1995). Microbial Biofilms. *Microbial Biofilms.*, 49, 711–745. <https://doi.org/10.1146/annurev.micro.49.1.711>
- Cowen, L. E. (2008). The evolution of fungal drug resistance: modulating the trajectory from genotype to phenotype. *Nat.Rev.Microbiol.*, 6(1740–1534 (Electronic)), 187–198. <https://doi.org/10.1038/nrmicro1835>
- Creek, D. J., Jankevics, A., Breitling, R., Watson, D. G., Barrett, M. P., & Burgess, K. E. V. (2011). Toward global metabolomics analysis with hydrophilic interaction liquid chromatography-mass spectrometry: Improved metabolite identification by retention time prediction. *Analytical Chemistry*, 83(22), 8703–8710. <https://doi.org/10.1021/ac2021823>
- Creek, D. J., Jankevics, A., Burgess, K. E. V., Breitling, R., & Barrett, M. P. (2012). IDEOM: an Excel interface for analysis of LC-MS-based metabolomics data. *Bioinformatics*, 28(7), 1048–1049. <https://doi.org/10.1093/bioinformatics/bts069>
- Cugini, C., Kolter, R., & Hogan, D. A. (2008). Interdomain Cross Talk. In *Chemical Communication among Bacteria* (pp. 419–429). American Society of Microbiology. Retrieved from <http://www.asmscience.org/content/book/10.1128/9781555815578.ch26>
- Cunningham, M. W. (2000). Pathogenesis of group A streptococcal infections. *Clinical Microbiology Reviews*, 13(3), 470–511. <https://doi.org/10.1128/CMR.13.3.470-511.2000>
- Dahlén, G., Blomquist, S., & Carlén, A. (2009). A retrospective study on the microbiology in patients with oral complaints and oral mucosal lesions. *Oral Diseases*, 15(4), 265–272. <https://doi.org/10.1111/j.1601-0825.2009.01520.x>
- de Gontijo, F. A., Pascon, R. C., Fernandes, L., Machado, J., Alspaugh, J. A., & Vallim, M. A. (2014). The role of the de novo pyrimidine biosynthetic pathway in *Cryptococcus neoformans* high temperature growth and virulence. *Fungal Genetics and Biology*, 70, 12–23. <https://doi.org/10.1016/j.fgb.2014.06.003>
- de Hoffmann, E., & Stroobant, V. (2002). Mass analysers. In *Mass spectrometry: Principles and Applications* (2nd ed., pp. 63–132). West Sussex, UK: John Wiley & Sons Ltd.
- De Sordi, L., & Mühlshlegel, F. A. (2009). Quorum sensing and fungal-bacterial interactions in *Candida albicans*: A communicative network regulating microbial coexistence and virulence. *FEMS Yeast Research*, 9(7), 990–999. <https://doi.org/10.1111/j.1567-1364.2009.00573.x>
- Dell'Aversano, C., Hess, P., & Quilliam, M. a. (2005). Hydrophilic interaction liquid chromatography-mass spectrometry for the analysis of paralytic shellfish poisoning (PSP) toxins. *Journal of Chromatography A*, 1081(2), 190–201. <https://doi.org/10.1016/j.chroma.2005.05.056>
- Dettmer, K., Aronov, P. A., & Hammock, B. D. (2007). Mass spectrometry-based metabolomics. *Mass Spectrometry Reviews*, 26, 51–78. <https://doi.org/DOI.10.1002/mas.20108>

- Dinges, M. M., Orwin, P. M., & Schlievert, P. M. (2000). Exotoxins of *Staphylococcus aureus*. *Clinical Microbiology Reviews*, *13*(1), 16–34. <https://doi.org/10.1128/CMR.13.1.16-34.2000>
- Dole, M., Mack, L. ., & Hines, R. . (1968). Molecular Beams of Macroions. *The Journal of Chemical Physics*, *49*, 2240. <https://doi.org/http://dx.doi.org/10.1063/1.1670391>
- Dongari-Bagtzoglou, A., Kashleva, H., Dwivedi, P., Diaz, P., & Vasilakos, J. (2009). Characterization of mucosal *Candida albicans* biofilms. *PLoS ONE*, *4*(11). <https://doi.org/10.1371/journal.pone.0007967>
- Donlan, R. M. (2002). Biofilms: microbial life on surfaces. *Emerging Infectious Diseases*, *8*(9), 881–90. <https://doi.org/10.3201/eid0809.020063>
- Douglas, L. J. (2003). *Candida* biofilms and their role in infection. *Trends in Microbiology*, *11*(1), 30–36. [https://doi.org/10.1016/S0966-842X\(02\)00002-1](https://doi.org/10.1016/S0966-842X(02)00002-1)
- Duerden, B. I. (1994). Virulence factors in anaerobes. *Clinical Infectious Diseases*, *18*, S253–S259. [https://doi.org/10.1093/clinids/18.Supplement\\_4.S253](https://doi.org/10.1093/clinids/18.Supplement_4.S253)
- Edelmann, M. J. (2011). Strong cation exchange chromatography in analysis of posttranslational modifications: innovations and perspectives. *Journal of Biomedicine & Biotechnology*, *2011*, 936508. <https://doi.org/10.1155/2011/936508>
- Edwards, J. E. (2012). Fungal cell wall vaccines: An update. *Journal of Medical Microbiology*, *61*(PART7), 895–903. <https://doi.org/10.1099/jmm.0.041665-0>
- Ekwempu, C. C., Lawande, R. V., & Egler, L. J. (1981). Microbial flora of the lower genital tract of women in labour in Zaria, Nigeria. *J Clin Pathol*, *34*(1), 82–83.
- El Rassi, Z., & Horváth, C. (1986). Tandem columns and mixed-bed columns in high-performance liquid chromatography of proteins. *Journal of Chromatography A*, *359*(C), 255–264. [https://doi.org/10.1016/0021-9673\(86\)80079-6](https://doi.org/10.1016/0021-9673(86)80079-6)
- Enjalbert, B., Letisse, F., & Portais, J.-C. (2013). Physiological and Molecular Timing of the Glucose to Acetate Transition in *Escherichia coli*. *Metabolites*, *3*(3), 820–837. <https://doi.org/10.3390/metabo3030820>
- Falasca, S., Petruzzello, F., Kretz, R., Rainer, G., & Zhang, X. (2012). Analysis of multiple quaternary ammonium compounds in the brain using tandem capillary column separation and high resolution mass spectrometric detection. *Journal of Chromatography A*, *1241*, 46–51. <https://doi.org/10.1016/j.chroma.2012.04.002>
- Farag, M. A., Porzel, A., Schmidt, J., & Wessjohann, L. A. (2012). Metabolite profiling and fingerprinting of commercial cultivars of *Humulus lupulus* L. (hop): A comparison of MS and NMR methods in metabolomics. *Metabolomics*, *8*(3), 492–507. <https://doi.org/10.1007/s11306-011-0335-y>
- Fekete, S., Veuthey, J. L., & Guillarme, D. (2015). Comparison of the most recent chromatographic approaches applied for fast and high resolution separations: Theory and practice. *Journal of Chromatography A*, *1408*, 1–14. <https://doi.org/10.1016/j.chroma.2015.07.014>
- Fernández-Ramos, C., Šatínský, D., & Solich, P. (2014). New method for the

determination of carbamate and pyrethroid insecticides in water samples using on-line SPE fused core column chromatography. *Talanta*, *129*, 579–585.  
<https://doi.org/10.1016/j.talanta.2014.06.037>

- Fiehn, O. (2002). Metabolomics - the link between genotypes and phenotypes. *Plant Molecular Biology*, *48*, 155–171.
- Fiehn, O., Kopka, J., Dörmann, P., Altmann, T., Trethewey, R. N., & Willmitzer, L. (2000). Metabolite profiling for plant functional genomics. *Nature Biotechnology*, *18*(11), 1157–1161. <https://doi.org/10.1038/81137>
- Fiehn, O., Kopka, J., Trethewey, R. N., & Willmitzer, L. (2000). Identification of uncommon plant metabolites based on calculation of elemental compositions using gas chromatography and quadrupole mass spectrometry. *Analytical Chemistry*, *72*(15), 3573–3580. <https://doi.org/10.1021/ac991142i>
- Flemming, H.-C., & Wingender, J. (2010). The biofilm matrix. *Nature Reviews Microbiology*, *19*(2), 139–150. <https://doi.org/10.1038/nrmicro2415>
- Fontanals, N., Marcé, R. M., Borrull, F., & Cormack, P. A. G. (2010). Mixed-mode ion-exchange polymeric sorbents: dual-phase materials that improve selectivity and capacity. *TrAC - Trends in Analytical Chemistry*, *29*(7), 765–779. <https://doi.org/10.1016/j.trac.2010.03.015>
- Forcisi, S., Moritz, F., Kanawati, B., Tziotis, D., Lehmann, R., & Schmitt-Kopplin, P. (2013). Liquid chromatography-mass spectrometry in metabolomics research: Mass analyzers in ultra high pressure liquid chromatography coupling. *Journal of Chromatography A*, *1292*, 51–65. <https://doi.org/10.1016/j.chroma.2013.04.017>
- Foster, T. J. (2005). Immune evasion by staphylococci. *Nature Reviews Microbiology*, *3*(12), 948–958. <https://doi.org/10.1038/nrmicro1289>
- Foster, T. J., & Höök, M. (1998). Surface protein adhesins of *Staphylococcus aureus*. *Trends in Microbiology*, *6*(12), 484–488. [https://doi.org/10.1016/S0966-842X\(98\)01400-0](https://doi.org/10.1016/S0966-842X(98)01400-0)
- François, I., Sandra, K., & Sandra, P. (2009). Comprehensive liquid chromatography: Fundamental aspects and practical considerations-A review. *Analytica Chimica Acta*, *641*(1–2), 14–31. <https://doi.org/10.1016/j.aca.2009.03.041>
- Fu, J., Wu, J., Jiang, J., Wang, Z., & Ma, Z. (2013). Cystathionine gamma-synthase is essential for methionine biosynthesis in *Fusarium graminearum*. *Fungal Biology*, *117*(1), 13–21. <https://doi.org/10.1016/j.funbio.2012.11.001>
- Fugère, A., Séguin, D. L., Mitchell, G., Déziel, E., Dekimpe, V., Cantin, A. M., ... Malouin, F. (2014). Interspecific small molecule interactions between clinical isolates of *Pseudomonas aeruginosa* and *Staphylococcus aureus* from adult cystic fibrosis patients. *PLoS ONE*, *9*(1). <https://doi.org/10.1371/journal.pone.0086705>
- Gabriela Bowden, M., Visai, L., Longshaw, C. M., Holland, K. T., Speziale, P., & Höök, M. (2002). Is the GehD lipase from *Staphylococcus epidermidis* a collagen binding adhesin? *Journal of Biological Chemistry*, *277*(45), 43017–43023. <https://doi.org/10.1074/jbc.M207921200>

- Ganguly, S., & Mitchell, A. P. (2011). Mucosal biofilms of *Candida albicans*. *Current Opinion in Microbiology*, 14(4), 380–385. <https://doi.org/10.1016/j.mib.2011.06.001>
- García-Cañaveras, J. C., López, S., Castell, J. V., Donato, M. T., & Lahoz, A. (2016). Extending metabolome coverage for untargeted metabolite profiling of adherent cultured hepatic cells. *Analytical and Bioanalytical Chemistry*, 408(4), 1217–1230. <https://doi.org/10.1007/s00216-015-9227-8>
- García, M. C., Hogenboom, A. C., Zappey, H., & Irth, H. (2002). Effect of the mobile phase composition on the separation and detection of intact proteins by reversed-phase liquid chromatography–electrospray mass spectrometry. *Journal of Chromatography A*, 957(2), 187–199. [https://doi.org/10.1016/S0021-9673\(02\)00345-X](https://doi.org/10.1016/S0021-9673(02)00345-X)
- Gaskell, S. J. (1997). Electrospray : Principles and Practice, 32(April), 677–688.
- Ge, X., Kitten, T., Chen, Z., Lee, S. P., Munro, C. L., & Xu, P. (2008). Identification of *Streptococcus sanguinis* genes required for biofilm formation and examination of their role in endocarditis virulence. *Infection and Immunity*, 76(6), 2551–2559. <https://doi.org/10.1128/IAI.00338-08>
- Gheorghe, A., van Nuijs, A., Pecceu, B., Bervoets, L., Jorens, P. G., Blust, R., ... Covaci, A. (2008). Analysis of cocaine and its principal metabolites in waste and surface water using solid-phase extraction and liquid chromatography-ion trap tandem mass spectrometry. *Analytical and Bioanalytical Chemistry*, 391(4), 1309–19. <https://doi.org/10.1007/s00216-007-1754-5>
- Gibson, J., Sood, A., & Hogan, D. A. (2009). *Pseudomonas aeruginosa*-*Candida albicans* interactions: Localization and fungal toxicity of a phenazine derivative. *Applied and Environmental Microbiology*, 75(2), 504–513. <https://doi.org/10.1128/AEM.01037-08>
- Glajch, J. ., Gluckman, J. ., Charikofsky, J. ., Minor, J. ., & Kirkland, J. . (1985). Simultaneous selectivity optimization of mobile and stationary phases in reversed-phased liquid chromatography for isocratic separations of phenylthiohydantoin amino acid derivatives. *Journal of Chromatography A*, 318(March 1982), 23–39. [https://doi.org/10.1016/S0021-9673\(01\)90661-2](https://doi.org/10.1016/S0021-9673(01)90661-2)
- Gloaguen, Y., Morton, F., Daly, R., Gurden, R., Rogers, S., Wandy, J., ... Burgess, K. (2017). PiMP my metabolome: An integrated, webbased tool for LC-MS metabolomics data. *Bioinformatics*. Retrieved from <https://academic.oup.com/bioinformatics/article/doi/10.1093/bioinformatics/btx499/4082268/PiMP-my-metabolome-An-integrated-web-based-tool>
- Götz, F. (2002). *Staphylococcus* and biofilms. *Molecular Microbiology*, 43(6), 1367–1378. <https://doi.org/10.1046/j.1365-2958.2002.02827.x>
- Greco, G., Grosse, S., & Letzel, T. (2013). Serial coupling of reversed-phase and zwitterionic hydrophilic interaction LC/MS for the analysis of polar and nonpolar phenols in wine. *Journal of Separation Science*, 36(8), 1379–88. <https://doi.org/10.1002/jssc.201200920>
- Gross, M., Cramton, S. E., Götz, F., & Peschel, A. (2001). Key Role of Teichoic Acid Net Charge in *Staphylococcus aureus* Colonization of Artificial Surfaces Key Role of

Teichoic Acid Net Charge in *Staphylococcus aureus* Colonization of Artificial Surfaces. *Infection and Immunity*, 69(5), 3423–2426.  
<https://doi.org/10.1128/IAI.69.5.3423>

- Groussac, E., Ortiz, M., & Francois, J. (2000). Improved protocols for quantitative determination of metabolites from biological samples using high performance ionic-exchange chromatography with conductimetric and pulsed amperometric detection. *Enzyme and Microbial Technology*, 26(9–10), 715–723. Retrieved from <http://cat.inist.fr/?aModele=afficheN&cpsid=1450532>
- Guédon, E., & Martin-Verstraete, I. (1997). Cysteine Metabolism and Its Regulation in Bacteria. In *Amino Acid Biosynthesis ~ Pathways, Regulation and Metabolic Engineering* (Vol. 43, pp. 195–218). Berlin, Heidelberg: Springer Berlin Heidelberg.  
[https://doi.org/10.1007/7171\\_2006\\_060](https://doi.org/10.1007/7171_2006_060)
- Guiochon, G., Marchetti, N., Mriziq, K., & Shalliker, R. A. (2008). Implementations of two-dimensional liquid chromatography. *Journal of Chromatography A*, 1189(1–2), 109–168. <https://doi.org/10.1016/j.chroma.2008.01.086>
- Guo, Y., & Gaiki, S. (2005). Retention behavior of small polar compounds on polar stationary phases in hydrophilic interaction chromatography. *Journal of Chromatography A*, 1074(1–2), 71–80. <https://doi.org/10.1016/j.chroma.2005.03.058>
- Haddad, P. R., Nesterenko, P. N., & Buchberger, W. (2008). Recent developments and emerging directions in ion chromatography. *Journal of Chromatography A*, 1184(1–2), 456–473. <https://doi.org/10.1016/j.chroma.2007.10.022>
- Haggarty, J., & Burgess, K. E. (2017). Recent advances in liquid and gas chromatography methodology for extending coverage of the metabolome. *Current Opinion in Biotechnology*, 43, 77–85. <https://doi.org/10.1016/j.copbio.2016.09.006>
- Haggarty, J., Oppermann, M., Dalby, M. J., Burchmore, R. J., Cook, K., Weidt, S., & Burgess, K. E. V. (2015). Serially coupling hydrophobic interaction and reversed-phase chromatography with simultaneous gradients provides greater coverage of the metabolome. *Metabolomics*, 1465–1470. <https://doi.org/10.1007/s11306-014-0770-7>
- Hall-Stoodley, L., Costerton, J. W., & Stoodley, P. (2004). Bacterial biofilms: from the Natural environment to infectious diseases. *Nature Reviews Microbiology*, 2(2), 95–108. <https://doi.org/10.1038/nrmicro821>
- Hammel, M., Nemecek, D., Keightley, J. A., Thomas, G. J., & Geisbrecht, B. V. (2007). The *Staphylococcus aureus* extracellular adherence protein (Eap) adopts an elongated but structured conformation in solution. *Protein Science : A Publication of the Protein Society*, 16(12), 2605–17. <https://doi.org/10.1110/ps.073170807>
- Hammond, A., Dertien, J., Colmer-Hamood, J. A., Griswold, J. A., & Hamood, A. N. (2010). Serum Inhibits *P. aeruginosa* Biofilm Formation on Plastic Surfaces and Intravenous Catheters. *Journal of Surgical Research*, 159(2), 735–746.  
<https://doi.org/10.1016/j.jss.2008.09.003>
- Han, T. li, Cannon, R. D., & Villas-Bôas, S. G. (2012). Metabolome analysis during the morphological transition of *Candida albicans*. *Metabolomics*, 8(6), 1204–1217.  
<https://doi.org/10.1007/s11306-012-0416-6>

- Han, Y. K., Lee, T., Han, K. H., Yun, S. H., & Lee, Y. W. (2004). Functional analysis of the homoserine O-acetyltransferase gene and its identification as a selectable marker in *Gibberella zeae*. *Current Genetics*, *46*(4), 205–212. <https://doi.org/10.1007/s00294-004-0528-2>
- Harriott, M. M., & Noverr, M. C. (2009). *Candida albicans* and *Staphylococcus aureus* form polymicrobial biofilms: effects on antimicrobial resistance. *Antimicrobial Agents and Chemotherapy*, *53*(9), 3914–22. <https://doi.org/10.1128/AAC.00657-09>
- Harriott, M. M., & Noverr, M. C. (2010). Ability of *Candida albicans* mutants to induce *Staphylococcus aureus* vancomycin resistance during polymicrobial biofilm formation. *Antimicrobial Agents and Chemotherapy*, *54*(9), 3746–55. <https://doi.org/10.1128/AAC.00573-10>
- Harris, L. G., Foster, S. J., & Richards, R. G. (2002). An introduction to *Staphylococcus aureus*, and techniques for identifying and quantifying *S. aureus* adhesins in relation to adhesion to biomaterials: review. *European Cells & Materials*, *4*, 39–60. Retrieved from <http://www.ncbi.nlm.nih.gov/pubmed/14562246>
- Hatanaka, H., Ariga, N., Nagai, J., & Katsuki, H. (1974). Accumulation of a sterol intermediate during reaction in the presence of homocysteine with cell-free extract of yeast. *Biochemical and Biophysical Research Communications*, *60*(2), 787–793. [https://doi.org/10.1016/0006-291X\(74\)90309-X](https://doi.org/10.1016/0006-291X(74)90309-X)
- Hawser, S. P., & Douglas, L. J. (1994). Biofilm formation by *Candida* species on the surface of catheter materials in vitro. *Infection and Immunity*, *62*(3), 915–921.
- He, W., Miao, F. J.-P., Lin, D. C.-H., Schwandner, R. T., Wang, Z., Gao, J., ... Ling, L. (2004). Citric acid cycle intermediates as ligands for orphan G-protein-coupled receptors. *Nature*, *429*(6988), 188–193. <https://doi.org/10.1038/nature02488>
- Hemström, P., & Irgum, K. (2006). *Hydrophilic interaction chromatography*. *Journal of Separation Science* (Vol. 29). <https://doi.org/10.1002/jssc.200600199>
- Hochberg, Y., & Benjamini, Y. (1990). More powerful procedures for multiple statistical significance testing. *Stat Med*, *9*(September 1989), 811–818.
- Hogan, D. A., & Kolter, R. (2002). *Pseudomonas-Candida* Interactions: An Ecological Role for Virulence Factors. *Science*, *296*(June), 2229–2232. <https://doi.org/10.1126/science.1070784>
- Hogan, D. a, Wargo, M. J., & Beck, N. (2007). Bacterial Biofilms on Fungal Surfaces 13. *The Biofilm Mode of Life: Mechanisms and adaptations.2*, 235–245.
- Holzschneider, M. (1995). A brief history in time of ion traps and their achievements in science. *Physica Scripta*, *T59*, 69–76. Retrieved from <http://iopscience.iop.org/1402-4896/1995/T59/009>
- Horai, H., Arita, M., Kanaya, S., Nihei, Y., Ikeda, T., Suwa, K., ... Nishioka, T. (2010). MassBank: a public repository for sharing mass spectral data for life sciences. *Journal of Mass Spectrometry: JMS*, *45*(7), 703–14. <https://doi.org/10.1002/jms.1777>
- Howard, B., & Kloos, W. (1987). *Staphylococcus*. In B. Howard, J. I. Klass, S. Rubin, A. Weissfeld, & R. Tilton (Eds.), *Clinical and Pathogenic Microbiology* (pp. 231–244).

Washington (DC): Mosby.

- Hsieh, Y. (2008). Potential of HILIC-MS in quantitative bioanalysis of drugs and drug metabolites. *Journal of Separation Science*, *31*(9), 1481–91.  
<https://doi.org/10.1002/jssc.200700451>
- Hsieh, Y., & Chen, J. (2005). Simultaneous determination of nicotinic acid and its metabolites using hydrophilic interaction chromatography with tandem mass spectrometry. *Rapid Communications in Mass Spectrometry : RCM*, *19*(21), 3031–6.  
<https://doi.org/10.1002/rcm.2171>
- Hu, Q., Noll, R. J., Li, H., Makarov, A., Hardman, M., & Cooks, R. G. (2005). The Orbitrap: A new mass spectrometer. *Journal of Mass Spectrometry*, *40*(4), 430–443.  
<https://doi.org/10.1002/jms.856>
- Ikegami, T., Tomomatsu, K., Takubo, H., Horie, K., & Tanaka, N. (2008). Separation efficiencies in hydrophilic interaction chromatography. *Journal of Chromatography A*, *1184*(1–2), 474–503. <https://doi.org/10.1016/j.chroma.2008.01.075>
- Issaq, H. J., Gutierrez, J., Issaq, H. J., & Gutierrez, J. (2017). Mixed Packings in High Performance Liquid Chromatography . II . Mixed Packings vs . Mixed Ligands PERFORMANCE LIQUID CHROMATOGRAPHY :, *3919*(January).  
<https://doi.org/10.1080/01483918808076765>
- Jabra-Rizk, M. a, Meiller, T. F., James, C. E., & Shirliff, M. E. (2006). Effect of farnesol on *Staphylococcus aureus* biofilm formation and antimicrobial susceptibility. *Antimicrobial Agents and Chemotherapy*, *50*(4), 1463–9.  
<https://doi.org/10.1128/AAC.50.4.1463-1469.2006>
- Jandera, P. (2008). Stationary phases for hydrophilic interaction chromatography, their characterization and implementation into multidimensional chromatography concepts. *Journal of Separation Science*, *31*(9), 1421–1437.  
<https://doi.org/10.1002/jssc.200800051>
- Jandera, P. (2011). Stationary and mobile phases in hydrophilic interaction chromatography: a review. *Analytica Chimica Acta*, *692*(1–2), 1–25.  
<https://doi.org/10.1016/j.aca.2011.02.047>
- Jastrzębowska, K., & Gabriel, I. (2015). Inhibitors of amino acids biosynthesis as antifungal agents. *Amino Acids*, *47*(2), 227–249. <https://doi.org/10.1007/s00726-014-1873-1>
- Jey, Y., Alsad, L., Vogel, F., Koppar, S., Auguste, F., Seymour, J., ... Nevarez, L. (2013). Interactions between *Candida albicans* and *Staphylococcus aureus* within mixed species biofilms. *Bios*, *84*(1), 30–39. <https://doi.org/130.209.6.41>
- Jiang, W., Fischer, G., Girmay, Y., & Irgum, K. (2006). Zwitterionic stationary phase with covalently bonded phosphorylcholine type polymer grafts and its applicability to separation of peptides in the hydrophilic interaction liquid chromatography mode. *Journal of Chromatography A*, *1127*(1–2), 82–91.  
<https://doi.org/10.1016/j.chroma.2006.05.080>
- Jiang, W., & Irgum, K. (1999). Stationary Phase for Simultaneous Separation of Inorganic

Cations and Anions, *71*(2), 2985–2996.

- Johnson, C. H., & Gonzalez, F. J. (2012). Challenges and opportunities of metabolomics. *Journal of Cellular Physiology*, *227*(8), 2975–2981. <https://doi.org/10.1002/jcp.24002>
- Jung, J. Y., & Oh, M. K. (2015). Isotope labeling pattern study of central carbon metabolites using GC/MS. *Journal of Chromatography. B: Analytical Technologies in the Biomedical and Life Sciences*, *974*, 101–108. <https://doi.org/10.1016/j.jchromb.2014.10.033>
- Kahsay, G., Song, H., Van Schepdael, A., Cabooter, D., & Adams, E. (2014). Hydrophilic interaction chromatography (HILIC) in the analysis of antibiotics. *Journal of Pharmaceutical and Biomedical Analysis*, *87*, 142–54. <https://doi.org/10.1016/j.jpba.2013.04.015>
- Kaito, C., & Sekimizu, K. (2007). Colony spreading in *Staphylococcus aureus*. *Journal of Bacteriology*, *189*(6), 2553–2557. <https://doi.org/10.1128/JB.01635-06>
- Kanehisa, M., & Goto, S. (2000). KEGG: Kyoto encyclopedia of genes and genomes. *Nucleic Acids Research*, *28*(1), 27–30.
- Kaneko, J., & Kamio, Y. (2004). Bacterial Two-component and Hetero-heptameric Pore-forming Cytolytic Toxins: Structures, Pore-forming Mechanism, and Organization of the Genes. *Bioscience, Biotechnology, and Biochemistry*, *68*(5), 981–1003. <https://doi.org/10.1271/bbb.68.981>
- Karas, M., Bachmann, D., & Hillenkamp, F. (1985). Influence of the wavelength in high-irradiance ultraviolet laser desorption mass spectrometry of organic molecules. *Analytical Chemistry*, *57*(14), 2935–2939. <https://doi.org/10.1021/ac00291a042>
- Kazarian, A. A., Nesterenko, P. N., Soisungnoen, P., Burakham, R., Srijaranai, S., & Paull, B. (2014). Comprehensive analysis of pharmaceutical products using simultaneous mixed-mode (ion-exchange/reversed-phase) and hydrophilic interaction liquid chromatography. *Journal of Separation Science*, *37*(16), 2138–2144. <https://doi.org/10.1002/jssc.201400411>
- Kebarle, P., & Tang, L. (1993). From ions in solution to ions in the gas phase. *Analytical Chemistry*, *65*(22), 972A–986A. <https://doi.org/10.1021/ac00070a001>
- Keefer, J. F., & Schuster, S. M. (1986). Separation of citric acid cycle intermediates by high-performance liquid chromatography with ion pairing. *Journal of Chromatography*, *383*(2), 297–305. [https://doi.org/10.1016/S0378-4347\(00\)83475-1](https://doi.org/10.1016/S0378-4347(00)83475-1)
- Keer, J., Smeulders, M. J., & Williams, H. D. (2001). A *purF* mutant of *Mycobacterium smegmatis* has impaired survival during oxygen-starved stationary phase. *Microbiology*, *147*(2), 473–481. <https://doi.org/10.1099/00221287-147-2-473>
- Kell, D. B. (2004). Metabolomics and systems biology : making sense of the soup, (1986), 296–307. <https://doi.org/10.1016/j.mib.2004.04.012>
- Kennedy, M. J., & Volz, P. A. (1985). Ecology of *Candida albicans* gut colonization: Inhibition of *Candida* adhesion, colonization, and dissemination from the gastrointestinal tract by bacterial antagonism. *Infection and Immunity*, *49*(3), 654–663.

- Ketelle, B. H., & Boyd, G. E. (1947). The Exchange Adsorption of Ions from Aqueous Solutions by Organic Zeolites. IV. The Separation of the Yttrium Group Rare Earths 1. *Journal of the American Chemical Society*, 69(11), 2800–2812. <https://doi.org/10.1021/ja01203a062>
- Khakimova, M., Ahlgren, H. G., Harrison, J. J., English, A. M., & Nguyen, D. (2013). The stringent response controls catalases in *Pseudomonas aeruginosa* and is required for hydrogen peroxide and antibiotic tolerance. *Journal of Bacteriology*, 195(9), 2011–2020. <https://doi.org/10.1128/JB.02061-12>
- Kiefer, P., Nicolas, C., Letisse, F., & Portais, J.-C. (2007). Determination of carbon labeling distribution of intracellular metabolites from single fragment ions by ion chromatography tandem mass spectrometry. *Analytical Biochemistry*, 360(2), 182–188. <https://doi.org/10.1016/j.ab.2006.06.032>
- Kim, J. K., Jang, H. A., Won, Y. J., Kikuchi, Y., Han, S. H., Kim, C. H., ... Lee, B. L. (2014). Purine biosynthesis-deficient Burkholderia mutants are incapable of symbiotic accommodation in the stinkbug. *The ISME Journal*, 8(3), 552–563. <https://doi.org/10.1038/ismej.2013.168>
- Kim, S., Thiessen, P. A., Bolton, E. E., Chen, J., Fu, G., Gindulyte, A., ... Bryant, S. H. (2016). PubChem substance and compound databases. *Nucleic Acids Research*, 44(D1), D1202–D1213. <https://doi.org/10.1093/nar/gkv951>
- Kimball, E., & Rabinowitz, J. D. (2006). Identifying decomposition products in extracts of cellular metabolites. *Analytical Biochemistry*, 358(2), 273–280. <https://doi.org/10.1016/j.ab.2006.07.038>
- Kloos, D., Derks, R. J. E., Wijtmans, M., Lingeman, H., Mayboroda, O. A., Deelder, A. M., ... Giera, M. (2012). Derivatization of the tricarboxylic acid cycle intermediates and analysis by online solid-phase extraction-liquid chromatography-mass spectrometry with positive-ion electrospray ionization. *Journal of Chromatography A*, 1232, 19–26. <https://doi.org/10.1016/j.chroma.2011.07.095>
- Kloos, W. E., & Lambe, D. R. J. (1991). Staphylococcus. In A. Barlows, W. Hausler, K. Hermann, H. Isenberg, & H. Shadomy (Eds.), *Manual of Clinical Microbiology* (5th ed., pp. 222–237). Washington (DC): ASM.
- Kloos, W. E., & Musselwhite, M. S. (1975). Distribution and persistence of *Staphylococcus* and *Micrococcus* species and other aerobic bacteria on human skin. *American Society of Microbiology*, 30(3), 381–395.
- Klotz, S. a., Chasin, B. S., Powell, B., Gaur, N. K., & Lipke, P. N. (2007). Polymicrobial bloodstream infections involving *Candida* species: analysis of patients and review of the literature. *Diagnostic Microbiology and Infectious Disease*, 59(4), 401–406. <https://doi.org/10.1016/j.diagmicrobio.2007.07.001>
- Klotz, S. A., Gaur, N. K., De Armond, R., Sheppard, D., Khardori, N., Edwards, J. E., ... El-Azizi, M. (2007). *Candida albicans* Als proteins mediate aggregation with bacteria and yeasts. *Medical Mycology*, 45(4), 363–370. <https://doi.org/10.1080/13693780701299333>
- Knapp, D. R. (1979). *Handbook of Analytical Derivatization Reactions* (1st ed.). New

York, USA: John Wiley & Sons.

- Knot, P. D., Suci, P. A., Miller, R. L., Nelson, R. D., & Tyler, B. J. (2006). A small subpopulation of blastospores in *Candida albicans* biofilms exhibit resistance to amphotericin B associated with differential regulation of ergosterol and  $\beta$ -1,6-glucan pathway genes. *Antimicrobial Agents and Chemotherapy*, *50*(11), 3708–3716. <https://doi.org/10.1128/AAC.00997-06>
- Knox, K. W., & Wicken, A. J. (1973). Immunological properties of teichoic acids. *Bacteriological Reviews*, *37*(2), 215–257.
- Koek, M., Muilwijk, B., Werf, M. J., & Hankemeier, T. (2006). Microbial metabolomics with gas chromatography mass spectrometry. *Anal Chem*, *78*(4), 1272–1281. <https://doi.org/10.1021/ac051683+>
- Kojic, E. M., & Darouiche, R. O. (2004). *Candida* Infections of Medical Devices. *Clinical Microbiology Revi*, *17*(2), 255–267. <https://doi.org/10.1128/CMR.17.2.255>
- Konermann, L., Ahadi, E., Rodriguez, A. D., & Vahidi, S. (2013). Unraveling the mechanism of electrospray ionization. *Analytical Chemistry*, *85*(1), 2–9. <https://doi.org/10.1021/ac302789c>
- Krismer, B., Liebeke, M., Janek, D., Nega, M., Rautenberg, M., Hornig, G., ... Peschel, A. (2014). Nutrient Limitation Governs *Staphylococcus aureus* Metabolism and Niche Adaptation in the Human Nose. *PLoS Pathogens*, *10*(1). <https://doi.org/10.1371/journal.ppat.1003862>
- Kumamoto, C. A. (2002). *Candida* biofilms. *Current Opinion in Microbiology*, *5*(6), 608–611. [https://doi.org/10.1016/S1369-5274\(02\)00371-5](https://doi.org/10.1016/S1369-5274(02)00371-5)
- Kumamoto, C. A. (2011). Inflammation and gastrointestinal *Candida* colonization. *Current Opinion in Microbiology*, *14*(4), 386–391. <https://doi.org/10.1016/j.mib.2011.07.015>
- Kümmel, A., Panke, S., & Heinemann, M. (2006). Putative regulatory sites unraveled by network-embedded thermodynamic analysis of metabolome data. *Molecular Systems Biology*, *2*, 2006.0034. <https://doi.org/10.1038/msb4100074>
- LaFleur, M. D., Kumamoto, C. A., & Lewis, K. (2006). *Candida albicans* biofilms produce antifungal-tolerant persister cells. *Antimicrobial Agents and Chemotherapy*, *50*(11), 3839–3846. <https://doi.org/10.1128/AAC.00684-06>
- Le Masle, A., Angot, D., Gouin, C., D'Attoma, A., Ponthus, J., Quignard, A., & Heinisch, S. (2014). Development of on-line comprehensive two-dimensional liquid chromatography method for the separation of biomass compounds. *Journal of Chromatography A*, *1340*, 90–98. <https://doi.org/10.1016/j.chroma.2014.03.020>
- Levdikov, V. M., Blagova, E., Joseph, P., Sonenshein, A. L., & Wilkinson, A. J. (2006). The structure of CodY, a GTP- and isoleucine-responsive regulator of stationary phase and virulence in gram-positive bacteria. *Journal of Biological Chemistry*, *281*(16), 11366–11373. <https://doi.org/10.1074/jbc.M513015200>
- Li, Y., Zhang, Z., Liu, X., Li, A., Hou, Z., Wang, Y., & Zhang, Y. (2015). A novel approach to the simultaneous extraction and non-targeted analysis of the small molecules metabolome and lipidome using 96-well solid phase extraction plates with

- column-switching technology. *Journal of Chromatography A*, 1409, 277–281. <https://doi.org/10.1016/j.chroma.2015.07.048>
- Li, Z., Chen, K., Guo, M., & Tang, D. (2016). Two-dimensional liquid chromatography and its application in traditional Chinese medicine analysis and metabonomic investigation. *Journal of Separation Science*, 39(1), 21–37. <https://doi.org/10.1002/jssc.201500634>
- Link, H., Fuhrer, T., Gerosa, L., Zamboni, N., & Sauer, U. (2015). Real-time metabolome profiling of the metabolic switch between starvation and growth, 12(11). <https://doi.org/10.1038/nmeth.3584>
- Little, E. L., Jeansonne, M. S., & Foley, J. P. (1991). Sequential Multimodal Elution for Pseudomultidimensional Liquid Chromatography on a Single Column. *Analytical Chemistry*, 63(Iii), 33–44.
- Livak, K. J., & Schmittgen, T. D. (2001). Analysis of Relative Gene Expression Data Using Real-Time Quantitative PCR and the 2- $\Delta\Delta$ CT Method. *Methods*, 25(4), 402–408. <https://doi.org/10.1006/meth.2001.1262>
- Lortholary, O., Petrikos, G., Akova, M., Arendrup, M. C., Arıkan-Akdagli, S., Bassetti, M., ... Ullmann, A. J. (2012). ESCMID guideline for the diagnosis and management of Candida diseases 2012: Patients with HIV infection or AIDS. *Clinical Microbiology and Infection*, 18(SUPPL.7), 68–77. <https://doi.org/10.1111/1469-0691.12042>
- Louw, S., Pereira, A. S., Lynen, F., Hanna-Brown, M., & Sandra, P. (2008). Serial coupling of reversed-phase and hydrophilic interaction liquid chromatography to broaden the elution window for the analysis of pharmaceutical compounds. *Journal of Chromatography. A*, 1208(1–2), 90–4. <https://doi.org/10.1016/j.chroma.2008.08.058>
- Lowy, F. (1998). the chromosome, as well as the extrachromosomal elements. 6 These genes are transferred between staphylococcal strains, species, or other gram-positive bacterial species through the extrachromosomal elements. 7. *New England Journal of Medicine*, 339, 520–532. <https://doi.org/10.1056/NEJM199808203390806>
- Lu, W., Bennett, B. D., & Rabinowitz, J. D. (2008). Analytical strategies for LC-MS-based targeted metabolomics. *Journal of Chromatography. B, Analytical Technologies in the Biomedical and Life Sciences*, 871(2), 236–42. <https://doi.org/10.1016/j.jchromb.2008.04.031>
- Lu, W., Bennett, B. D., & Rabinowitz, J. D. (2009). Analytical strategies for LC-MS-based targeted metabolomics, (609). <https://doi.org/10.1016/j.jchromb.2008.04.031>.Analytical
- Lu, W., Clasquin, M. F., Melamud, E., Amador-Noguez, D., Caudy, A. A., & Rabinowitz, J. D. (2010). Metabolomic analysis via reversed-phase ion-pairing liquid chromatography coupled to a stand alone orbitrap mass spectrometer. *Analytical Chemistry*, 82(8), 3212–3221. <https://doi.org/10.1021/ac902837x>
- Lu, W., Zhang, S., Teng, X., Melamud, E., Lazar, M. a, White, E., & Rabinowitz, J. D. (2014). LC-MS and GC-MS based metabolomics platform for cancer research. *Cancer & Metabolism*, 2(Suppl 1), P41. <https://doi.org/10.1186/2049-3002-2-S1-P41>

- Luo, B., Groenke, K., Takors, R., Wandrey, C., & Oldiges, M. (2007). Simultaneous determination of multiple intracellular metabolites in glycolysis, pentose phosphate pathway and tricarboxylic acid cycle by liquid chromatography-mass spectrometry. *Journal of Chromatography. A*, *1147*(2), 153–64. <https://doi.org/10.1016/j.chroma.2007.02.034>
- Lv, H., Palacios, G., Hartil, K., & Kurland, I. J. (2011). Advantages of tandem LC-MS for the rapid assessment of tissue-specific metabolic complexity using a pentafluorophenylpropyl stationary phase. *Journal of Proteome Research*, *10*(4), 2104–2112. <https://doi.org/10.1021/pr1011119>
- Mack, D., Becker, P., Chatterjee, I., Dobinsky, S., Knobloch, J. K. M., Peters, G., ... Herrmann, M. (2004). Mechanisms of biofilm formation in *Staphylococcus epidermidis* and *Staphylococcus aureus*: Functional molecules, regulatory circuits, and adaptive responses. *International Journal of Medical Microbiology*, *294*(2–3), 203–212. <https://doi.org/10.1016/j.ijmm.2004.06.015>
- Mack, L. ., Kralik, P., Rheude, A., & Dole, M. (1970). Molecular Beams of Macroions. II. *The Journal of Chemical Physics*, *52*, 4977. <https://doi.org/http://dx.doi.org/10.1063/1.1672733>
- Makarov, A., & Scigelova, M. (2010). Coupling liquid chromatography to Orbitrap mass spectrometry. *Journal of Chromatography A*, *1217*(25), 3938–3945. <https://doi.org/10.1016/j.chroma.2010.02.022>
- Makarov, a. (2000). Electrostatic axially harmonic orbital trapping: a high-performance technique of mass analysis. *Analytical Chemistry*, *72*(6), 1156–62. Retrieved from <http://www.ncbi.nlm.nih.gov/pubmed/10740853>
- Mallet, A. I., & Down, S. (2009). *Dictionary of Mass Spectrometry*. West Sussex, UK: John Wiley & Sons Ltd.
- Mangram, A. J., Horan, T. C., Pearson, M. L., Silver, L. C., & Jarvis, W. R. (1999). Guideline for Prevention of Surgical Site Infection, 1999. Centers for Disease Control and Prevention (CDC) Hospital Infection Control Practices Advisory Committee. *American Journal of Infection Control*, *27*(2), 97–132; quiz 133–4; discussion 96. [https://doi.org/10.1016/S0196-6553\(99\)70088-X](https://doi.org/10.1016/S0196-6553(99)70088-X)
- Maresso, A. W., & Schneewind, O. (2008). Sortase as a Target of Anti-Infective Therapy. *Pharmacological Reviews*, *60*(1), 128–141. <https://doi.org/10.1124/pr.107.07110>
- Marraffini, L. A., DeDent, A. C., & Schneewind, O. (2006). Sortases and the Art of Anchoring Proteins to the Envelopes of Gram-Positive Bacteria. *Microbiology and Molecular Biology Reviews*, *70*(1), 192–221. <https://doi.org/10.1128/MMBR.70.1.192-221.2006>
- Martin, a. J. P., & Synge, R. L. M. (1941). A new form of chromatogram employing two liquid phases. *Biochemical Journal*, *35*(12), 1358–1368. <https://doi.org/10.1042/bj0351358>
- Martínez, V., & Krömer, J. (2016). Quantification of Microbial Phenotypes. *Metabolites*, *6*(4), 45. <https://doi.org/10.3390/metabo6040045>

- Martins, M., Henriques, M., Lopez-Ribot, J. L., & Oliveira, R. (2012). Addition of DNase Improves the In Vitro Activity of Antifungal Drugs against *Candida albicans* Biofilms. *Mycoses*, *55*(1), 80–85.
- Martins, M., Uppuluri, P., Thomas, D. P., Cleary, I. A., Henriques, M., Lopez-Ribot, J. L., & Oliveira, R. (2010). Presence of extracellular DNA in the *Candida albicans* biofilm matrix and its contribution to biofilms. *Mycopathologia*, *169*(5), 323–331. <https://doi.org/10.1007/s11046-009-9264-y>
- Martzolff, A., Cahoreau, E., Cogne, G., Peyriga, L., Portais, J.-C., Dechandol, E., ... Legrand, J. (2012). Photobioreactor design for isotopic non-stationary <sup>13</sup>C-metabolic flux analysis (INST <sup>13</sup>C-MFA) under photoautotrophic conditions. *Biotechnology and Bioengineering*, *109*(12), 3030–3040. <https://doi.org/10.1002/bit.24575>
- Marx, A., De Graaf, A. A., Wiechert, W., Eggeling, L., & Sahm, H. (1996). Determination of the fluxes in the central metabolism of *Corynebacterium glutamicum* by nuclear magnetic resonance spectroscopy combined with metabolite balancing. *Biotechnology and Bioengineering*, *49*(2), 111–129. [https://doi.org/10.1002/\(SICI\)1097-0290\(19960120\)49:2<111::AID-BIT1>3.0.CO;2-T](https://doi.org/10.1002/(SICI)1097-0290(19960120)49:2<111::AID-BIT1>3.0.CO;2-T)
- Mashego, M. R., Wu, L., Van Dam, J. C., Ras, C., Vinke, J. L., Van Winden, W. a., ... Heijnen, J. J. (2004). MIRACLE: mass isotopomer ratio analysis of U-13C-labeled extracts. A new method for accurate quantification of changes in concentrations of intracellular metabolites. *Biotechnology and Bioengineering*, *85*(6), 620–8. <https://doi.org/10.1002/bit.10907>
- Mateus, C., Crow, S. A., & Ahearn, D. G. (2004). Adherence of *Candida albicans* to silicone induces immediate enhanced tolerance to fluconazole. *Antimicrobial Agents and Chemotherapy*, *48*(9), 3358–3366. <https://doi.org/10.1128/AAC.48.9.3358-3366.2004>
- Mayer, S. W., & Tompkins, E. R. (1947). Ion Exchange as a Separations Method. IV. A Theoretical Analysis of the Column Separations Process 1. *Journal of the American Chemical Society*, *69*(11), 2866–2874. <https://doi.org/10.1021/ja01203a069>
- McCalley, D. V. (2007). Is hydrophilic interaction chromatography with silica columns a viable alternative to reversed-phase liquid chromatography for the analysis of ionisable compounds? *Journal of Chromatography. A*, *1171*(1–2), 46–55. <https://doi.org/10.1016/j.chroma.2007.09.047>
- McCalley, D. V. (2010). The challenges of the analysis of basic compounds by high performance liquid chromatography: some possible approaches for improved separations. *Journal of Chromatography. A*, *1217*(6), 858–80. <https://doi.org/10.1016/j.chroma.2009.11.068>
- McCammon, M. T., & Parks, L. W. (1981). Inhibition of sterol transmethylation by S-adenosylhomocysteine analogs. *Journal of Bacteriology*, *145*(1), 106–112.
- McCrea, K. W., Hartford, O., Davis, S., Eidhin, D. N., Lina, G., Speziale, P., ... Höök, M. (2000). The serine-aspartate repeat (Sdr) protein family in *Staphylococcus epidermidis*. *Microbiology*, *146*(7), 1535–1546. <https://doi.org/10.1099/00221287-146-7-1535>

- McDougald, D., Rice, S. A., Barraud, N., Steinberg, P. D., & Kjelleberg, S. (2011). Should we stay or should we go: mechanisms and ecological consequences for biofilm dispersal. *Nature Reviews Microbiology*, *10*(1), 39–50. <https://doi.org/10.1038/nrmicro2695>
- McLaughlin, L. (1989). Mixed-Mode Chromatography of Nucleic Acids. *Chemical Reviews*, *89*(2), 309–319. <https://doi.org/10.1021/cr00092a003>
- Mei, J. M., Nourbakhsh, F., Ford, C. W., & Holden, D. W. (1997). Identification of *Staphylococcus aureus* virulence genes in a murine model of bacteraemia using signature-tagged mutagenesis. *Molecular Microbiology*, *26*, 399–407. <https://doi.org/10.1046/j.1365-2958.1997.5911966.x>
- Menestrina, G., Dalla Serra, M., & Prévost, G. (2001). Mode of action of  $\beta$ -barrel pore-forming toxins of the staphylococcal  $\alpha$ -hemolysin family. *Toxicon*, *39*(11), 1661–1672. [https://doi.org/10.1016/S0041-0101\(01\)00153-2](https://doi.org/10.1016/S0041-0101(01)00153-2)
- Mermel, L. A., Allon, M., Bouza, E., Craven, D. E., Flynn, P., O'Grady, N. P., ... Warren, D. K. (2009). Clinical Practice Guidelines for the Diagnosis and Management of Intravascular Catheter-Related Infection: 2009 Update by the Infectious Diseases Society of America. *Clinical Infectious Diseases*, *49*(1), 1–45. <https://doi.org/10.1086/599376>
- Millard, P., Massou, S., Wittmann, C., Portais, J.-C., & Létisse, F. (2014). Sampling of intracellular metabolites for stationary and non-stationary  $^{13}\text{C}$  metabolic flux analysis in *Escherichia coli*. *Analytical Biochemistry*, *465*, 38–49. <https://doi.org/10.1016/j.ab.2014.07.026>
- Mitchell, K. F., Taff, H. T., Cuevas, M. A., Reinicke, E. L., Sanchez, H., & Andes, D. R. (2013). Role of matrix  $\beta$ -1,3 glucan in antifungal resistance of non-albicans *Candida* biofilms. *Antimicrobial Agents and Chemotherapy*, *57*(4), 1918–1920. <https://doi.org/10.1128/AAC.02378-12>
- Monds, R. D., & O'Toole, G. A. (2008). Metabolites as Intercellular Signals for Regulation of Community-Level Traits. In *Chemical Communication among Bacteria* (pp. 105–129). American Society of Microbiology. Retrieved from <http://www.asmscience.org/content/book/10.1128/9781555815578.ch08>
- Monds, R. D., & O'Toole, G. A. (2009). The developmental model of microbial biofilms: ten years of a paradigm up for review. *Trends in Microbiology*, *17*(2), 73–87. <https://doi.org/10.1016/j.tim.2008.11.001>
- Mongodin, E., Climo, M. W., Rosato, A., Gill, S., & Archer, G. L. (2003). Microarray Transcription Analysis of Clinical. *Society*, *185*(15), 4638–4643. <https://doi.org/10.1128/JB.185.15.4638>
- Moore, S., Spackman, D. H., & Stein, W. H. (1958). Chromatography of Amino Acids on Sulfonated Polystyrene Resins. An Improved System. *Analytical Chemistry*, *30*(7), 1185–1190. <https://doi.org/10.1021/ac60139a005>
- Moormeier, D. E., Bose, J. L., Horswill, A. R., & Bayles, K. W. (2014). Temporal and stochastic control of *Staphylococcus aureus* biofilm development. *mBio*, *5*(5), 1–12. <https://doi.org/10.1128/mBio.01341-14>

- Mozzi, F., Ortiz, M. E., Bleckwedel, J., De Vuyst, L., & Pescuma, M. (2013). Metabolomics as a tool for the comprehensive understanding of fermented and functional foods with lactic acid bacteria. *Food Research International*, *54*(1), 1152–1161. <https://doi.org/10.1016/j.foodres.2012.11.010>
- Muenter, M. M., Stokes, K. C., Obie, R. T., & Jezorek, J. R. (1999). Simultaneous separation of inorganic ions and neutral organics on ion-exchange stationary phases. *Journal of Chromatography A*, *844*(1–2), 39–51. [https://doi.org/10.1016/S0021-9673\(99\)00406-9](https://doi.org/10.1016/S0021-9673(99)00406-9)
- Mukherjee, P. K., Chandra, J., Kuhn, D. M., & Ghannoum, M. A. (2003). Mechanism of fluconazole resistance in *Candida albicans* biofilms: Phase-specific role of efflux pumps and membrane sterols. *Infection and Immunity*, *71*(8), 4333–4340. <https://doi.org/10.1128/IAI.71.8.4333-4340.2003>
- Muzenda, E. (2012). Analysis of Chromatographic Theories and Thermodynamics Calculation Procedure. *International Conference on Nanotechnology and Chemical Engineering (ICNCS'2012)*, 41–46.
- Myres, R., Ratziu, V., Benhamou, Y., Di Martino, V., Moussalli, J., Tainturier, M., & Poynard, T. (2002). Infections with Multiple Hepatotropic Viruses - Polymicrobial Diseases. In K. A. Brogen & J. M. Guthmiller (Eds.), *Polymicrobial Diseases* (pp. 51–73). Washington (DC): ASM Press.
- Nair, N., Biswas, R., Götz, F., & Biswas, L. (2014). Impact of *Staphylococcus aureus* on pathogenesis in polymicrobial infections. *Infection and Immunity*, *82*(6), 2162–9. <https://doi.org/10.1128/IAI.00059-14>
- Nash, E. E., Peters, B. M., Fidel, P. L., & Noverr, M. C. (2015). Morphology-independent virulence of *Candida* species during polymicrobial intra-abdominal infections with *Staphylococcus aureus*. *Infection and Immunity*, *84*(1), 90–98. <https://doi.org/10.1128/IAI.01059-15>
- Nash, E. E., Peters, B. M., Palmer, G. E., Fidel, P. L., & Noverr, M. C. (2014). Morphogenesis is not required for *Candida albicans*-*Staphylococcus aureus* intra-abdominal infection-mediated dissemination and lethal sepsis. *Infection and Immunity*, *82*(8), 3426–35. <https://doi.org/10.1128/IAI.01746-14>
- Nazi, I., Scott, A., Sham, A., Rossi, L., Williamson, P. R., Kronstad, J. W., & Wright, G. D. (2007). Role of homoserine transacetylase as a new target for antifungal agents. *Antimicrobial Agents and Chemotherapy*, *51*(5), 1731–1736. <https://doi.org/10.1128/AAC.01400-06>
- Nesterenko, P. N., & Paull, B. (2017). Ion chromatography. In S. Fanali, P. R. Haddad, C. F. Poole, & M.-L. Riekkola (Eds.), *Liquid Chromatography* (2nd ed., pp. 205–244). Elsevier. <https://doi.org/10.1016/B978-0-12-805393-5.00009-9>
- Nett, J. E., Lepak, A. J., Marchillo, K., & Andes, D. R. (2009). Time Course Global Gene Expression Analysis of an In Vivo *Candida* Biofilm. *Gene Expression*, *53792*, 307–313. <https://doi.org/10.1086/599838>
- Nett, J. E., Sanchez, H., Cain, M. T., & Andes, D. R. (2010). Genetic Basis of *Candida* Biofilm Resistance Due to Drug-Sequestering Matrix Glucan. *The Journal of*

- Infectious Diseases*, 202(1), 171–175. <https://doi.org/10.1086/651200>
- Nett, J., Lincoln, L., Marchillo, K., Massey, R., Holoyda, K., Hoff, B., ... Andes, D. (2007). Putative role of  $\beta$ -1,3 glucans in *Candida albicans* biofilm resistance. *Antimicrobial Agents and Chemotherapy*, 51(2), 510–520. <https://doi.org/10.1128/AAC.01056-06>
- Nielsen, J., & Oliver, S. (2005). The next wave in metabolome analysis. *Trends in Biotechnology*, 23(11), 544–546. <https://doi.org/10.1016/j.tibtech.2005.08.005>
- Nobile, C. J., Fox, E. P., Nett, J. E., Sorrells, T. R., Mitrovich, Q. M., Hernday, A. D., ... Johnson, A. D. (2012). A recently evolved transcriptional network controls biofilm development in *Candida albicans*. *Cell*, 148(1–2), 126–138. <https://doi.org/10.1016/j.cell.2011.10.048>
- Nobile, C. J., & Johnson, A. D. (2015). *Candida albicans* Biofilms and Human Disease. *Annual Review of Microbiology*, 69(1), 71–92. <https://doi.org/10.1146/annurev-micro-091014-104330>
- Nobile, C. J., & Mitchell, A. P. (2006). Genetics and genomics of *Candida albicans* biofilm formation. *Cellular Microbiology*, 8(9), 1382–1391. <https://doi.org/10.1111/j.1462-5822.2006.00761.x>
- Nobile, C. J., Nett, J. E., Andes, D. R., & Mitchell, A. P. (2006). Function of *Candida albicans* adhesin hwp1 in biofilm formation. *Eukaryotic Cell*, 5(10), 1604–1610. <https://doi.org/10.1128/EC.00194-06>
- Nogueira, R., Michael, L., & Lindner, W. (2005). Alternative high-performance liquid chromatographic peptide separation and purification concept using a new mixed-mode reversed-phase / weak anion-exchange type stationary phase, 1089, 158–169. <https://doi.org/10.1016/j.chroma.2005.06.093>
- O'Toole, G., Kaplan, H. B., & Kolter, R. (2000). BIOFILM FORMATION ASMICROBIAL DEVELOPMENT. *Annual Review of Microbiology*, 54, 49–79.
- Ochsner, U. A., Young, C. L., Stone, K. C., Dean, B., Janjic, N., Critchley, I. A., & Dean, F. B. (2005). Mode of Action and Biochemical Characterization of REP8839 , a Novel Inhibitor of Methionyl-tRNA Synthetase Mode of Action and Biochemical Characterization of REP8839 , a Novel Inhibitor of Methionyl-tRNA Synthetase. *Antimicrobial Agents and Chemotherapy*, 49(10), 4253–4262. <https://doi.org/10.1128/AAC.49.10.4253>
- Oliver, S. G., Winson, M. K., Kell, D. B., & Baganz, F. (1998). Systematic functional analysis of the yeast genome. *Trends in Biotechnology*, 16(9), 373–378. [https://doi.org/10.1016/S0167-7799\(98\)01214-1](https://doi.org/10.1016/S0167-7799(98)01214-1)
- Ordoñez, E. Y., Quintana, J. B., Rodil, R., & Cela, R. (2012). Computer assisted optimization of liquid chromatographic separations of small molecules using mixed-mode stationary phases. *Journal of Chromatography A*, 1238, 91–104. <https://doi.org/10.1016/j.chroma.2012.03.055>
- Ortiz-Bolsico, C., Torres-Lapasió, J. R., Ruiz-ángel, M. J., & García-álvarez-Coque, M. C. (2013). Comparison of two serially coupled column systems and optimization

software in isocratic liquid chromatography for resolving complex mixtures. *Journal of Chromatography A*, 1281, 94–105. <https://doi.org/10.1016/j.chroma.2013.01.064>

- Otto, M. (2008). Staphylococcal biofilms. *Current Topics in Microbiology and Immunology*, 322, 207–28. Retrieved from <http://www.pubmedcentral.nih.gov/articlerender.fcgi?artid=2777538&tool=pmcentrez&rendertype=abstract>
- Pal, O. P., & Sharma, P. K. (2010). Journal of Global Pharma Technology. *Journal of Global Pharma Technology*, 2(5), 22–26. Retrieved from <http://www.jgpt.co.in/jgpt/index.php/jgptjournal/article/view/208>
- Palmer, R. J., Kazmerzak, K., Hansen, M. C., Palmer, J., Kazmerzak, K., Hansen, M. C., & Kolenbrander, P. E. (2001). Mutualism versus independence: Strategies of mixed-species oral biofilms in vitro using saliva as the sole nutrient source. *Infection and Immunity*, 69(9), 5794–5804. <https://doi.org/10.1128/IAI.69.9.5794-5804.2001>
- Parks, L. W., & Casey, W. M. (1995). PHYSIOLOGICAL, 95–116.
- Parveen, N., & Cornell, K. A. (2011). Methylthioadenosine/S-adenosylhomocysteine nucleosidase, a critical enzyme for bacterial metabolism. *Molecular Microbiology*, 79(1), 7–20. <https://doi.org/10.1111/j.1365-2958.2010.07455.x>
- Patti, G. J., Yanes, O., & Siuzdak, G. (2012a). Metabolomics: the apogee of the omic trilogy. *Nature Reviews. Molecular Cell Biology*, 13(4), 263–269. <https://doi.org/10.1038/nrm3314>
- Patti, G. J., Yanes, O., & Siuzdak, G. (2012b). Metabolomics: The apogee of the omics trilogy. *Nature Reviews Molecular Cell Biology*. Nature Publishing Group. <https://doi.org/10.1038/nrm3314>
- Patti, J. M., Allen, B. L., McGavin, M. J., & Hook, M. (1994). MSCRAMM-Mediated Adherence of Microorganisms to Host Tissues. *Annual Review of Microbiology*, 48(1), 585–617. <https://doi.org/10.1146/annurev.mi.48.100194.003101>
- Paul, W., & Raether, M. (1955). Das elektrische Massenfilter. *Zeitschrift für Physik*, 140(3), 262–273. <https://doi.org/10.1007/BF01328923>
- Peleg, A. Y., Hogan, D. A., & Mylonakis, E. (2010). Medically important bacterial – fungal interactions. *Nature Publishing Group*, 8(5), 340–349. <https://doi.org/10.1038/nrmicro2313>
- Peleg, A. Y., Tampakakis, E., Fuchs, B. B., Eliopoulos, G. M., Moellering, R. C., & Mylonakis, E. (2008). Prokaryote-eukaryote interactions identified by using *Caenorhabditis elegans*. *Proceedings of the National Academy of Sciences*, 105(38), 14585–14590. <https://doi.org/10.1073/pnas.0805048105>
- Peltola, V. T., & McCullers, J. A. (2004). Respiratory viruses predisposing to bacterial infections: role of neuraminidase. *Pediatr Infect Dis J*, 23(1), 87–97.
- Pence, H. E., & Williams, A. (2010). Chemspider: An online chemical information resource. *Journal of Chemical Education*, 87(11), 1123–1124. <https://doi.org/10.1021/ed100697w>

- Perlroth, J., Choi, B., & Spellberg, B. (2007). Nosocomial fungal infections: epidemiology, diagnosis, and treatment. *Medical Mycology*, *45*(4), 321–346. <https://doi.org/10.1080/13693780701218689>
- Peschel, A., Vuong, C., Otto, M., & Gotz, F. (2000). The D-alanine residues of *Staphylococcus aureus* teichoic acids alter the susceptibility to vancomycin and the activity of autolytic enzymes. *Antimicrobial Agents and Chemotherapy*, *44*(10), 2845–2847. <https://doi.org/10.1128/AAC.44.10.2845-2847.2000>
- Peters, B. M., Jabra-rizk, M. A., O'May, G. A., William Costerton, J., Shirtliff, M. E., Costerton, J. W., & Shirtliff, M. E. (2012). Polymicrobial interactions: impact on pathogenesis and human disease. *Clinical Microbiology Reviews*, *25*(1), 193–213. <https://doi.org/10.1128/CMR.00013-11>
- Peters, B. M., Jabra-Rizk, M. A., Scheper, M. a., Leid, J. G., Costerton, J. W., & Shirtliff, M. E. (2010a). Microbial interactions and differential protein expression in *Staphylococcus aureus* -*Candida albicans* dual-species biofilms. *FEMS Immunology and Medical Microbiology*, *59*(3), 493–503. <https://doi.org/10.1111/j.1574-695X.2010.00710.x>
- Peters, B. M., Jabra-Rizk, M. A., Scheper, M. A., Leid, J. G., Costerton, J. W., & Shirtliff, M. E. (2010b). Microbial interactions and differential protein expression in *Staphylococcus aureus*–*Candida albicans* dual-species biofilms. *FEMS Immunology & Medical Microbiology*, *59*(3), 493–503. <https://doi.org/10.1111/j.1574-695X.2010.00710.x>
- Peters, B. M., Jabra-Rizk, M. A., Scheper, M. A., Leid, J. G., Costerton, J. W., & Shirtliff, M. E. (2010c). Microbial interactions and differential protein expression in *Staphylococcus aureus* -*Candida albicans* dual-species biofilms. *FEMS Immunology and Medical Microbiology*. <https://doi.org/10.1111/j.1574-695X.2010.00710.x>
- Peters, B. M., Ovchinnikova, E. S., Krom, B. P., Schlecht, L. M., Zhou, H., Hoyer, L. L., ... Shirtliff, M. E. (2012). *Staphylococcus aureus* adherence to *Candida albicans* hyphae is mediated by the hyphal adhesin Als3p. *Microbiology (Reading, England)*, *158*(Pt 12), 2975–86. <https://doi.org/10.1099/mic.0.062109-0>
- Peters, B. M., Ward, R. M., Rane, H. S., Lee, S. a., & Noverr, M. C. (2013). Efficacy of ethanol against *Candida albicans* and *Staphylococcus aureus* polymicrobial biofilms. *Antimicrobial Agents and Chemotherapy*, *57*(1), 74–82. <https://doi.org/10.1128/AAC.01599-12>
- Pfaller, M. A., & Diekema, D. J. (2007). Epidemiology of invasive candidiasis: A persistent public health problem. *Clinical Microbiology Reviews*, *20*(1), 133–163. <https://doi.org/10.1128/CMR.00029-06>
- Pietiäinen, M., François, P., Hyyryläinen, H.-L., Tangomo, M., Sass, V., Sahl, H.-G., ... Kontinen, V. P. (2009). Transcriptome analysis of the responses of *Staphylococcus aureus* to antimicrobial peptides and characterization of the roles of *vraDE* and *vraSR* in antimicrobial resistance. *BMC Genomics*, *10*, 429. <https://doi.org/10.1186/1471-2164-10-429>
- Potrykus, K., Murphy, H., Philippe, N., & Cashel, M. (2011). ppGpp is the major source of growth rate control in *E. coli*. *Environmental Microbiology*, *13*(3), 563–575.

<https://doi.org/10.1111/j.1462-2920.2010.02357.x.ppGpp>

- Pulimood, S., Ganesan, L., Alangaden, G., & Chandrasekar, P. (2002). Polymicrobial candidemia. *Diagnostic Microbiology and Infectious Disease*, *44*(4), 353–357. [https://doi.org/10.1016/S0732-8893\(02\)00460-1](https://doi.org/10.1016/S0732-8893(02)00460-1)
- Rabinowitz, J. D. (2007). Cellular metabolomics of Escherichia coli. *Expert Review of Proteomics*. <https://doi.org/10.1586/14789450.4.2.187>
- Rabinowitz, J. D., & Kimball, E. (2007). Acidic Acetonitrile for Cellular Metabolome Extraction from Escherichia coli, *79*(16), 6167–6173.
- Rajendran, R., May, A., Sherry, L., Kean, R., Williams, C., Jones, B. L., ... Ramage, G. (2016). Metabolism With Biofilm Heterogeneity By Transcriptome Mapping. *Nature Publishing Group*, (July), 1–11. <https://doi.org/10.1038/srep35436>
- Ramage, G., Bachmann, S., Patterson, T. F., Wickes, B. L., & López-Ribot, J. L. (2002). Investigation of multidrug efflux pumps in relation to fluconazole resistance in Candida albicans biofilms. *The Journal of Antimicrobial Chemotherapy*, *49*(6), 973–980. <https://doi.org/10.1093/jac/dkf049>
- Ramautar, R., Somsen, G. W., & de Jong, G. J. (2015). CE-MS for metabolomics: Developments and applications in the period 2012–2014. *Electrophoresis*, *36*(1), 212–224. <https://doi.org/10.1002/elps.201400388>
- Rex, J. H., Walsh, T. J., Sobel, J. D., Filler, S. G., Pappas, P. G., Dismukes, W. E., & Edwards, J. E. (2004). Practice guidelines for the treatment of candidiasis. *Clinical Infectious Diseases*, (38), 661–689. <https://doi.org/10.1086/313749>
- Rice, K. C., Mann, E. E., Endres, J. L., Weiss, E. C., Cassat, J. E., Smeltzer, M. S., & Bayles, K. W. (2007). The cidA murein hydrolase regulator contributes to DNA release and biofilm development in Staphylococcus aureus. *Proceedings of the National Academy of Sciences*, *104*(19), 8113–8118. <https://doi.org/10.1073/pnas.0610226104>
- Riedel, K., Hentzer, M., Geisenberger, O., Huber, B., Steidle, A., Wu, H., ... Eberl, L. (2001). Communication between Pseudomonas aeruginosa and Burkholderia cepacia in mixed biofilms. *Microbiology*, *147*, 3249–3262.
- Roberts, L. D., Souza, A. L., Gerszten, R. E., & Clish, C. B. (2012). Targeted metabolomics. *Current protocols in molecular biology* (Vol. Chapter 30). <https://doi.org/10.1002/0471142727.mb3002s98>
- Rodionov, D. A., Vitreschak, A. G., Mironov, A. A., & Gelfand, M. S. (2004). Comparative genomics of the methionine metabolism in Gram-positive bacteria: A variety of regulatory systems. *Nucleic Acids Research*, *32*(11), 3340–3353. <https://doi.org/10.1093/nar/gkh659>
- Rühl, M., Rupp, B., Nöh, K., Wiechert, W., Sauer, U., & Zamboni, N. (2012). Collisional fragmentation of central carbon metabolites in LC-MS/MS increases precision of 13C metabolic flux analysis. *Biotechnology and Bioengineering*, *109*(3), 763–771. <https://doi.org/10.1002/bit.24344>
- Saito, K., & Matsuda, F. (2010). Metabolomics for Functional Genomics, Systems

- Biology, and Biotechnology. *Annu. Rev. Plant Biol.*, *61*, 463–89.  
<https://doi.org/10.1146/annurev.arplant.043008.092035>
- Saldanha Dominic, R. M., Shenoy, S., & Baliga, S. (2007). Candida biofilms in medical devices: Evolving trends. *Kathmandu University Medical Journal*, *5*(19), 431–436.
- Samant, S., Lee, H., Ghassemi, M., Chen, J., Cook, J. L., Mankin, A. S., & Neyfakh, A. A. (2008). Nucleotide biosynthesis is critical for growth of bacteria in human blood. *PLoS Pathogens*, *4*(2). <https://doi.org/10.1371/journal.ppat.0040037>
- Sato, S., Soga, T., Nishioka, T., & Tomita, M. (2004). Simultaneous determination of the main metabolites in rice leaves using capillary electrophoresis mass spectrometry and capillary electrophoresis diode array detection. *The Plant Journal*, *40*, 151–163.  
<https://doi.org/10.1111/j.1365-313X.2004.02187.x>
- Sauer, U. (2004). High-throughput phenomics: Experimental methods for mapping fluxomes. *Current Opinion in Biotechnology*, *15*(1), 58–63.  
<https://doi.org/10.1016/j.copbio.2003.11.001>
- Sauer, U. (2006). Metabolic networks in motion: <sup>13</sup>C-based flux analysis. *Molecular Systems Biology*, *2*, 62. <https://doi.org/10.1038/msb4100109>
- Saville, S. P., Lazzell, A. L., Monteagudo, C., & Lopez-ribot, J. L. (2003). Engineered Control of Cell Morphology In Vivo Reveals Distinct Roles for Yeast and Filamentous Forms of *Candida albicans* during Infection Engineered Control of Cell Morphology In Vivo Reveals Distinct Roles for Yeast and Filamentous Forms of *Candida albic*. *Eukaryotic Cell*, *2*(5), 1053–60. <https://doi.org/10.1128/EC.2.5.1053>
- Scheltema, R. A., Jankevics, A., Jansen, R. C., Swertz, M. A., & Breitling, R. (2011). PeakML/mzMatch: A file format, Java library, R library, and tool-chain for mass spectrometry data analysis. *Analytical Chemistry*, *83*(7), 2786–2793.  
<https://doi.org/10.1021/ac2000994>
- Schlecht, L. M. arie, Peters, B. M., Krom, B. P., Freiberg, J. A., Hänsch, G. M., Filler, S. G., ... Shirliff, M. E. (2015). Systemic *Staphylococcus aureus* infection mediated by *Candida albicans* hyphal invasion of mucosal tissue. *Microbiology (Reading, England)*, *161*(2015), 168–181. <https://doi.org/10.1099/mic.0.083485-0>
- Schoenfelder, S. M. K., Marincola, G., Geiger, T., Goerke, C., Wolz, C., & Ziebuhr, W. (2013). Methionine Biosynthesis in *Staphylococcus aureus* Is Tightly Controlled by a Hierarchical Network Involving an Initiator tRNA-Specific T-box Riboswitch. *PLoS Pathogens*, *9*(9), 1–9. <https://doi.org/10.1371/journal.ppat.1003606>
- Seddiki, S. M. L., Boucherit-Otmani, Z., Boucherit, K., Badsı-Amir, S., Taleb, M., & Kunkel, D. (2013). Assessment of the types of catheter infectivity caused by *Candida* species and their biofilm formation. First study in an intensive care unit in Algeria. *International Journal of General Medicine*, *6*, 1–7.  
<https://doi.org/10.2147/IJGM.S38065>
- Seiflein, T. A., & Lawrence, J. G. (2001). Methionine-to-Cysteine Recycling in *Klebsiella aerogenes*, *183*(1), 336–346. <https://doi.org/10.1128/JB.183.1.336>
- Sekowska, a, & Danchin, a. (1999). Identification of yrrU as the methylthioadenosine

nucleosidase gene in *Bacillus subtilis*. *DNA Research : An International Journal for Rapid Publication of Reports on Genes and Genomes*, 6(5), 255–264.

- Sharkey, L. L., McNemar, M. D., Saporito-Irwin, S. M., Sypherd, P. S., & Fonzi, W. A. (1999). HWP1 functions in the morphological development of *Candida albicans* downstream of EFG1, TUP1, and RBF1. *Journal of Bacteriology*, 181(17), 5273–5279.
- Sherertz, R. J., Raad, I. I., Belani, A., Koo, L. C., Rand, K. H., Pickett, D. L., ... Fauerbach, L. L. (1990). Three-Year Experience with Sonicated Vascular Catheter Cultures in a Clinical Microbiology Laboratory, 28(1), 76–82.
- Sherry, L., Rajendran, R., Lappin, D. F., Borghi, E., Perdoni, F., Falleni, M., ... Ramage, G. (2014). Biofilms formed by *Candida albicans* bloodstream isolates display phenotypic and transcriptional heterogeneity that are associated with resistance and pathogenicity. *BMC Microbiology*, 14(1), 182. <https://doi.org/10.1186/1471-2180-14-182>
- Shirtliff, M. E., Peters, B. M., & Jabra-Rizk, M. A. (2009). Cross-kingdom interactions: *Candida albicans* and bacteria. *FEMS Microbiology Letters*, 299(1), 1–8. <https://doi.org/10.1111/j.1574-6968.2009.01668.x>
- Shockman, G. D., & Barrett, J. F. (1983). and Assembly of Cell Walls of Gram-Positive, 132–134.
- Short, F. L., Murdoch, S. L., & Ryan, R. P. (2014). Polybacterial human disease: the ills of social networking. *Trends in Microbiology*, 22(9), 508–516. <https://doi.org/10.1016/j.tim.2014.05.007>
- Siegmán-Igra, Y., Schwartz, D., & Konforti, N. (1988). Polymicrobial bacteremia. *Medical Microbiology and Immunology*, 177(3), 169–179. <https://doi.org/10.1007/BF00232896>
- Small, H., Stevens, T. S., & Bauman, W. C. (1975). Novel ion exchange chromatographic method using conductimetric detection. *Analytical Chemistry*, 47(11), 1801–1809. <https://doi.org/10.1021/ac60361a017>
- Smith, A. J., Robertson, D., Tang, M. K., Jackson, M. S., MacKenzie, D., & Bagg, J. (2003). *Staphylococcus aureus* in the oral cavity: a three-year retrospective analysis of clinical laboratory data. *British Dental Journal*, 195(12), 701–703. <https://doi.org/10.1038/sj.bdj.4810832>
- Smith, C. A., Want, E. J., O'Maille, G., Abagyan, R., & Siuzdak, G. (2006). XCMS: Processing mass spectrometry data for metabolite profiling using nonlinear peak alignment, matching, and identification. *Analytical Chemistry*, 78(3), 779–787. <https://doi.org/10.1021/ac051437y>
- Smyth, G. K. (2004). Linear Models and Empirical Bayes Methods for Assessing Differential Expression in Microarray Experiments. *Statistical Applications in Genetics and Molecular Biology*, 3(1), 1–25. <https://doi.org/10.2202/1544-6115.1027>
- Socia, A., & Foley, J. P. (2014). Sequential elution liquid chromatography can significantly increase the probability of a successful separation by simultaneously

- increasing the peak capacity and reducing the separation disorder. *Journal of Chromatography A*, 1324, 36–48. <https://doi.org/10.1016/j.chroma.2013.11.016>
- Söderquist, B., Kanclerski, K., Sundqvist, K. G., Colque-Navarro, P., Holmberg, H., Vikersfors, T., & Möllby, R. (1998). Cytokine response to staphylococcal exotoxins in *Staphylococcus aureus* septicemia. *Clin.Microbiol.Infect.*, 4(1198–743X JC–DY9), 366–372. <https://doi.org/10.1111/j.1469-0691.1998.tb00080.x>
- Soga, T., Igarashi, K., Ito, C., Mizobuchi, K., Zimmermann, H. P., & Tomita, M. (2009). Metabolomic profiling of anionic metabolites by capillary electrophoresis mass spectrometry. *Analytical Chemistry*, 81(15), 6165–6174. <https://doi.org/10.1021/ac900675k>
- Soga, T., Ishikawa, T., Igarashi, S., Sugawara, K., Kakazu, Y., & Tomita, M. (2007). Analysis of nucleotides by pressure-assisted capillary electrophoresis-mass spectrometry using silanol mask technique. *Journal of Chromatography A*, 1159(1–2), 125–133. <https://doi.org/10.1016/j.chroma.2007.05.054>
- Soga, T., Ueno, Y., Naraoka, H., Ohashi, Y., Tomita, M., & Nishioka, T. (2002). Simultaneous Determination of Anionic Intermediates for *Bacillus subtilis* Metabolic Pathways by Capillary Electrophoresis Electrospray Ionization Mass Spectrometry. *Analytical Chemistry*, 74(10), 2233–2239. <https://doi.org/10.1021/ac020064n>
- Speziale, P., Pietrocola, G., Rindi, S., Provenzano, M., Provenza, G., Poto, A. Di, ... Arciola, C. R. (2009). Structural and functional role of, 1337–1352.
- Staib, F., Geier, R., & (Germany), R. K.-I. B. (1971). *Proteolysis Products of Candida Albicans as a Substratum for Growth of Staphylococcus Aureus - A Preliminary Report (Proteolyseprodukte Von Candida Albicans Als Naehrsubstrat Fuer Staphylococcus Aureus - Eine Vorlaeufige Mitteilung)*. Defense Technical Information Center. Retrieved from <https://books.google.co.uk/books?id=80ZBOAAACAAJ>
- Stewart, P. S., & William Costerton, J. (2001). Antibiotic resistance of bacteria in biofilms. *The Lancet*, 358(9276), 135–138. [https://doi.org/10.1016/S0140-6736\(01\)05321-1](https://doi.org/10.1016/S0140-6736(01)05321-1)
- Stitt, M., & Fernie, A. R. (2003). From measurements of metabolites to metabolomics: An “on the fly” perspective illustrated by recent studies of carbon-nitrogen interactions. *Current Opinion in Biotechnology*, 14(2), 136–144. [https://doi.org/10.1016/S0958-1669\(03\)00023-5](https://doi.org/10.1016/S0958-1669(03)00023-5)
- Sudbery, P., Gow, N., & Berman, J. (2004). The distinct morphogenic states of *Candida albicans*. *Trends in Microbiology*, 12(7), 317–324. <https://doi.org/10.1016/j.tim.2004.05.008>
- Sumner, L. W., Amberg, A., Barrett, D., Beale, M. H., Beger, R., Daykin, C. a, ... Viant, M. R. (2007). Proposed minimum reporting standards for chemical analysis Chemical Analysis Working Group (CAWG) Metabolomics Standards Initiative (MSI). *Metabolomics : Official Journal of the Metabolomic Society*, 3(3), 211–221. <https://doi.org/10.1007/s11306-007-0082-2>
- Sumner, L. W., Lei, Z., Nikolau, B. J., Saito, K., Roessner, U., & Trengove, R. (2014). Proposed quantitative and alphanumeric metabolite identification metrics.

*Metabolomics*, 10(6), 1047–1049. <https://doi.org/10.1007/s11306-014-0739-6>

- Suzuki, H., Hashimoto, W., & Kumagai, H. (1993). Escherichia coli K-12 can utilize an exogenous gamma-glutamyl peptide as an amino acid source, for which gamma-glutamyltranspeptidase is essential. *Journal of Bacteriology*, 175(18), 6038–6040.
- Suzuki, H., Kamatani, S., Kim, E. S., & Kumagai, H. (2001). Aminopeptidases A, B, and N and dipeptidase D are the four cysteinylglycinases of Escherichia coli K-12. *Journal of Bacteriology*, 183(4), 1489–1490. <https://doi.org/10.1128/JB.183.4.1489-1490.2001>
- Takats, Z. (2004). Mass Spectrometry Sampling Under Ambient Conditions with Desorption Electrospray Ionization. *Science*, 306(5695), 471–473. <https://doi.org/10.1126/science.1104404>
- Tampakakis, E., Peleg, A. Y., & Mylonakis, E. (2009). Interaction of candida albicans with an intestinal pathogen, salmonella enterica serovar typhimurium. *Eukaryotic Cell*, 8(5), 732–737. <https://doi.org/10.1128/EC.00016-09>
- Tan, B., Lu, Z., Dong, S., Zhao, G., & Kuo, M. (2014). Derivatization of the tricarboxylic acid intermediates with O -benzylhydroxylamine for liquid chromatography – tandem mass spectrometry detection. *ANALYTICAL BIOCHEMISTRY*, 465, 134–147. <https://doi.org/10.1016/j.ab.2014.07.027>
- Tanaka, K., Waki, H., Ido, Y., Akita, S., Yoshida, Y., Yoshida, T., & Matsuo, T. (1988). Protein and polymer analyses up to  $m/z$  100 000 by laser ionization time-of-flight mass spectrometry. *Rapid Communications in Mass Spectrometry*, 2(8), 151–153. <https://doi.org/10.1002/rcm.1290020802>
- Tawara, Y., Honma, K., & Naito, Y. (1996). Methicillin-resistant Staphylococcus aureus and Candida albicans on denture surfaces. *The Bulletin of Tokyo Dental College*, 37(3), 119–28. Retrieved from <http://www.ncbi.nlm.nih.gov/pubmed/9151568>
- Taylor, G. (1964). Disintegration of Water Drops in an Electric Field. *Proceedings of the Royal Society A: Mathematical, Physical and Engineering Sciences*, 280(1382), 383–397. <https://doi.org/10.1098/rspa.1964.0151>
- Terborg, L., Nowak, S., Passerini, S., Winter, M., Karst, U., Haddad, P. R., & Nesterenko, P. N. (2012). Ion chromatographic determination of hydrolysis products of hexafluorophosphate salts in aqueous solution. *Analytica Chimica Acta*, 714, 121–126. <https://doi.org/10.1016/j.aca.2011.11.056>
- Teusink, B., Walsh, M. C., Van Dam, K., & Westerhoff, H. V. (1998). The danger of metabolic pathways with turbo design. *Trends in Biochemical Sciences*, 23(5), 162–169. [https://doi.org/10.1016/S0968-0004\(98\)01205-5](https://doi.org/10.1016/S0968-0004(98)01205-5)
- Thakker, M., Park, J. S., Carey, V., & Lee, J. C. (1998). Staphylococcus aureus serotype 5 capsular polysaccharide is antiphagocytic and enhances bacterial virulence in a murine bacteremia model. *Infection and Immunity*, 66(11), 5183–5189.
- Thomas, D., & Surdin-Kerjan, Y. (1997). Metabolism of sulfur amino acids in Saccharomyces cerevisiae. *Microbiology and Molecular Biology ...*, 61(4), 503–532. Retrieved from <http://mmbr.asm.org/content/61/4/503.short>

- Tomellini, S. a, Hsu, S. H., & Hartwick, R. a. (1986). Prediction of retention for coupled column gradient elution high-performance liquid chromatography. *Analytical Chemistry*, 58(4), 904–6. Retrieved from <http://www.ncbi.nlm.nih.gov/pubmed/3706753>
- Tzagoloff, H., & Novick, R. P. (1977). Geometry of cell division in *Staphylococcus aureus*. *Journal of Bacteriology*, 129(1), 343–350.
- Unnanuntana, A., Bonsignore, L., Shirtliff, M. E., & Greenfield, E. M. (2009). The effects of farnesol on *Staphylococcus aureus* biofilms and osteoblasts. An in vitro study. *The Journal of Bone and Joint Surgery. American Volume*, 91(11), 2683–92. <https://doi.org/10.2106/JBJS.H.01699>
- Uppuluri, P., Chaturvedi, A. K., Srinivasan, A., Banerjee, M., Ramasubramaniam, A. K., K?hler, J. R., ... Lopez-Ribot, J. L. (2010). Dispersion as an important step in the *Candida albicans* biofilm developmental cycle. *PLoS Pathogens*, 6(3). <https://doi.org/10.1371/journal.ppat.1000828>
- Valenza, G., Tappe, D., Turnwald, D., Frosch, M., K?nig, C., Hebestreit, H., & Abele-Horn, M. (2008). Prevalence and antimicrobial susceptibility of microorganisms isolated from sputa of patients with cystic fibrosis. *Journal of Cystic Fibrosis*, 7(2), 123–127. <https://doi.org/10.1016/j.jcf.2007.06.006>
- Van Berkel, G. J., & Kertesz, V. (2007). Using the Electro Electrochemistry spray Ion Source. *Analytical Chemistry*, 79(15), 5510–5520. <https://doi.org/10.1021/ac071944a>
- Van Dam, J. C., Eman, M. R., Frank, J., Lange, H. C., Van Dedem, G. W. K., & Heijnen, S. J. (2002). Analysis of glycolytic intermediates in *Saccharomyces cerevisiae* using anion exchange chromatography and electrospray ionization with tandem mass spectrometric detection. *Analytica Chimica Acta*, 460(2), 209–218. [https://doi.org/10.1016/S0003-2670\(02\)00240-4](https://doi.org/10.1016/S0003-2670(02)00240-4)
- Van Winden, W. A., Van Dam, J. C., Ras, C., Kleijn, R. J., Vinke, J. L., Van Gulik, W. M., & Heijnen, J. J. (2005). Metabolic-flux analysis of *Saccharomyces cerevisiae* CEN.PK113-7D based on mass isotopomer measurements of <sup>13</sup>C-labeled primary metabolites. *FEMS Yeast Research*, 5(6–7), 559–568. <https://doi.org/10.1016/j.femsyr.2004.10.007>
- Vermeij, P., & Kertesz, M. a. (1999). Pathways of Assimilative Sulfur Metabolism in *Pseudomonas putida* Pathways of Assimilative Sulfur Metabolism in *Pseudomonas putida*, 181(18), 1–6.
- Viklund, C., & Irgum, K. (2000). Synthesis of Porous Zwitterionic Sulfobetaine Monoliths and Characterization of Their Interaction with Proteins, 2539–2544.
- Walshe, M., Kelly, M. T., Smyth, M. R., & Ritchie, H. (1995). Retention studies on mixed-mode columns in high-performance liquid chromatography. *Journal of Chromatography A*, 708(1), 31–40. [https://doi.org/10.1016/0021-9673\(95\)00260-T](https://doi.org/10.1016/0021-9673(95)00260-T)
- Wang, Y., Liu, S., Hu, Y., Li, P., & Wan, J.-B. (2015). Current state of the art of mass spectrometry-based metabolomics studies - a review focusing on wide coverage, high throughput and easy identification. *RSC Advances*, 5(96), 78728–78737. <https://doi.org/10.1039/C5RA14058G>

- Want, E. J., Nordström, A., Morita, H., & Siuzdak, G. (2007). From exogenous to endogenous: The inevitable imprint of mass spectrometry in metabolomics. *Journal of Proteome Research*, 6(2), 459–468. <https://doi.org/10.1021/pr060505+>
- Weckwerth, W. (2003). Metabolomics in systems biology. *Annual Review of Plant Biology*, 54(1), 669–689. <https://doi.org/10.1146/annurev.arplant.54.031902.135014>
- Weckwerth, W., Loureiro, M. E., Wenzel, K., & Fiehn, O. (2004). Differential metabolic networks unravel the effects of silent plant phenotypes. *Proceedings of the National Academy of Sciences of the United States of America*, 101(20), 7809–7814. <https://doi.org/10.1073/pnas.0303415101>
- Weig, M., Gross, U., & Muhlschlegel, F. (1998). Clinical aspects and pathogenesis of *Candida* infection. *Trends in Microbiology*, 6(12), 468–470. [https://doi.org/10.1016/S0966-842X\(98\)01407-3](https://doi.org/10.1016/S0966-842X(98)01407-3)
- Wendisch, V. F., Bott, M., Kalinowski, J., Oldiges, M., & Wiechert, W. (2006). Emerging *Corynebacterium glutamicum* systems biology. *Journal of Biotechnology*, 124(1), 74–92. <https://doi.org/10.1016/j.jbiotec.2005.12.002>
- Wenzel, R. P. (1995). Nosocomial Candidemia: Risk Factors and Attributable Mortality. *Clinical Infectious Diseases*, 20(6), 1531–1534. <https://doi.org/10.1093/clinids/20.6.1531>
- Wertheim, H. F. L., Melles, D. C., Vos, M. C., van Leeuwen, W., van Belkum, A., Verbrugh, H. a, & Nouwen, J. L. (2005). The role of nasal carriage in *Staphylococcus aureus* infections. *The Lancet Infectious Diseases*, 5(12), 751–762. [https://doi.org/10.1016/S1473-3099\(05\)70295-4](https://doi.org/10.1016/S1473-3099(05)70295-4)
- Wheeler, P. R., Coldham, N. G., Keating, L., Gordon, S. V., Wooff, E. E., Parish, T., & Hewinson, R. G. (2005). Functional demonstration of reverse transsulfuration in the *Mycobacterium tuberculosis* complex reveals that methionine is the preferred sulfur source for pathogenic mycobacteria. *Journal of Biological Chemistry*, 280(9), 8069–8078. <https://doi.org/10.1074/jbc.M412540200>
- Wiechert, W. (2001). *C Metabolic Flux Analysis*, 206.
- Wilkinson, B. (1997). Biology. In K. Crossley & G. Archer (Eds.), *The Staphylococci in Human Diseases* (pp. 1–38). London: Churchill Livingstone.
- Wilkinson, B. J., & Holmes, K. M. (1979). *Staphylococcus aureus* cell surface: Capsule as a barrier to bacteriophage adsorption. *Infection and Immunity*, 23(2), 549–552.
- Williams, R. E. (1963). Healthy carriage of *Staphylococcus aureus*: its prevalence and importance. *Bacteriological Reviews*, 27(96), 56–71.
- Wilm, M. S., & Mann, M. (1994). Electrospray and Taylor-Cone theory, Dole's beam of macromolecules at last? *International Journal of Mass Spectrometry and Ion Processes*, 136(2–3), 167–180. [https://doi.org/10.1016/0168-1176\(94\)04024-9](https://doi.org/10.1016/0168-1176(94)04024-9)
- Wisplinghoff, H., Bischoff, T., Tallent, S. M., Seifert, H., Wenzel, R. P., & Edmond, M. B. (2004). Nosocomial bloodstream infections in US hospitals: analysis of 24,179 cases from a prospective nationwide surveillance study. *Clinical Infectious Diseases : An Official Publication of the Infectious Diseases Society of America*, 39(3), 309–17.

<https://doi.org/10.1086/421946>

- Wu, L., Mashego, M. R., Van Dam, J. C., Proell, A. M., Vinke, J. L., Ras, C., ... Heijnen, J. J. (2005). Quantitative analysis of the microbial metabolome by isotope dilution mass spectrometry using uniformly <sup>13</sup>C-labeled cell extracts as internal standards. *Analytical Biochemistry*, *336*(2), 164–171. <https://doi.org/10.1016/j.ab.2004.09.001>
- Wunschel, D. S., Fox, K. F., Fox, A., Nagpal, M. L., Kim, K., & Stewart, G. C. (1997). Quantitative analysis of neutral and acidic sugars in whole bacterial cell hydrolysates using high-performance anion-exchange liquid chromatography – electrospray ionization tandem mass spectrometry, *776*, 205–219.
- Xiang, Y., Liu, Y., & Lee, M. L. (2006). Ultrahigh pressure liquid chromatography using elevated temperature. *Journal of Chromatography. A*, *1104*(1–2), 198–202. <https://doi.org/10.1016/j.chroma.2005.11.118>
- Yamashita, M., & Fenn, B. J. (1984). Negative ion production with the electrospray ion source. *J Phys.Chem.*, *88*(20), 4671–4675. <https://doi.org/10.1021/j150664a046>
- Yang, S., Sadilek, M., & Lidstrom, M. E. (2010). Streamlined pentafluorophenylpropyl column liquid chromatography-tandem quadrupole mass spectrometry and global <sup>13</sup>C-labeled internal standards improve performance for quantitative metabolomics in bacteria. *Journal of Chromatography A*, *1217*(47), 7401–7410. <https://doi.org/10.1016/j.chroma.2010.09.055>
- Yang, W. C., Regnier, F. E., & Adamec, J. (2008). Comparative metabolite profiling of carboxylic acids in rat urine by CE-ESI MS/MS through positively pre-charged and 2H-coded derivatization. *Electrophoresis*, *29*(22), 4549–4560. <https://doi.org/10.1002/elps.200800156>
- Yarwood, J. M., Bartels, D. J., Volper, E. M., & Greenberg, E. P. (2004). Quorum Sensing in Staphylococcus aureus Biofilms Quorum Sensing in Staphylococcus aureus Biofilms, *186*(6). <https://doi.org/10.1128/JB.186.6.1838>
- Yeater, K. M., Chandra, J., Cheng, G., Mukherjee, P. K., Zhao, X., Rodriguez-Zas, S. L., ... Hoyer, L. L. (2007). Temporal analysis of *Candida albicans* gene expression during biofilm development. *Microbiology*, *153*(8), 2373–2385. <https://doi.org/10.1099/mic.0.2007/006163-0>
- Yee, R., Cui, P., Shi, W., Feng, J., & Zhang, Y. (2015). Genetic Screen Reveals the Role of Purine Metabolism in *Staphylococcus aureus* Persistence to Rifampicin. *Antibiotics*, *4*(4), 627–642. <https://doi.org/10.3390/antibiotics4040627>
- Yu, L. W., & Hartwick, R. A. (1989). Zwitterionic Stationary Phases in HPLC. *Journal of Chromatographic Science*, *27*(4), 176–185.
- Zamboni, N., Saghatelian, A., & Patti, G. J. (2015). Defining the Metabolome: Size, Flux, and Regulation. *Molecular Cell*, *58*(4), 699–706. <https://doi.org/10.1016/j.molcel.2015.04.021>
- Zarnowski, R., Westler, W. M., Lacmbouh, G. A. de, Marita, J. M., Bothe, J. R., Bernhardt, J., ... Andes, D. R. (2014). Novel entries in a fungal biofilm matrix encyclopedia. *mBio*, *5*(4), e01333–e01314. <https://doi.org/10.1128/mBio.01333-14>

- Zhang, K., & Liu, X. (2016). Mixed-mode chromatography in pharmaceutical and biopharmaceutical applications. *Journal of Pharmaceutical and Biomedical Analysis*, 128, 73–88. <https://doi.org/10.1016/j.jpba.2016.05.007>
- Zhang, X., Hou, H., Chen, H., Liu, Y., Wang, A., & Hu, Q. (2015). A column-switching LC-MS/MS method for simultaneous quantification of biomarkers for 1,3-butadiene exposure and oxidative damage in human urine. *Journal of Chromatography. B, Analytical Technologies in the Biomedical and Life Sciences*, 1002, 123–129. <https://doi.org/10.1016/j.jchromb.2015.08.012>